



Novel CD64-DTR mouse model generation using CRISPR-Cas9 technology and functional characterization of renal dendritic cells

Dissertation

zum Erwerb des Doctor of Philosophy (Ph.D.)

an der Medizinischen Fakultät der

Ludwig-Maximilians-Universität zu München

vorgelegt von

Dalia Pakalniškytė

aus

Kelmė

am

09.07.2019

Supervisor: Prof. Barbara Schraml

Second expert: Dr. Markus Moser

Third evaluator: Prof. Marc Schmidt-Supprian

Fourth evaluator: Prof. Peter Nelson

Dean: Prof. Dr. med. dent. Reinhard HICKEL

Date of oral examination: 22.11.2019

Acknowledgment

First, I would like to thank Prof. Dr. Barbara Schraml for giving me the excellent opportunity to make my PhD under her supervision. I appreciated her intensive guidance and support during my work. She helped me to sharpen my critical thinking, to interpret data without exception as well as to choose the most effective way to address scientific questions.

Particular, I would like to thank Dr. Markus Moser and his team for their intensive support and valuable suggestions during the generation of my mouse model.

Special thanks go to the other members of my TAC team, Prof. Dr. med. Christian Schulz and Prof. Dr. Anne Krug, for their helpful feedback and constant contribution to this work.

Of course, I would like to give special thanks to all my colleagues, particular Johanna Salvermoser, Stephan Rambischler, Claudia Schmalhofer and Dr. Natallia Salei, for their awesome support and cooperation during work, but also for the fun we had together in the institute and wherever we met.

I also would like to thank my friend for supporting me during all this time. He gave me the strength always to believe in the success of my work and to overcome all difficulties during this time.

Finally, the biggest gratitude goes to my family, especially my mum and my grandmother for their continual support and encouragement not to stop in my carrier and to reach the best in my life. Without my grandmother, who always believed in me and taught me how to follow my way, I would be not where I am now. Ačiū Tau, kad tu buvai ir esi mano gyvenime.

Summary

Generally, conventional dendritic cells (cDCs) are highly phagocytic non-lymphocytic motile cells that screen their surroundings for pathogens or tissue damage and after activation migrate from non-lymphoid organs to lymph nodes, where they can present antigen to naïve thymus derived (T) cells. Most of the tissue cDCs can be subdivided into two main subsets cDC1 and cDC2. However, fate mapping of DC using a reporter mouse model identified a renal specific cluster of differentiation (CD) 64⁺ cell population that displays features commonly associated with cDCs and monocytes (MOs)/macrophages (MØs). This discovery raised the question, weather CD64⁺ cells are specialized to regulate locally immune responses in the kidney microenvironment. Moreover, cells with features of DC and CD64⁺ population have been described to play a protective role in some pathological processes in the kidney, like in nephrotoxic acute kidney injury (AKI). However, the fact that these CD64⁺ cells are difficult to distinguish based on phenotypic properties hinders the exact delineation of the individual contributions of DCs, CD64⁺ cells, MOs and MØs for kidney immunity.

In order to investigate the specific function of CD64⁺ cells in kidney homeostasis, a novel transgenic mouse model was generated by clustered regularly interspaced short palindromic repeat (CRISPR)/CRIPSR-associated nuclease (Cas) technology in which cyclization recombination (Cre) recombinase-inducible diphtheria toxin receptor (iDTR) is expressed under the *CD64* promoter. Here, Cre-mediated excision of a locus of crossover in P1 (loxP) sequenced flanked STOP cassette (LSL) and *CD64* promoter activity renders the cell sensitivity to diphtheria toxin (DT) administration. Finally, the obtained transgenic CD64-LSL-2A-DTR strain was tested by breeding it with the DC specific C-type lectin domain family 9, member A (Clec9a)-Cre mouse line, and an efficient depletion of CD64⁺ cells in the offspring after DT treatment was observed. Importantly, DT exposure in these mice did not affect cDC1 and cDC2 and monocytosis or neutrophilia were not observed, as an unwanted side effects of cell ablation.

The second part of this work was focused on the establishment of a protocol to induce nephrotoxic AKI for the investigation of cDC and CD64⁺ cell function during this pathogenesis in the Clec9a-Cre x Rosa26-iDTR and X-C motif chemokine receptor 1 (XCR1)-DTR-Venus depletion mouse models. 15 milligram (mg)/ kilogram (kg) cisplatin was identified as the optimal dose for the induction of the disease within 48 hours (h) as confirmed by increased BUN and creatinine levels. Additionally, it was shown that the administration of 25 nanogram (ng)/gram (g) DT was enough to deplete renal cDC1 and cDC2 in Clec9a-Cre x Rosa26-iDTR mice and cDC1 in XCR1-DTR-Venus mice. DT administration followed by cisplatin injection showed for both models no effect of cell depletion on kidney function and on infiltration of MOs and neutrophils in renal tissue. Interestingly, the depletion of cDC1 and cDC2 in Clec9a-Cre x Rosa26-iDTR mouse model resulted in a slight decrease of CD64⁺ cell subsets.

Taken together, these results confirmed the establishment of a new CD64-LSL-2A-DTR depletion mouse model as a future *in vivo* tool for the functional investigation of CD64⁺ cells. Furthermore, a first AKI induction protocol was established for two DC depletion mouse models. The novel generated mouse model alone or in combination with this nephrotoxic AKI protocol will hopefully substantially contribute for a better and detailed understanding of cDC and CD64⁺ cell functions in renal immunity and may help to develop improved therapeutic strategies to treat kidney diseases.

Table of content

ACKNOWLEDGMENT	III
SUMMARY	IV
TABLE OF CONTENT	V
TABLE OF FIGURES AND TABLES	VII
1. INTRODUCTION	1
1.1. INNATE IMMUNE SYSTEM	1
1.1.1. <i>Mononuclear phagocyte system (MPS)</i>	1
1.1.2. <i>cDC subsets</i>	3
1.1.3. <i>Functional specialization of cDCs</i>	4
1.1.4. <i>Development of cDCs</i>	6
1.2. KIDNEY STRUCTURE, ROLE AND PARAMETERS OF RENAL FUNCTION.....	7
1.3. CDCs IN THE KIDNEY.....	9
1.3.1. <i>Renal DCs</i>	9
1.3.2. <i>Function of renal DCs</i>	10
1.3.3. <i>Renal DCs role during nephrotoxic AKI</i>	12
1.4. TRANSGENIC MOUSE MODELS TO DEplete DCs AND MØs.....	13
1.5. CONSIDERATIONS TO USE CD64 GENE AS A SELECTION MARKER FOR SPECIFIC DEPLETION OF DCs.....	17
1.6. GENOME ENGINEERING.....	19
1.6.1. <i>CRISPR-Cas9 technology as genome engineering tool</i>	21
1.6.2. <i>CRISPR-Cas9 technology in transgenic mouse model generation</i>	22
2. AIMS OF THE STUDY.....	24
3. MATERIALS AND METHODS	25
3.1. MATERIALS	25
3.1.1. <i>Solutions</i>	25
3.1.2. <i>Media</i>	26
3.1.3. <i>Plasmids and bacterial artificial chromosome (BAC) list</i>	26
3.1.4. <i>Antibodies</i>	27
3.1.5. <i>Oligonucleotides</i>	28
3.1.6. <i>Mouse strains</i>	30
3.1.7. <i>Bacterial strains</i>	31
3.1.8. <i>Analysis Software</i>	31
3.2. METHODS.....	32
3.2.1. <i>Molecular biology methods</i>	32
3.2.1.1. Absorbance based nucleic acid quantification and agarose gel electrophoresis.....	32
3.2.1.2. PCRs	33
3.2.1.3. Primer design.....	33
3.2.1.4. Restriction digestion and dephosphorylation of DNA	34
3.2.1.5. Ligation of DNA fragments using Quick Ligation™ Kit, Gibson Assembly® Master Mix Kit or pGEM®-T Easy Vector System	34
3.2.1.6. Measurement of bacterial cultures by optical density (OD) and bacterial glycerol stock preparation.....	35
3.2.1.7. Transformation of bacteria by heat shock and electroporation	35
3.2.1.8. Isolation of gDNA from mouse biopsies	37
3.2.1.9. Plasmid and DNA fragment purification	38
3.2.1.10. BAC isolation.....	39
3.2.1.11. Plasmid screening using Toothpick analysis	39
3.2.1.12. HR in EL350 cells	40
3.2.1.13. Southern blot and synthesis of Southern blot probes	40
3.2.1.14. BUN and creatinine measurement in the serum or plasma	42
3.2.2. <i>Flow cytometry</i>	42
3.2.2.1. Leukocyte isolation from spleen and kidney	42

Table of content

3.2.2.2. Cell number and viability determination	43
3.2.2.3. Cell surface marker staining using antibodies	44
3.2.3. <i>Animal Husbandry</i>	44
3.2.4. <i>In vivo methods</i>	45
3.2.4.1. CD64-LSL-2A-DTR mice generation using CRISPR-Cas9 technology	45
3.2.4.2. Blood collection and serum isolation	45
3.2.4.3. Depletion of DTR expressing cells	46
3.2.4.4. AKI induction	46
3.2.5. <i>Statistical analysis</i>	47
4. RESULTS	48
4.1. CD64-LSL-2A-DTR MOUSE MODEL GENERATION	48
4.1.1. <i>CD64 expression on cDC progenitors</i>	48
4.1.2. <i>In silico analysis of CD64 target region for DTR gene knock-in and design of DTR construct</i>	50
4.1.3. <i>Cloning of DTR construct (pBlueScript_LSL_2A_DTR_WPRE_Neo plasmid generation)</i>	52
4.1.4. <i>Design of homology arms</i>	56
4.1.5. <i>Cloning of homology arms (pBlueScript_Homo1_Homo2 rescue vector and pBlueScript_CD64 plasmid generation)</i>	56
4.1.6. <i>Synthesis of CD64-LSL-2A-DTR target vector</i>	62
4.1.7. <i>PCR approach for detection of DTR construct integration into mouse genome</i>	66
4.1.8. <i>PCR based screening assay identified two FM based on DTR construct integration into their gDNA</i>	69
4.1.9. <i>Generation of a specific Southern blot probe to detect DTR construct integration</i>	72
4.1.10. <i>Southern blot analysis confirmed successful CD64 gene editing for two CD64-LSL-2A-DTR FM</i>	75
4.1.11. <i>CD64-LSL-2A-DTR target vector integration into CD64 locus did not affect CD64 protein expression</i>	76
4.1.12. <i>DTR expression on renal CD64⁺ cells from Clec9a-Cre x CD64-LSL-2A-DTR mice is not detectable by FACS</i>	78
4.1.13. <i>CD64-LSL-2A-DTR target vector integration into CD64 locus did not cause frame shift</i>	81
4.1.14. <i>Cre recombinase removes LSL cassette allowing DTR expression in Clec9a-Cre x CD64-LSL-2A-DTR mice</i>	82
4.1.15. <i>Application of DT caused specific ablation of CLEC9A⁺ progenitor derived CD64⁺ cells in Clec9a-Cre x CD64-LSL-2A-DTR mice</i>	83
4.1.16. <i>Depletion of renal CD64⁺ cells did not cause monocytosis and neutrophilia</i>	87
4.2. ROLE OF DENDRITIC CELLS DURING AKI	90
4.2.1. <i>Effect of high concentrated cisplatin solution on AKI severity</i>	90
4.2.2. <i>Effect of different doses of cisplatin on AKI induction</i>	91
4.2.3. <i>Depletion of cDCs in Clec9a-Cre x Rosa26-iDTR mice</i>	92
4.2.4. <i>Depletion of cDC1 subset in XCR1-DTR-Venus mice</i>	94
4.2.5. <i>Cisplatin treatment fails to induce consistent AKI induction in female mice and to draw conclusions about cDCs role during nephrotoxicity</i>	95
5. DISCUSSION	99
5.1. MOUSE GENERATION	99
5.2. CDC ROLE IN AKI	105
6. LITERATURE	111
7. APPENDIX	126
7.1. PLASMID SEQUENCES	126
7.1.1. <i>GCDL-2A-DTR</i>	126
7.1.2. <i>195 FrtneokanaFrt DTA</i>	128
7.1.3. <i>pBlueScript® SK II (+)</i>	130
7.2. CURRICULUM VITAE	132
7.3. AFFIDAVIT	133
7.4. CONFIRMATION OF CONGRUENCY	134
7.5. LIST OF SCIENTIFIC PUBLICATIONS	135

Table of figures and tables

Figures

Figure 1. Phenotype of mononuclear phagocytic system cells.....	2
Figure 2. Mouse cDC populations in lymphoid and non-lymphoid tissues.....	4
Figure 3. The different compartments found in the murine kidney.....	8
Figure 4. CD64 expression analysis on cDC progenitors.....	49
Figure 5. Analysis of <i>CD64</i> region for repair construct insertion.....	50
Figure 6. Structure of DTR construct.....	51
Figure 7. Generation of pBlueScript_LSL_2A-DTR plasmid.....	53
Figure 8. Generation of pBlueScript_LSL_2A-DTR_WPRE_Neo plasmid.....	55
Figure 9. Schematic diagram of the <i>Mus musculus CD64</i> locus.....	56
Figure 10. Generation of pBlueScript_Homo1 plasmid.....	57
Figure 11. Generation of pBlueScript_Homo1_Homo2 plasmid.....	59
Figure 12. Verification of the transformed CD64_BAC integrity.....	60
Figure 13. Generation of pBlueScript_CD64 plasmid.....	62
Figure 14. Verification of the transformed pBlueScript_CD64 plasmid.....	63
Figure 15. Verification of the generated CD64-LSL-2A-DTR plasmid.....	65
Figure 16. Screening of single event uptake in Stbl2 for CD64-LSL-2A-DTR target vector.....	66
Figure 17. Generation of CD64_DTRconstruct_BAC.....	67
Figure 18. Establishment of positive control for DTR construct integration into genomic <i>CD64</i> screening to identify FM.....	69
Figure 19. PCR analysis to identify FM.....	72
Figure 20. Schematic diagram of Southern blot strategy for the specific detection of DTR construct integration.....	73
Figure 21. Cloning of Southern blot Probe1.....	74
Figure 22. Cloning of Southern blot probe Neo probe and quality control if DIG labelled probes.....	74
Figure 23. Southern blot analysis of gDNA isolated from FM.....	76
Figure 24. CD64 expression is not altered in <i>Clec9a^{+/-Cre}CD64^{+/-DTR}</i> mice compared to <i>Clec9a^{+/-Cre}CD64^{+/-+}</i> mouse.....	77
Figure 25. DTR expression on renal cDC1 from <i>Clec9a^{Cre/Cre}Rosa26^{+/-DTR}</i> mice.....	80
Figure 26. DTR expression on renal CD64 ⁺ cells from <i>Clec9a^{+/-Cre}CD64^{+/-DTR}</i> mice.....	81
Figure 27. Insertion of the transgenic <i>CD64</i> segment did not cause frame shift.....	82
Figure 28. Confirmation of successful LSL cassette excision in enriched Clec9a-Cre x CD64-LSL-2A-DTR mouse renal leukocytes.....	83
Figure 29. Depletion of renal CD64 ⁺ cells in Clec9a-Cre x CD64-LSL-2A-DTR mice.....	84
Figure 30. Depletion of cDCs in Clec9a-Cre x CD64-LSL-2A-DTR mice.....	86
Figure 31. Analysis of cDCs and RPM in the spleen of Clec9a-Cre x CD64-LSL-2A-DTR mice after DT or PBS administration.....	87
Figure 32. Analysis of neutrophils and MOs in the kidney of <i>Clec9a^{+/-Cre}CD64^{+/-DTR}</i> mice.....	89
Figure 33. AKI induction in C57BL/6 females using cisplatin.....	90
Figure 34. Dose response of C57BL/6 female mice to different cisplatin amounts to induce AKI.....	91
Figure 35. Gating strategy to identify cDC populations and CD64 ⁺ cells in kidney.....	92
Figure 36. Depletion of renal cDC populations in Clec9a-Cre x Rosa26-iDTR mice.....	94
Figure 37. Depletion of cDC1 in XCR1-DTR-Venus mice.....	95
Figure 38. Effect of cDC depletion on kidney function in cisplatin induced nephrotoxicity.....	96
Figure 39. Effect of cDC2 and/or cDC1 depletion on infiltrating leukocytes in cisplatin induced nephrotoxicity.....	98

Tables

Table 1. Stock Solutions.....	25
Table 2. Media.....	26
Table 3. Plasmid and BAC list.....	26

Table of figures and tables

Table 4. Antibodies	27
Table 5. DNA oligonucleotides for genotyping	28
Table 6. DNA oligonucleotides for Southern blot probe amplification	28
Table 7. DNA oligonucleotides for Gibson Assembly.....	29
Table 8. DNA oligonucleotides for PCR amplification.....	29
Table 9. DNA oligonucleotides for sequencing.....	29
Table 10. Mouse strains.....	30
Table 11. Bacterial strains.....	31
Table 12. Software used in the study	31

1. Introduction

1.1. Innate immune system

The mammalian immune system is a host defence system, which can be divided into an innate and adaptive arm¹. Evolutionarily, the innate immune system is older than the adaptive arm and provides rapid, but non-specific responses against invading pathogens and presents the first line of defence¹. The adaptive immune system includes immune cells that recognize a broad variety of potentially threatening pathogens with a high specificity and build a cellular memory against these infectious agents². However, development of adaptive immune responses requires about 4-7 days, which would provide a window of opportunity for pathogens to spread in the host without the help of the innate immune system²⁻⁴. The major cells of this ancient immune system include cDCs, plasmacytoid DCs (pDCs), MOs, MØs, natural killer (NK) cells, mast cells and granulocytes⁵⁻⁹.

1.1.1. Mononuclear phagocyte system (MPS)

Within the innate immune system, the MPS is represented by cDCs, pDCs, MØs and MOs. At the time of host defence in the mouse these cells play a prominent role, because they are one of the first cells to react to pathogens or tissue injury^{10,11}. Commonly, the cells of MPS are phenotypically similar, demonstrating stellate morphology and a capacity for fragment crystallizable region (Fc)-receptor mediated phagocytosis¹²⁻¹⁵. All MPS cells in tissue are mainly identified based on the expression of surface proteins (Fig. 1). However, most of these markers are not exclusively specific to a certain cell population and their expression levels can change based on the cell activation status, for instance after infection or during inflammation¹³. Nevertheless, all MPS cells express in common certain level of CD11c¹⁶. In consequence, cDCs are identified as double positive for CD11c and major histocompatibility complex II (MHCII) in all tissues. In addition, cDCs can express other markers such as C-X3-C motif chemokine receptor 1 (CX3CR1), CD24, CD135, CD8, CD103, XCR1, CD205, CLEC9A, CD4, CD172a, CD11b, CD64 (Fig. 1)^{13,17,18}. pDCs can be discriminated from other MPS cells using CD45R and sialic acid-binding immunoglobulin-like lectin H (Siglech) surface markers. Also, they express CD135, lymphocyte antigen 6 complex (Ly6C) and CLEC9A¹⁹. In case of MØs, the

most common expressed surface markers are CD64, CX3CR1 and epidermal growth factor-like module-containing mucin-like hormone receptor-like 1 (EMR1 or alternative name F4/80), but also expression of MHCII, CD11b, CD14, Mer tyrosine-protein kinase (MerTK), sialic acid-binding immunoglobulin-like lectin F (SiglecF) and CD172a can be found²⁰. The identification of MØs becomes even more aggravated, since they are well embedded into a tissue, where they adopt in addition a niche-specific phenotype and expression. For instance, CD11a and CD326 are more prominently expressed on lung MØs, but not on microglia, spleen and peritoneal MØs. In contrast to this, splenic MØs demonstrate higher expression of CD31, while peritoneal MØs are characterized by CD93 expression²¹. MOs represent a more phenotypically heterogeneous population generally characterised by Ly6C and CD11b expression and can be subdivided into Ly6C⁺CD11b⁺ and Ly6C⁻CD11b⁺ subsets. In addition, MOs can express surface markers such as CD64, CX3CR1 or MHCII, but also C-C chemokine receptor type 2 (CCR2), F4/80 (Fig. 1)²². However, the fact that MOs are able to differentiate into DC-like or MØ-like cells makes MO derived cells difficult to distinguish from DCs or MØs^{11,23,24}.

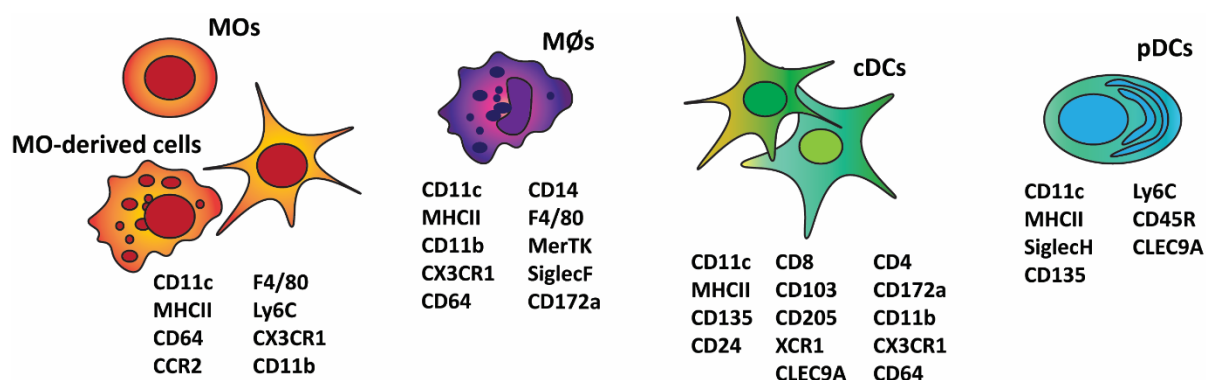


Figure 1. Phenotype of mononuclear phagocytic system cells.

Surface markers, commonly used to identify cDCs, MØs, pDCs, MOs and MO-derived cells are shown for each MPS cell population.

Even though the MPS represents a group of highly phenotypically similar cells, each cell population plays its specific role in tissue homeostasis. MØs are well known for their tissue sentience role²¹, where they are responsible for clearance of cellular debris and iron processing, regulation of tissue immune responses as well as being the first defence line against pathogens and environmental challenges²⁵. In contrast to MØs, MOs mainly circulate in the blood, but can be also found in small amounts in healthy tissues^{13,26,27}. Specifically, during tissue damage or infection MOs infiltrate in huge numbers to the site of inflammation,

where they acquire a functionally distinct phenotype enabling host defense^{11,28}. Similarly, pDCs are primarily found in the blood, but they can also infiltrate both lymphoid and non-lymphoid organs¹⁹. The main role of pDCs is to produce large amounts of type I interferon (IFN1) during viral infection²⁹⁻³¹. cDCs are non-lymphocytic motile cells located within the tissue at strategically important places to get in contact with cell associated antigens, bacteria or viruses. Consequently, cDCs are located in the spleen, which is highly rinsed by blood flow or found in the lymph node, where tissue draining lymphatic vessels enter the lymphoid system³²⁻³⁵. cDCs demonstrate the ability to process and present antigens following encounter with various pathogens and thus, their main function is to bridge the innate immune system to the adaptive part³⁶.

However, up to date the contrast between these distinct functions of the different myeloid populations within the MSP and coupled with the broad overlap in their phenotype create scientific challenges in the understanding of their individual specific contributions during pathogenic conditions, like infection or inflammation.

1.1.2. cDC subsets

cDCs can be further subdivided into so called cDC1 and cDC2 which can be discriminated based on specific transcription factor (TF) and surface marker expression^{13,17,18,35}. Specifically, cDC1 are characterised by dependence on inhibitor of deoxyribonucleic acid (DNA) binding 2 (ID2), basic leucine zipper activation transcription factor (ATF)-like transcription factor 3 (BATF3), interferon regulatory factor 8 (IRF8) and by the expression of XCR1, CD24 and CLEC9A. cDC2 on the other hand are characterised by dependence on interferon regulatory factor 4 (IRF4), neurogenic locus notch homolog protein 2 (NOTCH2) and kruppel like factor 4 (KLF4) and express CD11b or CD172^{18,37,38}.

Similarly to the before discussed MØs, the specific phenotype of surface markers of each cDC subset differs with their localization in the organism. It was shown, that lymphoid organs, such as thymus or spleen, contains two resident cDC1 and cDC2 subsets, which are described as CD8⁺CD4⁻ and CD8⁻CD4⁺ cDCs, respectively (Fig. 2)^{37,39}. In contrast, non-lymphoid tissue cDC subsets are phenotypically different and are identified as CD103⁺CD11b⁻ cDC1 and CD103⁻CD11b⁺ cDC2. Moreover, non-lymphoid tissues can also contain an additional tissue specific

cDC subset apart from the classical cDC1 and cDC2^{18,37,40}. Like this, the small intestine is equipped with a third CD103⁺CD11b⁺ cDC2 population, while the skin contains additional CD301b⁺ cDCs⁴¹⁻⁴⁵.

Therefore, any investigation aiming to understand the detailed contribution of each cDC subset in maintaining tissue homeostasis needs to consider, that each organ is equipped with two classical phenotypically and transcriptionally distinct cDC1 and cDC2 subsets, but may also contain additional cDC populations as a consequence of their adaptation to the niche-specific requirements.

	<u>Transcription factors</u>	<u>Surface markers</u>	
		<u>Lymphoid tissue</u>	<u>Non-lymphoid tissue</u>
 cDC1	BATF3 ID2 IRF8	CD24 CD8 CD205 XCR1 CLEC9A	CD24 CD103 XCR1 CLEC9A
 cDC2	IRF4 KLF4 NOTCH2	CD4 CD11b CD172a	CD11b CD172a

Figure 2. Mouse cDC populations in lymphoid and non-lymphoid tissues.

cDCs are subdivided into two main subsets cDC1 and cDC2 based on their TF and surface markers expression. Moreover, cDCs from lymphoid and non-lymphoid tissues can be distinguished by their specific phenotype as demonstrated by the indicated differentially expressed surface markers.

1.1.3. Functional specialization of cDCs

cDCs are the main antigen presenting cells, which regulate protective immune responses and the tolerance to self-antigens^{37,46,47}. In this context, cDCs are located in tissues at strategically important places that permit close proximity and exchange with possible environmental influences. This allows cDCs to efficiently sample antigens and after encounter, they migrate from the peripheral tissues via lymphatic vessels to the lymph nodes^{35,39}. Here, cDCs present these antigens mainly via MHCII to naïve T cells and activate them^{35,39}. Within the different cDC subsets, cDC1 is characterized by the key feature and unique ability to cross-present various internalized antigens via MHCI molecules^{48,49}. This unique feature predestines cDC1 to play an important role in tumour rejection as well as during viral infections⁵⁰⁻⁵³. Consequently, cDC1 are highly equipped with various receptors, such as toll-like receptors

(TLRs), C-type lectin receptors as well as chemokine receptors, that allow for the detection of particular pathogens, hence distinguishing cDC1 from cDC2^{35,54}. For example, cDC1 specifically express TLR3 for detecting double-stranded viral ribonucleic acid (RNA), TLR11, which senses flagellin and/or profilin on parasites, and CLEC9A, which interacts with necrotic bodies⁵⁵⁻⁵⁸. Additionally, cDC1 also express TLR12 receptor, which is highly homologous to TLR11, and play an important role in controlling of *Toxoplasma gondii* infection^{57,59,60}. Furthermore, cDC1 can shape immune responses by the secretion of specific cytokines. For instance, cDC1 are known to be the main source of interleukin (IL) 12, which is important in the defence against intracellular pathogens⁶¹⁻⁶⁴. It was shown that IL-12, produced by cDC1 in response to *Toxoplasma gondii* infection, induces interferon gamma production by natural killer and T cells, which in turn activates various cell intracellular defence pathways, leading to the clearance of the pathogen^{63,65}.

Similarly, cDC2 are equipped with a broad variety of partially overlapping receptors, required for tracking various pathogens, such as TLR2, TLR4, TLR9, but specifically cDC2 express CD209a, RIG-I-like receptor (RLR) and Nod-like receptor (NLR)^{37,66}. In contrast to cDC1, the cDC2 subset is more potent at activating CD4⁺ T cells than CD8⁺ T cells^{37,67}. Moreover, cDC2 are also highly involved in cytokine production and maintenance. As an example, they were identified as the essential IL-23 producers following bacterial flagellin administration or in response to *Citrobacter rodentium* infection^{68,69}. Here, cDC2 locally shape immune reactions by producing IL-23, which, in consequence, induces IL-22 production by type 3 innate lymphoid cells (ILC3s), required for efficient pathogen clearance⁶⁹. Other studies have shown, that cDC2 are involved in the promotion of T helper 2 (Th2) differentiation, by the production of IL-10 and IL-33 during lung inflammation⁷⁰. The cDC2 role in Th2 induction as a key mediator was further demonstrated after subcutaneous immunization with ovalbumin along with papain or alum and in response to a protease allergen, as well as after infection with *Nippostrongylus brasiliensis*^{44,71}. Finally, a potent implication of cDC2 in tissue homeostasis was demonstrated in mesenteric lymph nodes, where these cells maintained IL-17 producing CD4⁺ T cells⁷². In addition, cDC2 support skin IL-17 production by CD8⁺ T cells during commensal *Staphylococcus epidermidis* colonization⁷³.

Overall, specific cDC1 functions are better understood, since these cells are more easily distinguished from other myeloid cells by their surface markers and their targeted investigation is assisted by their TF dependency^{18,35,37}. In comparison to cDC1, the specific

functions of the cDC2 population still remain less characterized, mainly due to the absence of available cell specific markers to target this more heterogeneous cell population even against ontogenetically less related MØs and monocyte derived DCs (moDCs)^{18,35,37,72,74}. Therefore, studies investigating cDC2 function need to be always critically evaluated, like the data about the increased infiltration of cDC2 into the lungs of mice after ovalbumin induced asthma⁷⁵, which was later challenged by a more recent study⁷⁶. Here it was demonstrated, that moDCs, rather than cDC2, were the main infiltrating cells during asthma and producers of pro-inflammatory cytokines⁷⁶.

Therefore, the distinct identification of different DC populations within the myeloid cell lineage and the detailed investigation of more specially defined subpopulations of cDCs or DC-related cells, like the kidney resident CD64⁺ cells, is an indispensable requirement for the detailed understanding of the individual contribution of each cell subset to tissue immune homeostasis.

1.1.4. Development of cDCs

Initially, it was believed that DCs formed a specific subset of MOs⁷⁷⁻⁷⁹. However, detailed DC lineage tracing unravelled that DCs represented an independent myeloid cell lineage, which develop from hematopoietic stem cells over a cascade of various bone marrow (BM) resident progenitors^{24,30,80-82}. Macrophage and dendritic cell progenitors (MDPs) give rise to common dendritic cell precursors (CDPs), the first fully committed progenitors of the cDC lineage, which can be identified in tissue as lineage⁻CD115⁺CD135⁺CD117⁻ cells. Moreover, they are also characterised by high expression of CLEC9A²⁴. In the BM, these CDPs further differentiate into conventional DC precursors (pre-cDCs)⁸³⁻⁸⁵. These pre-cDCs can be identified in tissue as lineage⁻CD11c⁺CD135⁺CD172a^{lo} cells. Studies suggested that at the stage of pre-cDCs there is already a pre-commitment towards one or another cDC subset^{81,86,87}. After differentiation these pre-cDCs egress from the BM and enter the blood stream. Here they do not circulate for a long time and settle down in different tissues, where they finally differentiate into fully mature cDC1 or cDC2^{13,24}.

Development and survival of cDC are regulated by diverse endogenously expressed proteins and paracrine signalling molecules⁸⁰. However, the basic network and detailed contribution

of these molecules responsible for development and survival are up to date only partially understood. Nevertheless, several factors were already identified to play a pivotal role during these processes, like fms-like tyrosine kinase 3 ligand (Flt3L)^{88,89}. Others are granulocyte-macrophage colony-stimulating factor (GM-CSF), macrophage colony stimulating factor (M-CSF) or CX3CL1^{35,90-92}. Beside these molecules, there are also others TFs and ligands required for development and/or survival of the specific cDC1 and cDC2 subsets. Like this it was shown, that cDC1 require IRF8, BATF3 as well as ID2^{13,93}, while cDC2 are dependent on IRF4, NOTCH2 and KLF4^{72,94,95}. Moreover, ligands like transforming growth factor-beta (TGF β) or lymphotoxin β were described as requirements for maintenance of cDC2⁹⁶⁻⁹⁸.

Nevertheless, it needs to be mentioned here, that even through it is generally accepted that cDCs evolved from the myeloid lineage, recent studies have suggested that lymphoid progenitors may also contribute to the existing cDC2 pool⁹⁹⁻¹⁰¹. This in turn raises the question, if the existing conception for the development of cDC is yet complete. Moreover, since the molecular basics for the development and survival are not fully understood more detailed investigations need to be done to elucidate the processes leading to the diversification of the DC lineage.

1.2. Kidney structure, role and parameters of renal function

The urinary system can be subdivided into the upper and lower parts (Fig. 3A). While the lower urinary tract is composed of the bladder and urethra, the upper urinary tract includes kidneys and ureters¹⁰². The kidneys are a pair of bean-shaped organs, located on the right and left side of the abdomen. Each kidney is highly supplied with blood, flowing through the renal artery and collecting in renal vein (Fig. 3B)¹⁰³. Moreover, the kidney is covered by a thin fibrous layer, the kidney capsule, which protects it from trauma or damage. Each individual kidney can be further subdivided into two regions: an outer cortex and inner medulla¹⁰³. The cortical columns and pyramids start in the cortex and extend into the medulla. The nephron, the functional and structural unit of the kidney, is located in both kidney zones (Fig. 3C). Each adult kidney contains thousands of nephrons^{103,104}. The nephron by itself can be subdivided into renal corpuscle and renal tubules. The renal corpuscle is composed of glomerulus, a ball of blood capillaries, which is covered by Bowman's capsule¹⁰³. The renal proximal tubule

starts from the capsule, extends into the medulla, where it forms the so-called Henle's loop, and comes back into cortex forming distal tubules¹⁰³. Different distal nephron tubules join, forming a collecting duct, which enters the medulla, then the renal pelvis and finally fuses with the ureter^{103,105}.

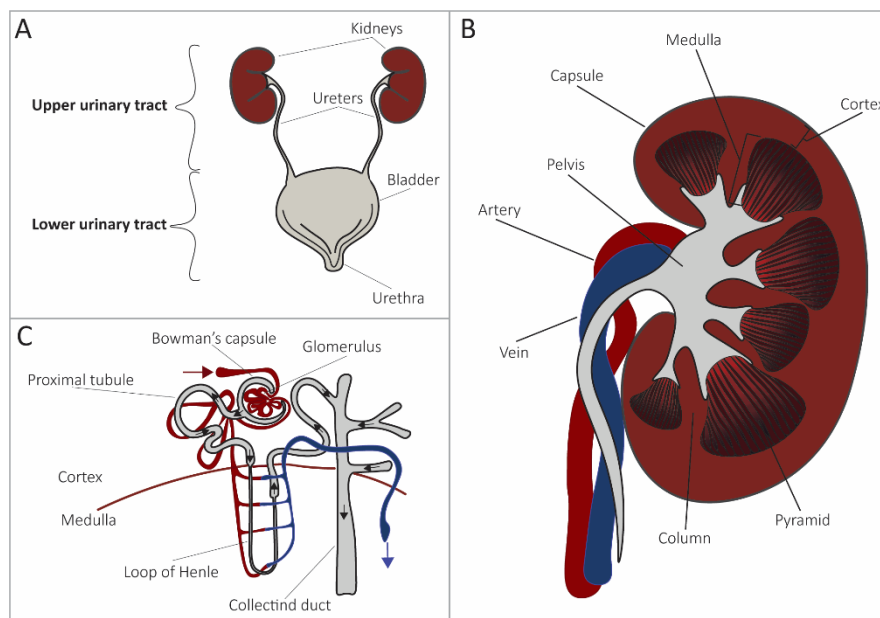


Figure 3. The different compartments found in the murine kidney.

(A) A diagram of the main parts that compose the murine urinary tract is shown. (B) A diagram of the main structures that make up the murine kidney is shown. (C) An overview of the main structures found in murine kidney is displayed.

In the glomerulus various micro and macromolecules and partially serum are filtrated from the blood into the capsule, due to high water pressure in the blood¹⁰³. This fluid from the capsule flows into the tubules, which are covered by capillaries. Here, most of the molecules are reabsorbed back, leaving behind toxic material, unnecessary salts, acids and excess water, which finally form the urine¹⁰³. Due to the fact that the kidneys remove excess water, as well as salt and acids, they are responsible for the regulation of blood pressure and pH¹⁰⁶⁻¹⁰⁸. Moreover, the kidney participates in the synthesis of important metabolites. For instance, it has been demonstrated that kidney cells produce the active form of vitamin D, which is required for calcium and phosphorus absorption^{109,110}. Aside the important role in regulating blood pH and salt homeostasis, the kidney is fully equipped for sensing and controlling the plasma volume as well as the mass of red blood cells¹¹¹. Kidney tissue produces the hormone erythropoietin, which acts on BM to differentiate more red blood cells^{111,112}.

Since a healthy kidney filtrates and removes toxic material as well as excess fluid from the organism, blood and urine are a commonly used materials to evaluate renal function¹¹³. Urine analysis can help to detect different kidney disorders, such as bladder infections, kidney stones, diabetes or chronic kidney diseases¹¹⁴. Typically, urine tests include a microscopic analysis of urine and dipstick test, measurement of protein amount in the urine, mostly albumin, and metabolic waste measurement, such as the muscle by-product creatinine or the liver waste product, blood urea nitrogen (BUN)^{113,114}. Increased protein levels in the urine indicate that kidneys became leaky, while low level of creatinine and BUN in the urine is associated with filtration ratio reduction and kidney function disruption¹¹³. Blood tests are used to evaluate the amount of several metabolic waste products, such as creatinine or BUN. The accumulation of these molecules in the blood indicates any disruption of kidney function^{115,116}.

1.3. cDCs in the kidney

1.3.1. Renal DCs

The kidney contains a heterogeneous cDC population, which phenotypically and functionally significantly overlap with MOs and MØs^{117,118}. Interestingly, the kidney exhibits typical non-lymphoid tissue cDC1 and cDC2 subsets, but also a third, highly tissue specific cell population^{24,93,119}. This specific population expresses CD64, a surface marker commonly used to separate MO derived cells from cDCs^{120,121}. Classical renal cDCs are identified as CD45⁺CD11c⁺MHCII⁺CD64⁻ cells and can be further subdivided as previously discussed before into cDC1 and cDC2 subsets based on their expression of additional surface markers, like CD24, CD103 or XCR1 and CD11b or CD172^{17,122,123}. The kidney specific CD64⁺ population shares a MO/MØ phenotype as well as cDC characteristics^{17,24,124-126}. CD64⁺ cells do not express zinc finger and BTB domain containing 46 (Zbtb46) TF, which is known to be restricted to DC lineage and some activated MOs, thereby supporting the notion that CD64⁺ cells are rather MØs^{37,125,127}. In contrast, CD64⁺ cells differentiate, like other cDCs, from a CLEC9A⁺ progenitor and therefore indicative of the DC lineage origin²⁴. In addition, these cells are able to stimulate *in vitro* T cells at a similar level as cDC2, further supporting the DC identity of

CD64⁺ cells²⁴. Renal CD64⁺ cells can be further subdivided into F4/80^{hi}CD11b^{lo} and F4/80^{lo}CD11b^{hi} subsets²⁴. F4/80^{hi}CD11b^{lo} cells, like yolk sack derived MØs, are characterised by a long life-span, as these cells do not exchange between parabiotic partners or do so just poorly^{124,128}. They also do not differentiate from DC progenitors in short-term transfer experiments^{24,124}. F4/80^{hi}CD11b^{lo} cells do not require FLT3 for their development and express low levels of the TFs IRF4 and IRF8, further supporting the notion that these cells are MØs rather than DCs. In contrast, the F4/80^{lo}CD11b^{hi} subset differentiates from pre-cDCs in short-term transfer experiments, depends on FLT3 and expresses high levels of IRF4^{17,24}. Taken together, the exact ontogeny of the unique kidney CD64⁺ cell population as well as F4/80^{hi}CD11b^{lo} and F4/80^{lo}CD11b^{hi} subsets is still an open question due to these opposing data.

All kidney cDC1, cDC2 as well as CD64⁺ cells are located in the tubulointerstitium and absent from the glomeruli^{125,129-131}. Specifically, the cDC1 subset preferentially seeds the cortex and is located around large blood vessels, while cDC2 subset is mainly found in the interstitium, close to smaller blood vessels^{122,125}. In contrast, CD64⁺ cells can be found across the kidney, forming an extensive network^{91,125,132}. Similar to cDC2, CD64⁺ cells express CX3CR1, which possibly is involved in the accumulation of these cells in the kidney^{91,131}. In addition, renal tubular epithelial cells express high amounts of CX3CL1 suggesting that CX3CR1/CX3CL1 is important for the survival of these cells in the kidney^{91,133,134}.

The identification of this unique renal CD64⁺ cell population, demonstrating the described cDC and MØ characteristics, has raised the actual question about their ontogeny and tissue related function. Therefore, it is believed that beside the classical cDCs, CLEC9A⁺ progenitor derived CD64⁺ cells may represent an additional and distinct kidney specific cDC population, leading to questions as to why these cells are located mainly in the kidney and what their role in kidney immune homeostasis could be²⁴.

1.3.2. Function of renal DCs

Even through, it is unquestionable today that renal DCs are critical for pathogen defence and tolerance to low-molecular-weight antigens, the elucidation of the specific functional role within the different renal DC subsets is still ongoing^{18,124,135}. This functional attribution is even more complicated by the fact that in large part studies on renal DC function are focused on

CD11c⁺ MPS cells, which allow no distinct conclusion on specific cDC subsets^{91,134,136-140}. For instance, the important role of CD11c⁺ cells as renal immune sentinels was demonstrated in bacterial pyelonephritis, where in response to bacteria CD11c⁺ cells recruited neutrophilic granulocytes by producing chemokine C-X-C motif ligand 2 (CXCL2)¹³⁶. In addition, renal CLEC9A⁺ progenitor derived cells play important protective role against systemic *Candida albicans* infection, by producing IL-23 in response to fungi, which further activates NK cells, which contribute to the elimination *Candida albicans*¹³⁷. The protective role of CD11c⁺ cells was also investigated in nephrotoxic nephritis (NTN), mouse model of crescentic glomerulonephritis (cGC). Depletion of CD11c⁺ cells at early stage of NTN resulted in aggravated kidney damage. These CD11c⁺ cells isolated from NTN mice induced IL-10 production in CD4⁺ T cells, indicating a possible CD11c⁺ cell protective mechanism, where IL-10 was shown to be already associated with a better disease outcome during NTN¹⁴¹⁻¹⁴⁴. Moreover, it was suggested that renal CD11c⁺ cells were important in the induction and maintenance of IL-17A production by renal resident gamma delta ($\gamma\delta$) T cells, which were shown to play a role at renal injury attenuation during cGC¹³⁸. The important protective role of antigen presenting cells during the early stage of NTN/cGC was also confirmed using CX3CR1-deficient mice, demonstrating a reduced number of CD11c⁺MHCII⁺ cells in the kidney^{91,134}. In contrast to this observed protective role, CD11c⁺ cell depletion at a later stage of NTN attenuated kidney damage. Such CD11c⁺ cells, isolated from mice at later stage of NTN, induced various pro-inflammatory cytokine production, like IL-2, TNF α , IFN γ , IL-17, IL-6 in CD4 T cells, indicating that CD11c⁺ cells acquired a pro-inflammatory phenotype over time¹³⁹. Additionally, CD11c⁺ cells were demonstrated to negatively contribute to sterile inflammation upon kidney ischemia reperfusion-injury by producing the pro-inflammatory cytokine tumour necrosis factor alpha (TNF α)¹⁴⁰.

A more subset-specific study of cGC demonstrated that cDC1 and cDC2 depletion prior to cGC induction attenuated kidney injury¹²⁵. Although M ϕ and neutrophil numbers were similar in this investigation, T cells as well as Th17 memory cells were reduced in cDC1/cDC2 depleted cGC mice. Additional detailed analysis demonstrated that the cDC1 subset specifically plays the protective role by limiting the recruitment of neutrophils^{125,145}. Moreover, another study demonstrated that the cDC1 subset fosters forkhead box P3 (FoxP3) expressing regulatory T (T_{reg}) cell accumulation in the kidney¹⁴⁵. Besides, it was also shown that during cGC cDC1 expressed high levels of anti-inflammatory genes, while cDC2 produced the neutrophil

recruiting CXCL2 cytokine¹²⁵. In contrast to the observed protective role of cDC1 subset in cGC, the same cell population acted in a pro-inflammatory manner by promoting renal damage in a murine model of adriamycin nephrotoxicity (AN). Here, a cDC1 mediated activation of CD8⁺ T cells and subsequent induction of kidney injury through cytotoxic CD8 T cells was observed¹²².

Overall, the renal CD11c⁺MHCII⁺ population is a heterogeneous group of cells that play an important role in kidney immune homeostasis through their role in immune surveillance and the instigation of immunity or tolerance. However, depending on the disease model the cells behave ambiguously and could act pro- or anti-inflammatory. However, a multitude of studies are mainly focused on the CD11c⁺ cell bulk population and have not investigated the individual contribution of each cell type. Therefore, a more detailed analysis of the individual contribution of each CD11c⁺ cell subset, especially the CD64⁺ cell population, could help in future to explain their individual contribution for the kidney immune homeostasis.

1.3.3. Renal DCs role during nephrotoxic AKI

Cisplatin is a chemical compound and cytostatic drug commonly used to treat patients with various solid tumours¹⁴⁶. However, cisplatin is also known to cause severe side effects, such as ototoxicity, gastrotoxicity, myelosuppression and nephrotoxicity^{146,147}. In the kidney, tubular epithelia cells actively take up cisplatin resulting in cell death and the induction of AKI^{146,148}.

Since most of the studies, dealing with renal DC functions, investigated CD11c⁺ MPS cells as a homogenous group, the specific role of the different DCs during AKI is limited and largely unknown. However, it was shown that CD11c⁺ cells play a protective role during this pathogenesis¹⁴⁹⁻¹⁵¹. Like this, inducible depletion of CD11c⁺ cells was shown to result in increased tubular necrosis, elevated blood BUN and creatinine levels during AKI^{16,149}. Depletion of these cells prior to AKI also lead to increased leukocyte infiltration into the kidney, where neutrophils were the major population¹⁴⁹. Even though, the extent of neutrophil infiltration has been shown to correlate with disease severity, their exact role during sterile kidney inflammation is not clear¹⁴⁹⁻¹⁵⁵. When CD11c⁺ cells were depleted at later time points of AKI, a disease protective effect was not observed, indicating that CD11c⁺ cells are important at the beginning of the disease¹⁴⁹. The protective role of CD11c⁺ cells appears

to be mediated by the anti-inflammatory cytokine IL-10, which inhibits pro-inflammatory cytokine production and kidney fibrosis^{150,156,157}. This observation was further supported by the use of mixed BM chimeric mice, lacking IL-10 in CD11c⁺ cells, which demonstrated a moderately increased disease severity compared with chimeric mice, still possessing functional CD11c⁺ cells¹⁵⁰. In contrast to this, chimeric mice, lacking CD11c⁺ cells, showed a severe renal pathology, indicating that CD11c⁺ cells provided additional protection against cisplatin nephrotoxicity, beside their IL-10 production¹⁵⁰. Interestingly, other studies observed no loss of protection against cisplatin nephrotoxicity in liposome-encapsulated clodronate treated mice or CX3CR1 deficient mice, which were characterized by a reduced number of renal CD11c⁺MHCII⁺ cells^{91,158}. Nevertheless, both strategies to reduce the cells of interest in the kidney were not cell type specific, affected a broad variety of cells and are prone to unspecific side effects. For instance, liposome-encapsulated clodronate treatment affects all professional phagocytic cells, including MØs/MOs as well as DCs¹⁵⁹. Similarly, CX3CR1 is not restricted to a specific cell type and can be found on MOs, pre-cDCs as well as on CD64⁺ cells and cDC2 subset. Moreover, CX3CR1 has been shown to play an important role in MO accumulation in the non-inflamed kidney as well as in ischemia–reperfusion injured kidney^{93,134,160-162}.

Although CD11c⁺ MPS cells were demonstrated to play a protective role during AKI, these investigations did not accommodate the heterogeneity of this cell system. Therefore, the individual contribution of each cDC subset, especially CD64⁺ cells, within this system is still not fully understood. Consequently, even the protective role of CD11c⁺ cells are indisputable, further detailed studies are still required to elucidate in the future the individual contribution of each cell population and their role during cisplatin nephrotoxicity.

1.4. Transgenic mouse models to deplete DCs and MØs

In vivo cell depletion mouse models are widely used in immunological studies and offer important tools to investigate cell specific functions in the development of various diseases¹⁶³⁻¹⁶⁶. Classically, transgenic cell depletion mouse models are generated by inactivation of essential cell genes, locus specific integration of a *DTR* gene or locus specific integration of a recombinase gene¹²⁷.

The first mouse models used to study cell specific functions were conventional gene knock-outs to deplete a cell type of interest. These mouse models lacked one or more cell-specific TFs, cytokine receptors or cytokines, required for the specific cell development, homeostasis or migration of the cell to a particular tissue^{127,164,165}. Consequently, such models were developed amongst others also to elucidate the functional impact of cDCs and MØs. Here, the most widely used knock-out mouse models for targeting DCs or specific cDC subset were *FLT3L*⁻, *Batf3*⁻, *IRF8*⁻, *Notch2*⁻, *Klf4*^{-52,89,167-169}. Following the same strategy, several MØ depletion models relied on the disruption of the genes for colony-stimulating factor 1 (CSF1) or CSF1 receptor (CSF1R), which are primary regulators of survival, proliferation, differentiation and function of MØs¹⁷⁰⁻¹⁷⁵. Nevertheless, the drawback of these approaches became quickly obvious, because the elimination of the desired gene was not restricted in these mouse models and occurred systematically in all tissues and cells. Therefore, these gene deficient mice exhibited a global phenotype, without the possibility to link the observed phenomenon to a distinct cell type.

Consequently, more advanced conditional cell depletion mouse models were developed on DTR-DT system basis, to prevent as much as possible the aforementioned side effects. DTR based mouse models are generated by knocking-in the *DTR* gene, which naturally does not occur in rodent cells, into a specific locus of choice within the murine genome, thereby making rodent cells susceptible to DT^{127,164,165}. Basically, the *DTR* gene is placed in frame downstream of the promoter of the desired cell type specific gene, expressed at the mature state of the cell or one of its progenitors. In most of cell depletion mouse models, the disruption of the targeted gene is accompanied with the cell type specific expression of DTR under the control of the original promoter. Now, DT administration in such transgenic mice leads to the selective apoptosis of these DTR⁺ cells, due to the disruption of the cellular protein synthesis^{127,176,177}. Therefore, selective cell depletion based on a DTR-DT system has a significant advantage over classical gene knock-out strategies, specifically if a heterozygote knock-in strategy is used or the knock-in does not disrupt the expression of the gene of interest. This is explained by the fact, that inducible cell depletion at a desired time point minimizes familiarization effects in the organism before an actual experiment starts^{176,177}. Common examples to make use of this approach and to address cDC function are CD11c based mouse models, like CD11c-DTR and CD11c-DOG or CD11c-LuciDTR¹⁷⁸⁻¹⁸⁰. Other examples for cell-targeted depletion are Zbtb46-DTR, CD207-DTR, CD205-DTR, Clec9a-DTR or

XCR1-DTR-Venus^{82,181-185}. There are several available MØ depletion models including CD11b-DTR, CD64-DTR, CD169-DTR^{166,186-188}. Even though DTR-DT based cell depletion mouse models became preferential over classical gene knock-out mouse models, they are still confronted with the problem and are criticized for their lack of specificity, because they also cannot solve the drawback, that one specific gene expression is rarely restricted to one particular cell population¹²⁷. This became especially obvious, for the first CD11c-DTR model, because here DT injection led to death of the treated animals due to lack of specificity of the targeted gene¹⁸⁹. Even with the approach to use BM chimeric animals to increase the targeted gene specificity for the CD11c-DTR mouse model or to generate more restricted CD11c.DOG mouse model, DT induced cell depletion was still not cDC specific and had a possible effect on pDCs, MØs, plasmablasts, activated T cells, NK cells or MOs^{127,164,178,189}. Even the later generated BM chimeric Zbtb46-DTR mouse model, which was believed to be more specific than the CD11c based ones, was still impaired by the observation that beside the cDC lineage cell some activated MOs were also depleted³⁰.

Another approach to achieve conditional cell depletion mouse models, is based on Cre-loxP system derived from P1 bacteriophage¹⁹⁰. Generally, these models are created by crossing two separately genetically manipulated mouse lines. One line is generated by knock-in a *Cre* gene into a specific locus of choice within the murine genome, thereby enabling the rodent cells to express this recombinase, which excises later any DNA sequence between two loxP sites¹⁹⁰⁻¹⁹². Typically, the Cre recombinase is placed under the control of a cell-specific promoter, which is active at the mature state of the cell or one of its progenitors, allowing the targeting of all later differentiated progeny¹²⁷. Similarly, the loxP sites need to be cloned into the genome of the second mouse line, thereby flanking a specific DNA sequence of interest.

Initially, this system was used to condition conventional gene knock-outs to specific cell population¹⁹³. This was achieved by cloning the *Cre* gene under the promoter of a cell population specific gene and to tag the gene for the actual cell depletion with the loxP sequences, which in turn ablate the desired cell population after the successful crossing. Typical examples for this strategy are *Irf4^{fl}* and *Notch2^{fl}* mouse models, to target the cDC2 population, and *IRF8^{fl}* for targeting cDC1^{167,194,195}.

Alternatively, such a cell depletion can be also made inducible, by crossing a Cre containing mouse line with any DTR containing mouse line, where the necessary constitutive DTR

expression is initially inhibited by the insertion of loxP sites tagged STOP cassette upstream of the transcriptional start side of the gene²³. With this strategy, mouse models like Clec9a-Cre, CD11c-Cre, XCR1-Cre, lysozyme M (LysM)-Cre, F4/80-Cre, CD64-Cre or CX3CR1-Cre, can be crossed with inducible DTR containing mouse lines to achieve DC, MO and M ϕ depletion, such as Rosa26-iDTR for instance resulting in Clec9a-Cre x Rosa26-iDTR mouse model allowing to target cDCs^{24,196-204}. However, also here the limited differential expression of most of the genes set boundaries for the specificity of such models, as demonstrated by the results obtained after crossing LysM-Cre with Rosa26-iDTR, which allowed depletion of 83-98% of the M ϕ s^{165,203}. However, also in this example the presence of LysM is not restricted to M ϕ s and can be also found in granulocytes and cDCs as well, supporting the notion that the pattern of one promoter activity is often insufficient to genetically define distinct cell populations¹⁹⁸. To further improve this inducible DT depending Cre-loxP strategy, DTR expression can be restricted to a certain cell population by placing not only *Cre*, but also the Cre-inducible *DTR* gene downstream of another cell specific promoter^{204,205}. Here, in contrast to the constitutive DTR expression before, now two specific promoter activities are required for cell depletion, which in turn can increase these mouse models specificity^{205,206}. Such inducible DTR-DT system for the investigations of cDCs or other MPS cell subsets after crossing with suitable *Cre* containing models can be provided from CX3CR1-iDTR or CD11c-iDTR^{205,206}. As an example, a study has generated CD11c-Cre x CX3CR1-iDTR mice, which demonstrated after DT treatment the specific deletion of small intestine CX3CR1^{hi} cells without affecting significantly cDC1 or CX3CR1^{lo} populations, even though all of these cells do express CD11c²⁰⁵. Finally, all these different approaches are strongly dependant on an accurate cell type-specific gene or transgene expression and the selection of the appropriate promoters^{127,207}. Nevertheless, all presented strategies to deplete a specific cell population are so far in most studies just the closest approximation to the final aim to investigate their unique functions in the body. To overcome this limitations strategic combination of targeting more than two highly specific genes in combination could be a future method of choice, like the proposed split Cre-system, which could expand the targeting of specific subpopulations of cells for a more precise investigation of their role during normal and pathogenic processes²⁰⁸.

1.5. Considerations to use CD64 gene as a selection marker for specific depletion of DCs

Leukocyte Fc receptor (FcRs) for IgG belong to the Ig superfamily^{209,210}. Up until now, four different classes of murine FcγRs have been described, in particular CD64, also known as a high affinity Fc receptor for IgG type I (FcγRI), CD32 (FcγRIIB), CD16 (FcγRIII) and CD16-2 (FcγRIV) based on the structural analysis. Moreover, FcγRs can be also divided functionally into the activating (CD64, CD16 and CD16-2) and inhibitory (CD32) receptors²⁰⁹⁻²¹¹. *CD64* is located in the *Mus musculus* genome at the reverse strand of 3rd chromosome, spanning the base pairs from 96,282,909 to 96,293,969 (Gene ID: 14129; ENS MUSG00000015947)²¹². The transcribed pre-RNA contains six exons and five introns. The sixth exon contains the stop codon, followed by the endogenous *CD64* poly(A) sequence. Moreover, the coding sequence for the extracellular part is located at the beginning of the *CD64* gene, while the coding sequence for the intracellular part is located at the end of the gene, upstream of poly(A) tail. Additionally, *CD64* messenger RNA (mRNA) has two spliced variants, Fcgr1-201 and Fcgr1-202, of which only the 2,589 base pair (bp) long Fcgr1-201 transcript is translated into the functional protein²¹³. The expressed murine CD64 is a 72-kDa integral membrane glycoprotein, which contains 404 amino acids, composed of a short signal peptide (23 amino acids) and the functionally important CD64 α chain²¹⁴. The CD64 α chain by itself is composed of an extracellular domain together with a membrane crossing helical domain and a cytoplasmic domain. Amongst them the extracellular domain is the biggest, composed of 273 amino acids, and contains three disulphide bonded extracellular Ig-like domains. The smaller cytoplasmic part contains 84 amino acids and the smallest helical domain is composed of 23 amino acids²¹⁵.

FcγRs are expressed on broad variety of immune cells, which makes them potentially attractive as selection markers for cell identification. Specifically, CD64 is highly expressed on murine MØ, MO and MO-derived cells, but are also expressed at low levels on cDCs^{210,216,217}. The CD64 expression level difference between moDCs and cDCs is so striking that several groups have proposed to use this marker for discrimination between moDCs and cDCs^{120,121}. Furthermore, CD64 has been recently established as a MO/MØ depletion selection marker in at last two independent CD64 based cell depletion mouse models^{186,200}. Interestingly, kidney tissue contains a bulk CLEC9A⁺ progenitor derived CD64 expressing population and recently

another CD64⁺ cDC population was identified in *Listeria monocytogenes* infected mice^{24,218}. Therefore, a closer investigation of the functions connected to such subpopulations becomes of paramount interest to understand the specific role of DCs and specifically CLEC9A⁺ progenitor derived CD64⁺ cells in detail. This implicate amongst others the generation of new more subpopulation specific depletion models, because the existing ones affect all CD64⁺ cells, which makes it impossible to conclude any specific function related to these unique populations^{186,200}.

Nevertheless, the use of the *CD64* gene to target specific cell populations for depletion bear the risk to induce a decrease in immune complex (IC)-induced inflammation, a reduction in antibody-dependent killing of pathogens by MØs and impaired protection from bacterial infection in the organism^{219,220}. As an example, *CD64*^{-/-} mice showed an impaired clearance of bacteria during *Bordetella Pertussis* infection²²⁰. Specifically, CD64 favourably interacts with IgG2a opsonised pathogens, forming IgG2a-IC, and induces IgG2a-IC phagocytosis. Moreover, the CD64 accessibility to IgG2a-IC is regulated by monomeric IgG2a, which occupies the CD64 recognition site²²¹. Later investigations, supported the assumption that the amount of CD64 bound monomeric IgG2a on the cell surface possibly influence the immune response to pathogens, because immunoglobulins lacking μ MT mice, treated with IgG2a, developed a IgG2a-induced systemic anaphylaxis²²⁰. Together, these data demonstrate that CD64 mediates IgG2a-IC induced effector functions on mononuclear cells²²⁰. Therefore, any approach to disrupt the expression of this receptor need to be avoided.

Furthermore, it needs to be taken under consideration, that the ligand binding CD64 alfa (α) chain interacts with the signal -transducing γ chain dimer, which contains two immune receptor tyrosine-based activation motifs (ITAMs)²¹¹. If this interaction is damaged, the extracellular signal is not further transmitted into the immune cell, where it normally triggers biological responses²¹⁰. In detail, ICs are recognised and bound by the Ig-like domains 1 and 2, which form an Ig-binding motif. The Ig-like domain 3 is not critical in this process, however it is important in determining the specific and high affinity interaction of CD64 with IgG2a²²². At last in human it has been shown, that the induced extracellular signal from the α chain is mediated by its transmembrane domain via the interaction with the γ chain, which is most likely the same for murine CD64²²³. It was demonstrated, that the cytoplasmic tail of CD64 does not have intrinsic enzymatic activity, but triggers immune cell activation, endocytosis

and phagocytosis^{224,225}. Additionally, the human and murine CD64 cytoplasmic tail was shown to be important in intracellular trafficking of receptor-antigen complexes^{226,227}. These data were further supported by the observation, that a serine residue of the cytoplasmic tail could be phosphorylated *in vitro* in response of phorbol-12-myristate-13-acetate (PMA) treatment in cell culture, leading to the conclusion of a possible involvement in signal transduction events after the binding of immune complexes²²⁸.

Taken together, following the strategy to use CD64 as a selection marker to target renal CD64⁺ cells for later depletion can be an efficient way to investigate the specific role of these cells in kidney immunity. However, due to the broad expression of CD64 on other immune cells, the specific depletion of such subpopulations needs in any case the usage of more sophisticated approaches, like the combination with an inducible depletion of the cells using DTR-DT system and an expression restriction using Cre-loxP system. Independent of the chosen depletion strategy the disruption of the *CD64* needs to be avoided in any case, to prevent any loss of function of the protein before cell depletion.

1.6. Genome engineering

Modern genomic engineering or gene editing offers the possibility of precisely manipulating genomic DNA (gDNA) of a living organism²²⁹⁻²³¹. The technique encompasses insertions, when foreign DNA is incorporated into the genome, deletions, when specific parts of the gDNA are removed, or replacements, when DNA sequences are removed from the genome and foreign DNA is inserted at the same time²³². The active engineering of living organisms at the drawing table, offers a huge potential for basic science, as well as for solving several medical needs or in the field of biotechnology. During the past decades genetic editing has been used for faster and easier generation of diverse genetic modified organisms and has become a promising tool for gene therapy²³²⁻²³⁸.

The implementation of most genomic engineering techniques is made possible by sequence-specific endonucleases, which create double-strand DNA breaks (DSBs) at the desired site of the genome, and is universally applicable to any cell type or organism that has DNA repair pathways^{236,239}. This is desired, because these controlled induced DSBs activates in turn the endogenous host DNA repair pathways, resulting in non-homologous end-joining (NHEJ) or

homologous recombination (HR) repair mechanisms²³². HR is a precise pathway, where a homologous sequence is utilized as a template for the repair of the DNA sequence at the break point^{240,241}. In contrast, NHEJ uses a variety of enzymes to directly join two DNA ends in DSB. However, NHEJ is error-prone and has been shown to cause mutations at the repair site, which consequently, can affect gene expression²⁴². Therefore, HR is the desired DNA repair pathway for generation of gene knock-in organisms or introduction of gene mutations in cell lines^{236,239,243,244}. However, the HR repair pathway is a more complex, slower process and mainly active in S and G2 cell cycle phases^{245,246}. Hence, it cannot be used for targeting post-mitotic cells such as neurons^{247,248}. However, the HR mechanism is not fully understood to date, making its use sometimes unpredictable. One of the most commonly accepted HR pathway models is based on the following steps. First, DSB activates HR and the DSB DNA ends are modified, by forming a 3'-OH single strand DNA (ssDNA) region^{249,250}. This ssDNA is covered by specific proteins forming a recombinase filament, which fuses into the homologous DNA molecule. This D-loop intermediate recruits the polymerase to extend the missing part of DSB ssDNA. Finally, the second DSB end is annealed to the extended D-loop forming a Holliday junction, which is later eliminated forming crossover or non-crossover products²⁴⁷. HR pathway uses donor DNA to restore lost information, as a template to repair the DSB²⁴⁷. This donor DNA can be a sister chromatid or foreign DNA, such as a plasmid containing a gene of interest or simply an oligonucleotide²⁴⁶. The aforementioned genetic changes can be introduced into gDNA during these repair mechanisms, with the prospect that these genetic modifications are later inherited by the daughter cells²⁵¹.

Due to the high interest and need of genome editing tools for various scientific and medical questions, several new editing technologies have been developed recent years, all with their own advantages and disadvantages^{236,239}. In general, DSB causing genome engineering reagents can be divided into the group of protein-DNA interaction driven nucleases, which includes meganucleases, zinc-finger nucleases (ZFNs) and transcription activator-like effector-based nucleases (TALENs)²⁵²⁻²⁵⁴. The second group of nucleases can be subdivided into the subgroup of RNA-guided nucleases, including the CRISPR/Cas9 system and targetrons^{255,256}. The other subgroup comprising DNA-based guided systems, includes peptide nucleic acids, triplex-forming oligonucleotides and structure guided endonucleases²³⁹.

Taken together, the discovery that various nucleases can be used as tools to precisely introduce changes at nearly any desired locus of the DNA of alive cell makes modern genome

editing tools highly attractive for generation of transgenic organisms as well as the investigation, prevention and treatment of various diseases.

1.6.1. CRISPR-Cas9 technology as genome engineering tool

Originally, the CRISPR/Cas systems was described to represent the adaptive immune system in prokaryotes by integrating short virus sequences in the CRISPR locus of the cell genome, allowing the cell to remember, recognize and remove the foreign genetic material²⁵⁷. Bacterial CRISPR/Cas systems, according to the phylogenetic analysis of the conserved Cas proteins, gene repertoires and arrangements in CRISPR-Cas loci, can be subdivided into the type I, II and III²⁵⁸. However, up to date the CRISPR/Cas system II from *Streptococcus pyogenes* provides the basic principle for CRISPR/Cas based genome editing^{257,259}. So far it is the best characterised system and based on a single multifunctional Cas9 protein, CRISPR RNA (crRNA) and trans-activating CRISPR RNA (tracrRNA). Cas digests the invaders DNA into short 20 bp long DNA fragments, which are incorporated into the bacterial CRISPR locus between short palindromic repeats, forming new protospacers²⁶⁰. This CRISPR locus is then transcribed into long precursor CRISPR RNA (pre-crRNA), for which maturation tracrRNAs are required. TracrRNAs recognise repeated sequences on pre-crRNA, hybridise with them resulting in a complex, which is recognised and cleaved by RNase III^{261,262}. Within the matured crRNA the protospacer, which is homologous to the targeted DNA is immediately followed by the protospacer adjacent motif (PAM) and serves as a guide for the Cas9 to bind and degrade the foreign DNA²⁶³. The recognised PAM sequence itself spans from 2 to 6 bp and is not conserved and depends on the species of the Cas9 protein²⁶⁴⁻²⁶⁶. Moreover, the PAM is an essential targeting component, not found in the bacteria genome and distinguishes host DNA from foreign DNA²⁶⁷. Additionally, it prevents the CRISPR locus from being targeted and destroyed by the nuclease. PAM is recognised by the Cas9 endonuclease, which creates than DSB 3 bp upstream of sequence²⁵⁹. The Cas9 protein itself is composed of two nuclease domains responsible for the cleavage of complementary and non-complementary DNA strand²⁶⁸. The CRISPR/Cas9 system as a gene editing tool has several advantages, it requires only few components and the protospacer sequence can be easily exchanged or adjusted to guide Cas9 to the desired locus. Moreover, the only limitation to recognize any desired sequence within a genome lies principally on the accessibility of a PAM sequence at the 3' end of the target

site^{268,269}. Consequently, the CRISPR/Cas based gene editing was quickly adopted by several groups and utilised for targeting various species and cell types²⁷⁰⁻²⁷³. Finally, the great efficiency as well as specificity in gene editing applications, promoted CRISPR system as the most popular method in targeted gene editing, specifically in the development of new transgenic animals.

1.6.2. CRISPR-Cas9 technology in transgenic mouse model generation

Up till now, most of the targeted genome editing based mouse models have been developed using embryonic stem cells (ESCs), whose role as the “gold standard” has been recently challenged by the CRISPR/Cas9 technology, mainly because this system has solved most of the limitations found in the ESC based methodologies^{232,274-276}. Aside the increased HR efficiency, the CRISPR/Cas technology can be applied to all mammalian cells and all required reagents are commercially available²⁷⁷. The generation of CRISPR/Cas based transgenic mouse models can be achieved using several delivery strategies. Common to all are Cas9, the guide RNA (gRNA) and a target vector with the desired DNA modification surrounded by homology arms to be delivered successfully *in vitro* into mouse pronuclear^{256,278,279}. Shortly after injection, the originating oocytes are implanted into pseudo-pregnant mice^{256,278,279}. In contrast to the ESCs strategy, the whole process is less time consuming. This is mainly justified by the fact, that manipulation with CRISPR/Cas9 does not require cell culture incubation before the injection, selection and validation step after injection of the target cells. This allows the performance of all essential steps within one day^{230,280,281}. Additionally, CRISPR/Cas9 technology permits double and triple-mutant generation simultaneously, drastically reducing the time and cost for three transgenic mouse line development via ESCs and subsequent breeding to obtain homozygote mice for desired mutations²⁸¹. Moreover, since the CRISPR/Cas system can be applied to all mouse lines, the mutation carrying founder mouse (FM) does not require any back breeding. However, the generated FM is mosaic and requires breeding for germline transmission²⁸⁰. Mice, with small genetic manipulations such as a single nucleotide exchange, can be even generated in not more than a month for subsequent investigations²⁸⁰. However, animals need to be first validated to exclude possible off-target effects and to confirm the correct targeting of the site, before they can be used for any experiment²⁸⁰.

In conclusion, CRISPR/Cas technology is an emerging genome editing tool, which has potential to replace completely the ESC-based transgenic animal development. Due to its versatile use, simplicity, robustness and efficiency this method greatly expands the opportunities to generate transgenic mouse models, like cell depletion models for basic and translational research.

2. Aims of the study

1. Develop a new strategy for the specific ablation of the CLEC9A⁺ progenitor derived CD64⁺ subpopulation by generating a new inducible DTR expression based mouse model.
2. Functionally validate the newly generated FM line by accessing DTR expression and cell depletion after DT treatment of CLEC9A⁺ progenitor derived CD64⁺ cells from Clec9a-Cre x CD64-LSL-2A-DTR mice *in vivo*.
3. Establish the cisplatin induced AKI model and assess the function of DCs in AKI by using Clec9a-Cre x Rosa26-iDTR and XCR1-DTR-Venus.

The results of this work will provide a new mouse model allowing to study the function of CLEC9A⁺ progenitor derived CD64⁺ cells by specific depletion of this subpopulation. Supplemented by cisplatin induced AKI based investigations, this offer a new tool to study DC functions not only during kidney steady state, but also under inflammatory conditions to understand better their role in modulating immune reactions. In a translational sense, understanding the role of renal CLEC9A⁺ progenitor derived CD64⁺ cells will help to gain a better understanding of the pathways underlying kidney inflammation and may help to develop an improved therapeutic strategy to treat kidney disease.

3. Materials and methods

3.1. Materials

3.1.1. Solutions

Table 1. Stock Solutions

Solution	Ingredients
Fluorescence-activated cell sorting (FACS) buffer	1X dulbecco's phosphate buffered saline (PBS) (Merck, Darmstadt, Germany) with 1% (v/v) fetal bovine serum (FBS) (Merck, Darmstadt, Germany), 0.02% (w/v) sodium azide (Merck, Darmstadt, Germany) and 2 mM ethylenediaminetetraacetic acid (EDTA) (pH 8) (Thermo Scientific Waltham MA, United States of America (USA))
Lysis buffer	0.1 M Tris(hydroxymethyl)aminomethane hydrochloride (Tris-HCl) (pH 8.0) (Merck, Darmstadt, Germany), 5 mM EDTA (pH 8.0), 0.2 M sodium chloride (NaCl) (Merck, Darmstadt, Germany) and 0.2% (w/v) sodium dodecyl sulfate (SDS) (Merck, Darmstadt, Germany)
1X Tris-EDTA (TE) buffer	10 mM Tris-HCl (pH 7.5), 1 mM EDTA (pH 8.0) in water
100% Percoll	90% (v/v) Percoll® (GE Healthcare Bio-Science, Piscataway, New Jersey, USA) and 10% (v/v) 10X phosphate-buffered saline
70% Percoll	70% (v/v) 100% Percoll in Hanks Balanced Salt Solution (HBSS) (Merck, Darmstadt, Germany)
37% Percoll	37% (v/v) 100% Percoll in 1X PBS
30% Percoll	30% (v/v) 100% Percoll in HBSS
Hydrolysis buffer	0.25 M hydrochloric acid (Merck, Darmstadt, Germany) in water
20X saline sodium citrate (SSC),pH7	3 M NaCl, 0.3 M trisodium citrate (Merck, Darmstadt, Germany) in water
Maleic acid buffer, pH 7.5	0.1 M maleic acid (Merck, Darmstadt, Germany) and 0.15 M NaCl in water
70% Ethanol	70% (v/v) ethanol (Merck, Darmstadt, Germany) in water
Wash buffer I	2X SSC and 0.1% (w/v) SDS in water
Wash buffer II	0.2X SSC and 0.1% (w/v) SDS in water
Wash buffer III	Maleic acid buffer with 3% (v/v) Tween® 20 (Merck, Darmstadt, Germany)
10X Phosphate-buffered saline	1.37 M NaCl, 27 mM potassium chloride (Merck, Darmstadt, Germany), 80 mM sodium phosphate dibasic (Merck, Darmstadt, Germany), 20 mM monopotassium phosphate (Merck, Darmstadt, Germany) in water
1X Tris-acetate-EDTA (TAE)	40 mM Tris-HCl, 20 mM acetic acid (Merck, Darmstadt, Germany), 1 mM EDTA in water
Toothpick lysis buffer	7% (w/v) Ficoll® PM 400 (Merck, Darmstadt, Germany), 0.5% (w/v) SDS, 5 mN sodium hydroxide (NaOH) (Merck, Darmstadt, Germany), 5 mM EDTA, 0.025% (w/v) bromphenol blue (Merck, Darmstadt, Germany) in water

Materials and Methods

Digestion solution	200 unit (U)/milliliter (ml) collagenase IV (Worthington Biochemical Corporation, Lakewood, New Jersey, USA), 0.2 milligram (mg)/ml DNase I (Roche, Basel, Switzerland) in Roswell park memorial institute (RPMI)-1640 medium (Merck, Darmstadt, Germany)
6X Loading buffer	14% (w/v) Ficoll® PM 400, 0.25% (w/v) bromphenol blue in water
Denaturation solution	1.5 M NaOH, 0.5 M NaCl in water
Neutralisation solution	1.5 M NaOH, 0.5 M Tris-HCl (pH 7.2), 10 mM EDTA in water
Detection buffer	0.1 M Tris-HCl (pH 9.5), 0.1 M NaOH in water
50% Glycerol solution	50% (v/v) glycerol (Merck, Darmstadt, Germany) in water
Microinjection solution	10 mM Tris-HCl, 0.1 mM EDTA, pH 7.5

3.1.2. Media

Table 2. Media

Solution	Ingredients
Lysogeny broth (LB)	0.17 M NaCl, 1% (w/v) tryptone, 0.5% (w/v) yeast extract in water
Luria agar plate	1.5% (w/v) agar (Roth, Karlsruhe, Germany) in lysogen broth

All solutions were sterilized by autoclavation.

3.1.3. Plasmids and bacterial artificial chromosome (BAC)

Table 3. Plasmid and BAC list

Plasmid	Sequence of interest	Source
Snap25-LSL-2A-green fluorescent protein (GFP)	LSL, woodchuck hepatitis virus posttranslational regulatory element (WPRE)	Addgene, Cambridge, Massachusetts, USA
RPCIB731E08452Q	<i>CD64</i> gene	Source BioScience, Nottingham, United Kingdom
195 FrtneokanaFrt DTA*	FrtneokanaFrt cassette	Research Department "Molecular Medicine", AG Moser, Max Planck Institute (MPI) of Biochemistry, Planegg-Martinsried, Germany
GCDL-2A-DTR*	2A-DTR	Department of Molecular Immunology, AG Garbi, Institute of Experimental Immunology, Bonn, Germany
pBlueScript® SK II (+)*	Backbone	Cardiovascular Physiology / Walter-Brendel Centrum, AG Brändli, Biomedical Center (BMC), Ludwig-Maximilians-Universität (LMU) Munich, Germany
pGem®-T Easy	Backbone	Promega, Madison, Wisconsin, USA

*the detailed plasmid sequences are provided in the Appendix

3.1.4. Antibodies

Table 4. Antibodies

AF488 - Alexa Fluor 488; **AF594** - Alexa Fluor 594; **AF647** - Alexa Fluor 647; **AF700** - Alexa Fluor 700; **APC** – Allophycocyanin; **BV421** - Brilliant™ Violet 421; **BV605** –Brilliant™ Violet 605; **BUV737** - Brilliant™ Ultraviolet 737; **BV785** - Brilliant™ Violet 785; **Cy5.5** - Cyanine-5.5; **Cy7** – Cyanine-7; **FITC** - Fluorescein isothiocyanate; **PB** – Pacific Blue; **PE** - Phycoerythrin; **PerCP** – peridinin-chlorophyll protein.

Antigen	Fluorophore	Clone	Catalogue number	Dilution factor	Provider
Biotin	PE	Non	405204	1:100	BioLegend, San Diego, California, USA
CD3epsilon (ε)	FITC	145-2C11	100306	1:100	BioLegend, San Diego, California, USA
CD3ε	PB	145-2C11	100334	1:100	BioLegend, San Diego, California, USA
CD3ε	PE	145-2C11	553063	1:100	BD Biosciences, San Jose, California, USA
CD4	PB	RM4-5	100531	1:400	BioLegend, San Diego, California, USA
CD8a	PB	53-6.7	100725	1:800	BioLegend, San Diego, California, USA
CD8a	BV605	53-6.7	100744	1:200	BioLegend, San Diego, California, USA
CD11b	APC/Cy7	M1/70	101226	1:200	BioLegend, San Diego, California, USA
CD11b	BUV737	M1/70	564443	1:800	BD Biosciences, San Jose, California, USA
CD11c	AF488	N418	117313	1:200	BioLegend, San Diego, California, USA
CD11c	AF647	N418	117314	1:200	BioLegend, San Diego, California, USA
CD11c	APC/Cy7	N418	117324	1:200	BioLegend, San Diego, California, USA
CD11c	BV785	N418	117335	1:200	BioLegend, San Diego, California, USA
CD11c	PerCP/Cy5.5	N418	117328	1 :200	BioLegend, San Diego, California, USA
CD16/CD32 (2.4G2)	Non	2.4G2	553142	1:50	BD Biosciences, San Jose, California, USA
CD16/CD32 (2.4G2)	Non	2.4G2	40-0161-M001	1:200	Tonbo bioscience, San Diego, California, USA
CD24	BV605	M1/69	101827	1:200	BioLegend, San Diego, California, USA
CD43	PE/Cy7	1B11	121218	1:300	BioLegend, San Diego, California, USA
CD45.2	AF700	104	109822	1:200	BioLegend, San Diego, California, USA
CD45.2	FITC	104	109806	1:200	BioLegend, San Diego, California, USA
CD45.2	PE/Cy7	104	109830	1:200	BioLegend, San Diego, California, USA
CD45R/B220	AF594	RA3-6B2	103254	1:200	BioLegend, San Diego, California, USA
CD45R/B220	PB	RA3-6B2	103227	1:400	BioLegend, San Diego, California, USA
CD64	APC	X54-5/7.1	139306	1:100	BioLegend, San Diego, California, USA
CD64	PE	X54-5/7.1	139304	1:100	BioLegend, San Diego, California, USA
CD64	PE/Cy7	X54-5/7.1	139314	1:100	BioLegend, San Diego, California, USA
CD115	BV605	AFS98	135517	1:200	BioLegend, San Diego, California, USA
CD117	APC/Cy7	2B8	105826	1:300	BioLegend, San Diego, California, USA
CD135	APC	A2F10	135310	1:200	BioLegend, San Diego, California, USA
CD161c/NK1.1	PB	PK136	108722	1:100	BioLegend, San Diego, California, USA
CD172a	PerCP/Cy5.5	P84	144009	1:300	BioLegend, San Diego, California, USA
F4/80	AF647	BM8	123122	1:100	BioLegend, San Diego, California, USA
F4/80	AF700	BM8	123130	1:100	BioLegend, San Diego, California, USA
F4/80	BV785	BM8	123141	1:100	BioLegend, San Diego, California, USA

Materials and Methods

HB-EGF	Biotin	polyclonal	BAF259	1:100	R&D Systems, Minneapolis, Minnesota, USA
MHCII	AF700	M5/114.1 5.2	107622	1:300	BioLegend, San Diego, California, USA
MHCII	PB	M5/114.1 5.2	107620	1:200	BioLegend, San Diego, California, USA
Isotype	PE/Cy7	MOPC-21	400125	1:100	BioLegend, San Diego, California, USA
Isotype	APC	MOPC-21	400119	1:100	BioLegend, San Diego, California, USA
Ly-6C	AF488	HK1.4	128022	1:200	BioLegend, San Diego, California, USA
Ly-6C	BV605	HK1.5	128036	1:200	BioLegend, San Diego, California, USA
Ly-6C	PerCP/Cy5.5	HK1.4	128012	1:200	BioLegend, San Diego, California, USA
Ly-6G	APC	1A8	127614	1:200	BioLegend, San Diego, California, USA
Ly-6G	PerCP/Cy5.5	1A8	127616	1:200	BioLegend, San Diego, California, USA
TER-119	PB	TER-119	116232	1:100	BioLegend, San Diego, California, USA
XCR1	BV421	ZET	148216	1:100	BioLegend, San Diego, California, USA

3.1.5. Oligonucleotides

All DNA oligonucleotides were purchased from Eurofins Genomics (Ebersberg, Germany). If not indicated in the text for specific primer combinations, the stated below melting temperature (T_m) was used for all experiments in this work.

Table 5. DNA oligonucleotides for genotyping

Primer	Sequence
BS49	5' –AAA AGT TCC ACT TTC TGG ATG ATG A-3'
BS47	5' –GGC TCT CTC CCC AGC ATC CAC A-3'
A65	5' –TCA CTT ACT CCT CCA TGC TGA CG-3'
Rosa 1	5' –AAA GTC GCT CTG AGT TGT TAT-3'
Rosa 3	5' –GGA GCG GGA GAA ATG GAT ATG-3'
oIMR4982	5' –AAG ACC GCG AAG AGT TTG TC-3'
iDTR-R BBO 0164	5' –AAT AGG AAC TTC GTC GAG C-3'
mouse XCR1-a	5' –CTA TCT TAA GAT TTC TCA GGG CCA GTC TAC-3'
mouse XCR1-b	5' –CAG GAC AAT GGT AGA GAT GGT GGA AAA G-3'
mouse XCR1-c	5' –CTG CAG CCA GAA AGA GCT TCA G-3'
CD64.3	5' –TCA GGG TCA ACT TTG GGA AG-3'
CD64.4	5' –CCA AAT GTA ACT TGG CTG GGT C-3'
CD64.5	5' –GGT ACT CTG TTC TCA CCC TTC-3'

Table 6. DNA oligonucleotides for Southern blot probe amplification

Primer	Sequence	T_m (Celsius (°C))
Neo1	5' –AAT ATC ACG GGT AGC CAA CG-3'	59
Neo2	5' –CAT TGA ACA AGA TGG ATT GCA CGC-3'	
Probe1.1	5' –ACT TCG CCC CAA AGT CCT AT-3'	58
Probe1.2	5' –TCT CGC TTA CTT GAG CAG CA-3'	

Materials and Methods

Table 7. DNA oligonucleotides for Gibson Assembly

Primer	Sequence	T _m (°C)
BL1 Fwd	5' –GGG CGA ATT GGG TAC CTG AAC CCC TTC CTC CCA GTG ACA GTA CTG GGG CAC AAA CTT CCC AAA GTA TAA CTT CGT ATA ATG TAT GCT ATA CGA AG-3'	63
Block1 Rev	5' –GCT CCG GAC GGT GCT CCA GAA CCT CT-3'	
DTR Fwd	5' –GAG CAC CGT CCG GAG CCA CGA ACT TC-3'	63
D Rev	5' –AGG GGG GGC CCG GTA CGT GGG AAT TAG TCA TGC CC-3'	
WPRE Fwd	5' –GTA CCG GGC CCC CCC GAA ATC ACG TGA GCT TAT C-3'	57.4
WPRE Rev	5' –TTG CGG CCA TCT ATG CCA AGC TTT TAC-3'	
F-Neo-F Fwd	5' –GGC ATA GAT GGC CGC AAG CTT GAT ATC-3'	
F-Neo-F Rev	5' –TCG ATA CCG TCG ACC TAT ATT TGC TTT ATT TAA GAG TTG CAT GCC ATG GTC CCA CAG TTT CAG GGC CTG ACT GAT GAA GTT CC-3'	60.2

Table 8. DNA oligonucleotides for PCR amplification

Primer	Sequence	T _m (°C)
Res_HOM1 Fwd	5' –ATG GCG GCC GCA GAC AGA CAT GCA GGC AAA A-3'	59
Res_HOM1 Rev	5' –CAT GTC GAC CCA GGA TAA CCC CTG TCC TT-3'	
Res_HOM2 Fwd	5' –ATG GTC GAC AAG GCA GGA AAT AGT GTA GCC-3'	58
Res_HOM2 Rev	5' –CAT CTC GAG CTG ATG CTG TCT GCT GTG TTC-3'	
DTR_Const Fwd	5' –CTG AAC CCC TTC CTC-3'	59
DTR_Const Rev	5' –TAT ATT TGC TTT ATT TAA GAG TTG CAT GC-3'	
CD64.1	5' –ACA AAG ATG TCC CCT TGC AC-3'	59
CD64.2	5' –CAA CAG GTG CTG GCA AGT AA-3'	59
CD64.6	5' –ACC CTC CAA AAA CCA AAT CC-3'	60

Table 9. DNA oligonucleotides for sequencing

Primer	Sequence
SeqPrimer1	5' –AGG GTT TTC CCA GTC ACG ACG TT-3'
SeqPrimer2	5' –GAA CTG CAG CCA GAA AGA GC-3'
SeqPrimer3	5' –TCA CGG GCT AAG AGA GGT TC-3'
SeqPrimer4	5' –GGG CTG CAG GAA TTC GAT A-3'
SeqPrimer5	5' –GGA AGT GTG GCC TTG TTG G-3'
SeqPrimer6	5' –GGC AGC TGT GAA TGG GAA G-3'
SeqPrimer7	5' –ACG GTA GGA AGG AGA GCA CA-3'
SeqPrimer8	5' –CAA GAC TCT GGC AGG GAA AA-3'
SeqPrimer9	5' –TGG GGC TTC TCA TGT TTA GG-3'
SeqPrimer10	5' –GCA CTG ACA ATT CCG TGG TGT-3'
SeqPrimer11	5' –GAG TTT ACG TCC AGC CAA GC-3'
SeqPrimer12	5' –CTT TGC TCC TTC GCT TTC TG-3'
SeqPrimer13	5' –TGC TCC TGC CGA GAA AGT AT-3'
SeqPrimer14	5' –CCC GGT ACG TGG GAA TTA G-3'
SeqPrimer15	5' –AAA GGG AGA TCC GAC TCG TCT G-3'
SeqPrimer16	5' –ATG TGG AATGTG TGC GAG GC-3'
SeqPrimer17	5' –GAT TAA TTG TCA ACA GGC TGC-3'
SeqPrimer18	5' –TCT TCG TCC AGA TCA TCC TG-3'
SeqPrimer19	5' –AGC CAC TGC ACC CTT CTA AA-3'
SeqPrimer20	5' –TTA ATC TGG GCC ACA CCT TC-3'
SeqPrimer21	5' –AGG GCA TGC AGA CAC AGA C-3'
SeqPrimer22	5' –GAC CAG GCT TTG AGG TTT CA-3'
SeqPrimer23	5' –GTG AGA TTC CTG CCC AGA AG-3'
SeqPrimer24	5' –TCG CCT TCT TGA CGA GTT CT-3'
SeqPrimer25	5' –GAC TGG GGA CCT GAA ACA GA-3'

Materials and Methods

SeqPrimer26	5' –TTT TGT CCT GCA TCC CTC TC-3'
SeqPrimer27	5' –TGA GTT CCT GTC CTG ACT TCC-3'
SeqPrimer28	5' –TTG GGG TGG CTA CTA ACC TG-3'
SeqPrimer29	5' –TGA GAC TCC CTC CCC TTT CT-3'
SeqPrimer30	5' –TGA GTC ACA GCG GCA TCT AC-3'
SeqPrimer31	5' –CGT GGA TGC TTT TGT AGT GG-3'
SeqPrimer32	5' –CAA GGT CAC CAG GAA CGT CT-3'
SeqPrimer33	5' –TCT CAG GGC TCA GAA GTT GG-3'
SeqPrimer34	5' –GCA TGA CAG AGG ACA GAA AGC-3'
SeqPrimer35	5' –ACA GCA AGA ACA GCC ATT CC-3'
SeqPrimer36	5' –AGT GGG AGG AAT GAG CTG G-3'
SeqPrimer37	5' –ATG TGT CCG TGT GTC GAA TG-3'
SeqPrimer38	5' –CAT ACG CTT GAT CCG GCT AC-3'
SeqPrimer39	5' –TCA CTC ACA ACC ACC CGT AA-3'
SeqPrimer40	5' –GCT TCA TTT TCT CGG TCC TG-3'
SeqPrimer41	5' –GAT GAT TTT GGC TCC CAT CT-3'
SeqPrimer42	5' –AGT CTA CGA GTT GTC AGT TTG A-3'
SeqPrimer44	5' –TGT AAA ACG ACG GCC AGT-3'
SeqPrimer45	5' –CAG GAA ACA GCT ATG ACC-3'
M13 rev (-49)	5' –CAG GAA ACA GCT ATG ACC-3'
T3	5'-AAT TAA CCC TCA CTA AAG GG-3'

3.1.6. Mouse strains

Table 10. Mouse strains

Mouse strain	Genetic modification	Background	Origin	Genotyping
Clec9a-Cre	<i>Cre</i> recombinase gene knock-in into <i>Clec9a</i> locus; Genetic defect in the <i>Clec9a</i> locus;	C57BL/6	²⁴	Primers: BS49, BS47, A65 T _m = 60 °C Wild type PCR: 407 bp Mutated PCR: 597 bp
Rosa26-iDTR	<i>DTR</i> gene knock-in into <i>Rosa26</i> locus; Genetic defect in the and <i>Rosa26</i> locus;	C57BL/6	²⁰³	Primers: Rosa1, Rosa3, iDTR BB00164 T _m = 61 °C Wild type PCR: 600 bp Mutated PCR: 845 bp
XCR1-DTR-Venus	<i>DTR-Venus</i> knock-in into <i>XCR1</i> locus; Genetic defect in <i>XCR1</i> locus;	C57BL/6	Institute for Immunology, AG Krug. BMC Munich Planegg-Martinsried, Germany; ¹⁸⁵	Primers: XCR1-a, XCR1-b, XCR1-c T _m = 62 °C Wild type PCR: 450 bp Mutated PCR: 450 bp
Rosa26-inducible enhanced yellow fluorescent protein (iEYFP)	<i>EYFP</i> gene knock-in into <i>Rosa26</i> locus; Genetic defect in the <i>Rosa26</i> locus;	C57BL/6	²⁸²	Primers: Rosa1, Rosa3, oIMR4982 T _m = 60 °C Wild type PCR: 320 bp Mutated PCR: 600 bp
CD64-LSL-2A-DTR	<i>LSL-2A-DTR-WPRE-Frt-flanked neomycin resistance cassette (Neo)</i>	C57BL/6	Made in this work	Primers: CD64.3, CD64.4, CD64.5 T _m = 60 °C Wild type PCR: 407 bp

Materials and Methods

	knock-in into CD64 locus;			Mutated PCR: 561 bp
C57BL/6	<i>Non</i>	C57BL/6	Charles River, Wilmington, Massachusetts, USA	Non

3.1.7. Bacterial strains

Table 11. Bacterial strains

Bacterial strain	Genotype	Origin
JM109	<i>recA1, endA1, gyrA96, thi, hsdR17</i> (<i>r_k-</i> , <i>m_k+</i>), <i>relA1, supE44, Δ(lac-proAB)</i> , [F', <i>traD36, proAB, lacI^qΔM15</i>]	Promega, Madison, Wisconsin, USA
MAX Efficiency[®] Stbl2[™]	F, <i>mcrA, Δ(mcrBC-hsdRMS-mrr), recA1, endA1lon, gyrA96, thi, supE44, relA1, λ⁻, Δ(lac-proAB)</i>	Thermo Scientific, Waltham, Massachusetts, USA
One Shot[®] TOP10	F, <i>mcrA, Δ(mrr-hsdRMS-mcrBC), φ80lacZΔM15, ΔlacX74, recA1, araD139, Δ(ara-leu)7697, galU, galK, rpsL, (Str^R), endA1, nupG, λ⁻</i>	Thermo Scientific, Waltham, Massachusetts, USA
EL350	DY380 [(<i>cro-bioA</i>) <> <i>araC-PBADcre</i>]	Research Department "Molecular Medicine", AG Moser, MPI of Biochemistry, Plannegg-Martinsried, Germany

3.1.8. Analysis Software

Table 12. Software used in the study

Analysis Software	Source
BD FACSDiva[™]	BD Biosciences, Franklin Lakes, New Jersey, USA
FlowJo[™] 10	FlowJo LLC, Ashland, Oregon, USA
GraphPad Prism 6	GraphPad Software Inc., La Jolla, California, USA
DNASTAR	DNASTAR, Madison, Wisconsin, USA

3.2. Methods

3.2.1. Molecular biology methods

3.2.1.1. Absorbance based nucleic acid quantification and agarose gel electrophoresis

DNA concentrations were measured using a NanoDrop 2000 Spectrophotometer (Thermo Scientific, Waltham, Massachusetts, USA) and the purity of the DNA was determined by the ratio of absorbance at 260 nanometre (nm) to 280 nm or 230 nm. Only samples showing a higher ratio than 1.8 (260/280) and 2.0 (260/230) were used for subsequent applications.

Linear DNA fragments were separated on agarose gels. Based on the DNA fragment size an agarose content (Thermo Scientific, Waltham, Massachusetts, USA) ranging from 0.8 - 1.5% (w/v) was used and visualized by the addition of Midori Green Direct dye (Biozym, Hessisch Oldendorf, Germany). In detail, a solution, containing the desired amount of agarose, was prepared with TAE buffer and heated up using a microwave until the agarose was dissolved completely. Next, Midori Green Direct was added directly to the cooled down solution or the solidified agarose gel was post-stained for 30 minutes (min) in the TAE buffer containing Midori Green Direct, with gentle shaking. Prior electrophoresis DNA samples were mixed with 6X DNA loading buffer (Thermo Scientific, Waltham, Massachusetts, USA; New England BioLabs, Ipswich, Massachusetts, USA) and loaded into prepared wells. Electrophoresis was carried out in 1X TAE buffer. Depending on fragment size, the procedure was carried out at 120 volts (V) or 90 V, until the separation of the individual bands was sufficient. Bands size was determined by adding appropriate DNA molecular weight standards to each gel (Gene ruler 1 kilobase (kb) DNA Ladder, GeneRuler 100 bp Plus DNA Ladder or TrackIt™ 1 kb Plus DNA Ladder (Thermo Scientific, Waltham, Massachusetts, USA), Quick-Load Purple 1 kb DNA Ladder (New England, BioLabs, Ipswich, Massachusetts, USA)). After electrophoresis, gel was visualized and pictures were made using UV-transilluminator (Intas, Göttingen, Germany) or Gel Doc™ XR+ Gel Documentation System (Bio Rad, Hercules, California, USA).

3.2.1.2. PCRs

To amplify DNA fragments by PCR for subsequent cloning experiments or sequencing reactions Q5[®] Hot Start High-Fidelity DNA Polymerase (New England BioLabs, Ipswich, Massachusetts, USA) or GoTaq[®] Long PCR Master Mix (Promega, Madison, Wisconsin, USA) were used according to the manufactures' instructions. For PCR reactions, which did not require the use of high fidelity polymerase, like bacterial colony screening or genotyping PCRs, A-tailing GoTaq[®] G2 Hot Start Polymerase (Promega, Madison, Wisconsin, USA) was used. All PCR reactions were performed using T-Advance Thermocycler or FlexCycler² Thermocycler (Biometra, Göttingen, Germany) with deoxyribonucleotide triphosphates (dNTPs) from Roche (Basel, Switzerland) according to the manufacturer's protocols for each polymerase with some modifications. For colony screening PCR, individual bacterial clones were picked with a plastic tip and directly placed into 30 microliter (µl) LB for up to 5 min and 2.5 µl of the obtained cell suspension was used for each amplification. In case of genotyping PCR, 1 µl of gDNA solution isolated from ear or toe biopsy tissues was used by default. Just for adenosine (A)-tailing, the individual amount of DNA used for the reaction was calculated at all times based on the required amount of insert for the optimal ratio between insert and vector backbone and incubated in a one-step reaction for 20 min at 72 °C using only deoxyadenosine triphosphates (dATPs). All PCR products were analysed using agarose gel electrophoresis using 1.5% agarose gels.

3.2.1.3. Primer design

Primers, used in sequencing and PCR reactions, were designed using the free available online program Primer3 Input (version 0.4.0) (<http://bioinfo.ut.ee/primer3-0.4.0/>). To standardize the PCR conditions, the optimal temperature was always set at 60 °C with a minimum at 57 °C and maximum at 63 °C values. Primer size was chosen to be 20 nucleotide (nt) with a minimum and maximum length of 18 nt to 27 nt. In case of the amplification of PCR fragments, which were later used for cloning, the primers sequences were generated in the same way by Primer3 Input and the appropriate restriction enzyme recognition sites were placed at the 5'-ends of forward and reverse primers, respectively.

Longer PCR primers (27-95 nt in size), which were used in Gibson Assembly cloning, were generated using New England BioLabs online tool (<http://nebuilder.neb.com/>). Different DNA sequences were supplied to the program for assembling primers with a minimal length of 18 nt and minimal overlap between the fragments 15 bp.

3.2.1.4. Restriction digestion and dephosphorylation of DNA

All restriction endonucleases were purchased from New England BioLabs (Ipswich, Massachusetts, USA). Depending on the experimental requirements, different amounts of DNA was digested in 20 µl, 50 µl or 500 µl volume using 20 U of enzyme per 1 microgram (µg) of DNA. Restriction digestion reactions were carried out for 2 h, 5 h or overnight at the recommended temperature by the supplier for each restriction enzyme in the Innova® incubator (Eppendorf, Hamburg, Germany).

For dephosphorylation of all restriction digested DNA the alkaline phosphatase calf intestinal (CIP) (New England BioLabs, Ipswich, Massachusetts, USA) was used in a 40 µl reaction mix, composed of 10 U CIP, 1X CutSmart buffer and restriction digested DNA. Reaction mix was incubated for 1 h at 37 °C in the Innova® incubator.

3.2.1.5. Ligation of DNA fragments using Quick Ligation™ Kit, Gibson Assembly® Master Mix Kit or pGEM®-T Easy Vector System

To ligate restriction digested DNA the Quick Ligation™ Kit (New England BioLabs, Ipswich, Massachusetts, USA) was used and procedure was carried out according to the manufacturer's instructions. Different ratios of linearized vector and DNA fragments were used, whereby the necessary amounts of DNA fragments were calculated using New England BioLab online calculator (<https://nebiocalculator.neb.com/#!/ligation>).

Gibson Assembly® Master Mix Kit (New England BioLabs, Ipswich, Massachusetts, USA) was used to assemble the fragments previously amplified using long primers with Q5® Hot Start High-Fidelity DNA Polymerase (New England BioLabs, Ipswich, Massachusetts, USA). Briefly, 1.25 µl of DNA mixture, containing vector and DNA fragments, was mixed with 1.25 µl Gibson Assembly Master Mix (2X). Reaction was carried out at 50 °C for 1 h using T-Advance

Thermocycler or FlexCycler² Thermocycler. The ratios between vector and DNA fragments as well as their amounts were calculated using online available NEBuilder Assembly tool (<http://nebuilder.neb.com/>) and online calculator (<https://nebiocalculator.neb.com/#!/ligation>).

The reaction mixture for pGEM[®]-T Easy Vector System (Promega, Madison, Wisconsin, USA) was prepared according to the manufacturer's protocol. Ratio between PCR product and vector was used 1:3 and the individual amounts were calculated using online calculator (<https://nebiocalculator.neb.com/#!/ligation>).

After incubation all ligation mixtures were placed at -20 °C or used immediately for transformation with competent bacteria.

3.2.1.6. Measurement of bacterial cultures by optical density (OD) and bacterial glycerol stock preparation

Cell density was measured using the Ultrospec10 (GE Healthcare Life Science, Massachusetts, USA). The OD around 0.6 was considered as an optimal cell density for further applications, representing bacteria growth in log phase.

To prepare glycerol stock from bacterial cultures, 500 µl of an overnight cell culture was transferred into cryovial and filled up with 500 µl of 50% glycerol solution (Merck, Darmstadt, Germany). The tube was shaken several times to mix the solutions, snap frozen on dry ice for 5 min and stored at -80 °C. Bacteria were recovered by placing the tip directly into LB media, supplemented with proper antibiotic after scraping the top of a glycerol stock with the tip. Inoculated LB was placed into incubator adjusted to the optimal bacterial growing temperature.

3.2.1.7. Transformation of bacteria by heat shock and electroporation

In this work, different high-efficiency competent cells for transformation were used: JM109 Competent cells, MAX Efficiency[®] Stbl2[™] Competent Cells, EL350 and One Shot[™] TOP10 Chemically Competent Cells.

For transformation using heat shock 1 μl of Gibson Assembly reaction mix, 2 μl of pGEM[®]-T Easy Vector System (Promega, Madison, Wisconsin, USA) reaction mix or 3-5 μl of Quick Ligation reaction mix after ligation was used to transform 25 μl of bacterial suspension. In detail, competent bacteria were placed into round bottom 2 ml Eppendorf tube, DNA was added directly to the bacterial suspension and the tube was gently swirled. This mixture was incubated for 20-30 min on ice followed by a 30 seconds (s) heat-shock at 42 °C in the water bath (Memmert, Schwabach, Germany). After this treatment, the tube was placed back on ice for 2 min. Next, 250-900 μl of LB was added to the cells and the tubes were incubated on a bacterial shaker with 150 revolutions per minute (rpm) for 1 h at the specific recommended temperature: 37 °C for JM109 and One Shot[™] TOP10 and 30 °C for Stbl2 cells. Subsequently, cells were centrifuged for 30 s at 13000 rpm using a table centrifuge (Eppendorf, Hamburg, Germany) and the supernatant was removed except for approximately 100 μl , which was used to re-suspend the bacterial pellet.

Transformation using electroporation was specifically used to introduce plasmid DNA into EL350 cells. For this purpose, 1 ml of the overnight cell culture was used to inoculate 50 ml fresh media. The flask, containing freshly inoculated media, was placed back into bacterial incubator and shook with 150 rpm at 32 °C. During this process, the bacterial density was measured several times until OD was around 0.6. Then the flask was placed into an ice water bath to cool down and cells were transferred into a pre-chilled 50 ml conical tube and centrifuged for 5 min at 4200 rpm and 0 °C in a Heraeus Multifuge X3R Centrifuge (Thermo Scientific, Waltham, MA, USA). The supernatant was removed completely and the residual cell pellet was first re-suspended in 1 ml ice cold sterile water and filled to a final volume of 10 ml. Cells were centrifuged as described above and the procedure was repeated two more times to remove the remaining medium. After that, cells were re-suspended in 1 ml sterile ice-cold water and transferred into a pre-chilled 2 ml Eppendorf tube. Cells were centrifuged for 30 s 12700 rpm at 4 °C, the supernatant was removed completely and the cells were re-suspended in 250 μl ice-cold sterile water. In a next step, the re-suspended cells were split into 5 pre-chilled 2 ml Eppendorf tubes and 1 μl of the DNA solution (150 ng- 1 μg) was added to each tube. Suspension was mixed gently tapping the tube and transferred each into a pre-chilled 1 mm cuvette, which was placed into Eporator[®] (Eppendorf, Hamburg, Germany). The specific electroporation parameters were 1750 V, 200 ohms (Ω), 25 farads (F). After

electroporation 1 ml LB was added to the cells and transferred into 2 ml Eppendorf tube. Cells were incubated for 1 h at 32 °C with horizontal shaking at 150 rpm. Then bacteria were centrifuged for 30 s 12700 rpm, most of the supernatant removed, and bacteria re-suspended remaining left over media.

In both methods the re-suspended bacterial cells were seeded after transformation on pre-warmed Luria agar plates with the appropriate antibiotic, ampicillin (100 µg/ml), chloramphenicol (25 µg/ml or 12.5 µg/ml) or kanamycin (50 µg/ml) (Merck, Darmstadt, Germany). Plates with JM109 competent cells were incubated at 37 °C and plates with MAX Efficiency® Stbl2™ competent cells were incubated at 30 °C for 16-24 h, respectively. Plates with One Shot™ TOP10 chemically competent cells were placed into bacterial incubator at 32 °C for 24-36 h.

3.2.1.8. Isolation of gDNA from mouse biopsies

Fresh tissue material was taken from mice at the age of 4-5 weeks by animal care takers. Tissue material was placed directly into 500 µl Lysis buffer, containing 0.2 mg/ml Proteinase K (Merck, Darmstadt, Germany). Digestion was carried on overnight at 56 °C in a ThermoMixer C (Eppendorf, Hamburg, Germany) at 300 rpm. To remove undigested material, samples were centrifuged at 12700 rpm for 10 min at room temperature in a 5427R centrifuge (Eppendorf, Hamburg, Germany). The DNA containing supernatant was transferred into fresh tubes. Depending on the DNA purity requirements, DNA was extracted from the Lysis buffer according phenol/chloroform method or precipitated with isopropanol.

For genotyping gDNA was precipitated from supernatant by adding 500 µl 2-propanol (Merck, Darmstadt, Germany) and inverting the tubes several times. The precipitated gDNA was spun down at 12700 rpm for 10 min at room temperature using a 5427R centrifuge. The obtained gDNA pellets were washed with 500 µl 70% ethanol, air dried at room temperature and dissolved in 100 µl TE buffer.

For Southern blot applications gDNA was extracted using the phenol/chloroform method. In detail, the gDNA containing lysate was mixed with equal volumes phenol:chloroform:isoamyl alcohol (25:24:1, v/v/v) (Merck, Darmstadt, Germany). Both solutions were mixed by shaking the tube for 10 s following centrifugation at 12700 rpm for 10 min at room temperature. The

tubes were carefully taken out without destroying the two formed phases. Then the top layer, referred as aqueous phase, was transferred to a fresh tube, mixed with an equal volume of chloroform (Merck, Darmstadt, Germany) and centrifuged again at 12700 rpm for 10 min at room temperature. From the two formed phases, the top layer (aqueous phase), was carefully collected. 3 M pH 5.2 sodium acetate (Merck, Darmstadt, Germany) to reach 10% (v/v) in the solution and 2 volumes of 99.8% ethanol (Merck, Darmstadt, Germany) were added to the aqueous phase and mixed. The obtained solution was kept on dry ice for 30 min and centrifuged at 12700 rpm for 30 min at room temperature in a 5427R centrifuge. The precipitated gDNA pellet was washed once with 500 μ l 70% ethanol, air dried and dissolved in 10-100 μ l 1X Loading Buffer or TE buffer.

3.2.1.9. Plasmid and DNA fragment purification

Depending on the individual needs, the following commercial plasmid DNA purification kits were used according to the manufacturer's instructions: QIAprep Spin Miniprep Kit and HiSpeed Plasmid Maxi Kit (Qiagen, Hilden, Germany). Typical elution volumes were 30 μ l for Miniprep isolations and 1 ml for Maxi Kit isolations. Plasmids were diluted in the water or TE buffer.

If necessary DNA fragments, from PCR reaction and restriction digestions ranging from 40-50 bp, were separated on agarose gels and cut out with a clean scalpel and extracted using QIAEX[®] Gel Extraction Kit (Qiagen, Hilden, Germany). All steps were carried out according to the manufacturer's protocol and the obtained DNA was diluted in 20 μ l DNase free water or TE buffer.

DNA fragments ranging from 100-10 bp, obtained from PCR and other enzymatic reactions, were purified using QIAquick PCR Purification Kit (Qiagen, Hilden, Germany). The procedure was done according to the manufacturer's instructions. All centrifugation steps were carried out on a 5427R centrifuge. Briefly, 5 volumes of Buffer PB was mixed with 1 volume of sample and applied on QIAquick spin column and centrifuged at 12700 rpm 30 s. After centrifugation, the column was washed with 0.75 ml Buffer PE, centrifuged at 12700 rpm for 1 min, followed by an additional centrifugation step at 12700 rpm, to remove residual liquid. The DNA was eluted in 30 μ l DNase free water, elution buffer or TE buffer.

3.2.1.10. BAC isolation

BAC was isolated from overnight bacterial culture using reagents from HiSpeed Plasmid Maxi Kit (Qiagen, Hilden, Germany) with some specific adjustments to the supplied standard protocol. First, an overnight cell culture was transferred into 50 ml conical tubes and centrifuged for 5 min at 4200 rpm at 4 °C in Heraeus Multifuge X3R Centrifuge. Supernatant was discarded, the cell pellet was re-suspended in 0.3 ml P1 solution and transferred to 2 ml fresh Eppendorf tube. Next, the tube was incubated for 5 min on ice and 0.3 ml P2 solution was added very slowly to cell lysate. The tube was gently inverted several times to mix solutions and left at room temperature for 5 min. Following, ice cold 0.3 ml P3 solution was added very slowly and the tube was gently inverted several times, until solutions were mixed. The cell lysate was further incubated for 15 min on ice with gently rocking on the ROCKER 2D digital (IKA, Staufen, Germany). Next, the lysate was centrifuged at 12700 rpm for 10 min at 4 °C in 5427R centrifuge. After centrifugation, the clear supernatant was transferred into new 1.5 ml Eppendorf tube and ice cold 0.8 ml 2-propanol was added. The tube was inverted several times and placed on ice for 5 min, following centrifugation for 15 min at 4 °C at 12700 rpm. The supernatant was removed and 0.5 ml 70% ethanol was added to wash the pellet. Finally, the tube was centrifuged at 12700 rpm for 5 min at 4 °C, supernatant was discarded and the DNA pellet air dried. The obtained DNA was re-suspended in 50 µl TE buffer. Specifically for Southern blot applications, BAC DNA was extracted using the phenol/chloroform method, which in detail is described in the section "Isolation gDNA from mouse biopsies".

3.2.1.11. Plasmid screening using Toothpick analysis

For Toothpick individual bacterial colonies were picked and wiped directly onto a 0.2 ml PCR tube walls after analysis after successful transformation and overnight incubation on Luria agar plates. 15 µl of Toothpick lysis buffer was added to each tube and vortexed on the Vortex-Genie 2 for a few seconds. Next, the tubes were incubated for 10 min at 68 °C in the T-Advance Thermocycler or FlexCycle² Thermocycler. After this incubation step, the cell lysate was directly loaded on an agarose gel and DNA was separated using agarose gel

electrophoresis. Only colonies showing the presence of the desired insert cloned into plasmid DNA the desired DNA fragment were used for further analysis.

3.2.1.12. HR in EL350 cells

In this study, genetically a modified *Escherichia coli* strain EL350 was used, which is characterized by a heat inducible expression of three lambda (λ) prophage recombination proteins. The expressions of these proteins are induced at 42 °C and switch off growing cells at 32 °C. HR was performed using EL350 cells, which already contained DNA of interest. Cells were placed into LB supplemented with appropriate antibiotic and were grown overnight. 1 ml of overnight cell culture was used to inoculate 50 ml LB containing appropriate antibiotic. Cells were left incubator at 32 °C 200 rpm and were let to divide until the OD 600 was around 0.6. Red protein expression was induced by transferring 10 ml of EL350 culture into pre-warmed 50 ml conical tubes and placing them into incubator for 15 min at 42 °C shaking at 200 rpm. The rest of the cell culture amount was incubated at 32 °C and used as non-induced control. Immediately after incubation cells were cooled down by placing tubes into slurry bath and proceeded with electrocompetent cell preparation and electroporation.

3.2.1.13. Southern blot and synthesis of Southern blot probes

The following protocol was developed in this work. gDNA or BAC was digested with PstI, EcoRI-HF[®] or KpnI-HF[®], restriction enzymes overnight in 500 μ l volume. The digested DNA was isolated with phenol-chloroform followed by ethanol precipitation. DNA pellets were air dried and re-suspended in 1X Loading Buffer and together with DNA Molecular Weight Marker II (Roche, Basel, Switzerland) loaded on a 0.8% agarose gel. After electrophoresis, the gel was incubated in hydrolysis buffer for 13 min at room temperature and washed shortly in water. Next, the hydrolysed gel was prepared for the transfer. Therefore, it was incubated in denaturation and neutralization buffer for 30 min each at room temperature with briefly rinsing the gel with water in between the incubations. To transfer DNA from the gel on a nylon membrane a transfer “sandwich” apparatus was set up as described as following. A tank was filled with 20X SSC solution and a platform was placed in the middle. Than the different layers

were placed using two filter papers soaked with 20X SSC, followed by the gel and covered with the nylon-membrane soaked with 2X SSC. On top of nylon-membrane 3 layers of filter papers soaked with 2X SSC were placed and topped with a stack of dry paper towels. All the levels were pressed together by a support weight. The final transfer “sandwich” apparatus was left overnight at room temperature using capillary forces to transfer DNA fragments from the gel onto nylon membrane. After successful transfer DNA fragments were cross-linked to the nylon membrane by exposing the membrane to UV light with CL508 UV-Cross-linker (Clever Scientific, Rugby, Warwickshire, UK). Next, the membrane was placed into pre-warmed 10 ml DIG Easy Hyb solution (Roche, Basel, Switzerland) for 30 min and placed into an incubator at 42 °C. After pre-hybridization step, old DIG Easy Hyb solution was replaced with fresh 4.5 ml pre-warmed digoxigenin(DIG)-labelled probe containing DIG Easy Hyb solution. The amount of the DIG labelled probe was calculated according to the DIG labelling efficiency. 9 µl of Neo probe and 13.5 µl of Probe1 was used for 4.5 ml DIG Easy Hyb solution. Afterwards, the membrane was incubated with the probe overnight at 42 °C. Next day the membrane was washed twice in Wash buffer I for 5 min at room temperature, twice in Wash buffer II for 15 min at 68 °C and once in Wash buffer III at room temperature for 3 min. DIG Luminescent Detection Kit (Roche, Basel, Switzerland) was used to detect DIG-labelled probe on the membrane. For this purpose, after washing, the membrane was placed into 1X Blocking solution for 30 min at room temperature and later incubated with anti-DIG-AP fragment (1:20 000 dilution) in 1X Blocking solution for 30 min room temperature. Subsequently, membrane was washed twice in Wash buffer III for 15 min at room temperature, incubated in the Detection buffer for 2 min at room temperature and placed in the reaction folder with disodium 3-(4-methoxyspiro {1,2-dioxetane-3,2'-(5'-chloro)tricyclo [3.3.1.1^{3,7}]decan}-4-yl)phenyl phosphate (CSPD) (1:100 dilution in Detection buffer). Membrane was placed in the incubator at 37 °C for 10 min. After incubation nylon membrane was transferred to a fresh bag, sealed and exposed to X-ray film.

To synthesize the DIG-label Southern blot DNA probes, a specific nucleotide sequence was PCR-amplified using appropriate sets of primers and PCR DIG Probe Synthesis kit (Roche, Basel, Switzerland). During this amplification, DIG-label was incorporated into the newly synthesized DNA. Using this method, the highly sensitive hybridization probes for Southern blot were generated, which was later used to detect low copy number DNA target sequences.

Neo1 and Neo2 primers with the $T_m = 59\text{ }^\circ\text{C}$ were used for the Neo probe synthesis. Probe1.1 and Probe1.2 primers with the $T_m = 58\text{ }^\circ\text{C}$ were used for Probe1 probe synthesis. As a template during the study generated pGemT_Probe1 plasmid was used for Probe1 probe synthesis and pGemT_Neo plasmid for Neo probe synthesis. Probes were synthesized according the manufacturer's instructions.

3.2.1.14. BUN and creatinine measurement in the serum or plasma

To evaluate kidney function and disease severity BUN and creatinine were measured in the murine blood. BUN levels in the serum were evaluated by Urea Assay Kit (Abcam, Cambridge, UK) according to the manufacturer's instructions and the absorption was measured using a Spark[®] 10M multimode microplate reader (Tecan, Männedorf, Switzerland). In addition to this, plasma samples were sent for BUN and creatinine laboratory evaluation to our collaborator PD Dr. med. vet., Dr. med. vet. habil. Karin Weber at the Medizinische Kleintierklinik, LMU München.

3.2.2. Flow cytometry

3.2.2.1. Leukocyte isolation from spleen and kidney

To analyse the leukocyte distribution and phenotype in the spleen and kidney, a single cell suspension from freshly tissue was prepared. In order to analyse the leukocyte distribution and phenotype in the kidney, mouse was overdosed with isoflurane (AbbBie Deutschland GmbH & Co. Ludwigshafen, Germany) and was perfused with cold PBS (Merck, Darmstadt, Germany) prior organ harvesting. Next, tissue homogenate was prepared by placing the harvested organ into Digestion solution for 30 min for spleen and 1 h for kidney at $37\text{ }^\circ\text{C}$ with shaking at 125 rpm. To remove undigested organ pieces, the obtained tissue homogenate was passed through $100\text{ }\mu\text{m}$ cell strainers. Cells were washed with cold FACS buffer and centrifuged at $4\text{ }^\circ\text{C}$ for 5 min at 1350 rpm and supernatant was removed. Afterwards red blood cell lysis was performed on the isolated splenocytes by re-suspended the cell in 2 ml

red blood cell (RBC) buffer (Merck, Darmstadt, Germany) and incubated for 2 min at room temperature. Then cold FACS buffer was added to stop lysis and cells were centrifuged at 4 °C for 5 min at 1350 rpm. Supernatant was removed and cell pellet was re-suspended in cold 5 ml FACS buffer. The isolated splenocytes were passed through 70 µm cell strainers and proceed with cell counting and staining.

In contrast to isolated cells from spleen, kidney leukocytes were enriched using low-speed iso-density percoll (GE Healthcare Bio-Science, Piscataway, New Jersey, USA) centrifugation method. After the digestion and washing, the cell pellet was re-suspended in 4 ml 70% percoll solution and transferred to a new 14 ml Conical tube. 4 ml of 37% and 30% percoll solutions were overlaid on top, without disturbing the individual layers. The tube was centrifuged for 30 min at room temperature at 2000 rpm without breaking. Leukocytes were collected from 70-37% interphase and once washed with FACS buffer. After supernatant was removed, pellet was re-suspended in 0.5 ml FACS buffer and proceeded with cell staining.

3.2.2.2. Cell number and viability determination

Prior the staining for flow cytometry, suspended in FACS buffer splenocytes were counted with Neubauer Chamber. Cell suspension was mixed 1:1 volume ratio with trypan blue solution (Merck, Darmstadt, Germany). Live cells were counted in four quadrats and the average cell per quadrat was multiple by dilution factor and 10^4 resulting in cell number per ml (cell/ml).

CountBright™ Absolute Counting Beads (Thermo Scientific, Waltham, Massachusetts, USA) were used for counting renal leukocytes. Cells were calculated by adding 10 µl 500 beads/µl counting beads directly into the cells suspension prior sample acquisition on the flow cytometry machine. Cell concentration was calculated according the formula:

$$\frac{m \text{ (counted cells)} * n \text{ (added beads)}}{g \text{ (counted beads)} * f \text{ (sample volume, } \mu\text{l)}} = \text{cell}/\mu\text{l}$$

3.2.2.3. Cell surface marker staining using antibodies

To identify and characterise different leukocyte cell populations within prepared single cell suspension, cells were stained with antibodies, conjugated with fluorescent dyes, against specific cell surface markers. First, Fc γ receptors were blocked by incubating cells in FACS buffer with CD16/CD32 antibody for 10 min dark at 4 °C. Next, master mix of prepared antibodies in the FACS buffer was added directly on the cells. Cells were stained at 4 °C in the dark for 20 min. After staining cells were washed three times with FACS buffer followed by centrifugation at 4 °C 1350 rpm 3 min. After the last wash, cells were re-suspended in the 100 μ l of FACS buffer. For live cell analysis, 4',6-diamidino-2-phenylindole (DAPI) (Merck, Darmstadt, Germany) was added to the cells prior the acquisition. For fixed cells analysis, after surface marker staining cells were stained using Zombie dyes (Biolegend, San Diego, California, USA) according to the manufactures' provided protocol and fixed with 2% paraformaldehyde (Thermo Scientific, Waltham, Massachusetts, USA) for 20 min at room temperature. After staining cells were washed three times with FACS buffer followed by centrifugation at 4 °C 1350 rpm 3 min. After the last wash, cells were re-suspended in the 100 μ l of FACS buffer and left at 4 °C until data was acquired on BD Fortessa (BD Biosciences, San Jose, California, USA).

3.2.3. Animal Husbandry

All animals were kept under specific pathogen free (SPF) conditions and routinely tested for pathogens. Clec9a-Cre, Rosa26-iDTR, XCR1-DTR-Venus, Rosa26-iEYFP, CD64-LSL-2A-DTR, C57BL/6 mice in the facility were kept under a 12 h light- 12 h dark light schedule. Food and water was available *ad libitum*.

3.2.4. *In vivo* methods

3.2.4.1. CD64-LSL-2A-DTR mice generation using CRISPR-Cas9 technology

After successful cloning of CD64-LSL-2A-DTR target vector the construct was sent to our collaborator Prof. Dr. Thorsten Buch in Switzerland and all further described steps were performed in his laboratory. Microinjection was done at the Institute of Laboratory Animal Science University of Zurich. 3-4 weeks old C57BL/6 female mice were superovulated prior embryos collection. For this purpose, the mice were intraperitoneal (*ip*) treated with 5 international unit (IU) pregnant mare serum gonadotropin (PMSG) (Folligon, MSD Animal Health GmbH, Luzern, Switzerland) and 48 h later were injected with 5 IU human chorionic gonadotropin (hCG) (Pregnyl MSD Animal Health GmbH, Luzern, Switzerland). Superovulated female mice were mated overnight with C57BL/6 stud males and later zygotes were isolated and used for microinjections. Prior the procedure Cas9:crRNA:tracrRNA complex was assembled by incubating Cas9 protein (New England BioLabs, Ipswich, Massachusetts, USA) with tracrRNA:crRNA duplex (Integrated DNA technologies, Coralville, Iowa, USA) for 15 min at 37 °C. The microinjection solution used to generate CD64-LSL-2A-DTR mice contained 30 ng/μl EnGen™ Cas9 nuclear location signal (NLS), 0.4 picomole (pmol)/μl tracrRNA and 0.4 pmol/μl crRNA and 10 ng/μl linearized CD64-LSL-2A-DTR target vector in microinjection solution. The *CD64* locus specific sequences, used to guide Cas9:tracrRNA:crRNA complex, were the following: fw AAAGTTGACCCTGAACTGT and rv ACAGTTTCAGGGTCAACTTT. Shortly after injection, oocytes have been implanted into a pseudo-pregnant mouse. All the zygote manipulations, including microinjection, culture and transfer into pseudopregnant foster female mice, were performed at the transgenesis core facility according to the standard mouse transgenesis protocols²⁸³ under license of the cantonal veterinary office in accordance with federal law.

3.2.4.2. Blood collection and serum isolation

The blood was collected from the heart of an isoflurane overdosed mouse into 2 ml syringe or into heparin coated 2 ml syringe (Hepatin-Nsturiu-25000-ratiopharma®, Ratiopharma,

Germany). The blood was transferred into a 1.5 ml tube and was kept on ice. All samples were centrifuged at 10000 rpm 4 °C for 10 min, to separate blood cells from serum or plasma. Top clear layer, containing plasma or serum, was carefully collected and transferred to new tubes and snap frozen on dry ice. The samples were kept at -80 °C until they were used.

3.2.4.3. Depletion of DTR expressing cells

To deplete DTR expressing cells, Clec9a-Cre x Rosa26-iDTR and XCR1-DTR-Venus mice were injected once and Clec9a-Cre x CD64-LSL-2A-DTR mice were treated twice, 24 h apart i.p. with a freshly prepared 4 ng/μl DT solution (Merck, Darmstadt, Germany) at the dose of 25 ng/kg body weight (PBS Merck, Darmstadt, Germany) was used as control. All animal experiments were performed at The Core Facility Animal Models at the BMC of the LMU, Munich, in accordance with national and institutional guidelines for animal care.

3.2.4.4. AKI induction

AKI experiments were performed using adult Clec9a-Cre x Rosa26-iDTR, XCR1-DTR-Venus and C57BL/6 mice at the age of 8-12 weeks old. AKI was induced in the animals by injecting i.p. a single dose of freshly laboratory prepared (2 mg/ml) cisplatin (Merck, Darmstadt, Germany) or commercial available (1 mg/ml) cisplatin solution (Petah Tikva, Israel) at the concentration of 10 – 20 mg/kg body weight, depending on the performed experiment, or 0.9% NaCl (Fresenius Kabi Deutschland GmbH, BAD Homburg, Germany). The 2 mg/ml cisplatin solution was prepared by sonicating 3 min, followed by 30 min stirring at 35 °C. Each animal was weighted and scored using an observation scoring system, evaluating mouse behaviour, fur condition, breathing, body weight lost, posture and excretion. Mice were monitored every morning/evening. Individual symptom scores were added together to give an overall symptom score and based on this score different actions were taken. Mice, which were given 20 points, were terminated immediately. All AKI experiments were performed at The Core Facility Animal Models at the BMC of the LMU, Munich in accordance with national and institutional guidelines for animal care.

3.2.5. Statistical analysis

Statistical analysis was performed using Prism 6 (GraphPad) program. Results with p value smaller than 0.5 was evaluated as statistically significant. In all analysis, unpaired Student's t-test with Welch's correction was used.

4. Results

4.1. CD64-LSL-2A-DTR mouse model generation

4.1.1. CD64 expression on cDC progenitors

The main aim of this thesis was the generation of a novel mouse model, allowing the selective depletion of CLEC9A⁺ progenitor derived CD64 expressing cells, in particular their renal CD64⁺ population. It was planned to achieve this by knock-in a Cre-inducible *DTR* gene in the *CD64* reading frame of a wild type mouse genome. To restrict later the DTR expression specifically to the renal CLEC9A⁺ progenitor derived CD64⁺ cells, a DC lineage *Clec9a*-Cre mouse line was planned to cross with this new generated DTR carrying mice. With this strategy DTR expression would be restricted to DCs, because a study has shown that *Clec9a*-Cre mice allowed the specific tracking of CLEC9A⁺ CDP derived cells, which was specifically demonstrated for crossing with *Rosa26*-iEYFP reporter mice^{24,282}. In consideration of the fact, that *Clec9a* promoter is active in CDPs as well as in pre-cDCs²⁴, it was mandatory to exclude the possibility, that DC progenitors express CD64, which would resulting in an unspecific depletion model. Thus, the CD64 expression was first investigated on the cDC progenitors using the *Clec9a*-Cre x *Rosa26*-iEYFP mice, which allow tracking of the CLEC9A⁺ expressing or CLEC9A⁺ progenitor derived cells based on EYFP expression. The BM of *Clec9a*^{Cre/Cre}*Rosa26*^{iEYFP/EYFP} mice were investigated by FACS for CD64 expression on EYFP positive and negative cDC progenitors pre-cDCs and CDPs as well as on MDPs (Fig. 4A). As shown in figure 4B, MDPs expressed similar levels of CD64 compared to MOs, used as a positive control^{17,121}. Importantly, CD64 expression was not found on pre-cDCs or CDPs (Fig. 4B). However, it was shown that not all pre-cDCs and CDPs are EYFP labelled in these mice. Nevertheless, an EYFP⁻ progenitors transfer study has demonstrated that EYFP⁻lin⁻ (lymphocyte antigen 76 (ly76 also known as Ter119), NK1.1, CD4, CD8, CD45R, CD11b, MHCII)CLEC9A⁺ cells are able to give rise to EYFP⁺ cells and thus, suggesting that EYFP⁺ and

Results

EYFP⁻ CDPs are not qualitative different²⁴. In line with this previous data, there was no difference detected for the CD64 expression between EYFP⁺ and EYFP⁻ CDPs in this study too (Fig. 4B). These data clearly demonstrated that CDPs and pre-cDCs isolated from *Clec9a^{Cre/Cre}Rosa26^{EYFP/EYFP}* mice do not express the CD64 making this model suitable for the later crossing.

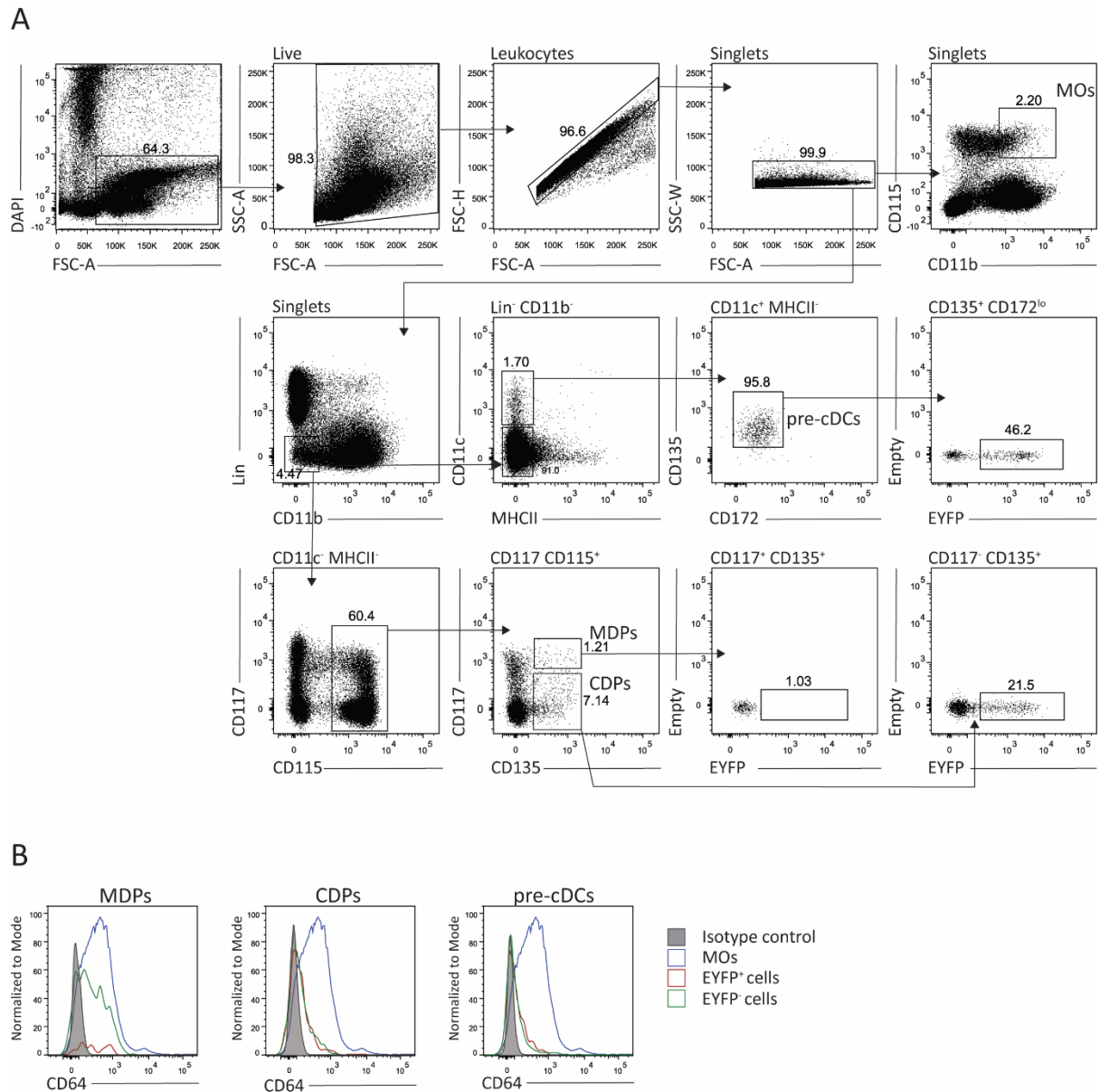


Figure 4. CD64 expression analysis on cDC progenitors.

(A) Gating strategy to identify MOs (CD115⁺CD11b⁺), pre-cDCs (lin⁻(CD3, CD4, CD8, Ter119, NK1.1, CD45R)CD11b⁻CD11c⁺CD135⁺CD172a^{lo}) as well as MDPs (lin⁻CD11b⁻CD11c⁺MHCII⁻CD115⁺CD135⁺CD117⁻) and CDPs (lin⁻CD11b⁻CD135⁺CD117⁺) in BM from *Clec9a^{Cre/Cre}Rosa26^{EYFP/EYFP}* mice by flow cytometry is shown. Cells from BM in *Clec9a^{Cre/Cre}Rosa26^{EYFP/EYFP}* mice were stained with antibodies against indicated surface markers. The numbers in the dot plots indicates the percentage of the cells within the indicated gates. (B) pre-cDCs, CDPs and MDPs were analysed for CD64 expression.

4.1.2. *In silico* analysis of *CD64* target region for *DTR* gene knock-in and design of DTR construct

The basic requirements for the successful generation of the novel DTR expressing transgenic mouse model were the knock-in of *DTR* gene into *CD64* locus reading frame and the prevention of undesired “neighborhood effects”. Therefore, the *CD64* locus (gene ID14129) itself and all relevant genes, in close proximity upstream and downstream of the possible insertion site, were analysed in advance *in silico*. As indicated in figure 5A, *CD64* gene is located between two histone cluster sequences and *n-TNgtt4 nuclear encoded tRNA asparagine 4 (anticodon GTT)*, located within a 13-28 kbp distance from the *CD64* gene. In detail, *histone cluster 2, H3b* sequence (geneID: 319154) was found 13,4 kbp and *histone H2B type 2-B* sequence (geneID: 319189) was found 12,7 kbp downstream of *CD64* gene 3' untranslated region (UTR) sequence. Additionally, 28,1 kbp upstream of the *CD64* 5'-UTR a *n-TNgtt4 nuclear encoded tRNA asparagine 4 (anticodon GTT)* (geneID: 102467475) sequence was found, making it most unlikely that knock-in into *CD64* locus would cause undesired side effects by affecting other important gene expression.

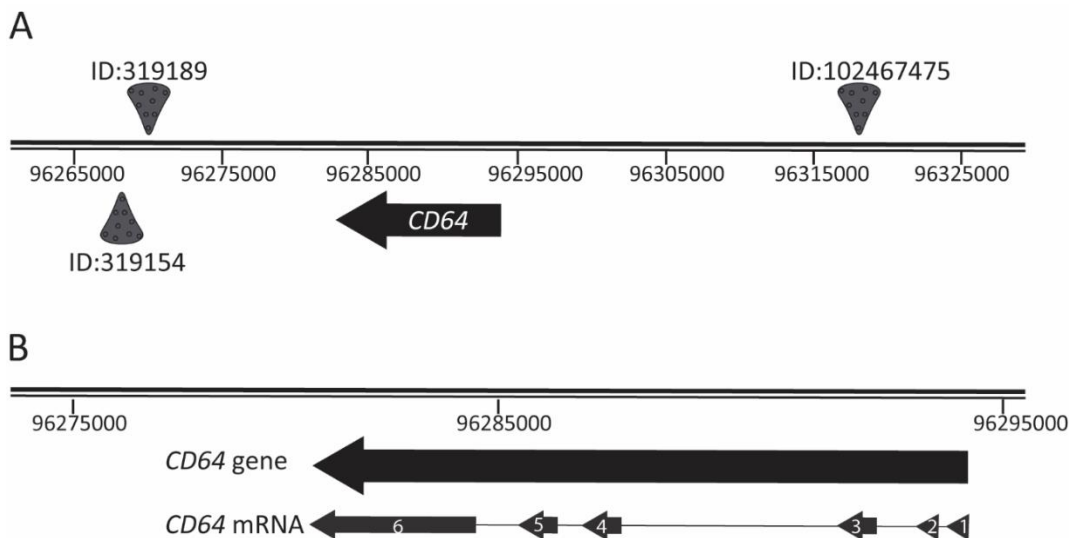


Figure 5. Analysis of *CD64* region for repair construct insertion.

(A) Part of *Mus musculus* 3rd chromosome is shown spanning the region of 96265000 - 96325000. In the track, dark triangles indicate histone cluster sequences derived by automated computational analysis. (B) *Mus musculus* *CD64* gene and mRNA is shown. In both tracks, black arrow indicates the *CD64* gene; the grey arrows represent different *CD64* exons.

Since it was described, that *CD64* gene deficient mice demonstrate a decrease in immune complex-induced inflammation, a reduction in antibody-dependent killing of pathogens by MØs and impaired protection from bacterial infection, it was taken in consideration to place the *DTR* gene downstream of the *CD64* protein coding sequence (CDS)^{219,220}. With this strategy, it was decided to fuse the *DTR* gene with *CD64* without disrupting or affecting the gene expression. In detail, the approach was to combine *CD64* with *DTR* by replacing the endogenous stop codon within the 6th exon of *CD64* at position 96,284,276 – 96,284,278 (Fig. 5B), resulting in a polycistronic mRNA. To ensure the production of equimolar levels of both genes a “self-cleaving” 2A peptide was placed between *CD64* and *DTR* genes. To increase *DTR* expression specificity, LSL was planned to be cloned in front of the 2A-DTR sequence. To stabilize the transcribed mRNA and to further increase gene expression efficacy, *WPRE* was designed to be cloned downstream of *DTR*. As a matter of course, it was taken into the consideration to place all these elements, LSL, 2A sequence, *DTR*, *WPRE* respectively in frame with *CD64* CDS. To keep at this point both possibilities for generating knock-in mice, using HR in ESC or CRISPR-Cas9 technology, a Neo cassette was additionally cloned behind the *WPRE* sequence. A schematic diagram illustrating the final design of the knock-in *DTR* construct, containing LSL, 2A, *DTR*, *WPRE* and Neo cassette sequences, is shown in figure 6.

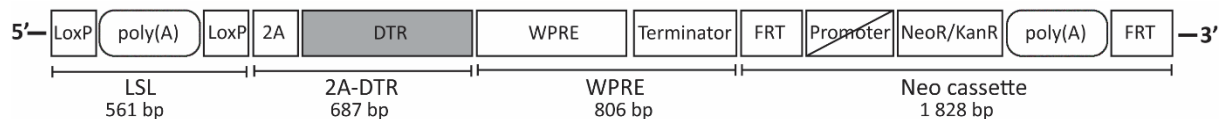


Figure 6. Structure of DTR construct.

Schematic overview of the 3882 bp DNA integration construct. All essential sequences, required for efficient *DTR* expression, are shown and indicated in 5'-3' order as boxes with the individual sequence name and length.

4.1.3. Cloning of DTR construct (pBlueScript_LSL_2A_DTR_WPRE_Neo plasmid generation)

To generate the designed DTR construct, I took advantage of Gibson Assembly method. Since the Gibson Assembly efficiency drops as the number of used DNA fragments of interest increases, synthesis of DTR construct was done in a two-step process. First, LSL cassette and 2A-DTR sequence were assembled into empty pBlueScript SK II (+) vector, generating the intermediate pBlueScript_LSL_2A-DTR plasmid. This was achieved by capturing a 590 bp fragment containing LSL cassette from Snap25-LSL-2A-GFP target vector and a 687 bp 2A-DTR sequence from GCDL-2A-DTR plasmid by PCR (Figure 7A, B). The forward primer to amplify LSL cassette sequence was designed to have a homology with the vector backbone and the fragment, containing the LSL cassette. Moreover, it contained an additional 50 nt sequence, which was homologous to 50 bp upstream of the endogenous the *CD64* stop codon. This 50 bp sequence was later used as a guide sequence for the replacement of the *CD64* endogenous stop codon. In detail, pBlueScript SK II (+) vector was linearized using KpnI-HF[®] restriction enzyme and assembled with the final 711 bp 2A-DTR PCR and 663 bp LSL PCR products. To confirm correct assembly, isolated plasmid DNA was restriction digested and analysed by agarose gel electrophoresis (Fig. 7C). Only plasmid isolations with the expected fragment pattern was sent for Sanger sequencing analysis using primers SeqPrimer 2-4 and was used for the next cloning step. A schematic overview of the finally obtained plasmid is shown in figure 7D.

Results

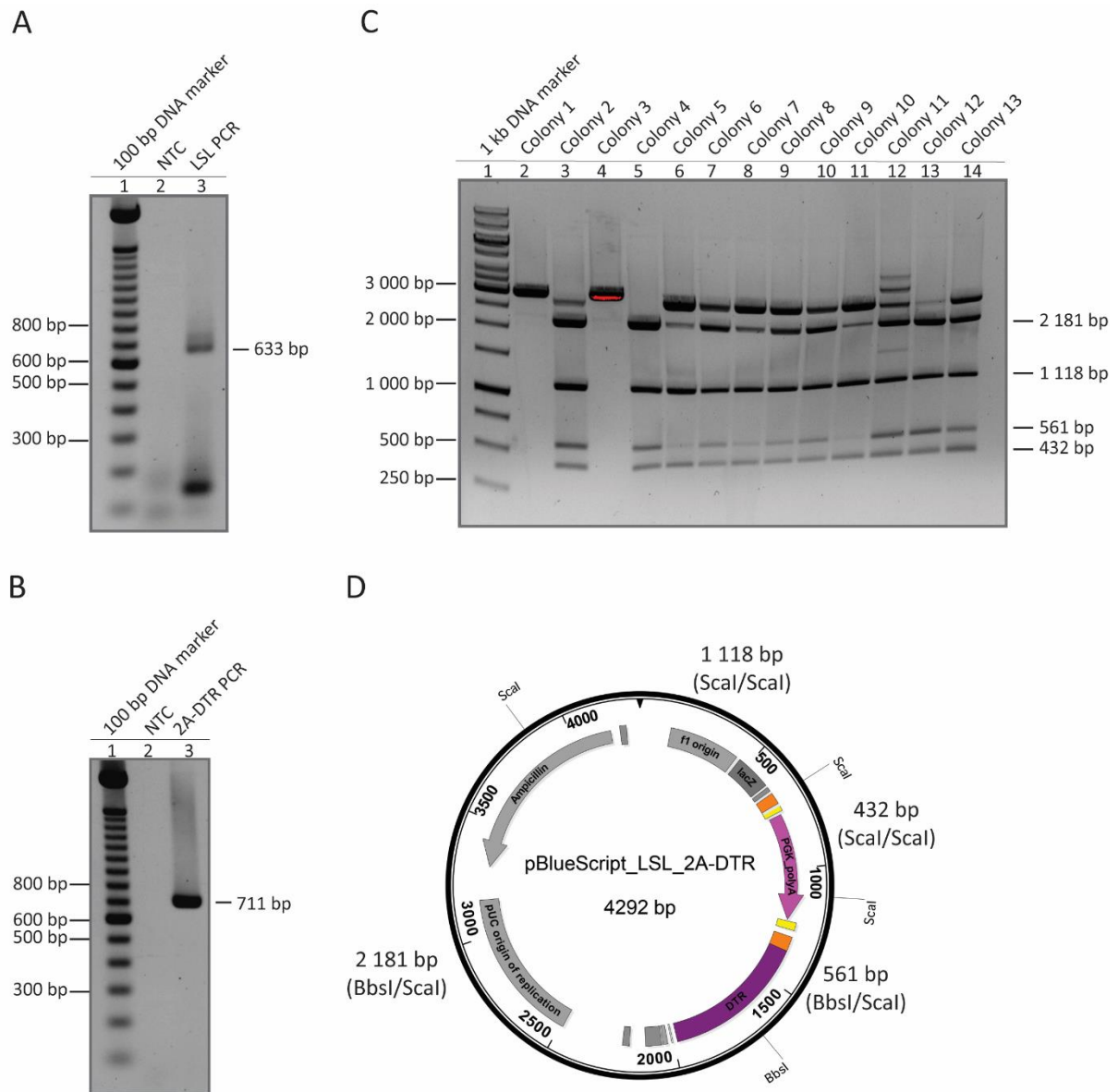


Figure 7. Generation of pBlueScript_LSL_2A-DTR plasmid.

(A) PCR of LSL cassette fragment using primers BL1 and Block1. A representative agarose gel electrophoresis image is shown. The expected 633 bp PCR product (lane 3), marker (lane 1) and non-template control (NTC) (lane 2) are indicated. (B) PCR of 2A-DTR fragment using DTR and D primers. A representative agarose gel electrophoresis image is shown. The expected 711 bp PCR product (lane 3), marker (lane 1) and NTC (lane 2) are indicated. (C) Restriction digestion of pBlueScript_LSL_2A-DTR plasmid. A representative agarose gel electrophoresis image of all plasmid DNAs isolated from different colonies after Scal-HF[®]/Bbsl digestion is shown. Clone 4 (lane 5) showed the expected digestion pattern of 2181 bp, 1118 bp, 561 bp and 432 bp fragments. (D) Plasmid map of pBlueScript_LSL_2A-DTR. All Scal-HF[®] and Bbsl restriction sites, to confirm the integrity of the plasmid, are indicated. The calculated fragment sizes after Scal-HF[®]/Bbsl digestion of 432 bp, 561 bp, 1118 bp and 2181 bp are shown.

Following the same strategy, *WPRE* sequence and Neo cassette were combined into the newly created pBlueScript_LSL_2A-DTR plasmid in the second step of assembly process. Therefore, the 864 bp fragment containing *WPRE* sequence was amplified by PCR from Snap25-LSL-2A-GFP target and the 1864 bp fragment containing Neo cassette from 195 FrtneokanaFrt DTA plasmid (Fig. 8A). Analogue to the first step, reverse primer to amplify Neo cassette was designed to include a 50 nt sequence, which was homologous to the 50 bp downstream of the endogenous *CD64* stop codon. The pBlueScript_LSL_2A-DTR plasmid was linearized using *XhoI* restriction enzyme and the *WPRE* and Neo cassette sequences were assembled into the linearized vector. Different individual bacterial clones were picked and verified by colony screening PCR for correct assembly (Fig. 8B). Only clones showing the expected fragment size, were used for pBlueScript_LSL_2A-DTR_ *WPRE*_Neo plasmids isolation and sent for Sanger sequencing using primers SeqPrimer 1-4, SeqPrimer 9-18, and M13 rev (-49) to confirm the correct assembly. The validated pBlueScript_LSL_2A-DTR_ *WPRE*_Neo plasmid contained the full length DTR construct, composed of LSL cassette, 2A sequence, *DTR* gene, *WPRE* sequence and Neo cassette is shown in figure 8C.

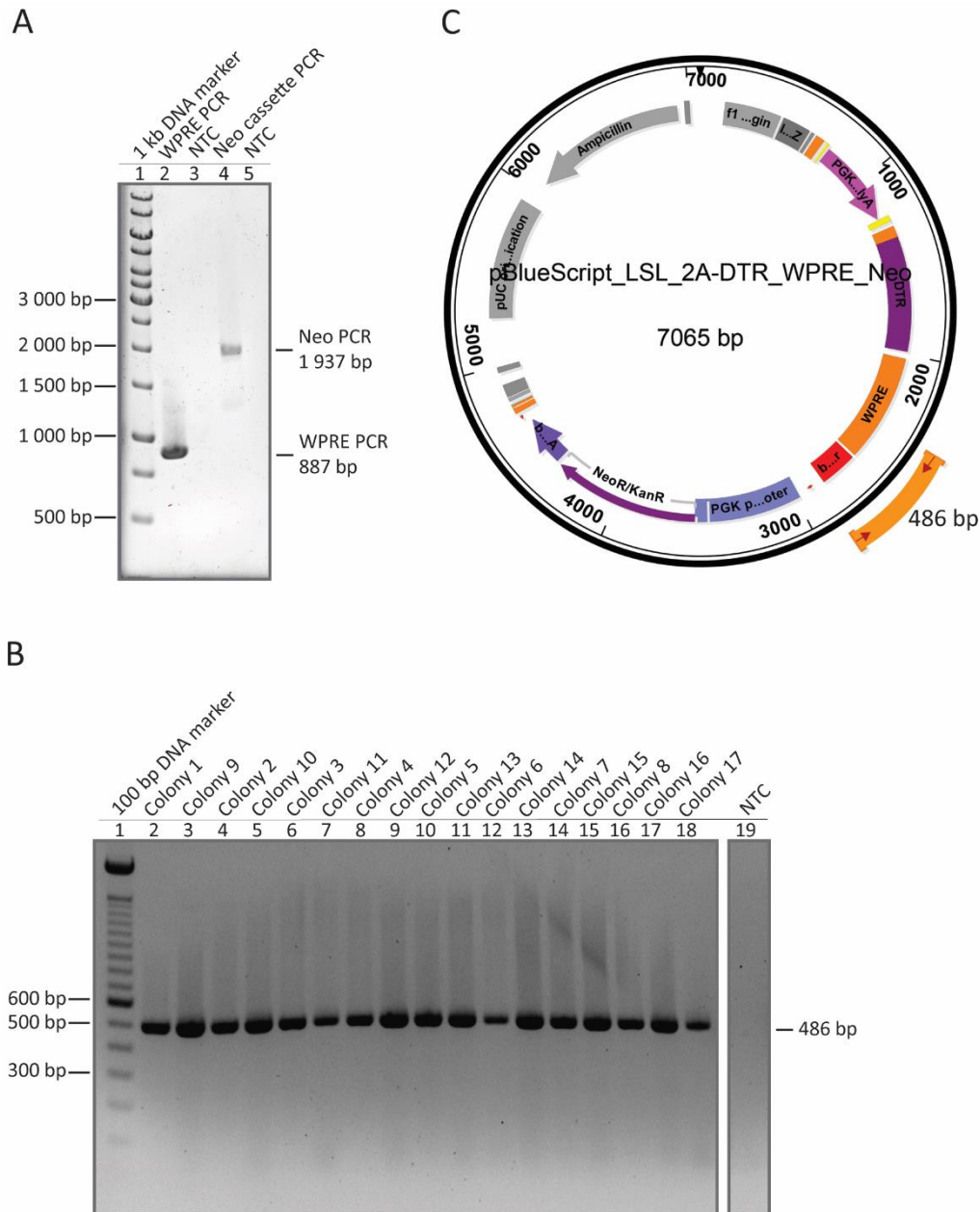


Figure 8. Generation of pBlueScript_LSL_2A-DTR_WPRE_Neo plasmid.

(A) PCR of WPRE and Neo cassette fragments using WPRE Fwd/WPRE Rev and F NeoF Fwd/F Neo F PRE Rev primers respectively. A representative agarose gel electrophoresis image is shown. The expected 887 bp of WPRE and 1937 bp of Neo PCR products, marker (lane 1) and NTC (lane 3, 5) are indicated. (B) Colony screening PCR to confirm pBlueScript_LSL_2A-DTR_WPRE_Neo integrity. A representative agarose gel electrophoresis image is shown. The primer combination SeqPrimer10 and WPRE Rev (T_m 57.4 °C) were used to identify positive clones. A representative agarose gel electrophoresis image of the fragments obtained from all screened colonies is shown. All samples showed the expected fragment size of 486 bp as indicated (lane 2-18). Marker (lane 1), NTC (lane 19) are indicated. (C) Plasmid map of pBlueScript_LSL_2A-DTR_WPRE_Neo. The location and amplified region of the SeqPrimer10 and WPRE Rev used for colony screening is indicated.

4.1.4. Design of homology arms

At this step, the generated DTR construct contained all necessary elements, required for the successful DTR expression. To accomplish the later targeted-orientated integration into the mouse genome, two homology arms were designed at the 5' and 3' end of DTR construct, with the length of 5497 bp for the main guiding 5' arm and 3885 bp for the shorter 3' arm (Fig. 9). In detail, these homology arms contained a partial *CD64* gene sequence spanning from intron 3rd intron until the endogenous poly(A) sequence followed by a sequence of 2,5 kbp 3rd mouse chromosome. A RPCIB731E08452Q BAC, below designed as CD64_BAC, containing a part of the *Mus musculus* 3rd chromosome (spanning 96,173,608 – 96,349,578 bp) was used as a template for the source of *CD64* gene sequence.

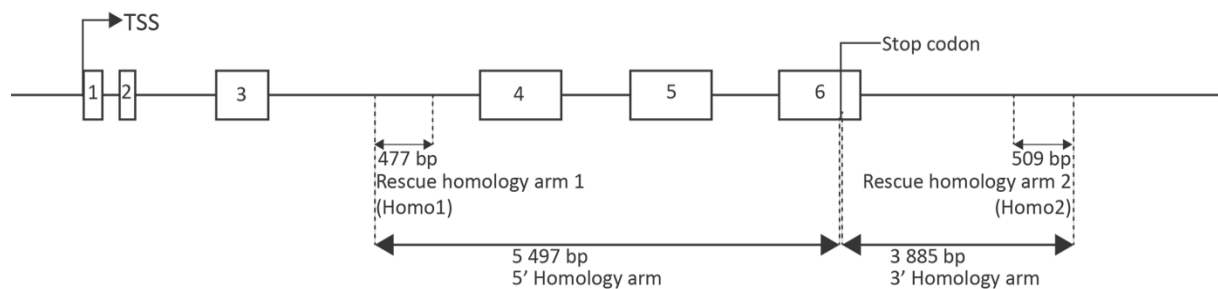


Figure 9. Schematic diagram of the *Mus musculus* *CD64* locus.

Boxes represent *CD64* gene exons, with the name indicated in the box, and bold black lines indicates introns. Double side arrows indicate right and left rescue homology and homology arms, with the specific name, size and position in the *CD64* locus; TSS- transcription start site.

4.1.5. Cloning of homology arms (pBlueScript_Homo1_Homo2 rescue vector and pBlueScript_CD64 plasmid generation)

For capturing the necessary homology arms from the CD64_BAC by HR, a rescue vector was generated. The recombination mediated rescue vector was planned to contain two short rescue homology arms called Homo1 and Homo2, which designed to serve as guides (Fig. 9). Homo1 sequence was homologous to the 477 bp upstream of homology arm 5' and Homo2 was identical to 508 bp downstream of homology arm 3'. These rescue homology arms were planned to get ligated into empty pBlueScript SK II (+) vector in a two-step process. First, Homo1 fragment was amplified from the CD64_BAC (Fig. 10A). The initially designed primer sequences to capture Homo1 were modified by introducing a Sall-HF[®] restriction site to

Results

Res_HOM1_Rev primer and a NotI-HF[®] site to Res_HOM1_Fwd primer 5'-ends. Prior ligation the obtained PCR product and pBlueScript SK II (+) vector were digested with Sall-HF[®] and NotI-HF[®] to generate the intermediate pBlueScript_Homo1 plasmid. To assure the correct plasmid sequence, several bacterial clones were screened for Homo1 integration by fragment analysis after restriction digestion. Only plasmids, which showed the expected fragment size, were further confirmed by sequencing using SeqPrimer44 and T3 primers (Fig. 10B). A schematic overview of the finally obtained plasmid is shown in figure 10C.

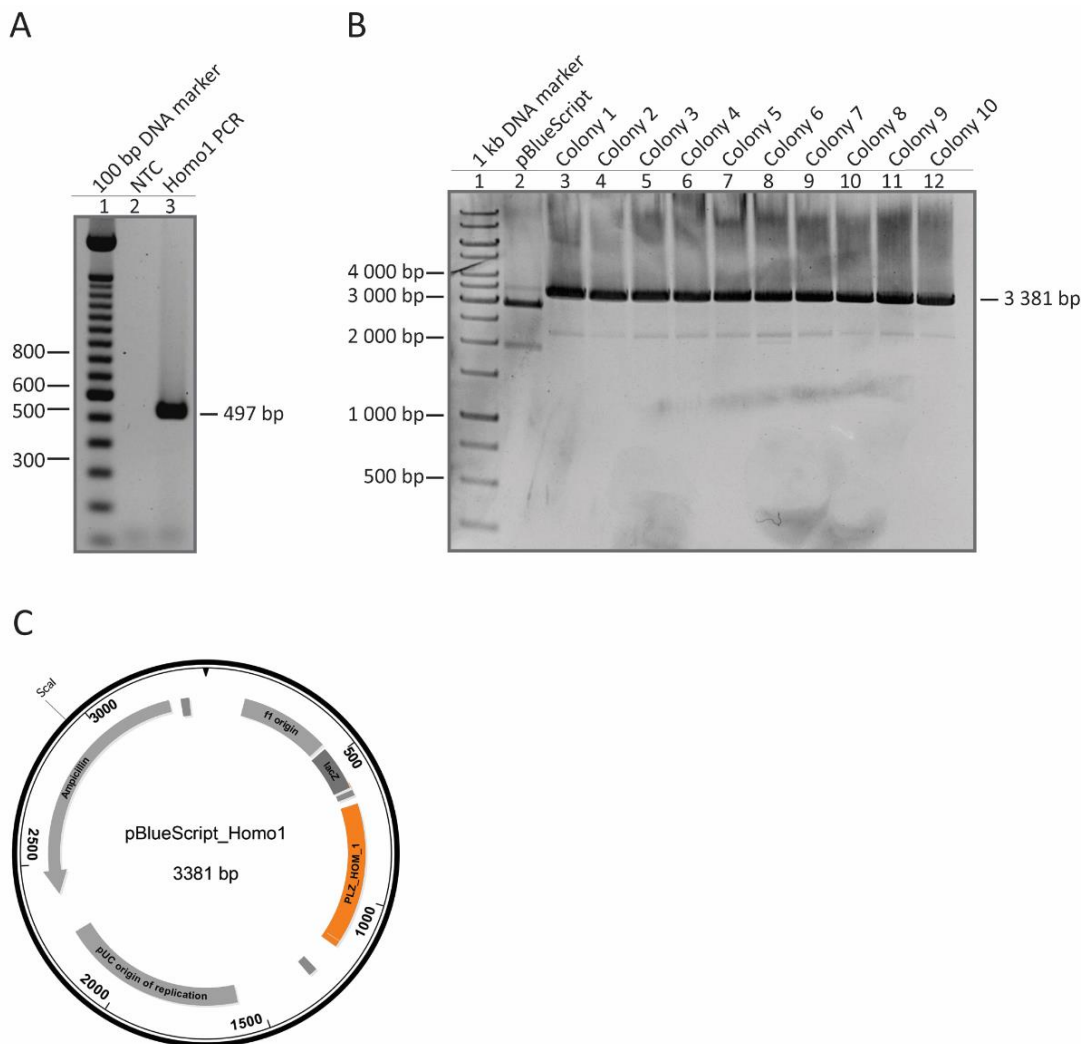


Figure 10. Generation of pBlueScript_Homo1 plasmid.

(A) PCR of Homo1 fragment using primers Res_Homo1 Fwd and Rev. A representative agarose gel electrophoresis image is shown. The expected 497 bp PCR product (lane 3), marker (lane 1) and NTC (lane 2) are indicated. (B) Restriction digestion of pBlueScript_Homo1 plasmid. A representative agarose gel electrophoresis image of all plasmid DNAs isolated from different clones after Sall-HF[®] digestion is shown (lane 3-12). All samples showed the expected fragment size of 3381 bp as indicated. The marker (lane 1) and pBlueScript plasmid (lane 2), used as a negative control, are shown. (C) Plasmid map of pBlueScript_Homo1. The Sall-HF[®] recognition site, to confirm the integrity of the plasmid, are indicated.

In the next step of rescue vector generation, Homo2 sequence was cloned behind the Homo1 sequence using pBlueScript_Homo1 plasmid. The specific Homo2 fragment was amplified from the same CD64_BAC (Fig. 11A). Initially designed primer sequences were modified by adding a Sall-HF[®] restriction site to Res_HOM2_Fwd and a XhoI site to Res_HOM2_Rev primer 5'-end. The obtained PCR product of Homo2 PCR and the pBlueScript_Homo1 plasmid were digested with XhoI and Sall-HF[®] ligated to generate pBlueScript_Homo1_Homo2 plasmid. For pre-screening several bacterial clones were picked-up for Toothpick analysis (Fig. 11B). To finally confirm the correct Homo2 orientation, plasmid DNA was restriction digested and the fragments were analysed (Fig. 11C). To further confirm that the cloned Homo2 sequence was without mutations, pBlueScript_Homo1_Homo2 plasmid sequence was confirmed by Sanger sequencing using SeqPrimer44 primer. The final rescue vector map is shown in figure 11D.

Results

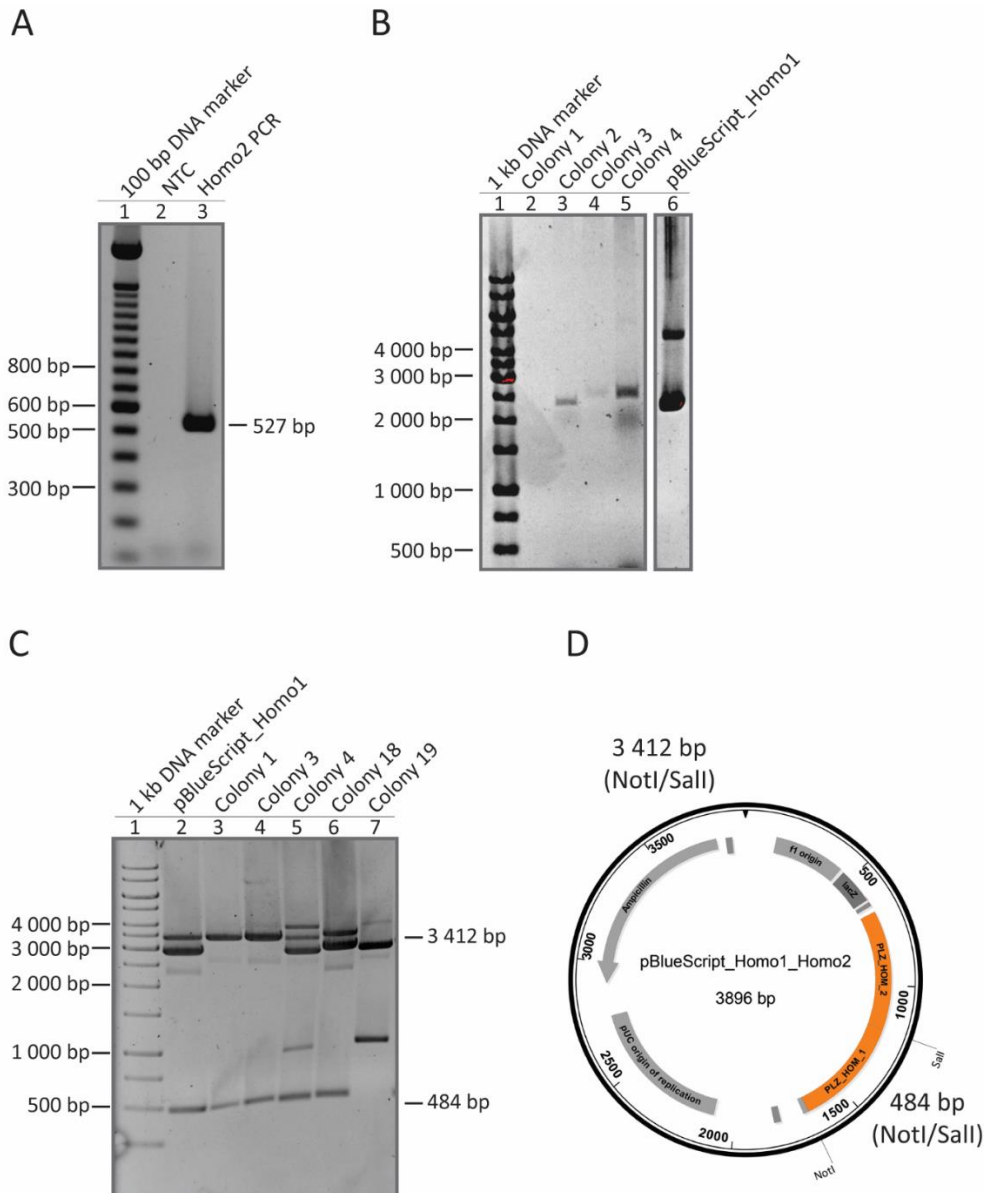


Figure 11. Generation of pBlueScript_Homo1_Homo2 plasmid.

(A) PCR of Homo2 fragment using primer Res_Homo2_ Fwd and Rev. A representative agarose gel electrophoresis image is shown. The expected 527 bp PCR product, marker (lane 1) and NTC (lane 2) are indicated. (B) Toothpick analysis. Representative agarose gel electrophoresis image of crude plasmid DNA extracts from agar plate of different colonies (lane 2-5). Colony 3 (lane 4) and 4 (lane 5) displayed the expected shift of the supercoiled DNA and confirmed for Homo2 sequence integration into the pBlueScript_Homo1 plasmid. The marker (lane 1) and pBlueScript_Homo1 (lane 6), used as a negative control, are indicated. (C) Restriction digestion of pBlueScript_Homo1_Homo2 plasmid. Agarose gel electrophoresis image of 5 representative plasmid DNAs isolated from different colonies after Sall-HF[®]/NotI-HF[®] digestion (lane 3-7) is shown. Out of 29 samples tested only colony 1 (lane 3) and 3 (lane 4) showed the expected fragment size of 484 bp and 3412 bp. Marker (lane 1) and pBlueScript_Homo1 plasmid (lane 2), used as the negative control, are indicated. (D) Plasmid map of pBlueScript_Homo1_Homo2. All Sall-HF[®] and NotI-HF[®] restriction sites, to confirm the integrity of the plasmid, are indicated. The calculated fragment sizes after Sall-HF[®]/NotI-HF[®] digestion of 484 bp and 3412 bp are shown.

Results

For capturing homologous arms from the CD64_BAC into rescue vector by HR, first EL350 cells were transformed. To exclude at this step any occurring rearrangements during transformation, CD64_BAC integrity was confirmed by two PCRs and restriction digest (Fig 12A, B, C). As shown in figure 12 all clones showed the expected amplification product and the same digestion pattern of 6 prominent fragments above 8000 bp compared to the original CD64_BAC DNA (Fig. 12C). Finally, one of these bacterial clones, which contained the validated CD64_BAC, was used for homology arm generation. This was achieved by transformation with linearized pBlueScript_Homo1_Homo2 rescue vector, after Sall-HF® digestion, to generate the homology arms containing pBlueScript_CD64 plasmid.

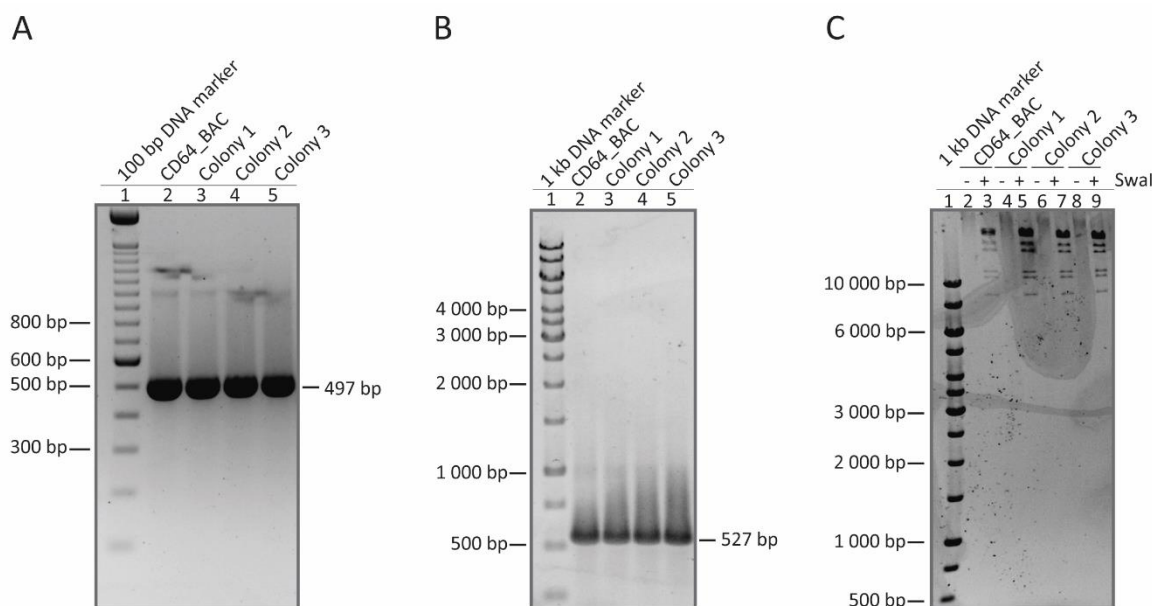


Figure 12. Verification of the transformed CD64_BAC integrity.

(A) PCR of Homo1 using primers Res_Homo1 Fwd and Rev. A representative agarose gel electrophoresis image is shown. The expected 497 bp PCR product, marker (lane 1) and original CD64_BAC (lane 2), used as a positive control, are indicated. (B) PCR of Homo2 fragments using primers Res_Homo2 Fwd and Rev. A representative agarose gel electrophoresis image is shown. The expected 527 bp PCR product, marker (lane 1) and original CD64_BAC (lane 2), used as a positive control, are indicated. (C) Restriction digestion of isolated BAC after transformation. A representative agarose gel electrophoresis image of BAC DNAs isolated from different colonies is shown before and after Swal digestion (lane 4-9). The expected signature of 6 prominent fragments, marker (lane 1) and original undigested and digested CD64_BAC (lane 2-3), used as a positive control, are indicated.

To confirm successful homology arm insertion into pBlueScript_Homo1_Homo2, isolated plasmid from different clones was digested individually with restriction enzymes. Unexpectedly, only the BamHI-HF® digestion showed for all clones the expected restriction digestion pattern of three bands (6916 bp, 4498 bp, 881 bp) (Fig. 13A). In contrast to that,

Results

two fragments (1562 bp and 907 bp) out of five expected ones (4833 bp, 3590 bp, 1562 bp, 1397 bp, 907 bp) were missing after XbaI digestion, as shown in figure 13C. Instead, only four fragments (4833 bp, 3590 bp, 2469 bp, 1397 bp) could be detected, leading to the assumption that this site was not cut by the enzyme. However, sequencing with primers SeqPrimer6-7 of the respective DNA area spanning the uncut XbaI site confirmed the integrity of the questionable enzyme recognition sequence in all clones and confirmed thereby the plasmid integrity. To further verify the two sequences of homology arms at the start position of gap repair mechanism, the obtained pBlueScript_CD64 plasmid was sent for Sanger sequencing analysis using SeqPrimer44 and T3 primers. The final plasmid map is shown in figure 13B, D.

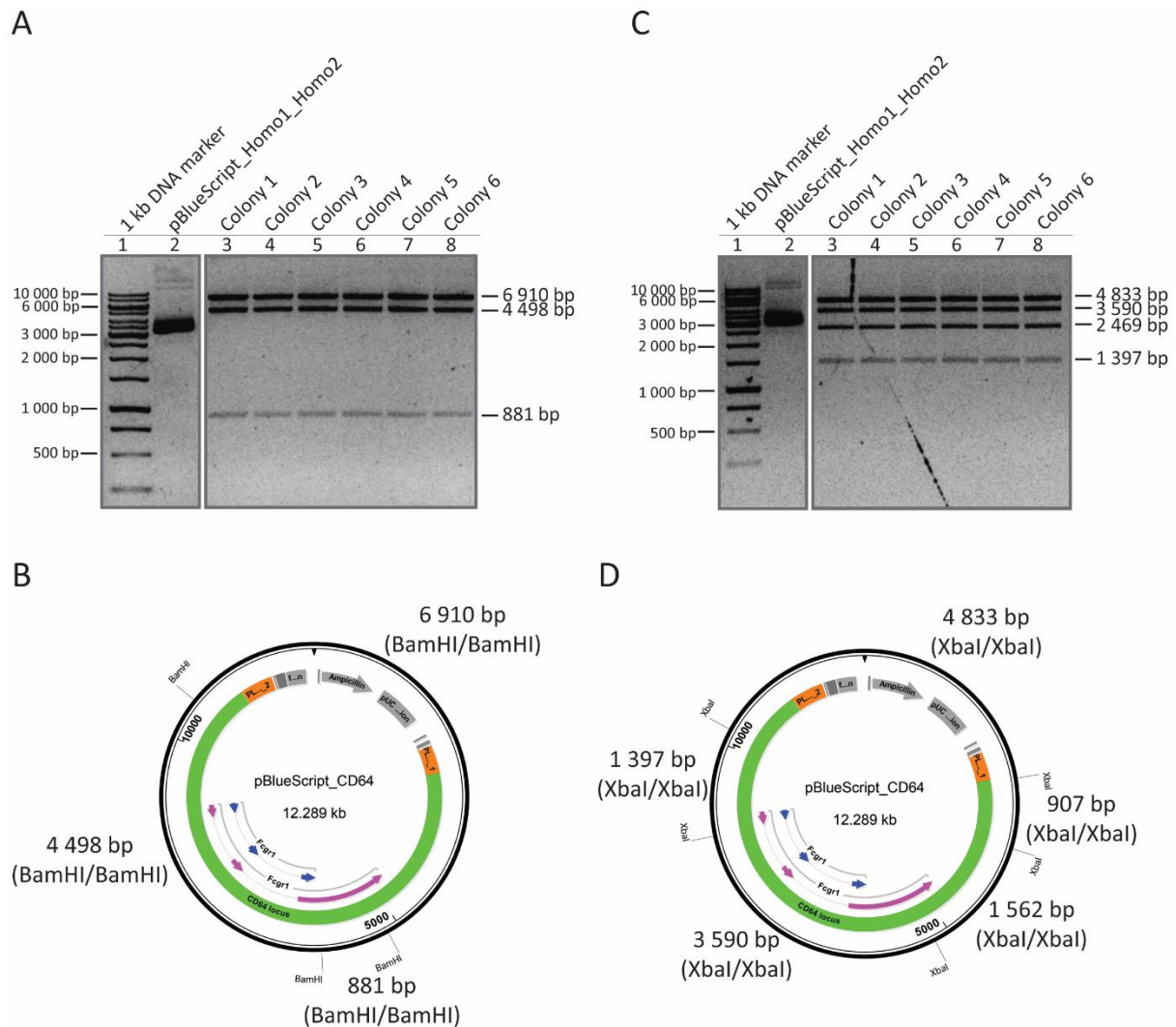


Figure 13. Generation of pBlueScript_CD64 plasmid.

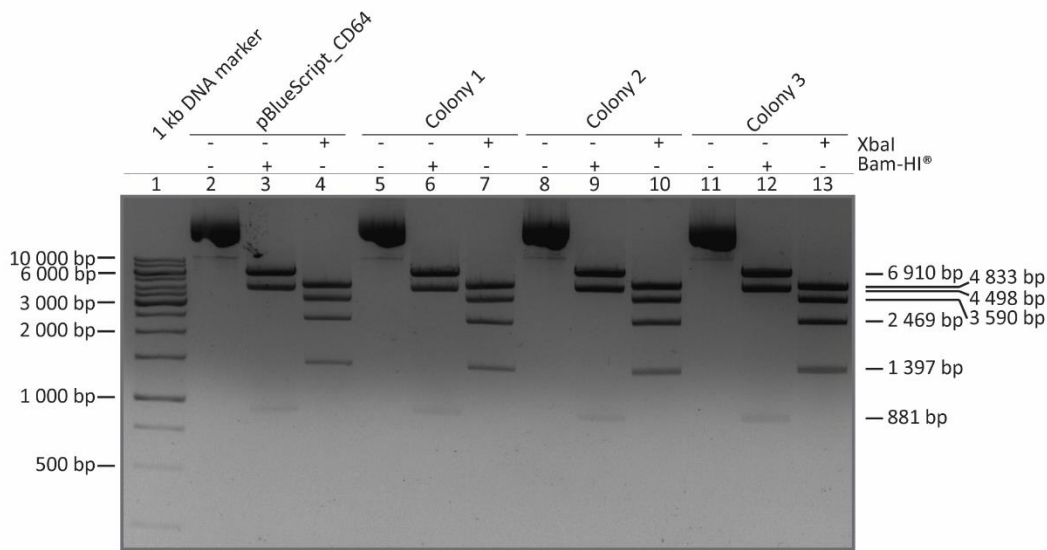
(A) Restriction digestion of pBlueScript_CD64 plasmid. Agarose gel electrophoresis image of 6 representative plasmid DNAs isolated from different colonies and BamHI-HF[®] digestion is shown (lane 3-8). All samples showed the expected fragment sizes of 881 bp, 4498 bp and 6910 bp. Marker (lane 1) and pBlueScript_Homo1_Homo2 plasmid (lane 2), used as a negative control, are indicated. (B) Plasmid map of pBlueScript_CD64. All BamHI-HF[®] restriction sites, to confirm the integrity of the plasmid, are indicated. The calculated fragment sizes after BamHI-HF[®] digestion of 881 bp, 4498 bp and 6910 bp are shown. (C) Restriction digestion of pBlueScript_CD64 plasmid. Agarose gel electrophoresis image of 6 representative plasmid DNAs isolated from different colonies and XbaI digestion is shown (lane 3-8). All samples showed the expected fragment sizes of 4833 bp, 3590 bp and 1397 bp. Instead of expected 907 bp and 1562 bp fragments, a 2469 bp fragment was found. Marker (lane 1) and pBlueScript_Homo1_Homo2 plasmid (lane 2), used as a negative control, are indicated. (D) Plasmid map of pBlueScript_CD64. All XbaI restriction sites, to confirm the integrity of the plasmid, are indicated. The calculated fragment sizes after XbaI digestion of 907 bp, 1397 bp, 1562bp, 3590 bp and 4833 bp are shown.

4.1.6. Synthesis of CD64-LSL-2A-DTR target vector

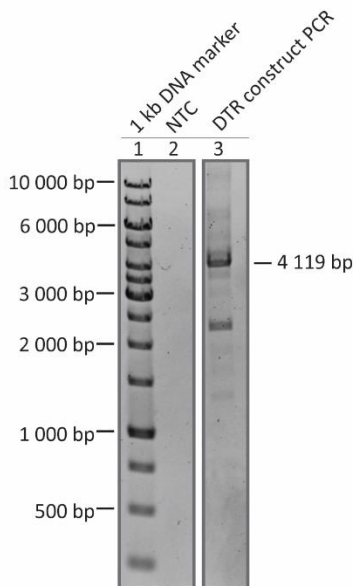
Using HR, the full length CD64-LSL-2A-DTR target vector was generated by insertion of the DTR construct from pBlueScript_LSL_2A_DTR_WPRE_Neo between the homology arms of pBlueScript_CD64. Therefore, first pBlueScript_CD64 plasmid was electroporated into EL350 cells and the integrity was verified by restriction digestion after plasmid isolation. As shown in figure 14A all digested plasmids showed the expected three fragments (6916 bp, 4498 bp and 881 bp) after BamHI-HF[®] digestion and four fragments (4774 bp, 3590 bp, 2469 bp and 1397 bp) after XbaI, thereby confirming that no rearrangements have occurred. Second, the DTR construct was amplified from pBlueScript_LSL_2A-DTR_WPRE_Neo plasmid (Fig. 14B) and the fragment (Fig. 14C) was purified and transformed for HR into EL350 cells harbouring validated pBlueScript_CD64 plasmid.

Results

A



B



C

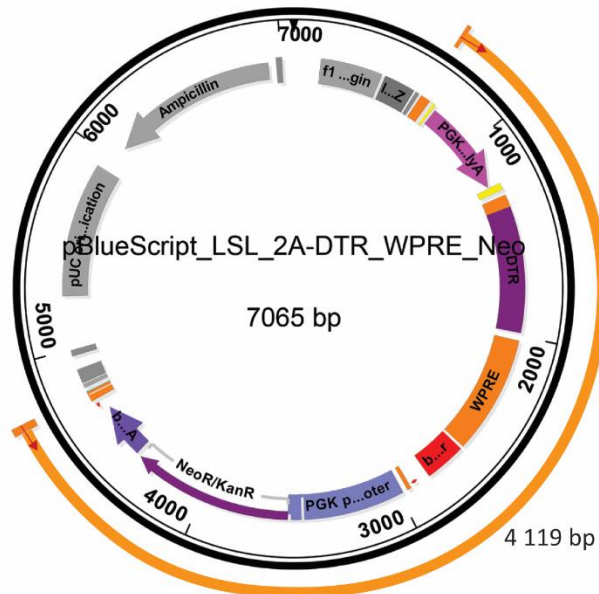


Figure 14. Verification of the transformed pBlueScript_CD64 plasmid.

(A) Restriction digestion of isolated pBlueScript_CD64 plasmid after transformation. A representative agarose gel electrophoresis image of plasmid DNAs isolated from different colonies is shown before and after BamHI-HF® (lane 6, 9, 12) or XbaI digestion (lane 7, 10, 13). All samples showed the expected fragment sizes of 881 bp, 4498 bp and 6910 bp for BamHI-HF® and 1397 bp, 2469 bp, 3590 bp and 4774 bp for XbaI. Marker (lane 1) and the original pBlueScript_CD64 plasmid (lane 2-4), used as a positive control, are indicated. (B) PCR of DTR construct fragment using DTR_Const Fwd and DTR_Const Rev. A representative agarose gel electrophoresis image is shown. The expected 4119 bp PCR product, marker (lane 1) and NTC (lane 2) are indicated. (C) Plasmid map of pBlueScript_LSL_2A-DTR_WPRE_Neo. The expected DNA construct of 4119 bp and amplification primers DTR_Const Fwd and Rev are indicated.

Results

Two colonies were picked and DTR construct integration between the homology arms was confirmed by PCR and restriction digestion. First, a colony screening PCR was performed. As shown in figure 15A, only one clone showed the desired DTR construct integration. This result was confirmed by specific single and double restriction digestions. As seen in figure 15C digestion with NotI-HF[®] resulted in the appearance of two bands, where one shows empty pBlueScript_CD64 and a second linearized plasmid with the expected size of 16305 bp, thereby confirming the successful integration. Additional digestion with NotI-HF[®] and EcoRV-HF[®] confirmed the correct orientation of the insert, due to the appearance of three additional bands below the linearized empty pBlueScript_CD64 plasmid band.

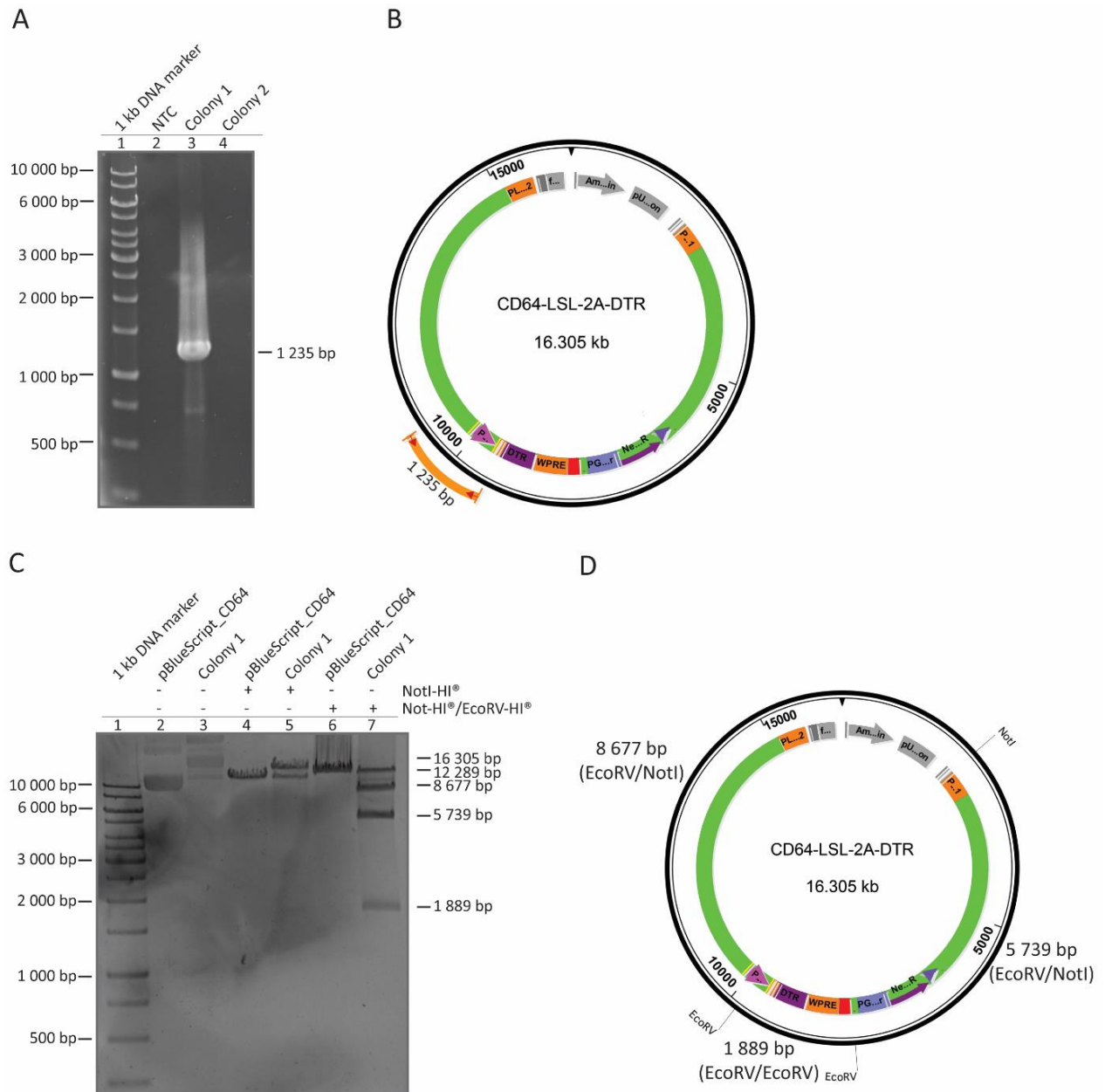


Figure 15. Verification of the generated CD64-LSL-2A-DTR plasmid.

(A) Colony screening PCR to confirm DTR construct knock-in into pBlueScreen_CD64 plasmid. A representative agarose gel electrophoresis image of the fragment obtained from all screened colonies (lane 3-4) is shown. The primer combination SeqPrimer2 and 8 (T_m 65 °C) was used to identify positive clones. Only colony 1 showed the expected fragment size of 1235 bp. Marker (lane 1) and NTC (lane 2) are indicated. (B) Plasmid map of CD64-LSL-2A-DTR target vector. The expected product of 1235 bp and amplification primers SeqPrimer 2 and 8 are indicated. (C) Restriction digestion of isolated CD64-LSL-2A-DTR plasmid. A representative agarose gel electrophoresis image of DNAs isolated from colony 1 is shown before (lane 3) and after NotI-HF[®] (lane 5) or NotI-HF[®]/EcoRV-HF[®] (lane 7) digestion. The colony 1 showed the expected fragment sizes of 1889 bp, 5739 bp, 8677 bp and 12289 bp. Marker (lane 1) and empty pBlueScript_CD64 plasmid (lane 2, 4, 6), used as negative control, are indicated. (D) Plasmid map of CD64-LSL-2A-DTR. All NotI-HF[®] and EcoRV-HF[®] restriction sites, to confirm the integrity of the plasmid, are indicated. The calculated fragments size after NotI-HF[®] digestion of 16305 bp and NotI-HF[®]/EcoRV-HF[®] digestion of 1889 bp, 5739 bp and 8677 bp are shown.

To separate the targeted pBlueScript_CD64 plasmid from the empty vector, the plasmids were isolated and transformed into Stbl2 cells. To exclude any colonies with multiple plasmid uptakes, isolated plasmid was double digested (Fig. 16). As shown in figure 16 plasmid isolation, that showed the expected bands, were further processed for Sanger sequencing to confirm integrity and to exclude any mutations, using the following primers: SeqPrimer 5-41, SeqPrimer 1-3 and SeqPrimer44. Finally, these data confirmed that the cloned CD64-LSL-2A-DTR target vector contained the desired sequence. After successful cloning of CD64-LSL-2A-DTR target vector it was sent to our collaborator Prof. Dr. Thorsten Buch in Switzerland for transgenic mouse generation using CRISPR-Cas9 technology.

Results

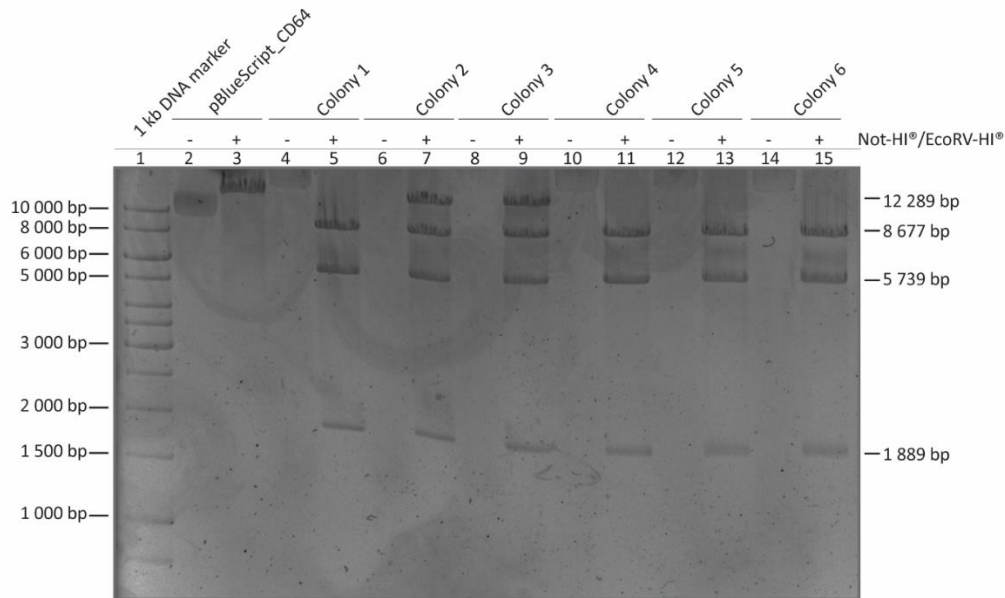


Figure 16. Screening of single event uptake in *Stbl2* for CD64-LSL-2A-DTR target vector.

Restriction digestion of isolated CD64-LSL-2A-DTR target vector after transformation into *Stbl2*. A representative agarose gel electrophoresis image of plasmid DNAs isolated from different colonies is shown before (lane 4, 6, 8, 10, 12, 14) and after NotI-HF[®]/EcoRV-HF[®] digestion (lane 5, 7, 9, 11, 13, 15). Plasmids from colonies 1 (lane 5), 4 (lane 11), 5 (lane 13) and 6 (lane 15) showed the expected fragment sizes of 1889 bp, 5739 bp, 8677 bp. Marker (lane 1) and the original empty pBlueScript_CD64 plasmid (lane 2-3), used as negative control, are indicated and showed the expected 12289 bp fragment.

4.1.7. PCR approach for detection of DTR construct integration into mouse genome

Due to the lack of a specific positive control to screen potential FM by PCR for DTR construct knock-in, I decided to mimic the existence of this sequence in the mouse genome by modifying the previously used wild type *CD64* locus containing CD64_BAC sequence. This was achieved by inclusion of the DTR construct into the existing *CD64* locus by HR. For this purpose, the previously generated CD64-LSL-2A-DTR target vector was linearized with *Xho*I and electroporated into CD64_BAC containing EL350 cells. To confirm the successful DTR construct integration, isolated plasmid was restriction digested (Fig. 17). Comparison between the original CD64_BAC and the modified BAC showed the same fragment pattern after *Swa*I digestion, indicating the integrity of the newly cloned CD64_DTRconstruct_BAC (Fig. 17A). Additionally, the integration of DTR construct was confirmed by *Kpn*I-HF[®] digestion. As expected the introduction of the additional *Kpn*I-HF[®] site led to the loss of the 17099 bp fragment and appearance of two 9635 bp and 11480 bp fragments instead (Fig.

Results

17A), compared to original CD64_BAC. Taken together, these results confirmed the successful generation of the desired positive control CD64_DTRconstruct_BAC.

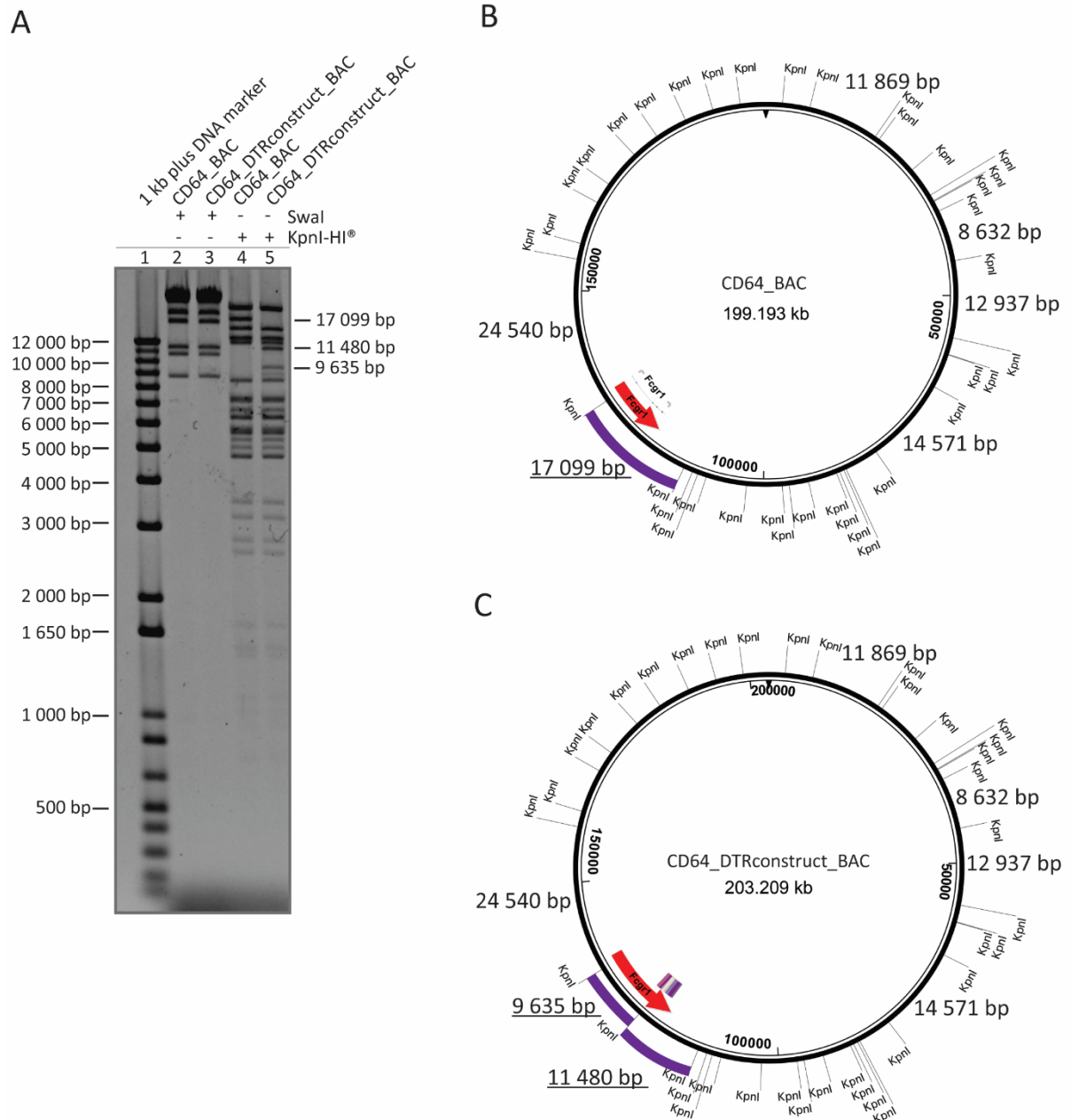


Figure 17. Generation of CD64_DTRconstruct_BAC.

(A) Restriction digestion of isolated BAC DNAs after HR. A representative agarose gel electrophoresis image of the comparison between isolated CD64_DTR (lane 2, 4) and CD64_DTRconstruct_BAC (lane 3, 5) after Swal or KpnI HF® digestion is shown. Marker (lane 1), the expected signature of 6 prominent fragments after Swal treatment and the expected 9635bp and 11480 bp products after KpnI-HF® digestion, confirming a positive DTR construct insertion, compared to the expected 17099 bp fragment for the empty BAC after KpnI-HF® digestion are indicated. (B) Plasmid map of CD64_BAC. All KpnI-HF® restriction sites and expected restriction fragments after KpnI-HF® digestion of 8632 bp, 11869 bp, 12937 bp, 14571 bp, 17099 bp and 24540 bp are indicated. (C) Plasmid map of CD64_DTRconstruct_BAC. All KpnI-HF® restriction sites and the expected restriction fragments after KpnI-HF® digestion of 8632 bp, 9635bp, 11480 bp, 11869 bp, 12937 bp, 14571 bp and 24540 bp are indicated.

Results

In order to confirm DTR construct integration and correct orientation into the genomic *CD64* locus for later FM screening, two PCR strategies, called 3'INS_PCR and 5'INS_PCR, were developed (Fig. 18A). To assure the quality of the isolated gDNA a third PCR assay, called WT_PCR, to amplify a product independent of integration or orientation (Fig 18A). Furthermore, to detect possible off targets, a fourth PCR (DTR_PCR), was designed to detect specifically any DTR gene integration independent from the targeted location (Fig. 18A). All PCR settings were tested and confirmed in advance using the previous generated positive control CD64_DTRconstruct_BAC, containing an integrated DTR construct within the *CD64* locus. As indicated in figure 18B, C, D all expected fragment sizes of 1992 bp, 4990 bp and 6021 bp were detected for each individual reaction, respectively.

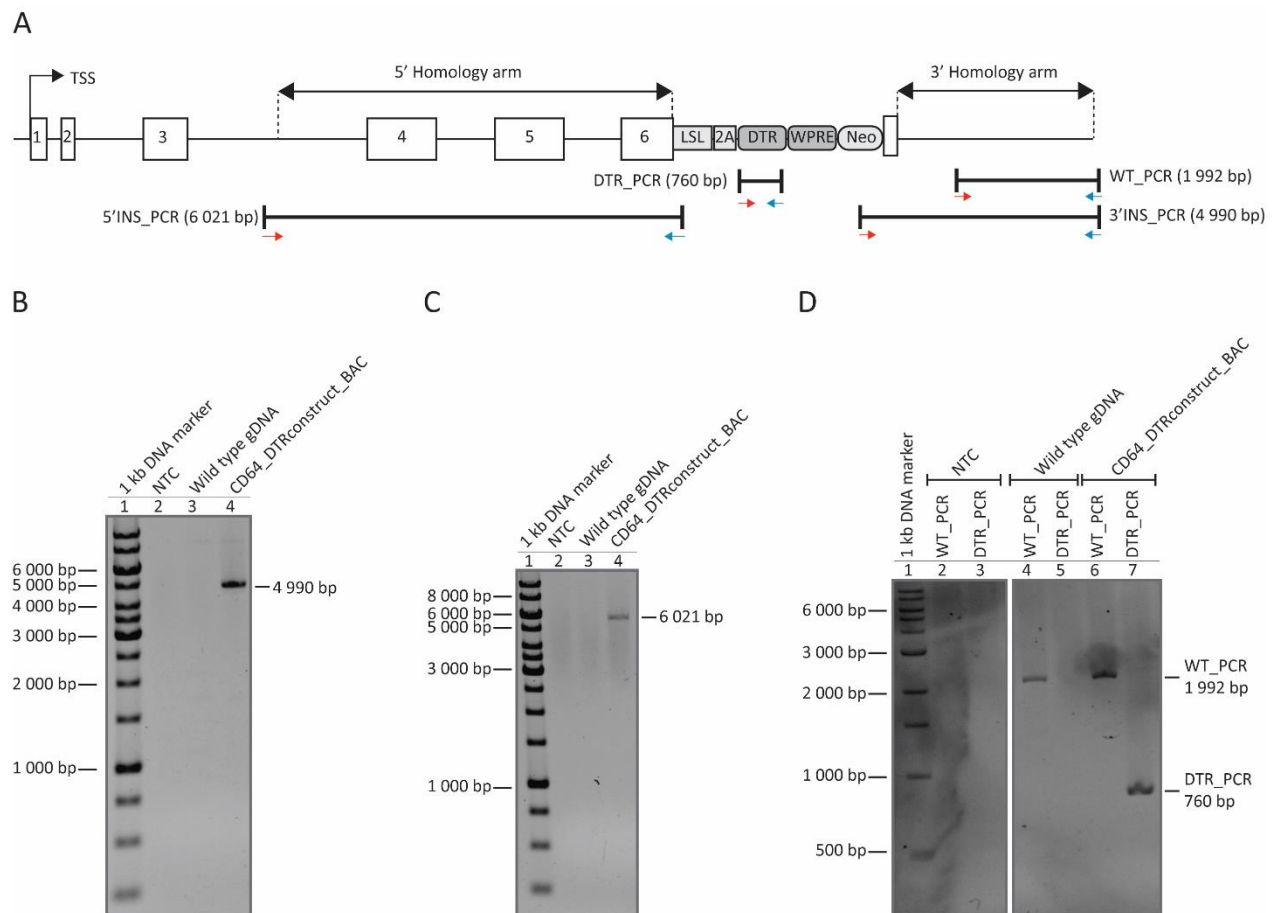


Figure 18. Establishment of positive control for DTR construct integration into genomic *CD64* screening to identify FM.

(A) PCR strategy to confirm successful DTR construct integration. A schematic diagram of the targeted *Mus musculus CD64* locus after DTR integration construct knock-in is shown. TSS represents the transcription start site. White boxes with numbers represent *CD64* gene exons. Grey boxes indicate the full length DTR construct, composed of LSL cassette, 2A sequence, *DTR* gene, *WPRE* sequence and Neo cassette, parts. The location of individual primers is indicated by arrows together with the resulting PCR fragment and name of the PCR. Double side arrows represent right and left homology arms, with the specific name, size and position in the *CD64* locus. The double side bar-head arrows indicate WT_PCR, 5'INS_PCR, DTR_PCR and 3'INS_PCR products. (B) 3'INS_PCR to confirm DTR construct integration and orientation into genome mouse DNA. A representative agarose gel electrophoresis image is shown. The primer combination SeqPrimer13 and CD64.1 ($T_m = 59^\circ\text{C}$) were used together with wild type genome mouse DNA (lane 3) or CD64_DTRconstruct_BAC (lane 4) and the expected fragment size of 4990 bp, marker (lane 1) and NTC (lane 2) are indicated. (C) 5'INS_PCR to confirm DTR construct integration and orientation into mouse gDNA. A representative agarose gel electrophoresis image is shown. The primer combination CD64.5 and CD64.6 ($T_m = 59^\circ\text{C}$) were used together with wild type mouse gDNA (lane 3) or CD64_DTRconstruct_BAC (lane 4) and the expected fragment size of 6021 bp, marker (lane 1) and NTC (lane 2) are indicated. (D) WT_PCR for quality control of the isolated mouse gDNA and DTR_PCR for the detection of off-target effects. A representative agarose gel electrophoresis image is shown. For WT_PCR the primer combination CD64.2 and CD64.1 ($T_m = 59^\circ\text{C}$) and for DTR_PCR SeqPrimer14 and SeqPrimer3 ($T_m = 59^\circ\text{C}$) were used together with wild type mouse gDNA (lane 4, 6) or RPCIB731E08452Q_DTR construct BAC (lane 5, 7), the expected fragment size of 1992 bp and 760 bp, marker (lane 1) and NTC (lane 2-3) are indicated.

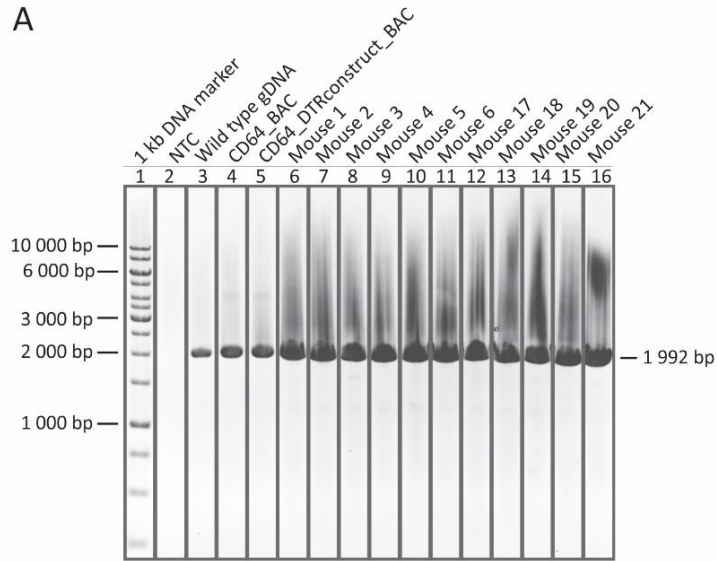
4.1.8. PCR based screening assay identified two FM based on DTR construct integration into their gDNA

After successful cloning of the CD64-LSL-2A-DTR target vector and application for CRISPR-Cas9 technology based knock-in, the generated mosaic offspring mice needed to be genotyped to ascertain the successful editing of the gene of interest. Therefore, previously established 3'INS_PCR, 5'INS_PCR, DTR_PCR and WT_PCR screening PCR assays were performed on gDNA isolated from ear biopsies. To ensure the quality of the PCR performance and to validate the correct size of the amplicons wild type mouse gDNA and CD64_BAC, containing the desired wild type *CD64* gene, were used as negative controls. Furthermore, the previously cloned CD64_DTRconstruct_BAC, containing the modified *CD64* locus, served as a positive control. Before the confirmation of DTR construct integration, all samples, passed through the quality control by WT_PCR application and demonstrated the appearance of a 1992 bp fragments (Fig. 19A), were further processed for DTR_PCR, 3'INS_PCR and 5'INS_PCR. The first pre-screening step using DTR_PCR analysis detected a knock-in within the genome of mouse 3, 21 and 4, as demonstrated by the presence of the expected fragment (Fig. 19B). To further exclude DTR construct insertion, independent from the targeted location, the 3'INS_PCR analysis was performed and identified only two mice out of the initial three, FM number 3 (FM3) and FM number 21 (FM21), bearing the successful DTR construct

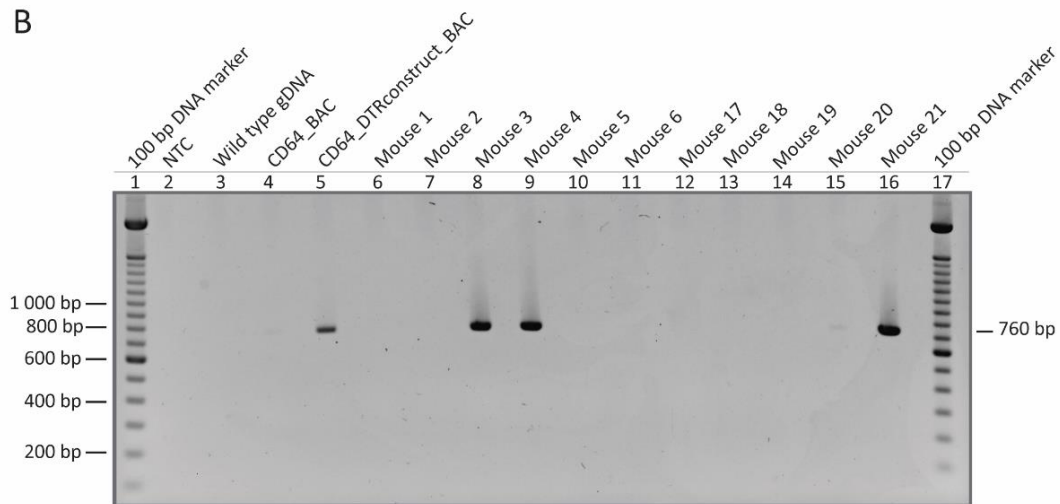
integration into their 3' *CD64* locus (Fig. 19C). Finally, these data were further confirmed by the use of 5'INS_PCR, which only shows a signal after integration of DTR construct in the 5' *CD64* locus (Fig. 19D). Since DTR_PCR confirmed that the genome of mouse 4 contained a *CD64* locus independent DTR construct integration (Fig. 19C), only gDNA from FM3 and FM21 was considered for the final verification of the successful knock-in by nonradioactive Southern blot, after they were used for line breeding.

Results

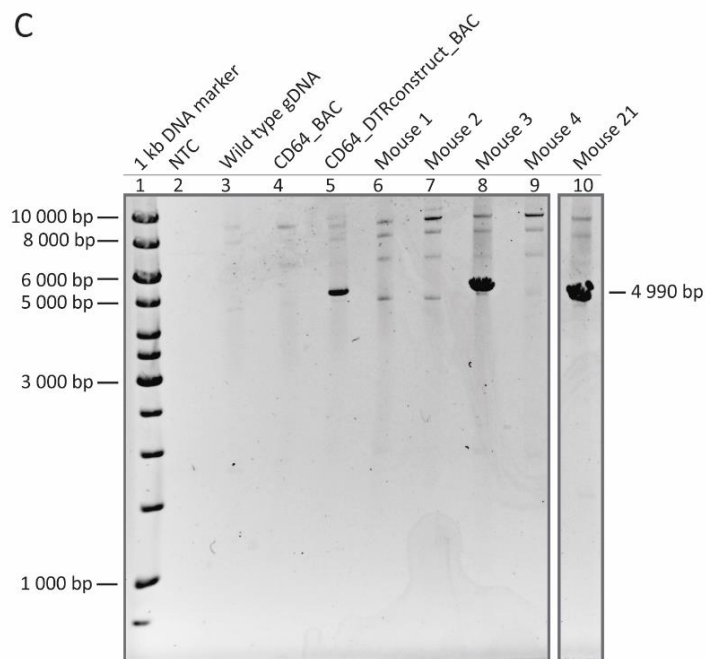
A



B



C



D

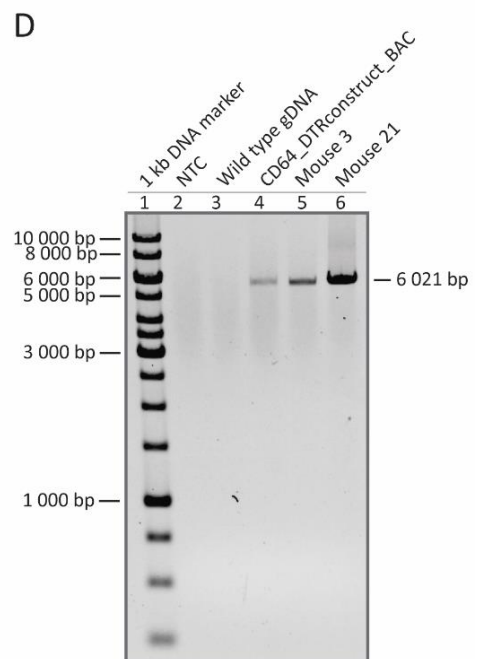


Figure 19. PCR analysis to identify FM.

(A) WT_PCR to confirm the isolated gDNA integrity. A representative agarose gel electrophoresis image is shown. CD64.1 and CD64.2 were used together with gDNA from possible FM to perform PCR analysis (lane 6-16). gDNA from a wild type mouse (lane 3) and CD64_BAC (lane 4) served as negative control, CD64_DTRconstruct_BAC (lane 5), served as positive control. The expected fragment size of 1992 bp, marker (lane 1) and NTC (lane 2) are indicated. (B) DTR_PCR for the detection of off-target effects. A representative agarose gel electrophoresis image is shown. SeqPrimer14 and SeqPrimer3 were used together with gDNA from possible FM to perform PCR analysis (lane 6-16). gDNA from a wild type mouse (lane 3) and CD64_BAC (lane 4) served as negative control, CD64_DTRconstruct_BAC (lane 5), served as positive control. The expected fragment size of 760 bp, marker (lane 1) and NTC (lane 2) are indicated. (C) 3'INS_PCR to confirm DTR construct insertion and orientation into mouse gDNA. A representative agarose gel electrophoresis image is shown. SeqPrimer13 and CD64.1 were used together with gDNA from three positive FM to perform PCR analysis (lane 8-10). gDNA from a wild type mouse (lane 3), CD64_BAC (lane 4) and gDNA from negative mice 1 (lane 6) and 2 (lane 7) served as negative controls, CD64_DTRconstruct_BAC (lane 5) served as positive control. The expected fragment size of 4990 bp, marker (lane 1) and NTC (lane 2) are indicated. (D) 5'INS_PCR to confirm DTR construct and orientation into mouse gDNA. A representative agarose gel electrophoresis image is shown. CD64.5 and CD64.6 were used together with gDNA from two positive FM to perform PCR analysis (lane 5-6). gDNA from a wild type mouse (lane 3) served as a negative control, CD64_DTRconstruct_BAC (lane 4) served as a positive control. The expected fragment size of 6021 bp, marker (lane 1) and NTC (lane 2) are indicated.

4.1.9. Generation of a specific Southern blot probe to detect DTR construct integration

As a second line of proof to verify the correct DTR construct integration into the gDNA of potential FM and to exclude possible off-targets like DNA rearrangements, a Southern blot strategy was planned additionally using two specific probes. Probe1 was designed to bind behind 3' homology arm and upstream of KpnI-HF[®] digestion site (Fig. 20). Another probe, called Neo, was chosen to recognise a sequence located inside the Neo cassette and to confirm the correct integration by the detection of 3' fragment (11480 bp) after KpnI-HF[®] digestion and 5' fragment (11224 bp) after PstI digestion (Fig. 20). With this strategy, it was possible to use Probe1 for the validation of the correct size and to distinguish between 3' part of wild type allele (18355 bp) and targeted allele (11480 bp) after KpnI-HF[®] digestion (Fig. 20).

Results

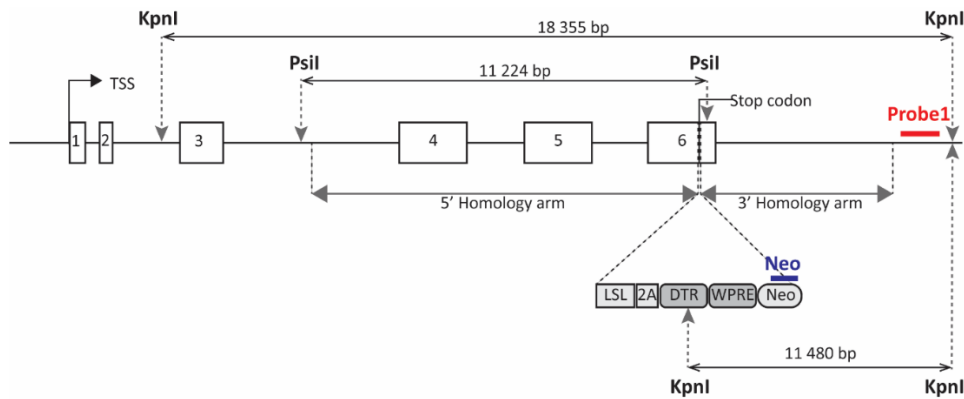


Figure 20. Schematic diagram of Southern blot strategy for the specific detection of DTR construct integration.

Southern blot strategy to confirm DTR construct integration into *CD64* using Probe1 and Neo probes. The location of Probe1 is indicated by the red bar together with the resulting fragment of 18355 bp after KpnI-HF[®] digestion of wild type gDNA and of 11480 bp after KpnI-HF[®] digestion of gDNA after DTR construct integration. Additionally, location of the Neo probe is indicated by a blue bar together with the resulting fragment of 11224 bp after PstI digestion of gDNA after DTR construct integration. White boxes represent *CD64* gene exons. Grey boxes indicate the full length DTR construct, composed of LSL cassette, 2A sequence, *DTR* gene, *WPRE* sequence and Neo cassette. 5' and 3' homology arms are illustrated by bold double side arrows. KpnI-HF[®] and PstI recognition sites are indicated. TSS- transcription start site.

To generate Probe1, a specific PCR was performed using CD64_BAC as a template (Fig. 21A). After A-tailing the PCR product was ligated into pGem-T vector resulting in pGem-T_Probe1 plasmid. Correct insert integration was confirmed by colony screening PCR and sequence integrity of positive clones was confirmed by Sanger sequencing with primers SeqPrimer42, SeqPrimer44-45.

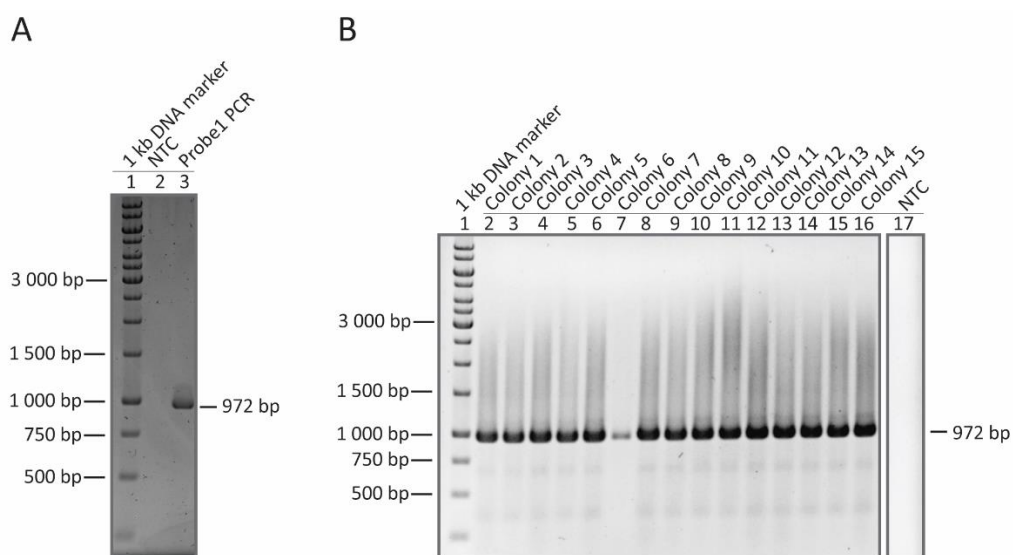


Figure 21. Cloning of Southern blot Probe1.

(A) PCR of Probe1 fragment using the primers Probe1.1 and Probe1.2. A representative agarose gel electrophoresis image is shown. The expected 972 bp PCR product, marker (lane 1) and NTC (lane 2) are indicated. (B) Colony screening PCR to confirm Probe1 sequence insertion into pGem-T. A representative agarose gel electrophoresis image of the fragment obtained from all screened colonies is shown (lane 2-16). The primer combination of Probe1.1 and Probe1.2 was used to identify the positive clones. All samples showed the expected fragment size of 972 bp. Marker (lane 1) and NTC (lane 17) are indicated.

The sequence of the second probe Neo was adopted from a published study²⁴ and captured from 195 FrtneoKanaFrt DTA plasmid (Fig. 22A) followed by the ligation into pGem-T vector resulting in pGem-T_Neo plasmid. To verify insert integration, a colony screening PCR was performed (Fig. 22B) and, that no mutations occurred, plasmids were sent for Sanger sequencing analysis along with SePrimer44 and SeqPrimer45 primers. In both cases mutation free plasmids were used for the probe synthesis.

Finally, these strategies ensured that the cloned pGem-T_Probe1 and pGEM-T_Neo plasmids contained the desired sequence for the following Probe1 and Neo probe synthesis and DIG labelling. As a quality control unlabelled and labelled PCR product was separated by electrophoresis and evaluated for a shift due to the DIG label (Fig. 22C).

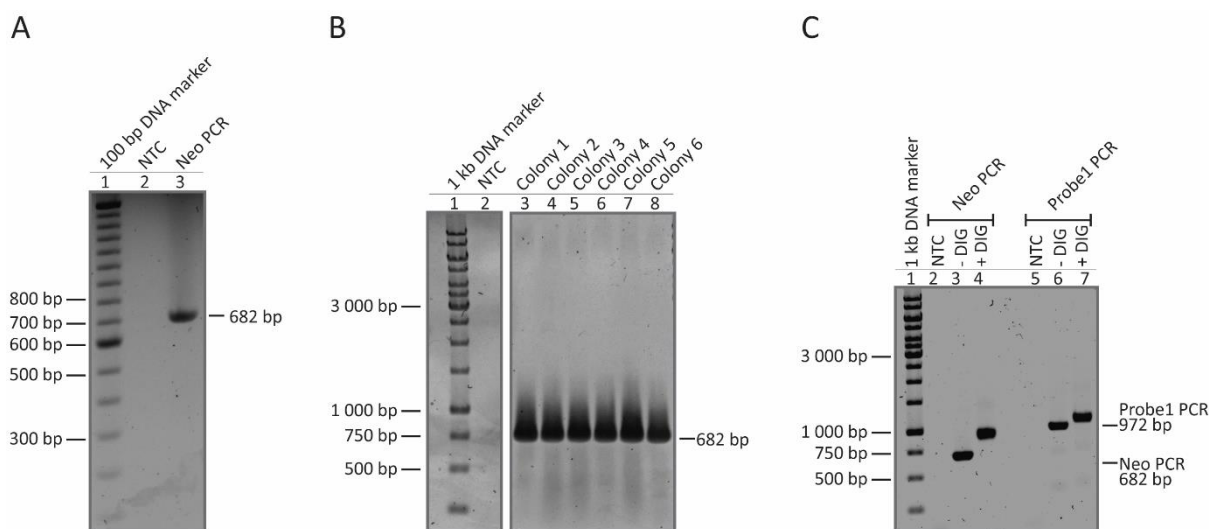


Figure 22. Cloning of Southern blot probe Neo probe and quality control of DIG labelled probes.

(A) PCR of Neo fragment using primers Neo1 and Neo2. A representative agarose gel electrophoresis image is shown. The expected 682 bp PCR product, marker (lane 1) and NTC (lane 2) are indicated. (B) Colony screening PCR to confirm Neo sequence insertion into pGem-T. A representative agarose gel electrophoresis image of fragment obtained from all screened colonies (lane 3-8) is shown. The primer combination Neo1 and Neo2 was used to identify positive clones. All samples showed the expected fragment size of 682 bp. Marker (lane 1) and NTS (lane 2) are indicated. (C) Agarose gel electrophoresis of PCR-labelled Neo and Probe1 fragments. A representative agarose gel electrophoresis image is shown. The expected unlabelled 682 bp and 972 bp and labelled products, marker (lane 1) and NTC (lane 2) are indicated. Labelled probes (lane 4, 7) demonstrated a higher molecular weight than the unlabelled products (lane 3, 6).

4.1.10. Southern blot analysis confirmed successful *CD64* gene editing for two CD64-LSL-2A-DTR FM

To further exclude possible undetected off-targets and DNA rearrangements in the *CD64* locus of FM3 and FM21 a nonradioactive Southern blot was performed on genomic DNA. A wild type mouse gDNA served as a negative control. For the positive control, wild type mouse gDNA was spiked with the modified CD64_DTRconstruct_BAC, containing the desired *CD64* locus. The amount of the spiked BAC was calculated in a way to ensure that it contained the same amount of *CD64* gene copy numbers as the expected single copy amount of the modified *CD64* of FM gDNA used for the screening. Southern blot analysis using Neo probe confirmed the knock-in of the desired DTR construct into the 5' *CD64* locus (Fig. 23A). However, a small shift in the band size was observed in both samples compared to the positive control (Fig. 23B). Moreover, Southern blot analysis from the gDNA samples obtained from FM21 identified an additional shorter band at approximately 10000 bp, below the expected band size of 11480 bp, which appeared exclusively after KpnI-HF[®] restriction digestion. Nevertheless, utilization of the second probe Probe1, which hybridizes with the same DNA fragment as the Neo probe (Fig. 20), resulted in the detection of fragments with the expected size (Fig. 23C). In addition, it needs to be mentioned that the knock-in and wild type bands of the gDNA of FM3 were slightly higher running. However, due to this worth mentioning difference between the artificial positive control CD64_DTRconstruct_BAC and the murine gDNA, we assumed at this point a successful DTR knock-in for these samples and included FM3 to be still valid to proceed together with FM21 for the further verification and establishment of the new mouse line.

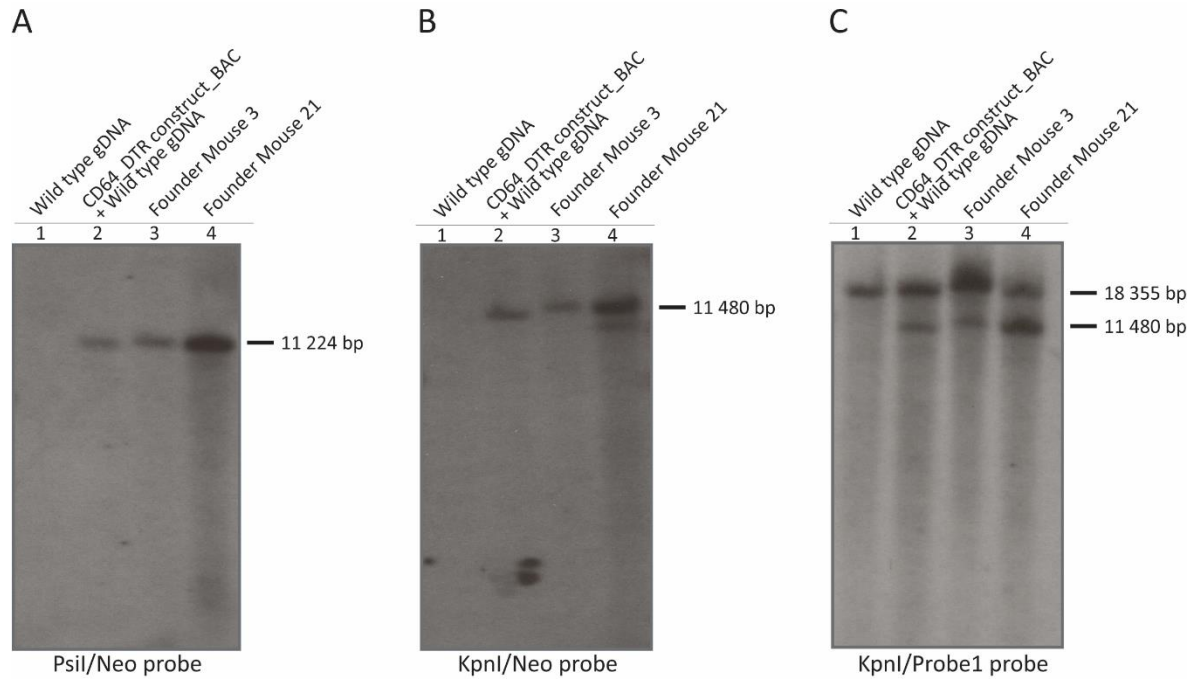


Figure 23. Southern blot analysis of gDNA isolated from FM.

(A) Southern blot to confirm DTR construct integration into 5' *CD64* gene. gDNA from FM3 and FM12 was digested with *Pst*I and further proceed for Southern blot analysis. A representative film after exposure is shown. DIG labelled probe Neo was used together with gDNA from FM3 (lane 3) and FM21 (lane 4) to perform the analysis. gDNA from wild type mouse (lane 1) served as negative control and CD64_DTRconstruct_BAC mixed with wild type gDNA (lane 2) served as a positive control. The expected fragment size 11224 bp is indicated. (B) Southern blot to confirm DTR construct integration into 3' *CD64* gene. gDNA from FM3 and FM21 was digested with *Kpn*I-HF® and further processed for Southern blot analysis. A representative film after exposure is shown. DIG labelled probe Neo was used together with gDNA from FM3 (lane 3) and FM21 (lane 4) to perform the analysis. gDNA from wild type mouse (lane 1) served as negative control and CD64_DTRconstruct_BAC mixed with wild type gDNA (lane 2) served as a positive control. The expected fragment size of 11480 bp is indicated. (C) Southern blot to confirm DTR construct integration into 3' *CD64* gene. gDNA from FM3 and FM21 was digested with *Kpn*I-HF® and further processed for Southern blot analysis. A representative film after exposure is shown. DIG labelled probe Probe1 was used together with gDNA from two positive FM (FM3 and FM21) (lane 3-4) to perform the analysis. gDNA from wild type mouse (lane 1) served as negative control and CD64_DTRconstruct_BAC mixed with wild type gDNA (lane 2) served as a positive control. The expected fragment sizes of 11480 bp and 18355 bp are indicated.

4.1.11. CD64-LSL-2A-DTR target vector integration into *CD64* locus did not affect CD64 protein expression

After successful confirmation, that the DTR construct was integrated into the *CD64* locus, it became necessary to exclude if the genetic manipulations of the *CD64* locus done so far together with the planned Cre excision of LSL cassette, had not affected CD64 expression level of the targeted cell population. To proceed in this regard, first offspring of both CD64-LSL-2A-DTR FM lines were crossed with Cre recombinase caring *Clec9a-Cre* mice²⁴ to enable the excision of the LSL cassette in these animals. Afterwards, renal leukocytes isolated from the

Results

obtained F1 generation mice, caring Cre and DTR knock-in, were stained against surface markers and analysed by FACS. As a positive control renal leukocytes from a wild type *CD64* locus caring *Clec9a*-Cre mouse was used. To get a valid read out of CD64 expression it was necessary to select first the cell population of interest independent of CD64. This was achieved by the use of F4/80 surface marker, because it is well established that the application of F4/80 surface glycoprotein can be used as a replacement of CD64 marker to identify CD64⁺ cells^{17,24,124}. With this strategy it was possible to prevent any falsification or misinterpretation of the final CD64 protein expression levels. The detailed gating strategy to identify renal CD64⁺ cells is shown in figure 24A.

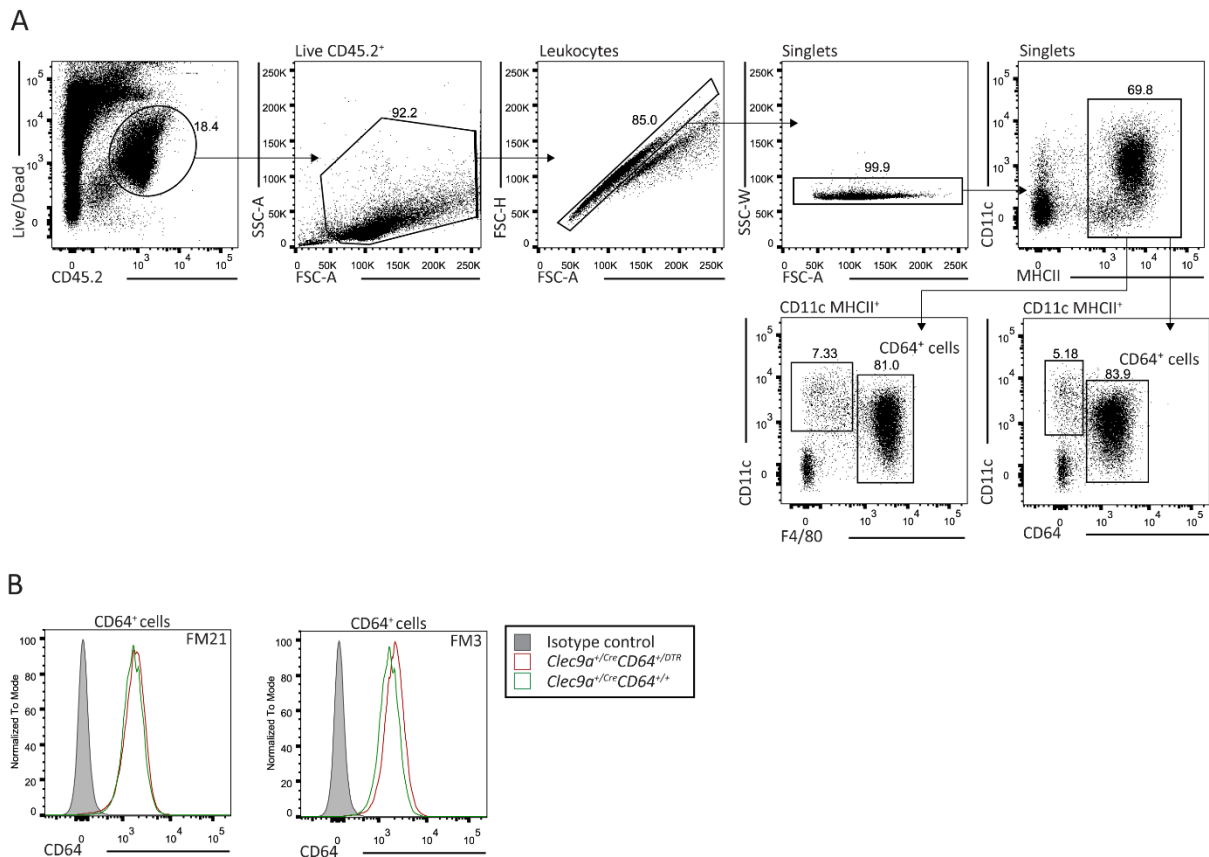


Figure 24. CD64 expression is not altered in *Clec9a*^{+/Cre}*CD64*^{+/DTR} mice compared to *Clec9a*^{+/Cre}*CD64*^{+/+} mouse. (A) Flow cytometry gating strategy to identify renal CD64⁺ cells (liveCD45.2⁺CD11cMHCII⁺CD64⁺ and liveCD45.2⁺CD11cMHCII⁺F4/80⁺). Cells from kidney in *Clec9a*^{+/Cre}*CD64*^{+/+} mice were stained with antibodies against indicated cell surface markers. The numbers in the dot plots indicate the percentages of the cells within the indicated gates. (B) Histogram overlay of CD64 expression on renal CD64⁺ cells (liveCD45.2⁺CD11cMHCII⁺F4/80⁺). The histograms for CD64 expression on renal CD64⁺ cells from FM3 and FM21 mouse line *Clec9a*^{+/Cre}*CD64*^{+/DTR} mice (red line box), *Clec9a*^{+/Cre}*CD64*^{+/+} mice (green line box) and isotype control (grey box) are indicated.

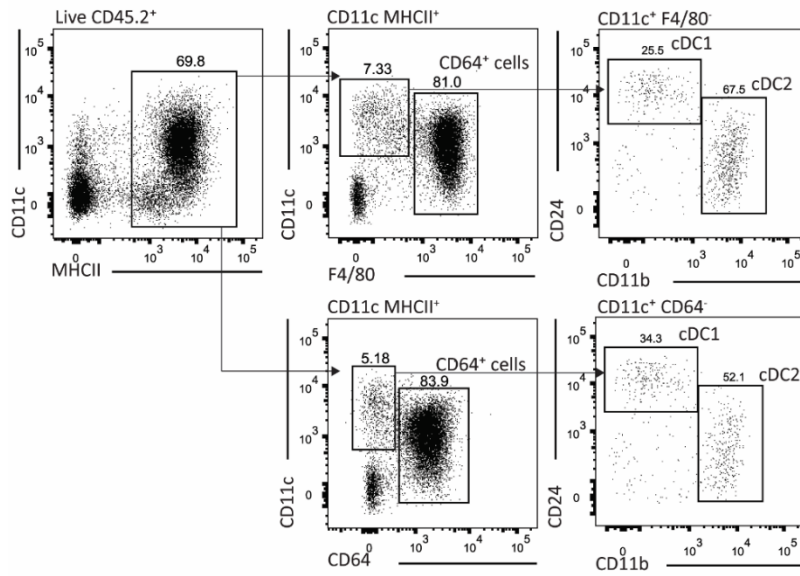
As shown in figure 24B, the subsequent CD64 expression analysis from *Clec9a^{+/-Cre}CD64^{+/-DTR}* mouse samples revealed, that CD64 receptor was highly expressed on renal CD64⁺ cells (liveCD45.2⁺CD11cMHCII⁺F4/80⁺), coming from both FM21 and FM3 lines. Moreover, the CD64 expression, independent of FM line, was comparable to the data obtained from the *Clec9a^{+/-Cre}CD64^{+/-+}* mouse sample, indicating that neither DTR construct integration behind CD64 gene, nor the expected LSL cassette excision did affect CD64 protein expression. Therefore, both FM lines were proceeded for further validation.

4.1.12. DTR expression on renal CD64⁺ cells from *Clec9a-Cre* x *CD64-LSL-2A-DTR* mice is not detectable by FACS

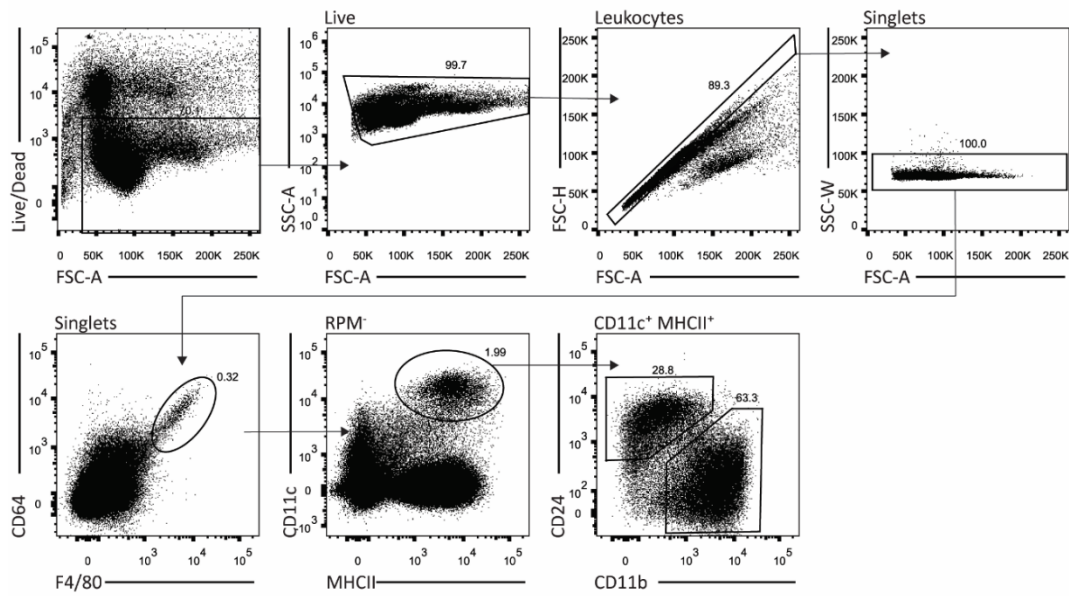
I next examined whether DTR was expressed on renal CD64⁺ cells coming from both FM21 and FM3 breeding mouse lines. Similar to the before described FACS approach, F4/80 and CD64 surface markers were used to first identify renal CD64⁺ cells, which were subsequently used for DTR expression analysis. The detailed gating strategy is indicated in figure 24A. As a positive control for DTR staining on renal CD64⁺ cells, renal and splenic cDC1 from a *Clec9a-Cre* x *Rosa26-iDTR* mouse were used, because of the genetic similarity to the new *Clec9a-Cre* x *CD64-LSL-2A-DTR* mouse model. Moreover cDC1 offer the advantage, that these cells express CLEC9A in their mature stage, which results in 95-100% prospective DTR⁺ cDC1 in the used *Clec9a-Cre* x *Rosa26-iDTR* mouse model^{24,204}. The detailed gating strategies to identify renal and splenic cDC1 populations is shown in figure 25A and 25B. It need to be noted, that this double strategy was chosen to ensure validation of DTR staining, because previous DTR staining on fresh cell isolations from renal tissue showed regularly a weaker DTR FACS signals compared to freshly isolated splenic probes as shown in figure 25C. However, these expression data were obtained from other mouse model and could not be automatically transferred to the situation in the new *Clec9a-Cre* x *CD64-LSL-2A-DTR* model.

Results

A



B



C

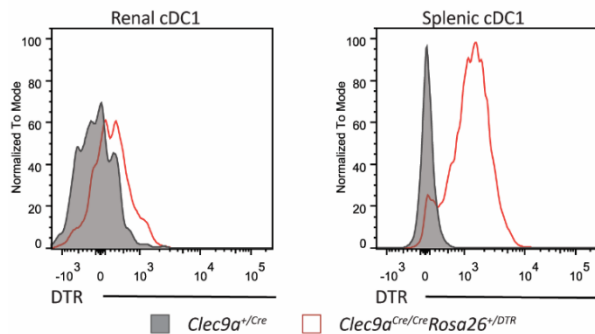


Figure 25. DTR expression on renal cDC1 from *Clec9a^{Cre/Cre}Rosa26^{+DTR}* mice.

(A) Flow cytometry gating strategy to identify renal cDC1 (liveCD45.2⁺MHCII⁺CD11c⁺CD64⁻CD24⁺CD11b⁻ and liveCD45.2⁺MHCII⁺CD11c⁺F4/80⁻CD24⁺CD11b⁻), cDC2 (liveCD45.2⁺MHCII⁺CD11c⁺CD64⁻CD24⁻CD11b⁺ and F4/80⁻CD24⁻CD11b⁺). Cells from kidney in *Clec9a^{+Cre}CD64^{+/+}* mice were stained with antibodies against indicated cell surface markers. The numbers in the dot plots indicate the percentages of the cells within the indicated gates. (B) Flow cytometry gating strategy to identify splenic red pulp MØs (RPM) (live⁺CD64⁺F4/80⁺), cDC1 (liveRPM⁻MHCII⁺CD11c⁺CD24⁺CD11b⁻) and cDC2 (liveRPM⁻MHCII⁺CD11c⁺CD24⁻CD11b⁺). Cells from spleen were stained with antibodies against indicated cell surface markers. The numbers in the dot plots indicate the percentages of the cells within the indicated gates. (C) Histogram overlay of DTR expression on cDC1. The histograms for DTR expression on splenic cDC1 and renal cDC1 (liveCD45.2⁺CD11c⁺MHCII⁺CD64⁻CD11b⁻CD24⁺) from *Clec9a^{Cre/Cre}Rosa26^{+DTR}* mouse (red line box) and *Clec9a^{+Cre}* mouse (grey box) are indicated.

Unfortunately, also for these samples DTR expression was not detected on renal CD64⁺ cells by flow cytometry (Fig. 26A). Similarly, the DTR control staining performed on isolated renal cDC1 from a *Clec9a-Cre* x *Rosa26-iDTR* mouse showed a negative result (Fig. 26B). Nevertheless, we were still able to verify with splenic control the efficacy of the DTR staining, because usage of splenic cDC1 from the same mouse still resulted in a slight positive shift in the FACS analysis (Fig. 26B). The lower expression compared to freshly isolated splenic samples shown in figure 25C can be most likely explained, by the suboptimal conditions caused by the originated time delay between tissue removal, isolation and analysis caused by tissue transport, since the experiment was not performed inwards. However, this inconsistent data did not allow final concluding evidence of DTR expression at this point.

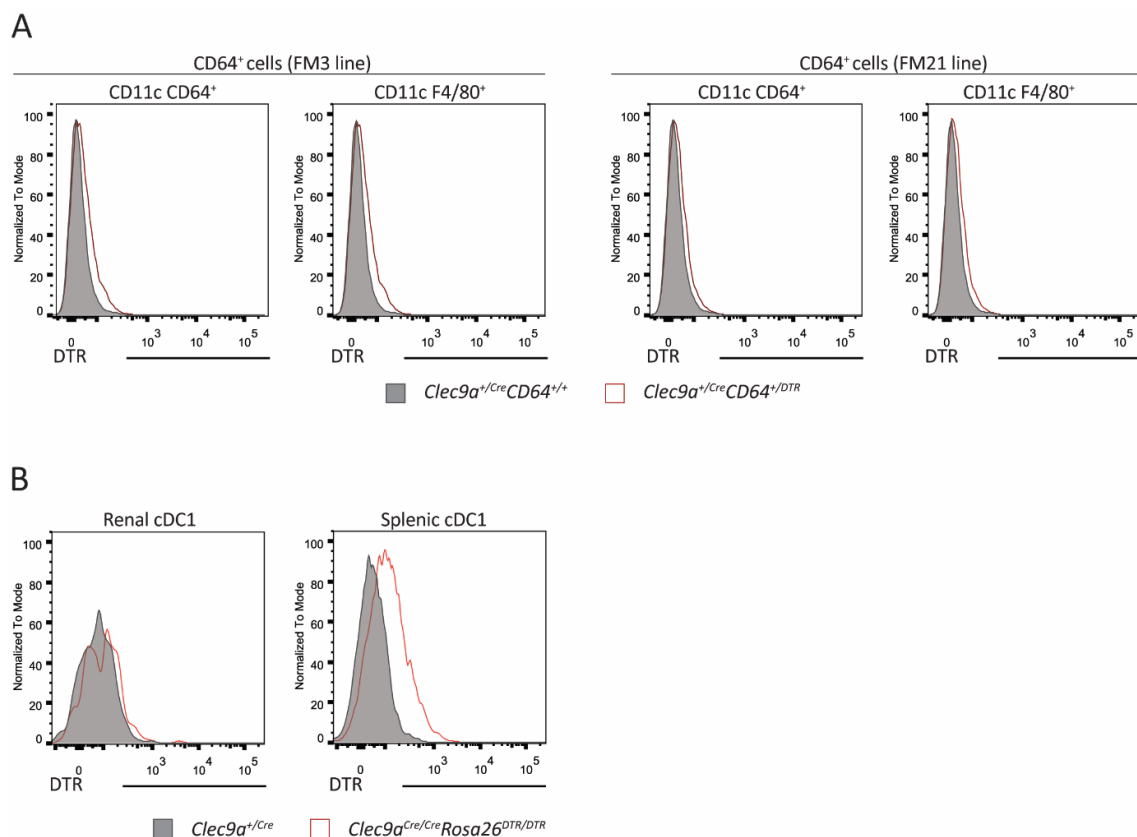


Figure 26. DTR expression on renal CD64⁺ cells from *Clec9a^{+/Cre}CD64^{+/DTR}* mice.

(A) Histogram overlay of DTR expression on renal CD64⁺ cells (liveCD45.2⁺CD11cMHCII⁺F4/80⁺ and liveCD45.2⁺CD11cMHCII⁺CD64⁺). The histograms for DTR expression on renal CD64⁺ cells from FM3 and FM21 mouse line *Clec9a^{+/Cre}CD64^{+/DTR}* mice (red line box) and *Clec9a^{+/Cre}* mice (grey box) are indicated. (B) Histogram overlay of DTR expression on cDC1. The histograms for DTR expression on splenic cDC1 and renal cDC1 (liveCD45.2⁺CD11c⁺MHCII⁺CD64⁺CD11b⁺CD24⁺) population from *Clec9a^{Cre/Cre}Rosa26^{DTR/DTR}* mouse (red line box) and *Clec9a^{+/Cre}* mice (grey box) are indicated.

4.1.13. CD64-LSL-2A-DTR target vector integration into *CD64* locus did not cause frame shift

To excluded at this point that the before observed absence of DTR expression on renal CD64⁺ cells is not caused by unwanted and undetected genomic sequence mutations occurred during the knock-in. Therefore, a more detailed *CD64* locus sequence analysis was performed. A specific region, starting within the 6th exon of *CD64* spanning the 5' loxP site in front of the DTR gene, and part of the poly(A) sequence was amplified by PCR (Fig. 27) using gDNA. gDNA from both FM showed the expected fragment, which was sent for Sanger sequencing analysis together with CD64.4 and SeqPrimer36 primers. This strategy confirmed the mutation free integrity of the targeted region for both FM and excluded the possibility to fail successful *CD64* induced DTR expression due to a frame shift within this region.

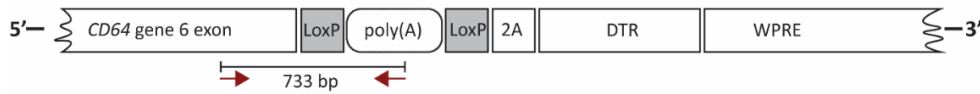


Figure 27. Insertion of the transgenic *CD64* segment did not cause frame shift.

PCR strategy to exclude frameshift caused by DTR construct integration. A schematic diagram of a section comprised of the targeted *Mus musculus CD64* locus, after DTR construct integration, is shown. White boxes represent *CD64* gene exon, poly(A), 2A sequence, *DTR* gene and a part of WPRE sequence. Grey boxes indicate loxP sequence. The location of the individual primers CD64.4 and SeqPrimer36 are indicated by arrows together with the resulting PCR fragment.

4.1.14. Cre recombinase removes LSL cassette allowing DTR expression in Clec9a-Cre x CD64-LSL-2A-DTR mice

As the analysis of *CD64* region in *Clec9a^{+/Cre}CD64^{+/DTR}* mice coming from both FM lines confirmed the absence of any unwanted mutations, next I determined if the LSL cassette was excised by Cre. To confirm LSL excision, which is required for successful DTR expression, gDNA from renal percoll enriched leukocytes was isolated from *Clec9a^{+/Cre}CD64^{+/DTR}* mice, originated from both FM lines and investigated by PCR, described in figure 28A. This PCR was designed to span the complete LSL cassette, resulting in fragment of 1100 bp, representing a full-length LSL cassette, or a 573 bp product, representing the excised LSL. As a negative control gDNA from both FM3 and FM21 was used, which were known to be Cre⁻. As expected, the data confirmed the presence of the additional 573 bp PCR products for the samples isolated from the F1 generation Clec9a-Cre x CD64-LSL-2A-DTR mouse lines compared to their parental probes from FM3 and FM21. These data clearly demonstrated that Cre recombinase was capable to remove the LSL cassette successfully as a requirement for later DTR gene expression within the renal leukocyte fraction of Clec9a-Cre x CD64-LSL-2A-DTR mice (Fig. 28B).

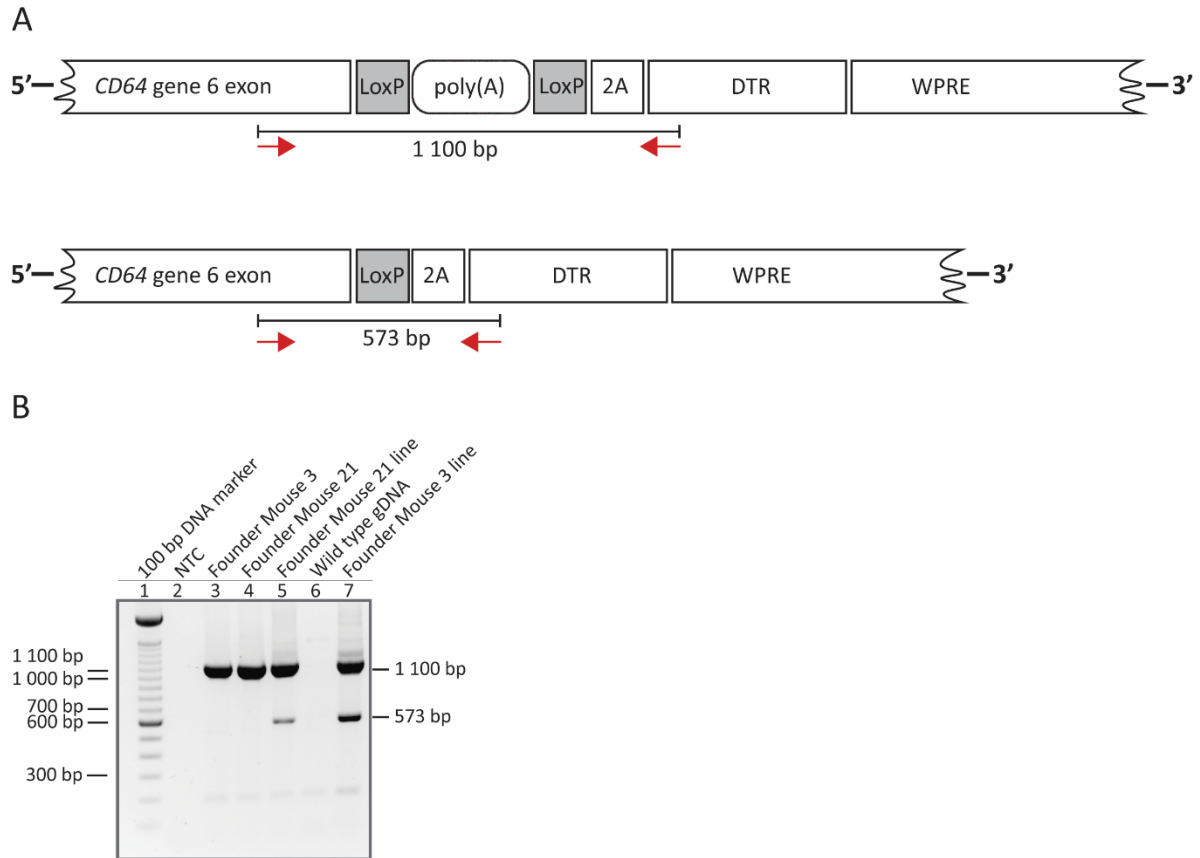


Figure 28. Confirmation of successful LSL cassette excision in enriched Clec9a-Cre x CD64-LSL-2A-DTR mouse renal leukocytes.

(A) PCR strategy to assess LSL cassette excision. A schematic diagram of a section comprised of the targeted *Mus musculus CD64* locus, after DTR construct integration, is shown. White boxes represent *CD64* gene exon, poly(A), 2A sequence, *DTR* gene and a part of *WPRE* sequence. Grey boxes indicate LoxP sequences. The location of the individual primers CD64.4 and SeqPrimer2 in the LSL cassette are indicated by red arrows. The resulting PCR fragments are indicated for the full length LSL cassette (1100 bp, upper panel) or after LSL cassette excision (573 bp, lower panel) as double side bar-head arrows. (B) PCR to confirm LSL cassette excision. A representative agarose gel electrophoresis image is shown. Primer combination of CD64.4 and SeqPrimer2 (T_m 61 °C) was used together with gDNA from two Clec9a-Cre x CD64-LSL-2A-DTR mice (lane 5, 7) to perform the analysis. gDNA from a wild type mouse (lane 6) and gDNA from FM21 and FM3 lines (lanes 3 and 4) served as negative controls. Marker (lane 1), NTC (lane 2) and the expected fragment sizes of 1100 bp and 573 bp are indicated.

4.1.15. Application of DT caused specific ablation of CLEC9A⁺ progenitor derived CD64⁺ cells in Clec9a-Cre x CD64-LSL-2A-DTR mice

After completion of the detailed genomic analysis of the *CD64* locus integrity of both FM lines and the finding, that the DTR construct was successfully integrated into the *CD64* gene without any frameshift or mutation potentially affecting DTR expression I decided to proceed with cell depletion experiment for Clec9a-Cre x CD64-LSL-2A-DTR mice verification. Two groups of *Clec9a^{+/Cre}CD64^{+/DTR}* mice, coming from FM3 line, were treated separately twice

Results

with DT or PBS as negative control and analyzed 48 h after the first injection for the presence of renal CD64⁺ cells. F4/80 surface markers were used to identify renal CD64⁺ cells, using the same gating strategy as in figure 24A. As demonstrated, the analysis of CD64⁺ cells identified as liveCD45.2⁺CD11cMHCII⁺F4/80⁺ cells (Fig. 29A), revealed a significant depletion of this population in the kidney of the DT treated animals, as shown by the reduction in frequency and the absolute cell numbers (Fig. 29B). As a second line of proof another part of the samples was used in an independent staining approach to detect CD64⁺ cells as liveCD45.2⁺CD11cMHCII⁺CD64⁺ cells. Again these data revealed that these CD64⁺ cells from the DT treated animals, were also significantly ablated (Fig. 29C, D).

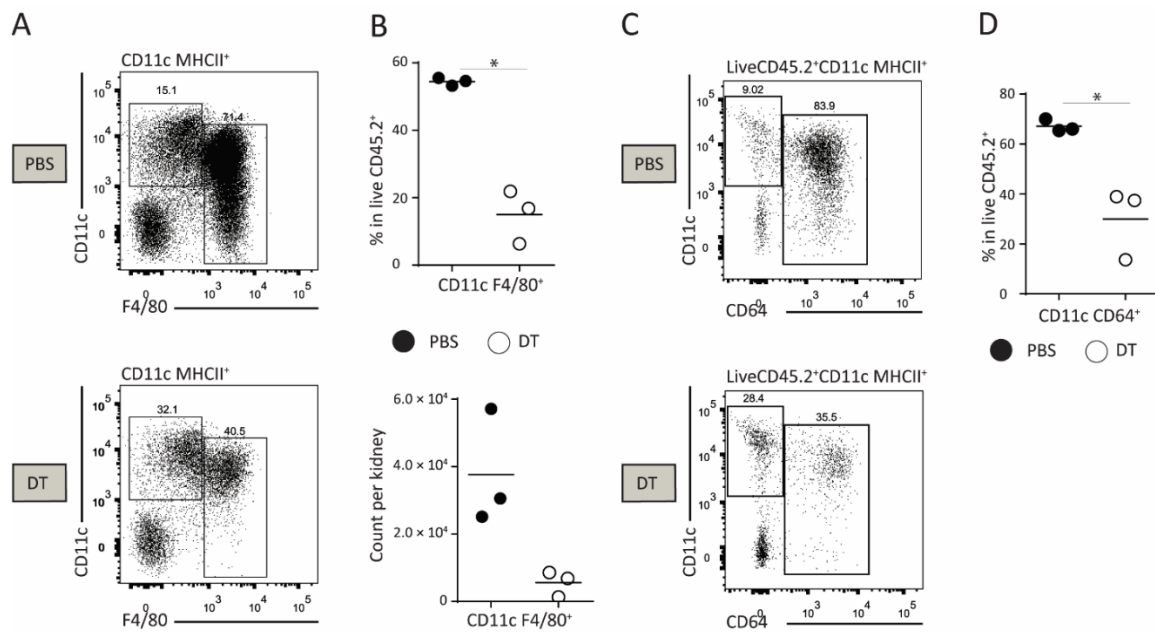


Figure 29. Depletion of renal CD64⁺ cells in Clec9a-Cre x CD64-LSL-2A-DTR mice.

(A) Depletion of CD64⁺ cells (liveCD45.2⁺CD11cMHCII⁺F4/80⁺) after DT treatment in Clec9a-Cre x CD64-LSL-2A-DTR mice. *Clec9a^{+/Cre}CD64^{+/DTR}* mice were treated i.p. twice 24 h apart, with DT (25 ng/g body weight) or PBS and one day after injections renal cells were stained using antibodies against surface markers as indicated figure 24A. Upper panel shows percentage of cell populations within the indicated gates in the group treated with PBS and the lower panel shows percentage in the DT treated group. (B) Analysis of renal CD64⁺ population in *Clec9a^{+/Cre}CD64^{+/DTR}* mice injected with PBS or DT. Total number and percentage with in the liveCD45.2⁺ cells per kidney is shown. Each symbol represents one mouse. (C) Depletion of CD64⁺ cells (liveCD45.2⁺CD11cMHCII⁺CD64⁺) after DT treatment in Clec9a-Cre x CD64-LSL-2A-DTR mice. Renal cells were stained using antibodies against surface markers as indicated figure 24A. Upper panel shows percentage of cell populations within the indicated gates in the group treated with PBS and the lower panel shows percentage in the DT treated group. (D) Analysis of renal CD64⁺ cells (identified as in C) in *Clec9a^{+/Cre}CD64^{+/DTR}* mice injected with PBS or DT. Percentage with in the liveCD45.2⁺ cells per kidney is shown. Each symbol represents one mouse. * $p < 0.05$.

After the confirmation of the successful depletion of CD64⁺ cells, it was also necessary to exclude that DT treatment had affected other CLEC9A⁺ progenitor derived cell populations in

Results

these mice. Consequently, the specificity of the *Clec9a^{+Cre}CD64^{+DTR}* mouse model was further tested by determining the presence of renal and splenic cDCs as well as RPM in the same samples. Similarly, F4/80 or CD64 surface markers were used to identify renal cDCs, using the same gating strategy as in figure 25A. As demonstrated by the comparison with the PBS treated animals, renal cDC1 and cDC2 were unaffected by DT treatment in the experimental group (Fig. 30A,B) as well as renal cDCs, identified as liveCD45.2⁺CD11cMHCII⁺CD64⁻ cells (Fig. 30C, D).

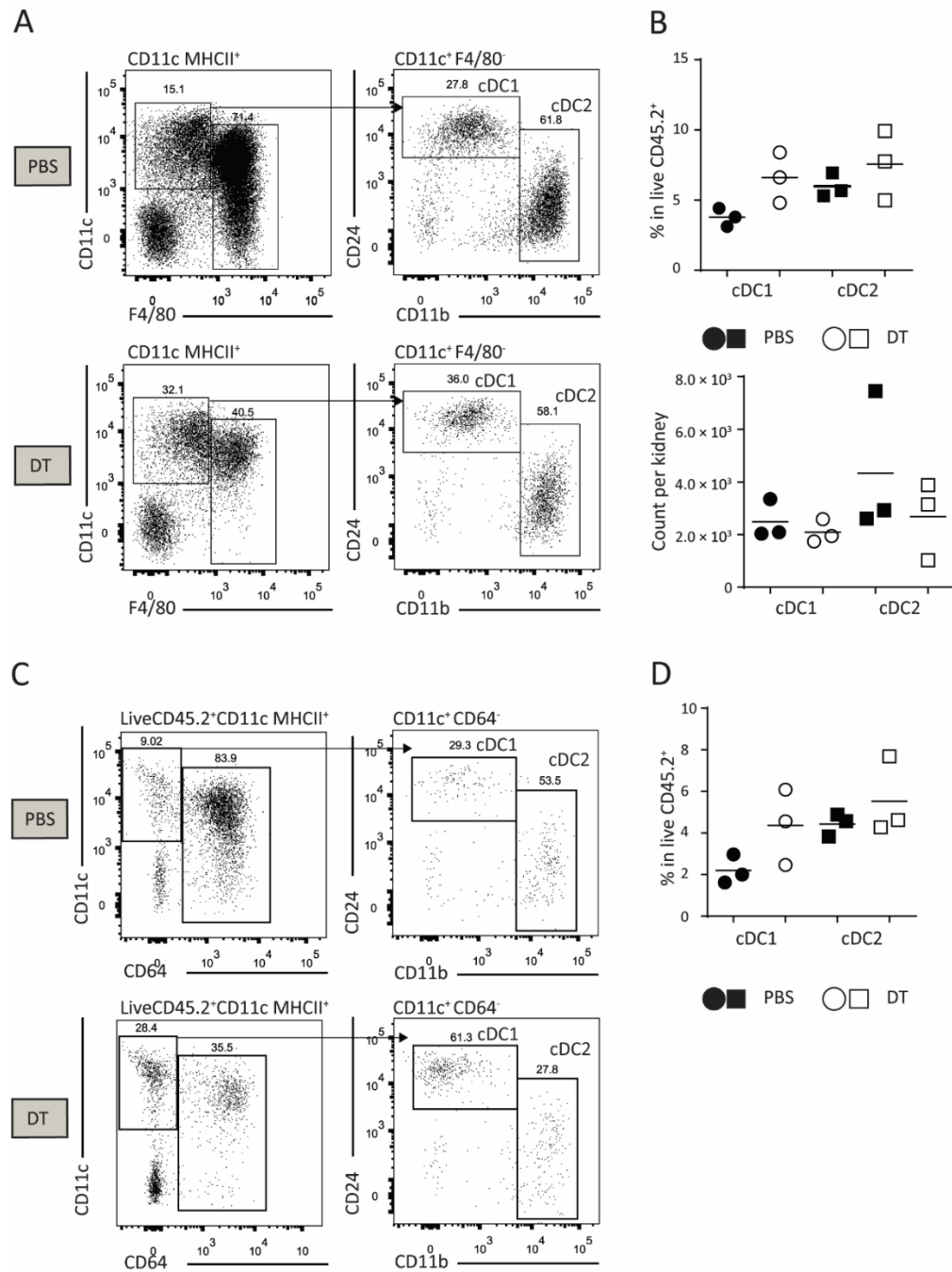


Figure 30. Depletion of cDCs in Clec9a-Cre x CD64-LSL-2A-DTR mice.

(A) Depletion of cDC1 (liveCD45.2⁺CD11cMHCII⁺F4/80⁻CD11b⁻CD24⁺) and cDC2 (liveCD45.2⁺CD11cMHCII⁺F4/80⁻CD11b⁺CD24) after DT treatment in Clec9a-Cre x CD64-LSL-2A-DTR mice. *Clec9a^{+/Cre}CD64^{+/DTR}* mice were treated i.p. twice 24 h apart, with DT (25 ng/g body weight) or PBS and one day after injections renal cells were stained using antibodies against surface markers as indicated figure 25A. Upper panel shows percentage of cell populations within the indicated gates in the group treated with PBS and the lower panel shows percentage in the DT treated group. (B) Analysis of renal cDC1 and cDC2 in *Clec9a^{+/Cre}CD64^{+/DTR}* mice injected with PBS or DT. Total number and percentage with in the liveCD45.2⁺ cells per kidney is shown. Each symbol represents one mouse. (C) Depletion of cDC1 (liveCD45.2⁺CD11cMHCII⁺CD64⁻CD11b⁻CD24⁺) and cDC2 (liveCD45.2⁺CD11cMHCII⁺CD64⁻CD11b⁺CD24) after DT treatment in Clec9a-Cre x CD64-LSL-2A-DTR mice. Renal cells were stained using antibodies against surface markers as indicated figure 25A. Upper panel shows percentage of cell populations within the indicated gates in the group treated with PBS and the lower panel shows percentage in the DT treated group. (D) Analysis of renal cDC1 and cDC2 (identified as in C) in *Clec9a^{+/Cre}CD64^{+/DTR}* mice injected with PBS or DT. Percentage with in the liveCD45.2⁺ cells per kidney is shown. Each symbol represents one mouse. * $p < 0.05$.

Next, I have analysed if splenic cDC1 and cDC2 are affected by DT treatment in these mice. In addition, RPM were investigated, because it is assumed that DCs could contribute to RPM pool in the spleen, as supported by the observation of one study in *Clec9a^{+/Cre}Rosa26^{+/EYFP}* mice²⁴. Therefore, I have examined whether RPM in these *Clec9a^{+/Cre}CD64^{+/DTR}* mice were affected by DT treatment, since these cells also express high level of CD64¹⁷. The detailed gating strategy to identify RPM as well as splenic cDCs is shown in figure 25B. Unexpectedly, RPM from DT administrated *Clec9a^{+/Cre}CD64^{+/DTR}* mice showed a strong reduction of more than 50% in counts and in frequency compared to the PBS treated controls (Fig. 31A, B). This was even more surprising, because according to previous published, only 2% of RPM are CLEC9A⁺ progenitor derived²⁴. In contrast to this, cDC1 and cDC2 were unaffected in these DT injected mice (Fig. 31A, C). These data further supported the notion, that Clec9a-Cre x CD64-LSL-2A-DTR mouse model allows to ablate CD64 expressing CLEC9A⁺ progenitor derived cells in the kidney and does not affect cDC subsets in this organ.

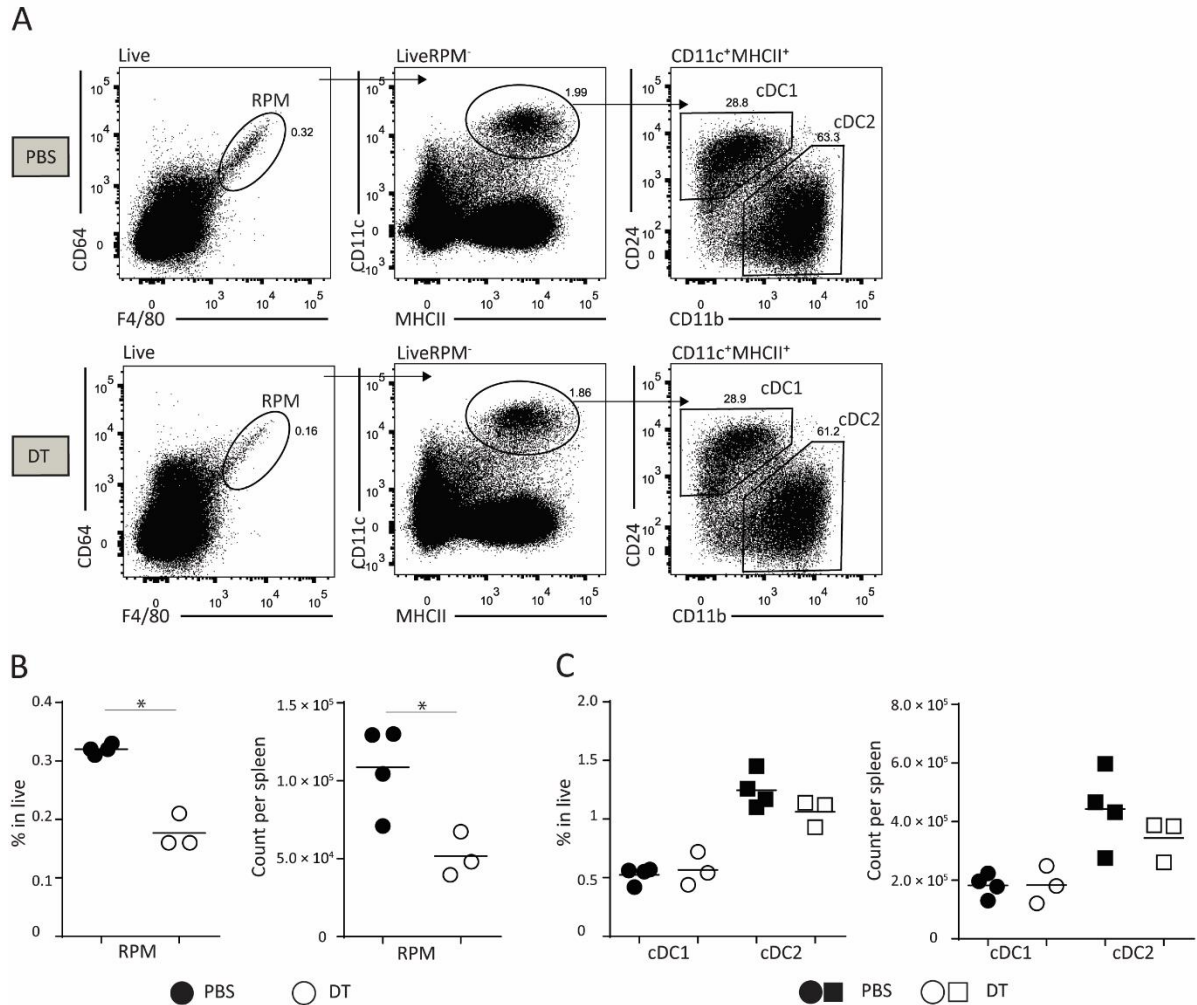


Figure 31. Analysis of cDCs and RPM in the spleen of *Clec9a-Cre x CD64-LSL-2A-DTR* mice after DT or PBS administration.

(A) Depletion of splenic cDC1 (liveCD64⁺F4/80⁻CD11c⁺MHCII⁺CD11b⁻CD24⁺), cDC2 (live CD64⁺F4/80⁻CD11c⁺MHCII⁺CD11b⁺CD24⁺) and RPM (live CD64⁺F4/80⁺) in *Clec9a-Cre x CD64-LSL-2A-DTR* mice. *Clec9a^{+/Cre}CD64^{+/DTR}* mice were treated as in figure 29A. Upper panel shows percentage of cell populations within the indicated gates in the group treated with PBS and the lower panel shows percentage in the DT treated group. (B) Analysis RPM in *Clec9a^{+/Cre}CD64^{+/DTR}* mice injected with PBS or DT. Total number and percentage with in the live cells per spleen is shown. Each symbol represents one mouse. (C) Analysis of cDC1 and cDC2 in *Clec9a^{+/Cre}CD64^{+/DTR}* mice injected with PBS or DT. Total number and percentage with in the live cells per spleen is shown. Each symbol represents one mouse. * $p < 0.05$.

4.1.16. Depletion of renal CD64⁺ cells did not cause monocytosis and neutrophilia

Since it is known, that other DC depletion models, such as CD11c-DTR, are prone to develop monocytosis and neutrophilia upon DT treatment, I have also assessed if DT treatment influenced the number of MO and neutrophil in the affected kidney of the same *Clec9a^{+/Cre}CD64^{+/DTR}* mice used before¹⁸⁰. The gating strategy to identify these cell populations is shown in figure 32A. Analysis of *Clec9a^{+/Cre}CD64^{+/DTR}* mice after DT treatment

demonstrated, in comparison to the PBS injected animals, a tendency of increased infiltration of MO and neutrophil into the kidney in counts and frequency within 48 h (Fig. 32B, C). Nevertheless, the observed effect of DT treatment on MOs and neutrophils was not statistically significant comparing to the PBS injected controls. Even though this observation needs to be taken into account for any further investigation of renal CD64⁺ cell function using these novel Clec9a-Cre x CD64-LSL-2A-DTR mice, the conclusion was made that this mouse model does not develop acute monocytosis or neutrophilia after DT treatment.

Results

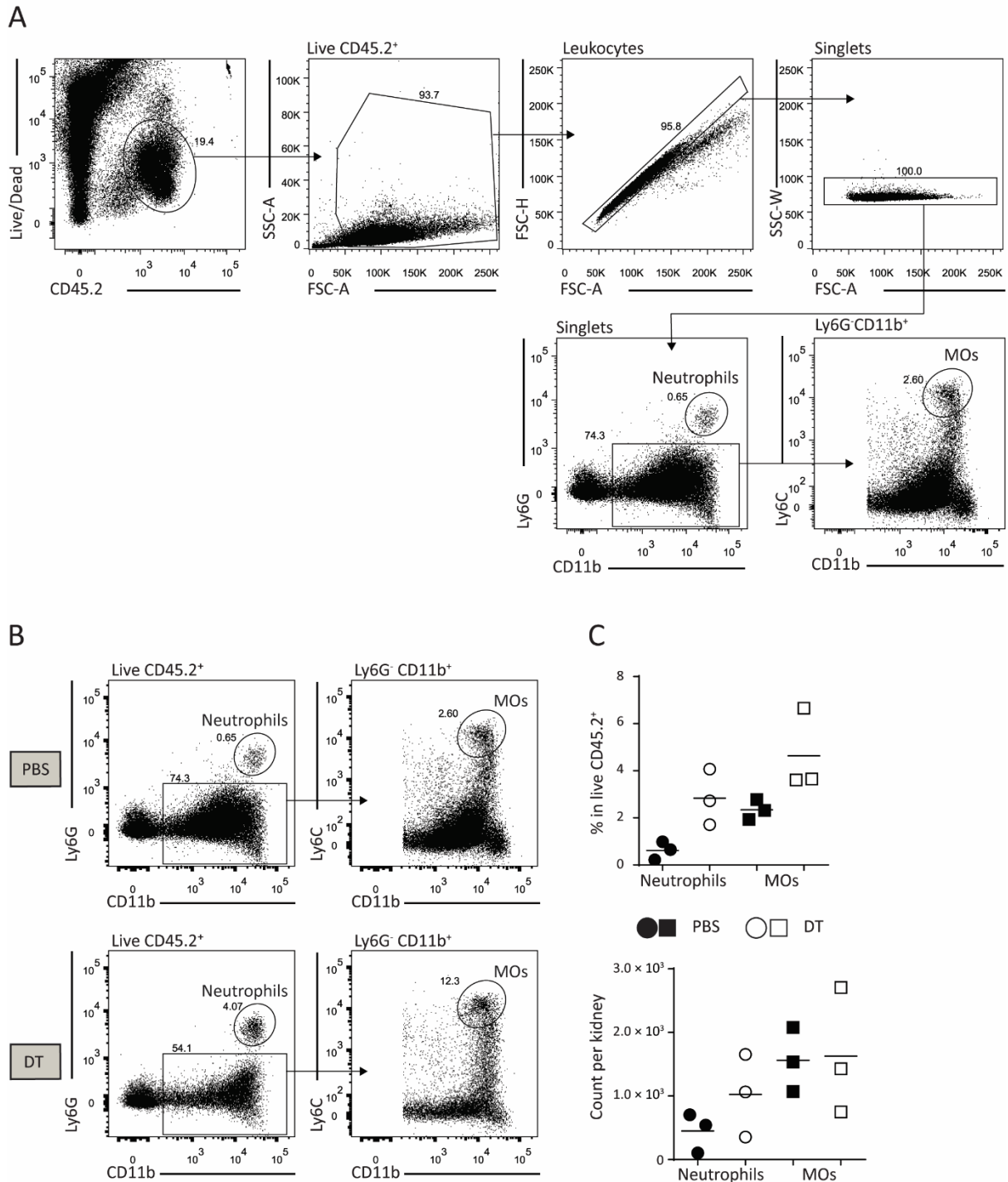


Figure 32. Analysis of neutrophils and MOs in the kidney of *Clec9a^{+Cre}CD64^{+DTR}* mice.

(A) Flow cytometry gating strategy to identify renal neutrophils (liveCD45.2⁺ lymphocyte antigen 6 complex, locus G (Ly6G)⁺CD11b⁺) and MOs (liveCD45.2⁺Ly6G⁻CD11b⁺ Ly6C⁺). Cells from kidney *Clec9a^{+Cre}CD64^{+DTR}* mice were stained with antibodies against indicated cell surface markers. The numbers in the dot plots indicate the percentages of the cells within the indicated gates. (B) Investigation of neutrophils (liveCD45.2⁺Ly6G⁺CD11b⁺) and MOs (liveCD45.2⁺Ly6G⁻CD11b⁺Ly6C⁺) after DT treatment in *Clec9a-Cre x CD64-LSL-2A-DTR* mice. *Clec9a^{+Cre}CD64^{+DTR}* mice were treated as described in figure 29A. Upper panel shows percentage of cell populations within the indicated gates in the group treated with PBS and the lower panel shows percentage in the DT treated group. (C) Analysis of renal neutrophils and MO in *Clec9a^{+Cre}CD64^{+DTR}* mice injected with PBS or DT. Total number and percentage with in the liveCD45.2⁺ cells per kidney is shown. Each symbol represents one mouse. * $p < 0.05$.

4.2. Role of dendritic cells during AKI

4.2.1. Effect of high concentrated cisplatin solution on AKI severity

Owed to the fact, that at this time point no established nephrotoxic AKI disease model existed in our laboratory, I first aimed to evaluate the optimal cisplatin administration regime for animal treatment. Considering the welfare of the experimental animals and to minimize pain, suffering or distress, I chose as a refinement to minimize the injectable volume per animal at this step. This was achieved by using a 2 mg/ml cisplatin solution.

According to previously published data for the induction of AKI, a set of C57BL/6 female mice were injected i.p. with a cisplatin dose of 20 mg/kg or the same volume of a 0.9% NaCl solution as a negative control. Since most of the published studies indicate 72 h to achieve cisplatin induced nephrotoxicity without reaching termination criteria I expected to see a similar result^{149,150}. In contrast to that, the cisplatin treated animals demonstrated an inconsistent response. In detail, overall 25%-75% of the investigated mice developed a severe stage of AKI and needed to be sacrificed within 24-48 h, while other cisplatin treated animals did not show any severe disease characteristics at this time points. However, all animals from this group that reached the earlier termination criteria developed a severe cisplatin caused nephrotoxicity, as demonstrated by strongly increased BUN values as compared to the control group. A representative experiment is shown in figure 33.

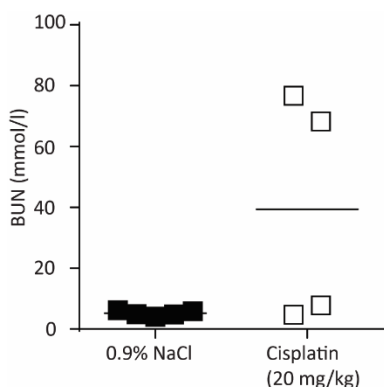


Figure 33. AKI induction in C57BL/6 females using cisplatin.

C57BL/6 female mice were treated with 2 mg/ml cisplatin solution (20 mg/kg) or injected with 0.9% NaCl. 48 h later mice were scarified and blood was collected from the heart to measure BUN levels for kidney function evaluation. Each symbol represents one mouse. * $p < 0.05$.

4.2.2. Effect of different doses of cisplatin on AKI induction

Due to the inconsistent result above, I decided to perform a cisplatin dose response experiment to find first the optimum drug dose to induce a uniform AKI severity in the experimental setting and to ensure the interpretability of any future AKI induction experiments. To investigate the optimal amount a 1 mg/ml cisplatin solution was used and 3 different sets of C57BL/6 female mice were injected i.p. with a final dose of either 10 mg/kg, 15 mg/kg or 20 mg/kg or an equivalent volume of 0.9% NaCl as a negative control. As before, in the experimental group treated with 20 mg/kg cisplatin, animals reached the termination criteria within 24 h after cisplatin administration and animals developed a kidney damage, as demonstrated by significantly increased creatinine and BUN levels in the plasma compared to the control group (Fig. 34A, B). In contrast to that, 3 out of 4 animals treated with 10 mg/kg and 1 out of 4 15 mg/kg cisplatin did not reach termination criteria within 48 h after cisplatin administration. Due to that, these experimental setups were determined after 48 h. Plasma creatinine and BUN levels later confirmed, that 1 out of 4 animals treated with 10 mg/kg and 2 out of 4 animals treated with 15 mg/kg cisplatin developed nephrotoxicity at this time point (Fig. 34A, B). Based on differences to disease induction to cisplatin treatment in this experimental setup, 15 mg/kg cisplatin amount was chosen as an optimal amount to induce AKI for the following experiments.

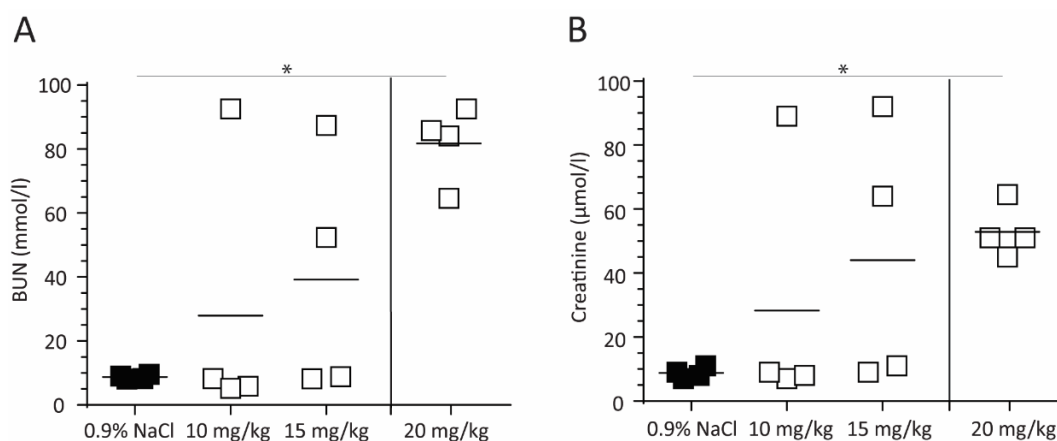


Figure 34. Dose response of C57BL/6 female mice to different cisplatin amounts to induce AKI.

(A) BUN amount in the blood of C57BL/6 female mice. C57BL/6 female mice were treated with 10, 15 or 20 mg/kg cisplatin or injected with 0.9% NaCl and monitored up till 48 h. 24-48 h later animals were scarified for blood collected from the heart. Each symbol represents one mouse. (B) Creatinine amount in the plasma of C57BL/6 female mice. Animals were treated as in indicated before and 24-48 h later scarified for blood collected from the heart. Each symbol represents one mouse. * $p < 0.05$.

4.2.3. Depletion of cDCs in *Clec9a-Cre x Rosa26-iDTR* mice

In order to study the specific role of cDCs and CD64⁺ cells during AKI development, the *in vivo* cell depletion mouse model *Clec9a-Cre x Rosa26-iDTR* was considered to be used²⁴. DT administration in these mice allows selective depletion of CLEC9A⁺ progenitor derived cells and does not induce monocytosis or neutrophilia^{24,99,204}. Since it was already shown that renal cDCs as well as both CD64⁺ cell subsets are derived from a CLEC9A⁺ progenitor²⁴, it was expected to see depletion of the same populations. To determine the functional reliability of renal cDC population depletion efficiency and kinetics, 2 sets of *Clec9a^{Cre/Cre}Rosa26^{DTR/DTR}* mice were treated i.p. with DT and compared with one control group for each time point. The presence of cDC subsets in the kidney was investigated on day 1 or day 2 after administration. The detailed gating strategy to identify renal cDCs as well as the CD64⁺ cell subsets F4/80^{hi} and F4/80^{lo} is shown in figure 35.

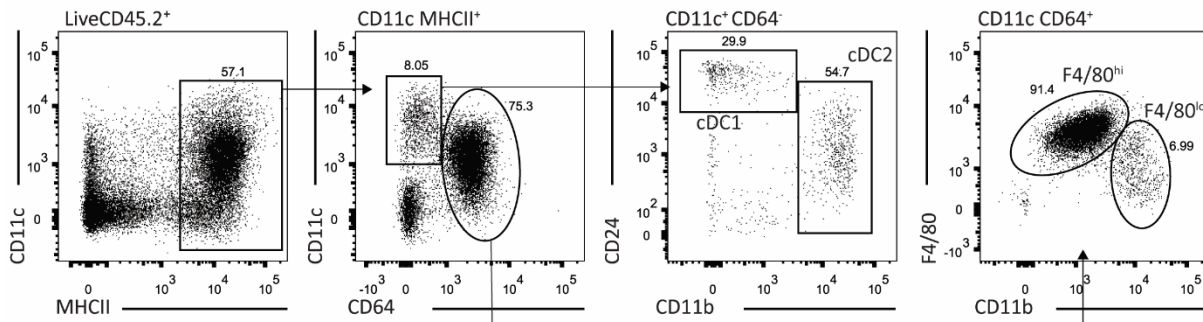


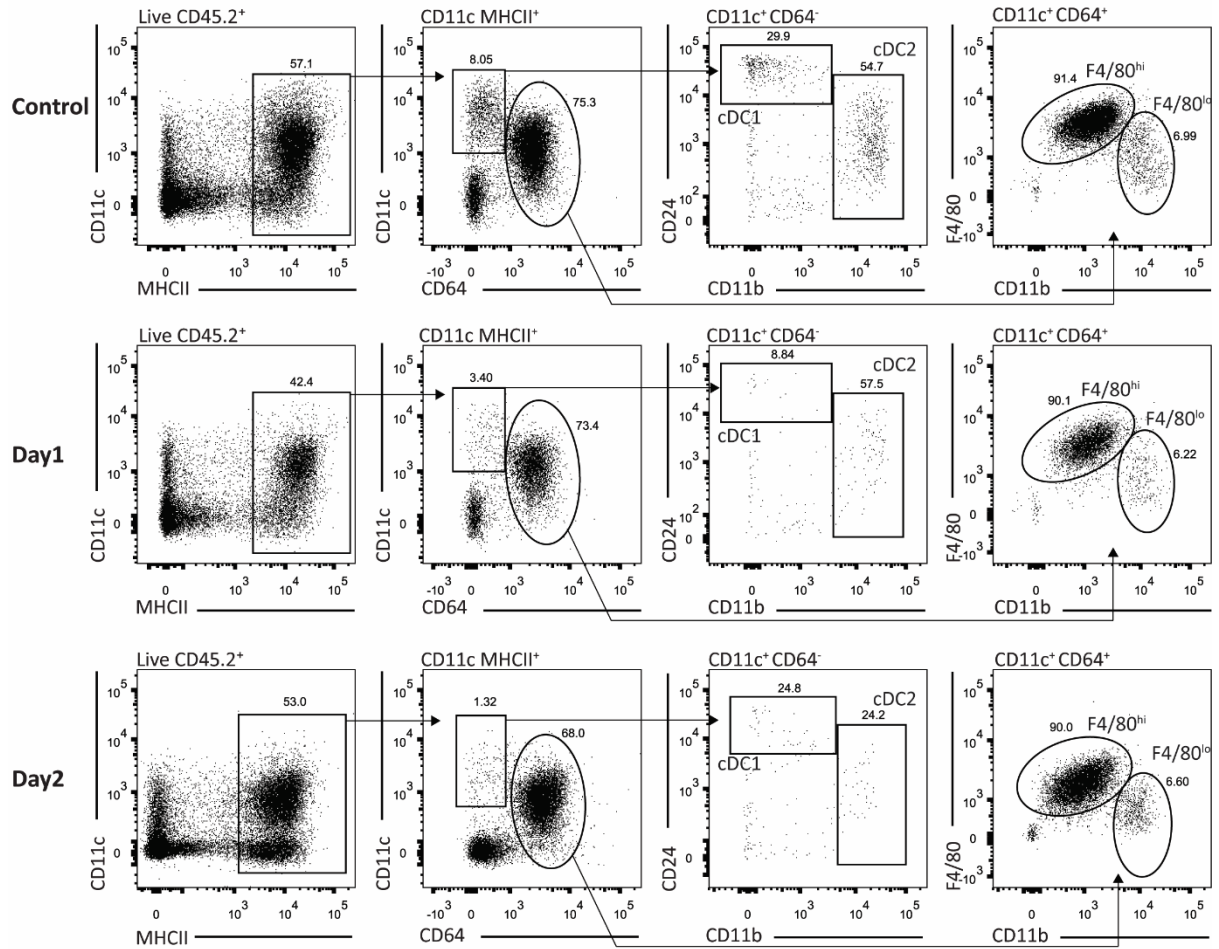
Figure 35. Gating strategy to identify cDC populations and CD64⁺ cells in kidney.

Flow cytometry gating strategy to identify renal cDC1 (liveCD45.2⁺CD11c⁺MHCII⁺CD64⁻CD24⁺CD11b⁺), cDC2 (liveCD45.2⁺CD11c⁺MHCII⁺CD64⁻CD24⁻CD11b⁺) as well as two CD64⁺ population subsets F4/80^{hi} cells (liveCD45.2⁺CD11c⁺MHCII⁺CD64⁺F4/80^{hi}CD11b⁺) and F4/80^{lo} cells (liveCD45.2⁺CD11c⁺MHCII⁺CD64⁺F4/80^{lo}CD11b⁺). Cells from kidney in *Clec9a^{Cre/Cre}Rosa26^{DTR/DTR}* mice were stained with antibodies against indicated cell surface markers. The numbers in the dot plots indicate the percentages of the cells within the indicated gates.

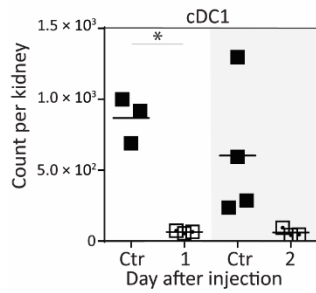
DT injection induced full depletion of renal cDC1 after 24 h and 48 h (Fig. 36A, B). In contrast to that cDC2 depletion efficiency was fully reached after 48 h (Fig. 36A, C). Surprisingly, none of the CD64⁺ cell subsets were affected by DT treatment, which is shown by count (Fig. 36A, D, E).

Results

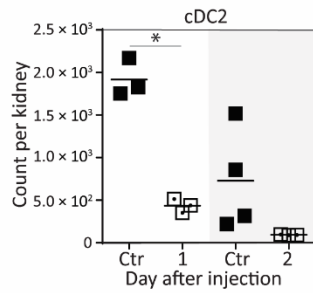
A



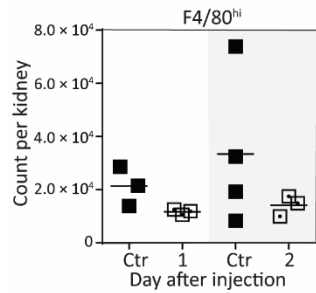
B



C



D



E

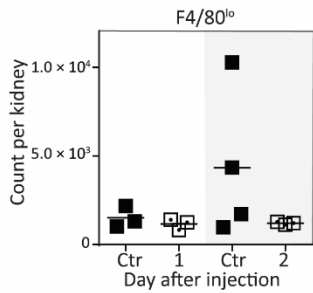


Figure 36. Depletion of renal cDC populations in Clec9a-Cre x Rosa26-iDTR mice.

(A) Depletion of renal cDC1, cDC2, F4/80^{hi} and F4/80^{lo} populations after DT treatment in Clec9a-Cre x Rosa26-iDTR mice. *Clec9a^{Cre/Cre}Rosa26^{DTR/DTR}* mice were treated i.p. with DT (25 ng/g body weight) and on day 1 and day 2 after injections renal cells were stained using antibodies against surface markers as indicated figure 35. Upper panel shows percentage of cell populations within the indicated gates in the control group and the lower panels show percentage in the DT treated group on different analysis days. (B) Analysis of renal cDC1 in *Clec9a^{Cre/Cre}Rosa26^{DTR/DTR}* mice injected with DT. Total number per kidney is shown. Each symbol represents one mouse. (C) Analysis of renal cDC2 in *Clec9a^{Cre/Cre}Rosa26^{DTR/DTR}* mice injected with DT. Total number per kidney is shown. Each symbol represents one mouse. (D) Analysis of renal F4/80^{hi} cells in *Clec9a^{Cre/Cre}Rosa26^{DTR/DTR}* mice upon DT administration. Total number per kidney is shown. Each symbol represents one mouse. (E) Analysis of renal F4/80^{lo} cell population in *Clec9a^{Cre/Cre}Rosa26^{DTR/DTR}* mice after DT administration. Total number per kidney is shown. Each symbol represents one mouse. * $p < 0.05$.

Therefore, I concluded that 25 ng/g DT should be sufficient to successfully deplete cDC1 and cDC2 in Clec9a-Cre x Rosa26-iDTR mice and that this mouse model can be used for the investigation of functional role of cDCs during the AKI induction experiments.

4.2.4. Depletion of cDC1 subset in XCR1-DTR-Venus mice

As a second DTR-DT system based mouse model, the XCR1-DTR-Venus mice were selected to investigate the role of renal cDC1 during AKI development. This model was chosen, because it allows the selective depletion of XCR1 expressing cells, specifically cDC1 subset, without affecting additional DC populations or other cells, such as MOs, neutrophils, granulocytes as well as T and bursa of fabricius (B) cells¹⁸⁵. XCR1-DTR-Venus mice were treated with DT as above. The presence of cDC1 in the kidneys was investigated on day 1 and day 2. In parallel one control group for each time point was also investigated. The gating strategy to identify renal cDC1 based on of the specific Venus expression of this model is shown in figure 37A. Similar to the before obtained results with Clec9a-Cre x Rosa26-iDTR, injection of DT induced full depletion of renal cDC1 in XCR1-DTR-Venus mouse samples after 24 h and 48 h (Fig. 37A, B).

In summary, these data conclusively demonstrated that the administration of 25 ng/g DT in XCR1-DTR-Venus mice is enough to fully ablate renal cDC1 and this mouse model can be used for the cDC1 functional role investigation during the AKI.

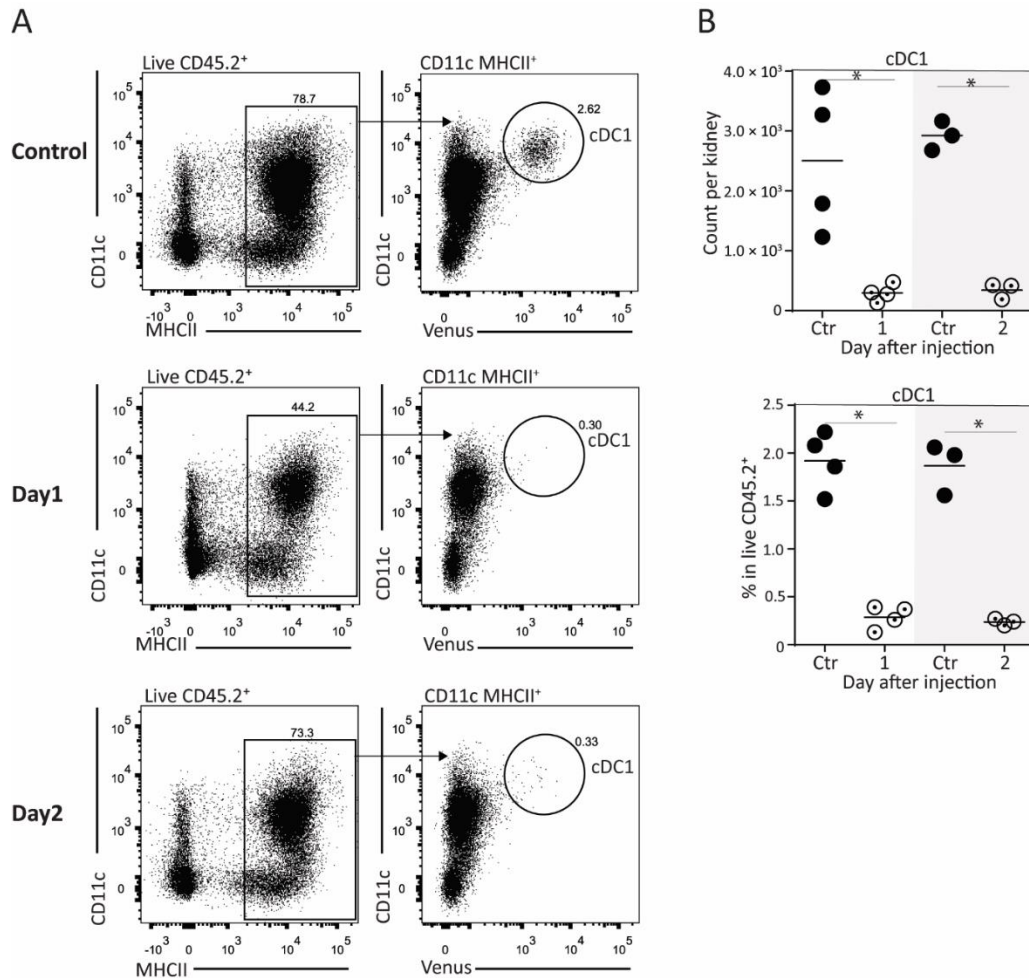


Figure 37. Depletion of cDC1 in XCR1-DTR-Venus mice. (A) Depletion of renal cDC1 after DT treatment in XCR1-DTR-Venus mice. *XCR1^{DTR-Venus/DTR-Venus}* mice were treated i.p. with DT (25 ng/g body weight) and on day 1 and day 2 after injections renal cells were stained using antibodies against surface markers. Flow cytometry gating strategy to identify renal cDC1 (liveCD45.2⁺CD11cMHCII⁺CD11c⁺Venus⁺) is indicated. The numbers in the dot plots indicate the percentages of the cells within the indicated gates. Upper panel shows percentage of cell populations within the indicated gates in the control group and the lower panels show percentage in the DT treated group on different analysis days. (B) Analysis of renal cDC1 in *XCR1^{DTR-Venus/DTR-Venus}* mice injected with DT. Total number and percentage with in the liveCD45.2⁺ cells per kidney is shown. Each symbol represents one mouse. * $p < 0.05$.

4.2.5. Cisplatin treatment fails to induce consistent AKI induction in female mice and to draw conclusions about cDCs role during nephrotoxicity

In order to investigate the contribution of cDC1 alone or cDC1 and cDC2 in combination during kidney homeostasis, the before validated XCR1-DTR-Venus and Clec9a-Cre x Rosa26-iDTR mouse models were used. To reach cell depletion a set of female mice were injected i.p. with a dose of 25 ng/g DT, followed one day later by i.p. injection with 15 mg/kg cisplatin to induce AKI or an equivalent volume of 0.9% NaCl used as a control (Fig. 38A). All cisplatin treated mice lost weight during the experiment (Fig. 38B). Unexpectedly, 20-34% of the animals

Results

reached the termination criteria within 24 h after cisplatin administration and therefore, the experiment was terminated at this point to be able to compare disease severity between mice. As expected, animals treated with saline did not show signs of kidney damage, as assessed by BUN and creatinine levels (Fig. 38C, D). Within the cisplatin treated animals, kidney damage was observed in some, but not all animals (Fig. 38C, D), indicating a degree of disease variation.

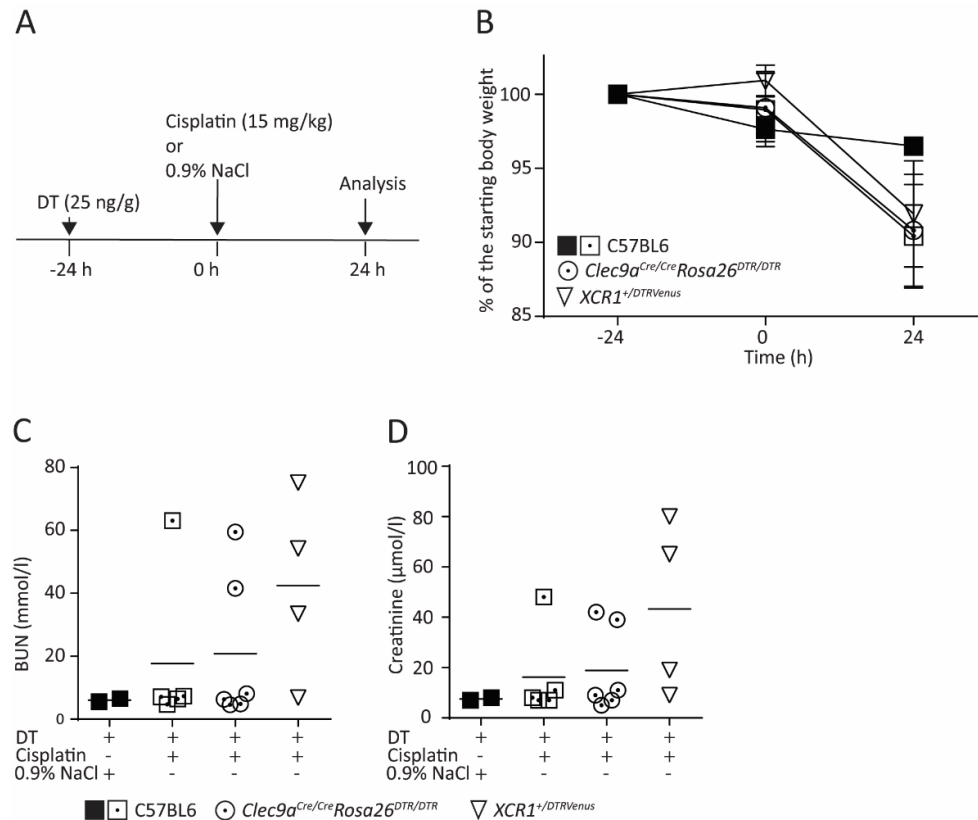


Figure 38. Effect of cDC depletion on kidney function in cisplatin induced nephrotoxicity.

(A) Schematic representation of the experimental design. C57BL/6, *Clec9a^{Cre/Cre}Rosa26^{DTR/DTR}* and *XCR1^{+/DTR-Venus}* female mice were i.p. treated with DT (25 ng/g), followed by 1 mg/ml cisplatin (15 mg/kg) or 0.9% NaCl administration. Mice were monitored up to 24 h after second injection. (B) Mouse body weight change during the experiment. Line with black squares represents C57BL/6 mice treated with DT and 0.9% NaCl combination. Lines with open symbols indicate mice injected with DT and cisplatin. (C) BUN amount in the mouse plasma. Animals were treated as indicated before and 24 h later scarified for blood collected from the heart. Each symbol represents one mouse. (D) Creatinine amount in the plasma of mice. Animals were treated as in indicated before and 24 h later scarified for blood collected from the heart. Each symbol represents one mouse. * $p < 0.05$.

Since tissue injury induced during AKI directly correlates with inflammation and infiltration of neutrophils^{149,152}, the infiltration rate of neutrophils and MOs was additionally assessed by FACS. In concordance with the kidney function parameters found before, the quantity of neutrophils and MOs of DT and cisplatin treated mice from *Clec9a*-Cre x *Rosa26*-iDTR and

Figure 39. Effect of cDC2 and/or cDC1 depletion on infiltrating leukocytes in cisplatin induced nephrotoxicity.

Analysis of renal neutrophils (A), MOs (B), cDC1 (C), cDC2 (D), F4/80^{hi} (E) and F4/80^{lo} (F) populations in C57BL/6, *Clec9a^{Cre/Cre} Rosa26^{DTR/DTR}* and *XCR1^{+DTR-Venus}* female mice treated as described in 38.A. Cells were identified as described in figure 32A and figure 35. Total number of the cells per kidney is shown. Each symbol represents one mouse. * $p < 0.05$.

Taken together, the observed inconsistent AKI induction data gained from these experimental setups at this point did not allow further conclusion about the role of cDCs during cisplatin induced nephrotoxicity. Furthermore, the unexpected termination after 24 h instead of 48 h after cisplatin injection challenge the before determined cisplatin dose of 15 mg/kg as the optimal amount to induce a reliable AKI response in these female animals.

5. Discussion

5.1. Mouse generation

In this thesis, a novel cell subset specific depletion mouse model, based on an inducible DTR-DT system, was successfully developed to target renal CLEC9A⁺ progenitor derived CD64⁺ cells. This approach was mainly hindered by the fact that most immune cells share a common set of surface markers. Therefore, a strategy to develop a mouse model based on a broadly expressed protein to target just one cell population is not easy to design. This problem is specifically evident for the ontogenetically independent DC lineage, which is phenotypically similar to other MPS cells^{35,77-79,84}. Like this, CD64 expression can be found on different MPS cell types^{24,120,121,218,284}. To overcome this problem, recombinase based intersectional genetic approaches became nowadays the method of choice for the successful generation of cell-specific depletion and labelling mouse models in multiple studies²⁸⁵⁻²⁸⁸. Another important requirement was the selection of a promising and efficient genome editing strategy. Therefore, as the basic concept to generate this mouse model I decided to use here a CRISPR-Cas9 genome editing strategy combined with Cre-loxP, which allowed to prevent the necessity to identify a unique cell-subset specific marker.

Even though CLEC9A⁺ progenitor derived CD64⁺ cell depletion was successfully reached in this work, some data were observed during the validation process of this mouse model, which need to be further investigated and discussed before it can be applied for future scientific applications.

One observation was the missing detection of DTR expression after DT treatment on CD64⁺ cells, isolated from the kidney of *Clec9a⁺/CreCD64⁺/DTR* mice. This data was noticeable, since DTR expression in *Clec9a⁺/CreCD64⁺/DTR* mice was expected to be found on approximately 30% of the renal CD64⁺ cells, as this labelling efficiency of this population was observed in a genetically similar mouse model *Clec9a⁺/CreRosa26⁺/EYFP²⁴*. However, here the expression of a cytosolic fluorescent dye was used to track CLEC9A⁺ progenitor derived cell. This had the advantage that a possible degradation of the reporter protein during the process of cell isolation from the tissue could be excluded, which in turn could explain the missing DTR signal

during FACS analysis in this work. Especially, the required conditions for renal cell isolation, including the necessary cell enrichment, were more prone for the loss of cell surface markers than for leukocyte isolation from spleen. This becomes especially evident for the direct comparison of DTR staining between splenic and renal cDC1, isolated from *Clec9a-Cre* x *Rosa26-iDTR* mouse samples used for this work. In consequence, the needed conditions for cell isolation can explain the occurred discrepancy, that the detected signal intensity most likely do not correlate with the real amount of protein expression on the isolated cells²⁸⁹⁻²⁹². Nevertheless, it cannot be excluded that a missing DTR detection can also be explained by too low protein expression. This assumption is supported by a similar controversy observation in another CD64 based depletion model¹⁸⁶. These CD64-DTR mice, generated by knocking-in of *EGFP* fused with *DTR* into *CD64* 3'-UTR sequence, showed also no detectable cytosolic EGFP expression by FACS¹⁸⁶. However, likewise the data generated in this thesis, DT treatment successfully depleted skin CD64⁺ MØs in CD64-DTR mice.

Unexpectedly, the depletion efficiency of renal CD64⁺ cells in *Clec9a^{+/Cre}CD64^{+/DTR}* mice was even higher than labelling efficiency in the aforementioned *Clec9a^{+/Cre}Rosa26^{+/EYFP}* model and accounted for approximately 80% of renal CD64⁺ cells after DT treatment. This was surprising, since the investigated animals were just heterozygous and raised the expectations, that the planned inbreeding to produce homozygous animals will improve the depletion efficiency even more significantly in future. These obvious differences between labelling and depletion efficiency in *Clec9a^{+/Cre}Rosa26^{+/EYFP}* and *Clec9a^{+/Cre}CD64^{+/DTR}* mice by itself can be most likely explained by different LSL excision efficiencies, because both mouse lines were heterozygous for all genetic manipulations and, more importantly, the same promoter was used to control Cre recombinase. Such differences between two genetically similar models can be caused by epigenetic modifications and DNA looping at the loxP sequence or the effective distance between the loxP sites^{192,293,294}. Specifically the fact is crucial, at which position the loxP sites are located in the genome and how big the physical distance for the Cre recombinase is to bring both loxP sites together^{192,293}.

Another striking observation was the higher depletion efficiency of splenic RPMs, because DT-administration in *Clec9a^{+/Cre}CD64^{+/DTR}* mice induced more than 50% depletion of this population, in contrast to the expected 2% positive labelled RPMs as observed for genetically similar *Clec9a^{+/Cre}Rosa26^{+/EYFP}* mice²⁴. However, recent studies indicate that RPMs mainly do not develop from DC lineage and are independent of CLEC9A⁺ CDPs or pre-cDCs^{20,295,296}.

Nevertheless, the observed high depletion of RPMs in this work indicates, that RPMs or one of their progenitor expressed CLEC9A, resulting in Cre recombinase translation and LSL cassette excision allowing DTR translation. It is less likely, that the observed RPM depletion is nonspecific, since DT treatment did not affect any splenic cDC populations. In addition to this, a detail study of DT entrance into the cell has shown that unspecific DT uptake via pinocytosis pathway leads to its degradation in the lysosomes without affecting cell viability^{176,177}. Only for very high concentration of DT a minimal protein synthesis inhibition in mouse MØs was observed^{176,177}. Therefore, the detected high depletion of RPMs in *Clec9a^{+/Cre}CD64^{+/DTR}* mice makes the Clec9a-Cre mouse model maybe not be an ideal *in vivo* model for an exclusive identification of DC lineage cells²⁴. However, it needs to be taken into account that the limited number of Clec9a-Cre x CD64-LSL-2A-DTR animals used for this study not allows a final conclusion at this point without further investigations. Importantly, more detailed studies need to be performed to exclude potential systemic MØ ablation upon DT administration in Clec9a-Cre X CD64-LSL-2A-DTR mice.

Even though the generated *Clec9a^{+/Cre}CD64^{+/DTR}* mouse model allows now the selective depletion of CLEC9A⁺ progenitor derived CD64 expressing cells, in particular renal CD64⁺ population, it needs to be considered, that several other cDC and MØ targeting DTR-DT system based transgenic mouse models do exist^{127,166}. However, most of them show a lower efficiency and specificity, because here DT administration affects not only the desired cell population^{127,164}. Therefore, the published data from these models need to be interpreted and discussed carefully. Examples are displayed by the different CD11c based mouse models, which are commonly used to study cDC functions, even though DT administration also affects MØs and MOs¹⁶⁴. In contrast to this, the Clec9a-Cre x CD64-LSL-2A-DTR mouse model allows the specific depletion of renal CLEC9A⁺ progenitor derived CD64⁺ cells, without affecting renal cDC1 and cDC2 and related subsets in spleen. This was expected, since cDCs develop from CLEC9A⁺ progenitors and do not or only at very low level express CD64^{24,120,121}.

Another drawback of several available DTR-DT based cDC depletion models so far was the reported an undesired development of neutrophilia or monocytosis upon DT treatment^{127,204,297}. This side effect of DT administration complicates the interpretation of the data, since is not clear if the observed outcome of the study is due to the absence of the cells or due to an increased count of MOs and neutrophils. Like this, a study reported that DT treated CD11c-DOG mice were able to faster overcome a bacterial infection during bacterial

pyelonephritis¹⁸⁰. Nevertheless, these data were put into question by Blijswijk et al., who stated that the observed result was rather due to the rapid influx of neutrophils, than due to the absence of CD11c⁺ cells¹²⁷. Especially, because neutrophils are involved in bacterial pyelonephritis²⁹⁸. In contrast to CD11c based depletion mouse models¹⁸⁰, DT treated *Clec9a^{+/Cre}CD64^{+/DTR}* mice in this work did not develop neutrophilia or monocytosis within 48 h. However, the development of neutrophilia in *Clec9a-Cre* x *CD64-LSL-2A-DTR* mice can be not excluded so far at later time points, based on the experimental setup used in this work. Finally, the question remains, how this new mouse model can be used in future to answer urgent basic scientific and translational questions. Generally, this new model has the advantage to offer the possibility to systemically deplete any CD64⁺ cell population, e.g. after crossing with any mouse model that contains generally expressed Cre. Beside this, the *CD64-LSL-2A-DTR* mouse model can be crossed with any murine model, which contains a cell subset specific promoter regulated Cre, allowing to target now a specific CD64 expressing cell subpopulation, in contrast to systemic CD64⁺ cell depletion.

Such a selective depletion of the cells could overcome the problem of multiplicity studies dealing with renal DC functions, which treated CD11c⁺ cells as a homogenous population without the possibility to resolve the observed effects to individual cDC1, cDC2 and CLEC9A⁺ progenitor derived CD64⁺ cell populations^{91,134,136-140}. Even though several of these studies has phenotypically characterized the kidney CD64⁺ cells and addressed the functional question using different kidney disease models, their investigations were limited in their expressiveness, since the specific ablation of renal CD64⁺ cells was not possible at this time^{124-126,128,299}. One study, that could have benefited from the inclusion of the *CD64-LSL-2A-DTR* mouse model, had the aim to investigate the role of tissue MØs in type III hypersensitivity and identified a physiological function of tissue-resident MØs in the kidney interstitium¹²⁸. In particular, the authors described a tissue-specific anatomical and functional unit, formed by resident MØs and peritubular capillary endothelial cells, which enabled them to detect potential infectious particles, in this case IC, and to initiate an immune response¹²⁸. Assuming that the authors would have included the *Clec9a-Cre* x *CD64-LSL-2A-DTR* mouse model in their studies, the role of the physical contribution of the MØs as well as CLEC9A⁺ progenitor derived CD64⁺ cells to the tissue-specific anatomical and functional unit could have been addressed in more detail. Similarly, the *CD64-LSL-2A-DTR* mouse model could support the data of Puranik et al., who described a specific protective role of MØs during chronic ischemic

injury¹²⁴. Especially because the role of kidney MØs was here investigated using liposomal clodronate based depletion, with the disadvantage to cause a possible neutrophil influx in the tissue, which was even critical discussed by the authors¹²⁴. Nevertheless, these data open another interesting field for the application of the CD64-LSL-2A-DTR mouse model, since this work has shown that kidney resident CD64⁺ cells are important and play protective role during ischemic injury. Therefore, it would be important to investigate if the CLEC9A⁺ progenitor derived CD64⁺ cells respond to the sterile inflammation during nephrotoxic AKI in the similar way. Moreover, studies similar to Lee et al., where the authors just characterized renal CD45^{int}CD11b^{int} and CD45^{hi}CD11b⁺ populations during ischemia-reperfusion injury, could be substantially improved by the application of the CD64-LSL-2A-DTR mouse model supplemented with a cDC specific depletion mouse models¹²⁶.

Beside the possibility to use the CD64-LSL-2A-DTR mouse model, crossed with Clec9a-Cre mice, to study CLEC9A⁺ progenitor derived CD64⁺ cells or CD64 expressing cDCs, also it can be crossed with Cre-carrying MO/MØ-specific mouse model. This would allow to specifically target MØs and MOs and to investigate their role in homeostasis of various tissues and disease models. Especially, because the recently developed CD64-DTR mouse model, which is the closest overlap in regard of applicability, is less specific due to the depletion of CD64 expressing cells including MOs, MØs, MDPs as well as CD64⁺ cDCs^{24,186,218}. The reason for this is the transcriptional regulation of DTR expression through the *CD64* promoter alone in this model¹⁸⁶. More importantly, these mice were generated by knock-in *EGFP* fused with *DTR* into the 3'-UTR region of *CD64*, which is known to be bound by various RNA-binding molecules involved in the fate of the expressed mRNA^{300,301}. Among others, it was shown that human CD64 3'-UTR is a direct target of micro RNA (miR)-127, resulting in a translational repression of this protein³⁰². Additionally, this study found that miR-127 expression in MØs was regulated during inflammation both *in vitro* and *in vivo*³⁰². Even though the translational repression of the murine 3'-UTR of CD64 is just poorly investigated, these data suggest a similar influence on the murine CD64 mRNA regulation by the murine homolog of miR-127 and other murine miRs. This assumption is made because the seed sequences within the transcribed mRNAs, responsible for the specific binding of the 3'-UTR, are normally highly conserved between *Homo sapiens* and *Mus musculus*³⁰³. Another possible drawback of this CD64-DTR mouse model, compared to the model developed in this thesis, is the dependency of DTR translation on an internal ribosome entry site (IRES) sequence. It is known, that such

IRES-based exogenous protein expression is often lower than the endogenous host protein, even though both proteins are translated from the same mRNA^{304,305}. Even though the authors did not discuss this point, it can contribute to the observed and before discussed undetectable EGFP protein expression but still successful depletion of CD64⁺ cells in CD64-DTR mice. Moreover, this could explain the high DT dose used in this study to compensate low DTR expression. Thus, not only the lack of specificity but also the required high DT amount to deplete the cells, which bear the risk of proteinuria³⁰⁶, make the CD64-DTR mouse model not the ideal choice for renal cell function investigations. In contrast, the new CD64-LSL-2A-DTR mice showed a nearly complete depletion of the targeted cells with a lower dose of DT thereby, most probably preventing unspecific high dose DT treatment caused side effects³⁰⁶. Since these promising results and the performed experiments in this work were still at the very beginning, even a lower and in consequence, more beneficial DT dose could be conceivable for future experiments to obtain the same depletion effect as described for the treatment of CD64-LSL-2A-DTR mice.

Another interesting application of the CD64-LSL-2A-DTR mouse model generated in this thesis is the crossing with Cre/loxP based MØ targeted mouse models, thereby generating novel MØ/MØ-specific depletion mouse models. Most popular models are LysM-Cre, CX3CR1-Cre and CD11b-Cre^{198,201,307}. Such a strategy could compensate that most of the Cre strains are indeed described to be specific to target certain cell population and tissues, but the detailed analysis often shows that increased efficiency is most of the time negatively correlated with the found specificity^{127,207}. In this context a study by Abram et al., made a substantial contribution by investigating the complete expression pattern of EYFP, between various MØ as well as DC Cre-models, crossed with the same reporter Rosa26-iEYFP model²⁰⁷. Amongst others, the authors showed conclusively that LysM-Cre significantly deleted LSL cassette in the *Rosa26* locus, thereby allowing high MØ labelling across the organism. Nevertheless, this was accompanied by a high EYFP labelling in polymorphonuclear neutrophils (PMNs) and some labelling in DCs. Moreover, similar observations were made for CD11c-Cre and CD11b-Cre²⁰⁷. Therefore, one can assume that the crossing of the newly established CD64-LSL-2A-DTR mouse model with one of these high efficient Cre recombinase models would help to overcome their specificity problem. Moreover, the strategy from this work to increase specificity and efficiency of depletion can be utilized as a basis for the design and generation for future mouse models. Especially the development of cDC2 subset specific depletion

mouse models could benefit from this, since they are up to date lacking specificity to target this population³⁰⁸.

In conclusion, the novel Clec9a-Cre x CD64-LSL-2A-DTR mouse model can be used to specifically deplete CLEC9A⁺ progenitor derived CD64⁺ cells. Additionally, the CD64-LSL-2A-DTR mouse model offers the possibility to increase the depletion specificity of other Cre-based models, opening the perspective to study highly selective any CD64 expressing cell subpopulation and draw conclusions about its specific functions. Therefore, this mouse model will hopefully be a substantial help in future to study the functional role of CD64⁺ cells in more detail for disease pathogenesis and progression with the long-term objective to test and develop convenient drugs for new therapeutic approaches and treatments.

5.2.cDC role in AKI

In the second part of this thesis cisplatin was used to induce AKI in mice with C57BL/6 background. The aim was to establish a spontaneous reproducible protocol with a high disease incidence for studying the role of cDC during nephrotoxic AKI. Since C57BL/6 have been used routinely in studies to investigate actual cancer related and immunological needs, I intended to use them as the basic background strain³⁰⁹. Furthermore, most of the routinely used mouse models in the laboratory were based on C57BL/6 and transgenic mice with C57BL/6 background at this time^{24,99,185,204}.

However, even though the cisplatin mouse model is widely accepted as a simple and reproducible disease model, the initial establishment can be extremely challenging if the method is not standardized and routinely used in the laboratory³¹⁰. Unfortunately, the success of AKI induction depends not only on obvious factors, like drug application, dose, and the biomarkers to estimate disease severity. It becomes more and more clear that also factors like animal age, genetic background, gender, circadian rhythm, diet, hydration status, or microenvironment can have a crucial impact on disease induction and reproducibility³¹⁰.

One of the most challenging problems in this study was the appearance of high disease variation within the experimental group. As it was mentioned before, the cisplatin mouse model is indeed often described as a reproducible model, which requires small amount of animals for the investigation^{311,312}. Most of the published studies refer to a protocol, which

contains a single injection of a high dose of 20 mg/kg cisplatin with a duration of 72 h before the successful AKI induction is measured by BUN and creatinine^{149-151,313-315}. Therefore, I decided in the present work to refer to a protocol published by Ramesh et al., where the authors used a dose of 20 mg/kg cisplatin for nephrotoxic AKI induction³¹¹. However, this dose was reduced to 15 mg/kg for the last investigations, because the mice got too sick and reached termination criteria before the expected end point with the initial cisplatin dose. Nevertheless, it was not possible to reproduce the previously published data for a study endpoint of 72 h, due to earlier termination of the experiments caused by low survival rate of the animals. Instead, only a part of the treated animals reached a severe stage and the experiments needed to be terminated within 24-48 h. After several modifications it was finally possible to induce AKI after a single i.p. injection of cisplatin with a dose of 15 mg/kg.

Cisplatin toxicity can be influenced by the animal genetic background, microbiological state or even physical conditions³¹⁰. Therefore, often rodents do not respond equally to cisplatin treatment, which in consequence, make it sometimes difficult to draw conclusions from the published studies to the data gained in this work. Additionally, valuable data about animal mortality during the experiments are rarely published in most of the cisplatin studies³¹⁰. Only a few investigations are an exception from that, supporting the notion that a high disease variation obviously sometimes occurs^{310,316}. One exception is the study published by Liu et al., where they reported similar observations, that only some animals in an experimental group showed an increased susceptibility, as demonstrated by the survival of less than 60% of treated mice over a period of 72 h³¹⁶. In contrast to these data, it was also observed that 9 out of 10 mice developed severe AKI, while 1 did not show any signs of cisplatin induced nephrotoxicity³¹⁰. These data keep the question unanswered if the group size of each individual setup in this pilot study may cause the absence of any significant difference even if it would exist in a setup with a higher number of animals.

Another obvious difference of this study to most of the published data is the preference to use male mice for AKI induction^{154,158,311,313,314,316-330}. This leads to the point, that the choice of the gender plays a potential role for the success of these experiments. This observation is further supported by recent scientific discussions that the observed susceptibility to damaging mechanism in the body often depends on the gender of the animals selected for the *in vivo* study^{310,331,332}. In line with this, several studies have analyzed such a gender based influence on AKI susceptibility during the last years. For instance, it was shown that males are

more susceptible to ischemia-reperfusion injury induced AKI than females, due to enhanced inflammatory responses observed in male mice³³³. Most probably some of these observed differences can be explained by sex hormones, since their influence on ischemia-reperfusion injury induced AKI was already demonstrated³³³⁻³³⁶. Nevertheless, in contrast to this, the exact role of the animal gender during nephrotoxic AKI is still not clear and needs to be further investigated, since one study concluded that males survived better than females, while another found that males were more susceptible^{337,338}. A recent study, which investigated the transcriptome and proteomic profile of male and female microglia, found, that male microglia expressed higher levels of MHCI and MHCI³³⁹. In consequence these MØs had a higher antigen presenting capacity compared to female microglia cells. These results gained from microglia cells even lead to the assumption that the observed differences need to be also considered for a critical interpretation of any data gained in relation to the role of renal MØs and other innate immune cells during AKI. Vice versa these gender dependent differences raise the question, to which extend preclinical animal models, that are based only on one gender, are representative enough to answer a scientific question in this field comprehensively.

Another problem with cisplatin treatment is the ability to penetrate systemically into all tissues, without a specific preference^{146,340}. Here it affects all fast dividing cells, but also tends to accumulate over the time in some tissues like kidney. Depending on the tissue, cisplatin can cause gastrointestinal toxicity, myelosuppression, nephrotoxicity, neuropathy, vascular injury and ototoxicity¹⁴⁷. Generally, mice treated with high dose of cisplatin develop minimal clinical signs of toxicity after 2 days, while obvious physiological reaction are observed on day 3, followed by the death of the animals on the 4th -7th day after treatment³¹⁰. Unexpectedly in this work and in contrast to published data, where the severe pain is normally observed after 4 days during cisplatin caused toxicity, several mice per experimental group reached termination criteria within the first 24 h after injection³¹⁰. Those mice showed rapidly developed signs of severe pain, such as hunched posture, lethargy, loss of coordination, rotating body movements after upholding mice by the tail, and were all confirmed for nephrotoxicity by increased BUN and creatinine levels. Importantly, these results were observed independent of the dose. In conclusion and to prevent most likely the loss of animals within the desired time frame of 72 h a lower dose of cisplatin (< 10 mg/kg) need to

be considered and tested in future experiments. Finally, this approach should rather lead to the desired induction of nephrotoxicity, than the observed systemic toxicity.

Cisplatin is not very soluble in the aquatic solutions³⁴¹. Nevertheless, injectable cisplatin solution is mostly prepared in 0.9% NaCl solution, where Cl ions help to stabilize cisplatin in the therapeutically active *cis*-isomerization form^{311,341}. Cisplatin is routinely administered i.p., but can be also injected intravenously or subcutaneously^{310,342}. This need to be taken in consideration, since it was shown that in rats i.p. administration of cisplatin resulted in a reservoir effect, which in consequence led to an increased half-life of the drug in the serum, compared to intravenous application³⁴². Beside the way of cisplatin administration, there are multiple other factors described to have an impact on the successful induction of nephrotoxicity using this drug. For instance, it is published that dietary plays an important role. In particular, magnesium depletion in the animal diet enhances cisplatin treatment nephrotoxicity, causing early death of the animals³⁴³. The same effect was observed with selenium, where selenium-reduced diet enhanced nephrotoxicity³²⁴. In addition to this, the hydration status of the animal also affects the animal sensitivity to cisplatin^{344,345}. It was shown that an increased hydration status led to reduced nephrotoxicity in rats by 60-70%³⁴⁴. To limit such variation in disease severity within the group, several studies decided to withhold food and water from the animals a few hours before the cisplatin injection^{154,158,318,346,347}. However, timing of cisplatin administration and circadian rhythm also needs to be taken into account^{328,329,348,349}. It was demonstrated that cisplatin treatment in rats near midactivity span, shortly after the maximum of the circadian rhythm reduces cisplatin caused nephrotoxicity³⁴⁵. In addition to this, it is speculated that inflammatory reactions depend on circadian rhythmicity in the kidney and contribute to cisplatin susceptibility, since murine renal interleukin IL-6 production shows circadian rhythmicity and IL-6 is known to play a protective role during cisplatin induced AKI^{325-327,329}. Moreover, the microbiological status of the animals is also considered to be the cause for nephrotoxic AKI severity variations^{317,330}. A study published by Ramesh et al., demonstrated that mice treated with cisplatin in combination with LPS developed severe renal failure and showed increased mortality compared to the just cisplatin treated control group³¹⁷. Therefore, all these examples of variables, that potentially can influence the data obtained from induced nephrotoxicity, show the importance of standardized conditions for the reproducibility of each experimental setup within a study, but also to compare the data obtained from different

studies. In consequence, the importance needs to be emphasized to include these additional variables to the initial experimental setup of this work to exclude, that variables like the way of administration, time point of administration or the diet of the animals caused the inconsistent data so far.

BUN and creatinine were used as a screening test for kidney function evaluation. These metabolic biomarkers were mainly chosen because they are routinely used as a fast and simple method for kidney function evaluation for clinical diagnostic and *in vivo* studies^{113,116}. However, it needs to be pointed out, that these biomarkers lack specificity and sensitivity and are obviously not fully reliable indicators of renal function¹¹³. For instance, they can be easily influenced by various physiological factors leading to an overestimation of the kidney tissue disruption degree. This include changes in protein synthesis, protein degradation due to loss of body weight, bleeding in intestine or stomach or dehydration³⁵⁰⁻³⁵². Indeed, since a drastic weight lost was also observed in this work for cisplatin treated mice, this effect may contribute to BUN and creatinine level variation. However, assuming that the elevated BUN and creatinine levels measured in this work were not significantly influenced by the described factors lead to the conclusion, that these animals developed a premature AKI. Especially because it was shown that BUN and creatinine levels in the blood do not increase before 70-75% of murine nephrons are damaged, which than refers as severe stage of kidney damage^{346,350}. Thus, it would be important to test first lower doses of cisplatin on both sex animals in the future to prevent the loss of animals before the planned experimental end point.

In this regard it need to be also mentioned, that apparently the age of the animals also influences susceptibility to cisplatin toxicity, because young mice as well as older mice are more susceptible for cisplatin treatment³¹⁰. For instance, a single dose of 16 mg/kg cisplatin injection into 24 month old mice resulted in 100% mortality, while 4-8 weeks old mice showed only 40% mortality within 7 days^{353,354}. Therefore, in this work exclusively 8-12 weeks old mice were selected for treatment, to eliminate the described age dependent increased susceptibility to cisplatin toxicity.

In conclusion, this work established a preliminary AKI induction protocol using female mice with a single dose of 15mg/kg. Since the initial goal to induce severe AKI not before 72 h was still not reached at this point, the before critically discussed variables need to be taken in

consideration for the future establishment of an adjusted and standardized protocol to induce AKI at an appropriate study end-point in a reliable and repeatable way.

The long-term objective of this AKI induction model is to investigate the role of each individual cDC subsets, with a special focus on CD64⁺ cells. Even though the final establishment of this cisplatin based nephrotoxic model is still owing, the pilot experiments to deplete cDC1/cDC2 or cDC1 in Clec9a-Cre x Rosa26-iDTR and XCR1-DTR-Venus mice were successfully done. Here, interesting observation applies to the decreased counts of F4/80^{hi} and F4/80^{lo} in Clec9a-Cre x Rosa26-iDTR mice after DT/Cisplatin treatment leading to the conclusion that DT/Cisplatin combination induces this effect, since the influence of DT treatment on these populations was not observed in previous experiments. However, these results are at moment in contrast to the majority of publications, where the cisplatin treatment led to increased infiltration of MØs^{158,320}. Since the establishment of the AKI induction model is still under investigation in the laboratory, future experiments will most probably answer the question, if this described discrepancy is just a unique effect of this experiment or will be reproduced significantly under these experimental conditions.

6. Literature

- 1 Alberts, B. *et al.* Molecular Biology of the Cell. 4th edition. Ch. 25, (Garland Science, 2002).
- 2 Chaplin, D. D. Overview of the immune response. *J Allergy Clin Immunol* **125**, S3-23, doi:10.1016/j.jaci.2009.12.980 (2010).
- 3 Janeway, C. *et al.* Immunobiology. 5th edition (Taylor & Francis, Inc., 2001).
- 4 Murphy, K. & Weaver, C. Janeways Immunobiology. 9th edition. ISBN: 978-0-815-34505-3 (2016).
- 5 Cruvinel, W. d. M. *et al.* Immune system - part I. Fundamentals of innate immunity with emphasis on molecular and cellular mechanisms of inflammatory response. *Revista brasileira de reumatologia* **50**, 434-461 (2010).
- 6 Medzhitov, R. & Janeway, C. Innate immunity. *The New England journal of medicine* **343**, 338-344, doi:10.1056/NEJM200008033430506 (2000).
- 7 Hato, T. *et al.* Sisters in arms: myeloid and tubular epithelial cells shape renal innate immunity. *American journal of physiology. Renal physiology* **304**, F1243-1251, doi:10.1152/ajprenal.00101.2013 (2013).
- 8 Akira, S., Uematsu, S. & Takeuchi, O. Pathogen Recognition and Innate Immunity. *Cell* **124**, 783-801, doi:10.1016/j.cell.2006.02.015 (2006).
- 9 Hato, T. & Dagher, P. C. How the Innate Immune System Senses Trouble and Causes Trouble. *Clinical journal of the American Society of Nephrology: CJASN* **10**, 1459-1469, doi:10.2215/CJN.04680514 (2015).
- 10 Hull, T. D., Agarwal, A. & George, J. F. The mononuclear phagocyte system in homeostasis and disease: a role for heme oxygenase-1. *Antioxid Redox Signal* **20**, 1770-1788, doi:10.1089/ars.2013.5673 (2014).
- 11 Jenkins, S. J. & Hume, D. A. Homeostasis in the mononuclear phagocyte system. *Trends in immunology* **35**, 358-367, doi:10.1016/j.it.2014.06.006 (2014).
- 12 Hume, D. A. The mononuclear phagocyte system. *Current opinion in immunology* **18**, 49-53, doi:10.1016/j.coi.2005.11.008 (2006).
- 13 Guilliams, M. *et al.* Dendritic cells, monocytes and macrophages: a unified nomenclature based on ontogeny. *Nature Publishing Group* **14**, 571-578, doi:10.1038/nri3712 (2014).
- 14 Hashimoto, D., Miller, J. & Merad, M. Dendritic Cell and Macrophage Heterogeneity In Vivo. *Immunity* **35**, 323-335, doi:10.1016/j.immuni.2011.09.007 (2011).
- 15 Bonten, E. J., Annunziata, I. & d'Azzo, A. Lysosomal multienzyme complex: pros and cons of working together. *Cell Mol Life Sci* **71**, 2017-2032, doi:10.1007/s00018-013-1538-3 (2014).
- 16 Bradford, B. M. *et al.* Defining the anatomical localisation of subsets of the murine mononuclear phagocyte system using integrin alpha X (Itgax, CD11c) and colony stimulating factor 1 receptor (Csf1r, CD115) expression fails to discriminate dendritic cells from macrophages. *Immunobiology* **216**, 1228-1237, doi:10.1016/j.imbio.2011.08.006 (2011).
- 17 Guilliams, M. *et al.* Unsupervised High-Dimensional Analysis Aligns Dendritic Cells across Tissues and Species. *Immunity* **45**, 669-684, doi:10.1016/j.immuni.2016.08.015 (2016).
- 18 Pakalniskyte, D. & Schraml, B. U. Tissue-Specific Diversity and Functions of Conventional Dendritic Cells. *Adv Immunol* **134**, 89-135, doi:10.1016/bs.ai.2017.01.003 (2017).
- 19 Swiecki, M. & Colonna, M. The multifaceted biology of plasmacytoid dendritic cells. *Nature Reviews Immunology* **15**, 471-485, doi:10.1038/nri3865 (2015).
- 20 Ginhoux, F. & Guilliams, M. Tissue-Resident Macrophage Ontogeny and Homeostasis. *Immunity* **44**, 439-449, doi:10.1016/j.immuni.2016.02.024 (2016).
- 21 Gautier, E. L. *et al.* Gene-expression profiles and transcriptional regulatory pathways that underlie the identity and diversity of mouse tissue macrophages. *Nature Immunology* **13**, 1118-1128, doi:10.1038/ni.2419 (2012).
- 22 Yang, J. *et al.* Monocyte and macrophage differentiation: circulation inflammatory monocyte as biomarker for inflammatory diseases. *Biomarker research* **2**, 1, doi:10.1186/2050-7771-2-1 (2014).
- 23 Poltorak, M. P. & Schraml, B. U. Fate Mapping of Dendritic Cells. *Frontiers in Immunology* **6**, 1-15, doi:10.3389/fimmu.2015.00199 (2015).
- 24 Schraml, B. U. *et al.* Genetic Tracing via DNGR-1 Expression History Defines Dendritic Cells as a Hematopoietic Lineage. *Cell* **154**, 843-858, doi:10.1016/j.cell.2013.07.014 (2013).

- 25 Davies, L. C. *et al.* Tissue-resident macrophages. *Nature Immunology* **14**, 986-995, doi:10.1038/ni.2705 (2013).
- 26 Jakubzick, C. *et al.* Minimal Differentiation of Classical Monocytes as They Survey Steady-State Tissues and Transport Antigen to Lymph Nodes. *Immunity* **39**, 599-610, doi:10.1016/j.immuni.2013.08.007 (2013).
- 27 Tamoutounour, S. *et al.* Origins and Functional Specialization of Macrophages and of Conventional and Monocyte-Derived Dendritic Cells in Mouse Skin. *Immunity* **39**, 925-938, doi:10.1016/j.immuni.2013.10.004 (2013).
- 28 Ginhoux, F. & Jung, S. Monocytes and macrophages: developmental pathways and tissue homeostasis. *Nature Reviews Immunology* **14**, 392-404, doi:10.1038/nri3671 (2014).
- 29 Cella, M. *et al.* Plasmacytoid monocytes migrate to inflamed lymph nodes and produce large amounts of type I interferon. *Nature Medicine* **5**, 919-923, doi:10.1038/11360 (1999).
- 30 Satpathy, A. T. *et al.* Zbtb46 expression distinguishes classical dendritic cells and their committed progenitors from other immune lineages. *Journal of Experimental Medicine* **209**, 1135-1152, doi:10.1084/jem.20120030 (2012).
- 31 Swiecki, M. *et al.* Plasmacytoid Dendritic Cell Ablation Impacts Early Interferon Responses and Antiviral NK and CD8+ T Cell Accrual. *Immunity* **33**, 955-966, doi:10.1016/j.immuni.2010.11.020 (2010).
- 32 Idoyaga, J. *et al.* M. Antibody to Langerin/CD207 localizes large numbers of CD8a+ dendritic cells to the marginal zone of mouse spleen. *Proceedings of the National Academy of Sciences* **106**, 1524-1529 (2009).
- 33 Qiu, C. H. *et al.* Novel Subset of CD8 + Dendritic Cells Localized in the Marginal Zone Is Responsible for Tolerance to Cell-Associated Antigens. *The Journal of Immunology* **182**, 4127-4136, doi:10.4049/jimmunol.0803364 (2009).
- 34 Eickhoff, S. *et al.* Robust Anti-viral Immunity Requires Multiple Distinct T Cell-Dendritic Cell Interactions. *Cell* **162**, 1322-1337, doi:10.1016/j.cell.2015.08.004 (2015).
- 35 Merad, M. *et al.* The dendritic cell lineage: ontogeny and function of dendritic cells and their subsets in the steady state and the inflamed setting. *Annual review of Immunology*, doi:10.1146/annurev-immunol-020711-074950 (2013).
- 36 Steinman, R. M. & Idoyaga, J. Features of the dendritic cell lineage. *Immunological reviews* **234**, 5-17, doi:10.1111/j.0105-2896.2009.00888.x (2010).
- 37 Mildner, A. & Jung, S. Development and Function of Dendritic Cell Subsets. *Immunity* **40**, 642-656, doi:10.1016/j.immuni.2014.04.016 (2014).
- 38 Paul, F. *et al.* Transcriptional Heterogeneity and Lineage Commitment in Myeloid Progenitors. *Cell* **163**, 1663-1677, doi:10.1016/j.cell.2015.11.013 (2015).
- 39 Satpathy, A. T. *et al.* Re(de)fining the dendritic cell lineage. *Nature Immunology* **13**, 1145-1154, doi:10.1038/ni.2467 (2012).
- 40 Sichien, D. *et al.* Development of conventional dendritic cells: from common bone marrow progenitors to multiple subsets in peripheral tissues. *Mucosal Immunology* **10**, 831-844, doi:10.1038/mi.2017.8 (2017).
- 41 Persson, E. K. *et al.* IRF4 Transcription-Factor-Dependent CD103+CD11b+ Dendritic Cells Drive Mucosal T Helper 17 Cell Differentiation. *Immunity* **38**, 958-969, doi:10.1016/j.immuni.2013.03.009 (2013).
- 42 Scott, C. L. *et al.* Signal regulatory protein alpha (SIRPα) regulates the homeostasis of CD103+CD11b+ DCs in the intestinal lamina propria. *European journal of immunology* **44**, 3658-3668, doi:10.1002/eji.201444859 (2014).
- 43 Fernández-Santoscoy, M. *et al.* A reduced population of CD103+CD11b+ dendritic cells has a limited impact on oral Salmonella infection. *Immunology Letters* **176**, 72-80, doi:10.1016/j.imlet.2016.05.012 (2016).
- 44 Kumamoto, Y. *et al.* CD301b+ Dermal Dendritic Cells Drive T Helper 2 Cell-Mediated Immunity. *Immunity* **39**, 733-743, doi:10.1016/j.immuni.2013.08.029 (2013).
- 45 Kumamoto, Y. *et al.* CD301b+ dendritic cells suppress T follicular helper cells and antibody responses to protein antigens. *eLife*, doi:10.7554/eLife.17979.001 (2016).
- 46 Dalod, M. *et al.* Dendritic cell maturation: functional specialization through signaling specificity and transcriptional programming. *The EMBO Journal* **33**, 1104-1116, doi:10.1002/embj.201488027 (2014).
- 47 Satpathy, A. T. *et al.* Runx1 and Cbf regulate the development of Flt3+ dendritic cell progenitors and restrict myeloproliferative disorder. *Blood* **123**, 2968-2977, doi:10.1182/blood-2013-11-539643 (2014).
- 48 den Haan, J. M. *et al.* CD8(+) but not CD8(-) dendritic cells cross-prime cytotoxic T cells in vivo. *Journal of Experimental Medicine* **192**, 1685-1696 (2000).

- 49 Bedoui, S. *et al.* Cross-presentation of viral and self antigens by skin-derived CD103+ dendritic cells. *Nature Immunology* **10**, 488-495, doi:10.1038/ni.1724 (2009).
- 50 Fuertes, M. B. *et al.* Host type I IFN signals are required for antitumor CD8+ T cell responses through CD8 α + dendritic cells. *The Journal of experimental medicine* **208**, 2005-2016, doi:10.1084/jem.20101159 (2011).
- 51 Diamond, M. S. *et al.* Type I interferon is selectively required by dendritic cells for immune rejection of tumors. *Journal of Experimental Medicine* **208**, 1989-2003, doi:10.1084/jem.20101158 (2011).
- 52 Hildner, K. *et al.* Batf3 Deficiency Reveals a Critical Role for CD8 α + Dendritic Cells in Cytotoxic T Cell Immunity. *Science* **322**, 1097-1100 (2009).
- 53 Sun, T. *et al.* Intestinal Batf3-dependent dendritic cells are required for optimal antiviral T-cell responses in adult and neonatal mice. *Mucosal Immunology*, doi:10.1038/mi.2016.79 (2016).
- 54 Miller, J. C. *et al.* Deciphering the transcriptional network of the dendritic cell lineage. *Nature Immunology* **13**, 888-899, doi:10.1038/ni.2370 (2012).
- 55 Edwards, A. D. *et al.* Toll-like receptor expression in murine DC subsets: lack of TLR7 expression by CD8 α + DC correlates with unresponsiveness to imidazoquinolines. *European journal of immunology* **33**, 827-833, doi:10.1002/eji.200323797 (2003).
- 56 Davey, G. M. *et al.* Cutting Edge: Priming of CD8 T Cell Immunity to Herpes Simplex Virus Type 1 Requires Cognate TLR3 Expression In Vivo. *The Journal of Immunology* **184**, ji_0903013-0902246, doi:10.4049/jimmunol.0903013 (2010).
- 57 Yarovinsky, F. *et al.* TLR11 activation of dendritic cells by a protozoan profilin-like protein. *Science* **308**, 1626-1629, doi:10.1126/science.1109893 (2005).
- 58 Sancho, D. *et al.* Identification of a dendritic cell receptor that couples sensing of necrosis to immunity. *Nature* **458**, 899-903, doi:10.1038/nature07750 (2009).
- 59 Koblansky, A. A. *et al.* Recognition of profilin by Toll-like receptor 12 is critical for host resistance to *Toxoplasma gondii*. *Immunity* **38**, 119-130, doi:10.1016/j.immuni.2012.09.016 (2013).
- 60 Van der Borgh, K. *et al.* Myocardial Infarction Primes Autoreactive T Cells through Activation of Dendritic Cells. *Cell Rep* **18**, 3005-3017, doi:10.1016/j.celrep.2017.02.079 (2017).
- 61 Zelenay, S. *et al.* The dendritic cell receptor DNGR-1 controls endocytic handling of necrotic cell antigens to favor cross-priming of CTLs in virus-infected mice. *Journal of Clinical Investigation* **122**, 1615-1627, doi:10.1172/JCI60644 (2012).
- 62 Torti, N. *et al.* Batf3 transcription factor-dependent DC subsets in murine CMV infection: Differential impact on T-cell priming and memory inflation. *European journal of immunology* **41**, 2612-2618, doi:10.1002/eji.201041075 (2011).
- 63 Mashayekhi, M. *et al.* CD8 α + dendritic cells are the critical source of interleukin-12 that controls acute infection by *Toxoplasma gondii* tachyzoites. *Immunity* **35**, 249-259 (2011).
- 64 Murphy, T. L. *et al.* Transcriptional Control of Dendritic Cell Development. *Annual Review of Immunology* **34**, 93-119, doi:10.1146/annurev-immunol-032713-120204 (2016).
- 65 Yap, G. S. *et al.* Genetic analysis of host resistance to intracellular pathogens: lessons from studies of *Toxoplasma gondii* infection. *Microbes Infect* **8**, 1174-1178, doi:10.1016/j.micinf.2005.10.031 (2006).
- 66 Schlitzer, A. *et al.* Recent advances in understanding dendritic cell development, classification, and phenotype. *F1000Res* **7**, doi:10.12688/f1000research.14793.1 (2018).
- 67 Dudziak, D. *et al.* Differential Antigen Processing by Dendritic Cell Subsets in Vivo. *Science* **315**, 107-111, doi:10.1126/science.1136080 (2007).
- 68 Kinnebrew, M. A. *et al.* Intestinal CD103+ CD11b+ lamina propria dendritic cells instruct intestinal epithelial cells to express antimicrobial proteins in response to Toll-like receptor 5 activation. *Immunity* **36**, 276-287, doi:10.1016/j.immuni.2011.12.011 (2012).
- 69 Satpathy, A. T. *et al.* Notch2-dependent classical dendritic cells orchestrate intestinal immunity to attaching-and-effacing bacterial pathogens. *Nature Immunology* **14**, 937-948, doi:10.1038/ni.2679 (2013).
- 70 Williams, J. W. *et al.* Transcription factor IRF4 drives dendritic cells to promote Th2 differentiation. *Nature Communications* **4**, 1-12, doi:10.1038/ncomms3990 (2016).
- 71 Gao, Y. *et al.* Control of T Helper 2 Responses by Transcription Factor IRF4-Dependent Dendritic Cells. *Immunity* **39**, 722-732, doi:10.1016/j.immuni.2013.08.028 (2013).
- 72 Lewis, K. L. *et al.* Notch2 Receptor Signaling Controls Functional Differentiation of Dendritic Cells in the Spleen and Intestine. *Immunity* **35**, 780-791, doi:10.1016/j.immuni.2011.08.013 (2011).
- 73 Naik, S. *et al.* Commensal-dendritic-cell interaction specifies a unique protective skin immune signature. *Nature* **520**, 104-108, doi:10.1038/nature14052 (2015).

- 74 Bajana, S. *et al.* IRF4 Promotes Cutaneous Dendritic Cell Migration to Lymph Nodes during Homeostasis and Inflammation. *The Journal of Immunology* **189**, 3368-3377, doi:10.4049/jimmunol.1102613 (2012).
- 75 Robays, L. J. *et al.* Chemokine Receptor CCR2 but Not CCR5 or CCR6 Mediates the Increase in Pulmonary Dendritic Cells during Allergic Airway Inflammation. *The Journal of Immunology* **178**, 5305-5311, doi:10.4049/jimmunol.178.8.5305 (2007).
- 76 Plantinga, M. *et al.* Conventional and Monocyte-Derived CD11b+ Dendritic Cells Initiate and Maintain T Helper 2 Cell-Mediated Immunity to House Dust Mite Allergen. *Immunity* **38**, 322-335, doi:10.1016/j.immuni.2012.10.016 (2013).
- 77 Van Furth, R. *et al.* The mononuclear phagocyte system: a new classification of macrophages, monocytes, and their precursor cells. *Bulletin of the World Health Organization* **46**, 845-852 (1972).
- 78 Sallusto F, L. A. Efficient presentation of soluble antigen by cultured human dendritic cells is maintained by granulocyte/macrophage colony-stimulating factor plus interleukin 4 and downregulated by tumor necrosis factor alpha. *The Journal of experimental medicine* **179**, 1109-1118 (1994).
- 79 Chomarat, P. *et al.* IL-6 switches the differentiation of monocytes from dendritic cells to macrophages. *Nat Immunol* **1**, 510-514, doi:10.1038/82763 (2000).
- 80 Anderson, D. A., 3rd, Murphy, K. M. & Brisen, C. G. Development, Diversity, and Function of Dendritic Cells in Mouse and Human. *Cold Spring Harb Perspect Biol* **10**, doi:10.1101/cshperspect.a028613 (2018).
- 81 Grajales-Reyes, G. E. *et al.* Batf3 maintains autoactivation of Irf8 for commitment of a CD8 α + conventional DC clonogenic progenitor. *Nature Immunology* **16**, 708-717, doi:10.1038/ni.3197 (2015).
- 82 Meredith, M. M. *et al.* Expression of the zinc finger transcription factor zDC (Zbtb46, Btd4) defines the classical dendritic cell lineage. *Journal of Experimental Medicine* **209**, 1153-1165, doi:10.1084/jem.20112675 (2012).
- 83 Schraml, B. U. & Sousa, C. R. e. Defining dendritic cells. *Current opinion in immunology* **32**, 13-20, doi:10.1016/j.coi.2014.11.001 (2015).
- 84 Haniffa, M., Collin, M. & Ginhoux, F. Ontogeny and Functional Specialization of Dendritic Cells in Human and Mouse. 1 edn, Vol. 120 (Elsevier Inc., 2013).
- 85 Merad, M. & Manz, M. G. Dendritic cell homeostasis. *Blood* **113**, 3418-3427, doi:10.1182/blood (2009).
- 86 Schlitzer, A. *et al.* Identification of cDC1- and cDC2-committed DC progenitors reveals early lineage priming at the common DC progenitor stage in the bone marrow. *Nature Immunology* **16**, 718-728, doi:10.1038/ni.3200 (2015).
- 87 Naik, S. H. *et al.* Intrasplenic steady-state dendritic cell precursors that are distinct from monocytes. *Nature Immunology* **7**, 663-671, doi:10.1038/ni1340 (2006).
- 88 Waskow, C. *et al.* The receptor tyrosine kinase Flt3 is required for dendritic cell development in peripheral lymphoid tissues. *Nature Immunology* **9**, 676-683, doi:10.1038/ni.1615 (2008).
- 89 McKenna, H. J. *et al.* Mice lacking flt3 ligand have deficient hematopoiesis affecting hematopoietic progenitor cells, dendritic cells, and natural killer cells. *Blood* **95**, 3489-3497 (2000).
- 90 Greter, M. *et al.* GM-CSF Controls Nonlymphoid Tissue Dendritic Cell Homeostasis but Is Dispensable for the Differentiation of Inflammatory Dendritic Cells. *Immunity* **36**, 1031-1046, doi:10.1016/j.immuni.2012.03.027 (2012).
- 91 Hochheiser, K. *et al.* Exclusive CX3CR1 dependence of kidney DCs impacts glomerulonephritis progression. *Journal of Clinical Investigation* **123**, 4242-4254, doi:10.1172/JCI70143 (2013).
- 92 Schmid, M. A. *et al.* Instructive cytokine signals in dendritic cell lineage commitment. *Immunol Rev* **234**, 32-44, doi:10.1111/j.0105-2896.2009.00877.x (2010).
- 93 Ginhoux, F. *et al.* The origin and development of nonlymphoid tissue CD103 +DCs. *Journal of Experimental Medicine* **206**, 3115-3130, doi:10.1084/jem.20091756 (2009).
- 94 Suzuki, S. *et al.* Critical roles of interferon regulatory factor 4 in CD11bhighCD8 α - dendritic cell development. *Proceedings of the National Academy of Sciences of the United States of America* **101**, 8981-8986, doi:10.1073/pnas.0402139101 (2004).
- 95 Tussiwand, R. *et al.* Klf4 expression in conventional dendritic cells is required for T helper 2 cell responses. *Immunity* **42**, 916-928, doi:10.1016/j.immuni.2015.04.017 (2015).
- 96 Bain, C. C. *et al.* TGF β R signalling controls CD103(+)CD11b(+) dendritic cell development in the intestine. *Nat Commun* **8**, 620, doi:10.1038/s41467-017-00658-6 (2017).
- 97 Kabashima, K. *et al.* Intrinsic Lymphotoxin- β Receptor Requirement for Homeostasis of Lymphoid Tissue Dendritic Cells. *Immunity* **22**, 439-450, doi:10.1016/j.immuni.2005.02.007 (2005).

- 98 Wang, Y.-G. *et al.* Stimulating lymphotoxin beta receptor on the dendritic cells is critical for their homeostasis and expansion. *The Journal of Immunology* **175**, 6997-7002, doi:10.4049/jimmunol.175.10.6997 (2005).
- 99 Salvermoser, J. *et al.* Clec9a-Mediated Ablation of Conventional Dendritic Cells Suggests a Lymphoid Path to Generating Dendritic Cells In Vivo. *Frontiers in Immunology* **9**, 699, doi:10.3389/fimmu.2018.00699 (2018).
- 100 Manz, M. G. Dendritic cell potentials of early lymphoid and myeloid progenitors. *Blood* **97**, 3333-3341, doi:10.1182/blood.V97.11.3333 (2001).
- 101 Izon, D. *et al.* A Common Pathway for Dendritic Cell and Early B Cell Development. *The Journal of Immunology* **167**, 1387-1392, doi:10.4049/jimmunol.167.3.1387 (2001).
- 102 Mendelsohn, C. Using mouse models to understand normal and abnormal urogenital tract development. *Organogenesis* **5**, 306-314 (2009).
- 103 Davidson, A. J. Mouse kidney development. *StemBook*, doi:10.3824/stembook.1.34.1 (2008).
- 104 Lindstrom, N. O. *et al.* Conserved and Divergent Features of Mesenchymal Progenitor Cell Types within the Cortical Nephrogenic Niche of the Human and Mouse Kidney. *J Am Soc Nephrol* **29**, 806-824, doi:10.1681/ASN.2017080890 (2018).
- 105 Liebelt, A. G. Unique Features of Anatomy, Histology, and Ultrastructure Kidney, Mause. *Urinary System* 37-57 (Springer, Berlin, Heidelberg, 1998).
- 106 Wall, S. M. Renal intercalated cells and blood pressure regulation. *Kidney Research and Clinical Practice* **36**, 305-317, doi:10.23876/j.krcp.2017.36.4.305 (2017).
- 107 Zhang, M.-Z. *et al.* Intrarenal dopamine deficiency leads to hypertension and decreased longevity in mice. *Journal of Clinical Investigation* **121**, 2845-2854, doi:10.1172/JCI57324 (2011).
- 108 Hartner, A. *et al.* Strain differences in the development of hypertension and glomerular lesions induced by deoxycorticosterone acetate salt in mice. *Nephrology Dialysis Transplantation* **18**, 1999-2004, doi:10.1093/ndt/gfg299 (2003).
- 109 Kumar, R. *et al.* Vitamin D and the kidney. *Archives of biochemistry and biophysics* **523**, 77-86, doi:10.1016/j.abb.2012.03.003 (2012).
- 110 Healy, K. D. *et al.* Regulation of the murine renal vitamin D receptor by 1,25-dihydroxyvitamin D3 and calcium. *Proceedings of the National Academy of Sciences* **100**, 9733-9737, doi:10.1073/pnas.1633774100 (2003).
- 111 Dunn, A. & Donnelly, S. The Role of the Kidney in Blood Volume Regulation: The Kidney as a Regulator of the Hematocrit. *The American Journal of the Medical Sciences* **334**, 65-71, doi:10.1097/MAJ.0b013e318095a4ae (2007).
- 112 Westenfelder, C. *et al.* Human, rat, and mouse kidney cells express functional erythropoietin receptors. *Kidney International* **55**, 808-820, doi:10.1046/j.1523-1755.1999.055003808.x (1999).
- 113 Gowda, S. *et al.* Markers of renal function test. *North American Journal of Medical Science* **2**, 170-173 (2010).
- 114 Kurien, B. T. *et al.* Experimental animal urine collection: a review. *Lab Anim* **38**, 333-361, doi:10.1258/0023677041958945 (2004).
- 115 Ronco, C. & Chawla, L. S. Glomerular and Tubular Kidney Stress Test: New Tools for a Deeper Evaluation of Kidney Function. *Nephron* **134**, 191-194, doi:10.1159/000449235 (2016).
- 116 Tesch, G. H. Review: Serum and urine biomarkers of kidney disease: A pathophysiological perspective. *Nephrology (Carlton)* **15**, 609-616, doi:10.1111/j.1440-1797.2010.01361.x (2010).
- 117 Kawakami, T. *et al.* Resident Renal Mononuclear Phagocytes Comprise Five Discrete Populations with Distinct Phenotypes and Functions. *The Journal of Immunology* **191**, 3358-3372, doi:10.4049/jimmunol.1300342 (2013).
- 118 Nelson, P. J. *et al.* The Renal Mononuclear Phagocytic System. *Journal of the American Society of Nephrology* **23**, 194-203, doi:10.1681/ASN.2011070680 (2012).
- 119 Schlitzer, A. *et al.* IRF4 Transcription Factor-Dependent CD11b+ Dendritic Cells in Human and Mouse Control Mucosal IL-17 Cytokine Responses. *Immunity* **38**, 970-983, doi:10.1016/j.immuni.2013.04.011 (2013).
- 120 Tamoutounour, S. *et al.* CD64 distinguishes macrophages from dendritic cells in the gut and reveals the Th1-inducing role of mesenteric lymph node macrophages during colitis. *European journal of immunology* **42**, 3150-3166, doi:10.1002/eji.201242847 (2012).
- 121 Langlet, C. *et al.* CD64 Expression Distinguishes Monocyte-Derived and Conventional Dendritic Cells and Reveals Their Distinct Role during Intramuscular Immunization. *The Journal of Immunology* **188**, 1751-1760, doi:10.4049/jimmunol.1102744 (2012).

- 122 Cao, Q. *et al.* CD103+ Dendritic Cells Elicit CD8+ T Cell Responses to Accelerate Kidney Injury in Adriamycin Nephropathy. *Journal of the American Society of Nephrology* **27**, 1344-1360, doi:10.1681/ASN.2015030229 (2016).
- 123 Poulin, L. F. *et al.* DNGR-1 is a specific and universal marker of mouse and human Batf3-dependent dendritic cells in lymphoid and nonlymphoid tissues. *Blood* **119**, 6052-6062, doi:10.1182/blood-2012-01-406967 (2012).
- 124 Puranik, A. S. *et al.* Kidney-resident macrophages promote a proangiogenic environment in the normal and chronically ischemic mouse kidney. *Scientific Reports* **8**, doi:10.1038/s41598-018-31887-4 (2018).
- 125 Brähler, S. *et al.* Opposing Roles of Dendritic Cell Subsets in Experimental GN. *Journal of the American Society of Nephrology : JASN* **29**, 138-154, doi:10.1681/ASN.2017030270 (2018).
- 126 Lee, S. A. *et al.* Characterization of kidney CD45intCD11bintF4/80+MHCII+CX3CR1+Ly6C- "intermediate mononuclear phagocytic cells". *PLoS One* **13**, e0198608, doi:10.1371/journal.pone.0198608 (2018).
- 127 van Blijswijk, J. *et al.* Advantages and limitations of mouse models to deplete dendritic cells. *European journal of immunology* **43**, 22-26, doi:10.1002/eji.201243022 (2013).
- 128 Stamatiades, E. G. *et al.* Immune Monitoring of Trans-endothelial Transport by Kidney-Resident Macrophages. *Cell* **166**, 991-1003, doi:10.1016/j.cell.2016.06.058 (2016).
- 129 Kurts, C. *et al.* The immune system and kidney disease: basic concepts and clinical implications. *Nature Reviews Immunology* **13**, 738-753, doi:10.1038/nri3523 (2013).
- 130 Weisheit, C. K. *et al.* Dendritic Cells and Macrophages: Sentinels in the Kidney. *Clinical Journal of the American Society of Nephrology* **10**, 1841-1851, doi:10.2215/CJN.07100714 (2015).
- 131 Yatim, K. M. *et al.* Renal dendritic cells sample blood-borne antigen and guide T-cell migration to the kidney by means of intravascular processes. *Kidney International* **90**, 818-827, doi:10.1016/j.kint.2016.05.030 (2016).
- 132 Soos, T. J. *et al.* CX3CR1+ interstitial dendritic cells form a contiguous network throughout the entire kidney. *Kidney International* **70**, 591-596, doi:10.1038/sj.ki.5001567 (2006).
- 133 Kim, K.-W. *et al.* In vivo structure/function and expression analysis of the CX3C chemokine fractalkine. *Blood* **118**, e156-167, doi:10.1182/blood-2011-04-348946 (2011).
- 134 Lionakis, M. S. *et al.* CX3CR1-dependent renal macrophage survival promotes Candida control and host survival. *Journal of Clinical Investigation* **123**, 5035-5051, doi:10.1172/JCI71307 (2013).
- 135 Gottschalk, C. *et al.* Batf3-Dependent Dendritic Cells in the Renal Lymph Node Induce Tolerance against Circulating Antigens. *Journal of the American Society of Nephrology* **24**, 543-549, doi:10.1681/ASN.2012101022 (2013).
- 136 Tittel, A. P. *et al.* Kidney Dendritic Cells Induce Innate Immunity against Bacterial Pyelonephritis. *Journal of the American Society of Nephrology* **22**, 1435-1441, doi:10.1681/ASN.2010101072 (2011).
- 137 Whitney, P. G. *et al.* Syk Signaling in Dendritic Cells Orchestrates Innate Resistance to Systemic Fungal Infection. *PLoS pathogens* **10**, e1004276-1004215, doi:10.1371/journal.ppat.1004276 (2014).
- 138 Turner, J. E. *et al.* IL-17A Production by Renal T Cells Promotes Kidney Injury in Crescentic GN. *Journal of the American Society of Nephrology* **23**, 1486-1495, doi:10.1681/ASN.2012010040 (2012).
- 139 Hochheiser, K. *et al.* Kidney Dendritic Cells Become Pathogenic during Crescentic Glomerulonephritis with Proteinuria. *Journal of the American Society of Nephrology* **22**, 306-316, doi:10.1681/ASN.2010050548 (2011).
- 140 Dong, X. *et al.* Resident dendritic cells are the predominant TNF-secreting cell in early renal ischemia-reperfusion injury. *Kidney International* **71**, 619-628, doi:10.1038/sj.ki.5002132 (2007).
- 141 Scholz, J. *et al.* Renal Dendritic Cells Stimulate IL-10 Production and Attenuate Nephrotoxic Nephritis. *Journal of the American Society of Nephrology* **19**, 527-537, doi:10.1681/ASN.2007060684 (2008).
- 142 Tipping, P. G. & Holdsworth, S. R. T cells in crescentic glomerulonephritis. *Journal of the American Society of Nephrology* **17**, 1253-1263, doi:10.1681/ASN.2005091013 (2006).
- 143 Kitching, A. R. *et al.* Interleukin-4 and interleukin-10 attenuate established crescentic glomerulonephritis in mice. *Kidney International* **52**, 52-59 (1997).
- 144 Wilson, H. M. *et al.* Bone-marrow-derived macrophages genetically modified to produce IL-10 reduce injury in experimental glomerulonephritis. *Molecular therapy : the journal of the American Society of Gene Therapy* **6**, 710-717 (2002).
- 145 Evers, B. D. G. *et al.* CD103+ Kidney Dendritic Cells Protect against Crescentic GN by Maintaining IL-10-Producing Regulatory T Cells. *Journal of the American Society of Nephrology*, 1-15, doi:10.1681/ASN.2015080873 (2016).
- 146 Ozkok, A. & Edelstein, C. L. Pathophysiology of Cisplatin-Induced Acute Kidney Injury. *BioMed Research International* **2014**, 1-17, doi:10.1155/2014/967826 (2014).

- 147 Miller, R. P., *et al.* Mechanisms of Cisplatin Nephrotoxicity. *Toxins* **2**, 2490-2518, doi:10.3390/toxins2112490 (2010).
- 148 Ramesh, G. & Reeves, W. B. TNFR2-mediated apoptosis and necrosis in cisplatin-induced acute renal failure. *Am J Physiol Renal Physiol* **285**, F610-618, doi:10.1152/ajprenal.00101.2003 (2003).
- 149 Tadagavadi, R. K. & Reeves, W. B. Renal Dendritic Cells Ameliorate Nephrotoxic Acute Kidney Injury. *Journal of the American Society of Nephrology* **21**, 53-63, doi:10.1681/ASN.2009040407 (2010).
- 150 Tadagavadi, R. K. & Reeves, W. B. Endogenous IL-10 Attenuates Cisplatin Nephrotoxicity: Role of Dendritic Cells. *The Journal of Immunology* **185**, 4904-4911, doi:10.4049/jimmunol.1000383 (2010).
- 151 Tadagavadi, R. *et al.* Dendritic Cell Protection from Cisplatin Nephrotoxicity Is Independent of Neutrophils. *Toxins* **7**, 3245-3256, doi:10.3390/toxins7083245 (2015).
- 152 Li, L. *et al.* IL-17 produced by neutrophils regulates IFN-gamma-mediated neutrophil migration in mouse kidney ischemia-reperfusion injury. *J Clin Invest* **120**, 331-342, doi:10.1172/JCI38702 (2010).
- 153 Bolisetty, S. & Agarwal, A. Neutrophils in acute kidney injury: not neutral any more. *Kidney Int* **75**, 674-676, doi:10.1038/ki.2008.689 (2009).
- 154 Faubel, S. *et al.* Cisplatin-Induced Acute Renal Failure Is Associated with an Increase in the Cytokines Interleukin (IL)-1beta, IL-18, IL-6, and Neutrophil Infiltration in the Kidney. *Journal of Pharmacology and Experimental Therapeutics* **322**, 8-15, doi:10.1124/jpet.107.119792 (2007).
- 155 Jang, H. R. & Rabb, H. The innate immune response in ischemic acute kidney injury. *Clin Immunol* **130**, 41-50, doi:10.1016/j.clim.2008.08.016 (2009).
- 156 Sinuani, I. *et al.* Role of IL-10 in the progression of kidney disease. *World J Transplant* **3**, 91-98, doi:10.5500/wjt.v3.i4.91 (2013).
- 157 Sziksz, E. *et al.* Fibrosis Related Inflammatory Mediators: Role of the IL-10 Cytokine Family. *Mediators Inflamm* **2015**, 764641, doi:10.1155/2015/764641 (2015).
- 158 Lu, L. H. *et al.* Increased macrophage infiltration and fractalkine expression in cisplatin-induced acute renal failure in mice. *The Journal of pharmacology and experimental therapeutics* **324**, 111-117, doi:10.1124/jpet.107.130161 (2008).
- 159 Weisser, S. B., van Rooijen, N. & Sly, L. M. Depletion and Reconstitution of Macrophages in Mice. *Journal of Visualized Experiments*, doi:10.3791/4105 (2012).
- 160 Nakano, H. *et al.* Distinct functions of CXCR4, CCR2, and CX3CR1 direct dendritic cell precursors from the bone marrow to the lung. *J Leukoc Biol* **101**, 1143-1153, doi:10.1189/jlb.1A0616-285R (2017).
- 161 Munro, D. A. D. & Hughes, J. The Origins and Functions of Tissue-Resident Macrophages in Kidney Development. *Frontiers in Physiology* **8**, 275-213, doi:10.3389/fphys.2017.00837 (2017).
- 162 Li, L. *et al.* The chemokine receptors CCR2 and CX3CR1 mediate monocyte/macrophage trafficking in kidney ischemia-reperfusion injury. *Kidney Int* **74**, 1526-1537, doi:10.1038/ki.2008.500 (2008).
- 163 Bar-On, L. & Jung, S. Defining dendritic cells by conditional and constitutive cell ablation. *Immunological reviews* **234**, 76-89, doi:10.1111/j.0105-2896.2009.00875.x (2010).
- 164 Bennett, C. L. & Clausen, B. E. DC ablation in mice: promises, pitfalls, and challenges. *Trends in immunology* **28**, 525-531, doi:10.1016/j.it.2007.08.011 (2007).
- 165 Goren, I. *et al.* A transgenic mouse model of inducible macrophage depletion: effects of diphtheria toxin-driven lysozyme M-specific cell lineage ablation on wound inflammatory, angiogenic, and contractive processes. *Am J Pathol* **175**, 132-147, doi:10.2353/ajpath.2009.081002 (2009).
- 166 Hua, L. *et al.* Genetic Models of Macrophage Depletion. *Methods in molecular biology (Clifton, N.J.)* **1784**, 243-258, doi:10.1007/978-1-4939-7837-3_22 (2018).
- 167 McCright, B., Lozier, J. & Gridley, T. Generation of new Notch2 mutant alleles. *Genesis* **44**, 29-33, doi:10.1002/gene.20181 (2006).
- 168 Holtschke, T. *et al.* Immunodeficiency and chronic myelogenous leukemia-like syndrome in mice with a targeted mutation of the ICSBP gene. *Cell* **87**, 307-317 (1996).
- 169 Katz, J. *et al.* The zinc-finger transcription factor Klf4 is required for terminal differentiation of goblet cells in the colon. *Development* **129**, 2619-2628 (2002).
- 170 Chitu, V. & Stanley, E. R. Colony-stimulating factor-1 in immunity and inflammation. *Curr Opin Immunol* **18**, 39-48, doi:10.1016/j.coi.2005.11.006 (2006).
- 171 Burnett, S. H. *et al.* Conditional macrophage ablation in transgenic mice expressing a Fas-based suicide gene. *J Leukoc Biol* **75**, 612-623, doi:10.1189/jlb.0903442 (2004).
- 172 Li, J., Chen, K., Zhu, L. & Pollard, J. W. Conditional deletion of the colony stimulating factor-1 receptor (c-fms proto-oncogene) in mice. *Genesis* **44**, 328-335, doi:10.1002/dvg.20219 (2006).

- 173 Dai, X. M. *et al.* Targeted disruption of the mouse colony-stimulating factor 1 receptor gene results in osteopetrosis, mononuclear phagocyte deficiency, increased primitive progenitor cell frequencies, and reproductive defects. *Blood* **99**, 111-120, doi:10.1182/blood.V99.1.111 (2002).
- 174 Yoshida, H. *et al.* The murine mutation osteopetrosis is in the coding region of the macrophage colony stimulating factor gene. *Nature* **345**, 442-444, doi:10.1038/345442a0 (1990).
- 175 Wiktor-Jedrzejczak, W. *et al.* Total absence of colony-stimulating factor 1 in the macrophage-deficient osteopetrotic (op/op) mouse. *Proceedings of the National Academy of Sciences* **87**, 4828-4832, doi:10.1073/pnas.87.12.4828 (1990).
- 176 Saelinger, C. B. *et al.* Uptake of diphtheria toxin and its fragment A moiety by mammalian cells in culture. *Infect Immun* **14**, 742-751 (1976).
- 177 Saelinger, C. *et al.* Interaction of Toxin of *Corynebacterium diphtheriae* with Phagocytes from Susceptible and Resistant Species. *Journal of Infectious Diseases* **131**, 431-438, doi:10.1093/infdis/131.4.431 (1975).
- 178 Jung, S. *et al.* In vivo depletion of CD11c+ dendritic cells abrogates priming of CD8+ T cells by exogenous cell-associated antigens. *Immunity* **17**, 211-220 (2002).
- 179 Hochweller, K. *et al.* A novel CD11c.DTR transgenic mouse for depletion of dendritic cells reveals their requirement for homeostatic proliferation of natural killer cells. *Eur J Immunol* **38**, 2776-2783, doi:10.1002/eji.200838659 (2008).
- 180 Tittel, A. P. *et al.* Functionally relevant neutrophilia in CD11c diphtheria toxin receptor transgenic mice. *Nat Methods* **9**, 385-390, doi:10.1038/nmeth.1905 (2012).
- 181 Piva, L. *et al.* Cutting edge: Clec9A+ dendritic cells mediate the development of experimental cerebral malaria. *J Immunol* **189**, 1128-1132, doi:10.4049/jimmunol.1201171 (2012).
- 182 Fukaya, T. *et al.* Conditional ablation of CD205+ conventional dendritic cells impacts the regulation of T-cell immunity and homeostasis in vivo. *Proc Natl Acad Sci U S A* **109**, 11288-11293, doi:10.1073/pnas.1202208109 (2012).
- 183 Bennett, C. L. *et al.* Inducible ablation of mouse Langerhans cells diminishes but fails to abrogate contact hypersensitivity. *The Journal of Cell Biology* **169**, 569-576, doi:10.1083/jcb.200501071 (2005).
- 184 Kissenpfennig, A. *et al.* Dynamics and function of Langerhans cells in vivo: dermal dendritic cells colonize lymph node areas distinct from slower migrating Langerhans cells. *Immunity* **22**, 643-654, doi:10.1016/j.immuni.2005.04.004 (2005).
- 185 Yamazaki, C. *et al.* Critical Roles of a Dendritic Cell Subset Expressing a Chemokine Receptor, XCR1. *The Journal of Immunology* **190**, 6071-6082, doi:10.4049/jimmunol.1202798 (2013).
- 186 Baranska, A. *et al.* Unveiling skin macrophage dynamics explains both tattoo persistence and strenuous removal. *Journal of Experimental Medicine* **215**, 1115-1133, doi:10.1084/jem.20171608 (2018).
- 187 Duffield, J. S. *et al.* Selective depletion of macrophages reveals distinct, opposing roles during liver injury and repair. *Journal of Clinical Investigation* **115**, 56-65, doi:10.1172/jci200522675 (2005).
- 188 Miyake, Y. *et al.* Critical role of macrophages in the marginal zone in the suppression of immune responses to apoptotic cell-associated antigens. *J Clin Invest* **117**, 2268-2278, doi:10.1172/JCI31990 (2007).
- 189 Zaft, T. *et al.* CD11c^{high} Dendritic Cell Ablation Impairs Lymphopenia-Driven Proliferation of Naive and Memory CD8+ T Cells. *The Journal of Immunology* **175**, 6428-6435, doi:10.4049/jimmunol.175.10.6428 (2005).
- 190 Maizels, N. Genome engineering with Cre-loxP. *J Immunol* **191**, 5-6, doi:10.4049/jimmunol.1301241 (2013).
- 191 Liu, J. *et al.* Non-parallel recombination limits cre-loxP-based reporters as precise indicators of conditional genetic manipulation. *Genesis* **51**, 436-442, doi:10.1002/dvg.22384 (2013).
- 192 Zheng, B. *et al.* Engineering mouse chromosomes with Cre-loxP: range, efficiency, and somatic applications. *Mol Cell Biol* **20**, 648-655 (2000).
- 193 Bouabe, H. & Okkenhaug, K. Gene targeting in mice: a review. *Methods Mol Biol* **1064**, 315-336, doi:10.1007/978-1-62703-601-6_23 (2013).
- 194 Feng, J. *et al.* IFN regulatory factor 8 restricts the size of the marginal zone and follicular B cell pools. *J Immunol* **186**, 1458-1466, doi:10.4049/jimmunol.1001950 (2011).
- 195 Klein, U. *et al.* Transcription factor IRF4 controls plasma cell differentiation and class-switch recombination. *Nature Immunology* **7**, 773-782, doi:10.1038/ni1357 (2006).
- 196 Caton, M. L., Smith-Raska, M. R. & Reizis, B. Notch-RBP-J signaling controls the homeostasis of CD8⁺-dendritic cells in the spleen. *Journal of Experimental Medicine* **204**, 1653-1664, doi:10.1084/jem.20062648 (2007).

- 197 Mattiuz, R. *et al.* Novel Cre-Expressing Mouse Strains Permitting to Selectively Track and Edit Type 1
Conventional Dendritic Cells Facilitate Disentangling Their Complexity in vivo. *Front Immunol* **9**, 2805,
doi:10.3389/fimmu.2018.02805 (2018).
- 198 Clausen, B. E. *et al.* Conditional gene targeting in macrophages and granulocytes using LysMcre mice.
Transgenic Research **8**, 265-277, doi:10.1023/a:1008942828960 (1999).
- 199 Schaller, E. *et al.* Inactivation of the F4/80 Glycoprotein in the Mouse Germ Line. *Molecular and Cellular
Biology* **22**, 8035-8043, doi:10.1128/mcb.22.22.8035-8043.2002 (2002).
- 200 Scott, C. L. *et al.* The Transcription Factor ZEB2 Is Required to Maintain the Tissue-Specific Identities of
Macrophages. *Immunity*, 1-36, doi:10.1016/j.immuni.2018.07.004 (2018).
- 201 Yona, S. *et al.* Fate mapping reveals origins and dynamics of monocytes and tissue macrophages under
homeostasis. *Immunity* **38**, 79-91, doi:10.1016/j.immuni.2012.12.001 (2013).
- 202 Bruttger, J. *et al.* Genetic Cell Ablation Reveals Clusters of Local Self-Renewing Microglia in the
Mammalian Central Nervous System. *Immunity* **43**, 92-106, doi:10.1016/j.immuni.2015.06.012 (2015).
- 203 Buch, T. *et al.* A Cre-inducible diphtheria toxin receptor mediates cell lineage ablation after toxin
administration. *Nature Methods* **2**, 419-426, doi:10.1038/nmeth762 (2005).
- 204 van Blijswijk, J. *et al.* Altered lymph node composition in diphtheria toxin receptor-based mouse models
to ablate dendritic cells. *Journal of immunology (Baltimore, Md. : 1950)* **194**, 307-315,
doi:10.4049/jimmunol.1401999 (2015).
- 205 Diehl, G. E. *et al.* Microbiota restricts trafficking of bacteria to mesenteric lymph nodes by CX(3)CR1(hi)
cells. *Nature* **494**, 116-120, doi:10.1038/nature11809 (2013).
- 206 Okuyama, M. *et al.* A novel in vivo inducible dendritic cell ablation model in mice. *Biochem Biophys Res
Commun* **397**, 559-563, doi:10.1016/j.bbrc.2010.05.157 (2010).
- 207 Abram, C. L. *et al.* Comparative analysis of the efficiency and specificity of myeloid-Cre deleting strains
using ROSA-EYFP reporter mice. *Journal of Immunological Methods* **408**, 89-100,
doi:10.1016/j.jim.2014.05.009 (2014).
- 208 Hirrlinger, J. *et al.* Split-cre complementation indicates coincident activity of different genes in vivo.
PLoS One **4**, e4286, doi:10.1371/journal.pone.0004286 (2009).
- 209 Nimmerjahn, F. & Ravetch, J. V. Fcγ receptors: old friends and new family members. *Immunity*
24, 19-28, doi:10.1016/j.immuni.2005.11.010 (2006).
- 210 Nimmerjahn, F. & Ravetch, J. V. Fcγ receptors as regulators of immune responses. *Nature Reviews
Immunology* **8**, 34-47, doi:10.1038/nri2206 (2008).
- 211 Guilliams, M. *et al.* The function of Fcγ receptors in dendritic cells and macrophages. *Nature Reviews
Immunology* **14**, 1-16, doi:10.1038/nri3582 (2014).
- 212 Gene [Internet]. Bethesda (MD): National Library of Medicine (US), National Center for Biotechnology
Information. 2004. Available from: <https://www.ncbi.nlm.nih.gov/gene/>.
- 213 Zerbino, D.R. *et al.* Ensembl 2018. PubMed PMID: 29155950. doi:10.1093/nar/gkx1098.
- 214 The UniProt Consortium. UniProt: a worldwide hub of protein knowledge. *Nucleic Acids Res.* **47**: D506-
515 (2019).
- 215 Sears, D. W. *et al.* Molecular cloning and expression of the mouse high affinity Fc receptor for IgG. *The
Journal of Immunology* **144**, 371-378 (1990).
- 216 Rosales, C. Fcγ Receptor Heterogeneity in Leukocyte Functional Responses. *Frontiers in Immunology* **8**,
280, doi:10.3389/fimmu.2017.00280 (2017).
- 217 Rosales, C. & Eileen Uribe-Querol, E. Fc receptors: Cell activators of antibody functions *Advances in
Bioscience and Biotechnology* **4**, 21-33, doi:<http://dx.doi.org/10.4236/abb.2013.44A004> (2013).
- 218 Min, J. *et al.* Inflammation induces two types of inflammatory dendritic cells in inflamed lymph nodes.
Experimental and Molecular Medicine **50**, e458-416, doi:10.1038/emm.2017.292 (2018).
- 219 Barnes, N. *et al.* FcγRI-deficient mice show multiple alterations to inflammatory and immune
responses. *Immunity* **16**, 379-389 (2002).
- 220 Ioan-Facsinay, A. *et al.* FcγRI (CD64) contributes substantially to severity of arthritis,
hypersensitivity responses, and protection from bacterial infection. *Immunity* **16**, 391-402 (2002).
- 221 Unkeless, J. C. & Eisen, H. N. Binding of monomeric immunoglobulins to Fc receptors of mouse
macrophages. *Journal of Experimental Medicine* **142**, 1520-1533, doi:10.1084/jem.142.6.1520 (1975).
- 222 Hulet, M. D. *et al.* Chimeric Fc receptors identify functional domains of the murine high affinity
receptor for IgG. *The Journal of Immunology* **147**, 1863-1868 (1991).
- 223 Harrison, P. T. *et al.* The interaction between human Fc γRI and the γ-chain is mediated
solely via the 21 amino acid transmembrane domain of Fc γRI. *Molecular membrane biology* **12**,
309-312 (1995).

- 224 Indik, Z. K. *et al.* The high affinity Fc gamma receptor (CD64) induces phagocytosis in the absence of its cytoplasmic domain: the gamma subunit of Fc gamma RIIIA imparts phagocytic function to Fc gamma RI. *Experimental hematology* **22**, 599-606 (1994).
- 225 Daeron, M. Intracytoplasmic sequences involved in the biological properties of low-affinity receptors for IgG expressed by murine macrophages. *Braz J Med Biol Res* **28**, 263-274 (1995).
- 226 van Vugt, M. J. *et al.* The Fc gamma RIa (CD64) ligand binding chain triggers major histocompatibility complex class II antigen presentation independently of its associated FcR gamma-chain. *Blood* **94**, 808-817 (1999).
- 227 Prins, J. B. *et al.* Linkage on chromosome 3 of autoimmune diabetes and defective Fc receptor for IgG in NOD mice. *Science* **260**, 695-698 (1993).
- 228 Quilliam, A. L. *et al.* Biochemical characterization of murine Fc gamma RI. *Immunology* **78**, 358-363 (1993).
- 229 Ran, F. A. *et al.* Genome engineering using the CRISPR-Cas9 system. *Nature Protocols* **8**, 2281-2308, doi:10.1038/nprot.2013.143 (2013).
- 230 Yang, H., Wang, H. & Jaenisch, R. Generating genetically modified mice using CRISPR/Cas-mediated genome engineering. *Nature Protocols* **9**, 1956-1968, doi:10.1038/nprot.2014.134 (2014).
- 231 Yang, H. *et al.* One-Step Generation of Mice Carrying Reporter and Conditional Alleles by CRISPR/Cas-Mediated Genome Engineering. *Cell* **154**, 1370-1379, doi:10.1016/j.cell.2013.08.022 (2013).
- 232 Baumgart, A.-K. & Beyer, M. Genetic engineering as a tool for the generation of mouse models to understand disease phenotypes and gene function. *Current opinion in biotechnology* **48**, 228-233, doi:10.1016/j.copbio.2017.06.012 (2017).
- 233 Ryu, J., Prather, R. S. & Lee, K. Use of gene-editing technology to introduce targeted modifications in pigs. *Journal of Animal Science and Biotechnology* **9**, 1-10, doi:10.1186/s40104-017-0228-7 (2018).
- 234 Capecchi, M. R. Gene targeting in mice: functional analysis of the mammalian genome for the twenty-first century. *Nature reviews. Genetics* **6**, 507-512, doi:10.1038/nrg1619 (2005).
- 235 Maggio, I., Chen, X. & Gonçalves, M. A. F. V. The emerging role of viral vectors as vehicles for DMD gene editing. *Genome Medicine*, 1-10, doi:10.1186/s13073-016-0316-x (2016).
- 236 Zych, A. O *et al.* Application of Genome Editing Techniques in Immunology. *Archivum Immunologiae et Therapiae Experimentalis* **66**, 289-298, doi:10.1007/s00005-018-0504-z (2018).
- 237 Nami, F. *et al.* Strategies for In Vivo Genome Editing in Nondividing Cells. *Trends in Biotechnology* **36**, 770-786, doi:10.1016/j.tibtech.2018.03.004 (2018).
- 238 Peddle, C. F. & Maclaren, R. E. The Application of CRISPR/Cas9 for the Treatment of Retinal Diseases. *The Yale journal of biology and medicine* **90**, 533-541 (2017).
- 239 Guha, T. K., Wai, A. & Hausner, G. Programmable Genome Editing Tools and their Regulation for Efficient Genome Engineering. *Computational and Structural Biotechnology Journal* **15**, 1-15, doi:10.1016/j.csbj.2016.12.006 (2017).
- 240 Ceccaldi, R., Rondinelli, B. & D'Andrea, A. D. Repair Pathway Choices and Consequences at the Double-Strand Break. *Trends Cell Biol* **26**, 52-64, doi:10.1016/j.tcb.2015.07.009 (2016).
- 241 Krejci, L. *et al.* Homologous recombination and its regulation. *Nucleic Acids Research* **40**, 5795-5818, doi:10.1093/nar/gks270 (2012).
- 242 Brinkman, E. K. *et al.* Kinetics and Fidelity of the Repair of Cas9-Induced Double-Strand DNA Breaks. *Molecular Cell* **70**, 801-813 e6, doi:10.1016/j.molcel.2018.04.016 (2018).
- 243 Babinet, C. Transgenic mice: an irreplaceable tool for the study of mammalian development and biology. *J Am Soc Nephrol* **11 Suppl 16**, S88-94 (2000).
- 244 Babinet, C. & Cohen-Tannoudji, M. Genome engineering via homologous recombination in mouse embryonic stem (ES) cells: an amazingly versatile tool for the study of mammalian biology. *Anais da Academia Brasileira de Ciências* **73**, 365-383, doi:10.1590/s0001-37652001000300007 (2001).
- 245 Mladenov, E., Magin, S., Soni, A. & Iliakis, G. DNA double-strand break repair as determinant of cellular radiosensitivity to killing and target in radiation therapy. *Frontiers in oncology* **3**, 113, doi:10.3389/fonc.2013.00113 (2013).
- 246 Kakarougkas, A. & Jeggo, P. A. DNA DSB repair pathway choice: an orchestrated handover mechanism. *The British journal of radiology* **87**, 20130685, doi:10.1259/bjr.20130685 (2014).
- 247 Filippo, J. S., Sung, P. & Klein, H. Mechanism of Eukaryotic Homologous Recombination. *Annual review of biochemistry* **77**, 229-257, doi:10.1146/annurev.biochem.77.061306.125255 (2008).
- 248 Jeppesen, D. K., Bohr, V. A. & Stevnsner, T. DNA repair deficiency in neurodegeneration. *Progress in Neurobiology* **94**, 166-200, doi:10.1016/j.pneurobio.2011.04.013 (2011).

- 249 West, S. C. Molecular views of recombination proteins and their control. *Nature reviews. Molecular cell biology* **4**, 435-445, doi:10.1038/nrm1127 (2003).
- 250 Wyman, C. & Kanaar, R. DNA double-strand break repair: all's well that ends well. *Annual review of genetics* **40**, 363-383, doi:10.1146/annurev.genet.40.110405.090451 (2006).
- 251 Mladenov, E. & Iliakis, G. The pathways of double-strand break repair. *intechopen.com* (2011).
- 252 Porteus, M. H. & Carroll, D. Gene targeting using zinc finger nucleases. *Nature Biotechnology* **23**, 967-973, doi:10.1038/nbt1125 (2005).
- 253 Stoddard, B. L. Homing endonucleases: from microbial genetic invaders to reagents for targeted DNA modification. *Structure (London, England : 1993)* **19**, 7-15, doi:10.1016/j.str.2010.12.003 (2011).
- 254 Doyle, E. L. *et al.* TAL effectors: highly adaptable phytobacterial virulence factors and readily engineered DNA-targeting proteins. *Trends in cell biology* **23**, 390-398, doi:10.1016/j.tcb.2013.04.003 (2013).
- 255 Ran, F. A. *et al.* Double nicking by RNA-guided CRISPR Cas9 for enhanced genome editing specificity. *Cell* **154**, 1380-1389, doi:10.1016/j.cell.2013.08.021 (2013).
- 256 Sander, J. D. & Joung, J. K. CRISPR-Cas systems for editing, regulating and targeting genomes. *Nature Biotechnology* **32**, 347-355, doi:10.1038/nbt.2842 (2014).
- 257 Rath, D. *et al.* The CRISPR-Cas immune system: biology, mechanisms and applications. *Biochimie* **117**, 119-128, doi:10.1016/j.biochi.2015.03.025 (2015).
- 258 Makarova, K. S. & Koonin, E. V. Annotation and Classification of CRISPR-Cas Systems. *Methods Mol Biol* **1311**, 47-75, doi:10.1007/978-1-4939-2687-9_4 (2015).
- 259 Richter, H., Randau, L. & Plagens, A. Exploiting CRISPR/Cas: interference mechanisms and applications. *International journal of molecular sciences* **14**, 14518-14531, doi:10.3390/ijms140714518 (2013).
- 260 Wiedenheft, B., Sternberg, S. H. & Doudna, J. A. RNA-guided genetic silencing systems in bacteria and archaea. *Nature* **482**, 331-338, doi:10.1038/nature10886 (2012).
- 261 Deltcheva, E. *et al.* CRISPR RNA maturation by trans-encoded small RNA and host factor RNase III. *Nature* **471**, 602-607, doi:10.1038/nature09886 (2011).
- 262 Pougach, K. *et al.* Transcription, processing and function of CRISPR cassettes in *Escherichia coli*. *Molecular microbiology* **77**, 1367-1379, doi:10.1111/j.1365-2958.2010.07265.x (2010).
- 263 Garneau, J. E. *et al.* The CRISPR/Cas bacterial immune system cleaves bacteriophage and plasmid DNA. *Nature* **468**, 67-71, doi:10.1038/nature09523 (2010).
- 264 Cho, S. W. *et al.* Targeted genome engineering in human cells with the Cas9 RNA-guided endonuclease. *Nature Biotechnology* **31**, 230-232, doi:10.1038/nbt.2507 (2013).
- 265 Hou, Z. *et al.* Efficient genome engineering in human pluripotent stem cells using Cas9 from *Neisseria meningitidis*. *Proceedings of the National Academy of Sciences of the United States of America* **110**, 15644-15649, doi:10.1073/pnas.1313587110 (2013).
- 266 Karvelis, T. *et al.* crRNA and tracrRNA guide Cas9-mediated DNA interference in *Streptococcus thermophilus*. *RNA Biology* **10**, 841-851, doi:10.4161/rna.24203 (2013).
- 267 Shah, S. A. *et al.* Protospacer recognition motifs: mixed identities and functional diversity. *RNA Biology* **10**, 891-899, doi:10.4161/rna.23764 (2013).
- 268 Jinek, M. *et al.* A Programmable Dual-RNA-Guided DNA Endonuclease in Adaptive Bacterial Immunity. *Science* **337**, 1225829-1225821, doi:10.1126/science.1225829 (2012).
- 269 Gasiunas, G. *et al.* Cas9-crRNA ribonucleoprotein complex mediates specific DNA cleavage for adaptive immunity in bacteria. *Proceedings of the National Academy of Sciences of the United States of America* **109**, E2579-E2586, doi:10.1073/pnas.1208507109 (2012).
- 270 Jiang, W. *et al.* Demonstration of CRISPR/Cas9/sgRNA-mediated targeted gene modification in *Arabidopsis*, tobacco, sorghum and rice. *Nucleic Acids Research* **41**, e188-e188, doi:10.1093/nar/gkt780 (2013).
- 271 Liang, P. *et al.* CRISPR/Cas9-mediated gene editing in human triploid zygotes. *Protein Cell* **6**, 363-372, doi:10.1007/s13238-015-0153-5 (2015).
- 272 Honda, A. *et al.* Single-step generation of rabbits carrying a targeted allele of the tyrosinase gene using CRISPR/Cas9. *Experimental animals* **64**, 31-37, doi:10.1538/expanim.14-0034 (2015).
- 273 Kimura, Y. *et al.* CRISPR/Cas9-mediated reporter knock-in in mouse haploid embryonic stem cells. *Scientific Reports* **5**, 10710, doi:10.1038/srep10710 (2015).
- 274 Skarnes, W. C. *et al.* A conditional knockout resource for the genome-wide study of mouse gene function. *Nature* **474**, 337-342, doi:10.1038/nature10163 (2011).
- 275 Skarnes, W. C. Is mouse embryonic stem cell technology obsolete? *Genome Biol* **16**, 109, doi:10.1186/s13059-015-0673-6 (2015).

- 276 Lee, J. *et al.* Developing genetically engineered mouse models using engineered nucleases: Current status, challenges, and the way forward. *Drug Discovery Today: Disease Models* **20**, 13-20, doi:10.1016/j.ddmod.2017.07.003 (2016).
- 277 Park, K. E. & Telugu, B. P. Role of stem cells in large animal genetic engineering in the TALENs-CRISPR era. *Reprod Fertil Dev* **26**, 65-73, doi:10.1071/RD13258 (2013).
- 278 Chen, S. *et al.* Highly Efficient Mouse Genome Editing by CRISPR Ribonucleoprotein Electroporation of Zygotes. *J Biol Chem* **291**, 14457-14467, doi:10.1074/jbc.M116.733154 (2016).
- 279 Wang, W. *et al.* Delivery of Cas9 Protein into Mouse Zygotes through a Series of Electroporation Dramatically Increases the Efficiency of Model Creation. *J Genet Genomics* **43**, 319-327, doi:10.1016/j.jgg.2016.02.004 (2016).
- 280 Singh, P. *et al.* A mouse geneticist's practical guide to CRISPR applications. *Genetics* **199**, 1-15, doi:10.1534/genetics.114.169771 (2015).
- 281 Wang, H. *et al.* One-Step Generation of Mice Carrying Mutations in Multiple Genes by CRISPR/Cas-Mediated Genome Engineering. *Cell* **153**, 910-918, doi:10.1016/j.cell.2013.04.025 (2013).
- 282 Srinivas, S. *et al.* Cre reporter strains produced by targeted insertion of EYFP and ECFP into the ROSA26 locus. *BMC developmental biology* **1**, 4 (2001).
- 283 Harms, D. W. *et al.* Mouse Genome Editing Using the CRISPR/Cas System. *Curr Protoc Hum Genet* **83**, 15 17 11-27, doi:10.1002/0471142905.hg1507s83 (2014).
- 284 De Calisto, J. *et al.* FcγRI (CD64): an identity card for intestinal macrophages. *European journal of immunology* **42**, 3136-3140, doi:10.1002/eji.201243061 (2012).
- 285 Madisen, L. *et al.* A robust and high-throughput Cre reporting and characterization system for the whole mouse brain. *Nature Neuroscience* **13**, 133-140, doi:10.1038/nn.2467 (2009).
- 286 Madisen, L. *et al.* A toolbox of Cre-dependent optogenetic transgenic mice for light-induced activation and silencing. *Nature Neuroscience* **15**, 793-802, doi:10.1038/nn.3078 (2012).
- 287 Madisen, L. *et al.* Transgenic Mice for Intersectional Targeting of Neural Sensors and Effectors with High Specificity and Performance. *Neuron* **85**, 942-958, doi:10.1016/j.neuron.2015.02.022 (2015).
- 288 Loschko, J. *et al.* Inducible targeting of cDCs and their subsets in vivo. *Journal of Immunological Methods* **434**, 32-38, doi:10.1016/j.jim.2016.04.004 (2016).
- 289 Anselmo, A. *et al.* Flow cytometry applications for the analysis of chemokine receptor expression and function. *Cytometry A* **85**, 292-301, doi:10.1002/cyto.a.22439 (2014).
- 290 Buehler, D. *et al.* An Optimized Procedure for Fluorescence-activated Cell Sorting (FACS) Isolation of Autonomic Neural Progenitors from Visceral Organs of Fetal Mice. *Journal of Visualized Experiments*, e4188, doi:10.3791/4188 (2012).
- 291 Benck, C. J. *et al.* Isolation of Infiltrating Leukocytes from Mouse Skin Using Enzymatic Digest and Gradient Separation. *J Vis Exp*, e53638, doi:10.3791/53638 (2016).
- 292 Menon, V. *et al.* Flow cytometry protocols for surface and intracellular antigen analyses of neural cell types. *J Vis Exp*, doi:10.3791/52241 (2014).
- 293 Coppoolse, E. R. *et al.* Size does matter: cre-mediated somatic deletion efficiency depends on the distance between the target lox-sites. *Plant Mol Biol* **58**, 687-698, doi:10.1007/s11103-005-7705-7 (2005).
- 294 Sharma, S. & Zhu, J. Immunologic applications of conditional gene modification technology in the mouse. *Curr Protoc Immunol* **105**, 10 34 11-13, doi:10.1002/0471142735.im1034s105 (2014).
- 295 Hoeffel, G. *et al.* C-Myb+ Erythro-Myeloid Progenitor-Derived Fetal Monocytes Give Rise to Adult Tissue-Resident Macrophages. *Immunity* **42**, 665-678, doi:10.1016/j.immuni.2015.03.011 (2015).
- 296 Kurotaki, D. *et al.* Functions and development of red pulp macrophages. *Microbiol Immunol* **59**, 55-62, doi:10.1111/1348-0421.12228 (2015).
- 297 Sivakumaran, S. *et al.* Depletion of CD11c(+) cells in the CD11c.DTR model drives expansion of unique CD64(+) Ly6C(+) monocytes that are poised to release TNF-alpha. *Eur J Immunol* **46**, 192-203, doi:10.1002/eji.201545789 (2016).
- 298 Svensson, M. *et al.* Acute pyelonephritis and renal scarring are caused by dysfunctional innate immunity in mCxcr2 heterozygous mice. *Kidney Int* **80**, 1064-1072, doi:10.1038/ki.2011.257 (2011).
- 299 Cao, Q. *et al.* Renal F4/80+CD11c+ Mononuclear Phagocytes Display Phenotypic and Functional Characteristics of Macrophages in Health and in Adriamycin Nephropathy. *Journal of the American Society of Nephrology* **26**, 349-363, doi:10.1681/ASN.2013121336 (2015).
- 300 Matoulkova, E. *et al.* The role of the 3' untranslated region in post-transcriptional regulation of protein expression in mammalian cells. *RNA Biol* **9**, 563-576, doi:10.4161/rna.20231 (2012).

- 301 Mayr, C. Regulation by 3'-Untranslated Regions. *Annu Rev Genet* **51**, 171-194, doi:10.1146/annurev-genet-120116-024704 (2017).
- 302 Xie, T. *et al.* MicroRNA-127 inhibits lung inflammation by targeting IgG Fcγ receptor I. *J Immunol* **188**, 2437-2444, doi:10.4049/jimmunol.1101070 (2012).
- 303 Friedman, R. C. *et al.* Most mammalian mRNAs are conserved targets of microRNAs. *Genome Res* **19**, 92-105, doi:10.1101/gr.082701.108 (2009).
- 304 Chan, H. Y. *et al.* Comparison of IRES and F2A-Based Locus-Specific Multicistronic Expression in Stable Mouse Lines. *PLoS ONE* **6**, e28885-28811, doi:10.1371/journal.pone.0028885 (2011).
- 305 Ha, S. H. *et al.* Application of two bicistronic systems involving 2A and IRES sequences to the biosynthesis of carotenoids in rice endosperm. *Plant Biotechnol J* **8**, 928-938, doi:10.1111/j.1467-7652.2010.00543.x (2010).
- 306 Goldwirth, A. *et al.* Impairment of podocyte function by diphtheria toxin—a new reversible proteinuria model in mice. *Lab Invest* **92**, 1674-1685, doi:10.1038/labinvest.2012.133 (2012).
- 307 Boillee, S. *et al.* Onset and progression in inherited ALS determined by motor neurons and microglia. *Science* **312**, 1389-1392, doi:10.1126/science.1123511 (2006).
- 308 Durai, V. & Murphy, K. M. Functions of Murine Dendritic Cells. *Immunity* **45**, 719-736, doi:10.1016/j.immuni.2016.10.010 (2016).
- 309 Song, H. K. & Hwang, D. Y. Use of C57BL/6N mice on the variety of immunological researches. *Lab Anim Res* **33**, 119-123, doi:10.5625/lar.2017.33.2.119 (2017).
- 310 Perše, M. & Večerić-Haler, Ž. Cisplatin-Induced Rodent Model of Kidney Injury: Characteristics and Challenges. *BioMed Research International* **2018**, 1-29, doi:10.1155/2018/1462802 (2018).
- 311 Ramesh, G. & Ranganathan, P. Mouse Models and Methods for Studying Human Disease, Acute Kidney Injury (AKI). *Methods in molecular biology* **1194**, 421-436 (Springer New York, 2014).
- 312 Heymann, F. *et al.* Kidney dendritic cell activation is required for progression of renal disease in a mouse model of glomerular injury. *Journal of Clinical Investigation* **119**, 1286-1297, doi:10.1172/JCI38399 (2009).
- 313 Deng, J. *et al.* Interleukin-10 inhibits ischemic and cisplatin-induced acute renal injury. *Kidney International* **60**, 2118-2128, doi:10.1046/j.1523-1755.2001.00043.x (2001).
- 314 Liang, H. *et al.* CXCL16 regulates cisplatin-induced acute kidney injury. *Oncotarget* **7**, 31652-31662, doi:10.18632/oncotarget.9386 (2016).
- 315 Liao, W. *et al.* MicroRNA-140-5p attenuated oxidative stress in Cisplatin induced acute kidney injury by activating Nrf2/ARE pathway through a Keap1-independent mechanism. *Experimental Cell Research* **360**, 292-302, doi:10.1016/j.yexcr.2017.09.019 (2017).
- 316 Liu, M. *et al.* A pathophysiologic role for T lymphocytes in murine acute cisplatin nephrotoxicity. *J Am Soc Nephrol* **17**, 765-774, doi:10.1681/ASN.2005010102 (2006).
- 317 Ramesh, G. *et al.* Endotoxin and cisplatin synergistically induce renal dysfunction and cytokine production in mice. *Am J Physiol Renal Physiol* **293**, F325-332, doi:10.1152/ajprenal.00158.2007 (2007).
- 318 Kim, H. J. *et al.* NLRP3 Inflammasome Knockout Mice Are Protected against Ischemic but Not Cisplatin-Induced Acute Kidney Injury. *Journal of Pharmacology and Experimental Therapeutics* **346**, 465-472, doi:10.1124/jpet.113.205732 (2013).
- 319 Kim, S. C. *et al.* Blocking junctional adhesion molecule C promotes the recovery of cisplatin-induced acute kidney injury. *The Korean Journal of Internal Medicine* **32**, 1053-1061, doi:10.3904/kjim.2016.060 (2017).
- 320 Lee, H. *et al.* CD4+CD25+ regulatory T cells attenuate cisplatin-induced nephrotoxicity in mice. *Kidney International* **78**, 1100-1109, doi:10.1038/ki.2010.139 (2010).
- 321 Linkermann, A. *et al.* Renal tubular Fas ligand mediates fratricide in cisplatin-induced acute kidney failure. *Kidney International* **79**, 169-78, doi:10.1038/ki.2010.317 (2010).
- 322 Ali, B. H. *et al.* Motor and behavioral changes in mice with cisplatin-induced acute renal failure. *Physiol Res* **63**, 35-45 (2014).
- 323 Liu, Y. L. *et al.* Pica—a model of nausea? Species differences in response to cisplatin. *Physiol Behav* **85**, 271-277, doi:10.1016/j.physbeh.2005.04.009 (2005).
- 324 Masahiko, S., Akira, N. & Nobumasa, I. Deficiency of selenium intake enhances manifestation of renal toxicity of cis-diamminedichloroplatinum in mice. *Toxicology Letters* **38**, 155-160, doi:10.1016/0378-4274(87)90123-8 (1987).
- 325 Mitazaki, S. *et al.* Interleukin-6 modulates oxidative stress produced during the development of cisplatin nephrotoxicity. *Life Sci* **92**, 694-700, doi:10.1016/j.lfs.2013.01.026 (2013).

- 326 Mitazaki, S. *et al.* Interleukin-6 plays a protective role in development of cisplatin-induced acute renal failure through upregulation of anti-oxidative stress factors. *Life Sci* **88**, 1142-1148, doi:10.1016/j.lfs.2011.04.016 (2011).
- 327 Mitazaki, S. *et al.* Interleukin-6 deficiency accelerates cisplatin-induced acute renal failure but not systemic injury. *Toxicology* **265**, 115-121, doi:10.1016/j.tox.2009.10.005 (2009).
- 328 Oda, M. *et al.* Renal circadian clock regulates the dosing-time dependency of cisplatin-induced nephrotoxicity in mice. *Mol Pharmacol* **85**, 715-722, doi:10.1124/mol.113.089805 (2014).
- 329 To, H. *et al.* Time-dependent Nephrotoxicity Associated with Daily Administration of Cisplatin in Mice. *Journal of Pharmacy and Pharmacology* **52**, 1499-1504, doi:10.1211/0022357001777711 (2000).
- 330 Zager, R. A. *et al.* Acute nephrotoxic and obstructive injury primes the kidney to endotoxin-driven cytokine/chemokine production. *Kidney Int* **69**, 1181-1188, doi:10.1038/sj.ki.5000022 (2006).
- 331 Rabe, M. & Schaefer, F. Non-Transgenic Mouse Models of Kidney Disease. *Nephron* **133**, 53-61, doi:10.1159/000445171 (2016).
- 332 Robert, R. *et al.* Gender difference and sex hormone production in rodent renal ischemia reperfusion injury and repair. *J Inflamm (Lond)* **8**, 14, doi:10.1186/1476-9255-8-14 (2011).
- 333 Kang, K. P. *et al.* Effect of gender differences on the regulation of renal ischemia-reperfusion-induced inflammation in mice. *Mol Med Rep* **9**, 2061-2068, doi:10.3892/mmr.2014.2089 (2014).
- 334 Kher, A. *et al.* Cellular and molecular mechanisms of sex differences in renal ischemia-reperfusion injury. *Cardiovasc Res* **67**, 594-603, doi:10.1016/j.cardiores.2005.05.005 (2005).
- 335 Park, K. M. *et al.* Testosterone is responsible for enhanced susceptibility of males to ischemic renal injury. *J Biol Chem* **279**, 52282-52292, doi:10.1074/jbc.M407629200 (2004).
- 336 Kim, J. *et al.* Orchiectomy attenuates post-ischemic oxidative stress and ischemia/reperfusion injury in mice. A role for manganese superoxide dismutase. *J Biol Chem* **281**, 20349-20356, doi:10.1074/jbc.M512740200 (2006).
- 337 Wei, Q. *et al.* Differential gender differences in ischemic and nephrotoxic acute renal failure. *Am J Nephrol* **25**, 491-499, doi:10.1159/000088171 (2005).
- 338 Townsend, D. M. *et al.* Role of glutathione S-transferase Pi in cisplatin-induced nephrotoxicity. *Biomed Pharmacother* **63**, 79-85, doi:10.1016/j.biopha.2008.08.004 (2009).
- 339 Guneykaya, D. *et al.* Transcriptional and Translational Differences of Microglia from Male and Female Brains. *Cell Rep* **24**, 2773-2783 e2776, doi:10.1016/j.celrep.2018.08.001 (2018).
- 340 Pabla, N. & Dong, Z. Cisplatin nephrotoxicity: Mechanisms and renoprotective strategies. *Kidney International* **73**, 994-1007, doi:10.1038/sj.ki.5002786 (2008).
- 341 Karbownik, A. *et al.* The physical and chemical stability of cisplatin (Teva) in concentrate and diluted in sodium chloride 0.9%. *Contemp Oncol (Pozn)* **16**, 435-439, doi:10.5114/wo.2012.31775 (2012).
- 342 Sekiya, S., Iwasawa, H. & Takamizawa, H. Comparison of the intraperitoneal and intravenous routes of cisplatin administration in an advanced ovarian cancer model of the rat. *American Journal of Obstetrics and Gynecology* **153**, 106-111, doi:10.1016/0002-9378(85)90605-2 (1985).
- 343 Lajer, H. *et al.* Magnesium depletion enhances cisplatin-induced nephrotoxicity. *Cancer Chemother Pharmacol* **56**, 535-542, doi:10.1007/s00280-005-1010-7 (2005).
- 344 Litterst, C. L. Alterations in the toxicity of cis-Dichlorodiammineplatinum-II and in tissue localization of platinum as a function of NaCl concentration in the vehicle of administration. *Toxicology and Applied Pharmacology* **61**, 99-108, doi:10.1016/0041-008x(81)90011-9 (1981).
- 345 Hrushesky, W. J. *et al.* Circadian stage dependence of cis-diamminedichloroplatinum lethal toxicity in rats. *Cancer Res* **42**, 945-949 (1982).
- 346 McKeage, M. J. *et al.* Lack of nephrotoxicity of oral ammine/amine platinum (IV) dicarboxylate complexes in rodents. *British Journal of Cancer* **67**, 996-1000, doi:10.1038/bjc.1993.182 (1993).
- 347 Faubel, S. *et al.* Caspase-1-deficient mice are protected against cisplatin-induced apoptosis and acute tubular necrosis. *Kidney International* **66**, 2202-2213, doi:10.1111/j.1523-1755.2004.66010.x (2004).
- 348 Levi, F. A. *et al.* Lethal Nephrotoxicity and Hematologic Toxicity of Cis-Diamminedichloroplatinum Ameliorated by Optimal Circadian Timing and Hydration. *The Journal of Urology* **129**, 446-447, doi:10.1016/s0022-5347(17)52160-6 (1983).
- 349 Levi, F. A. *et al.* Reduction of cis-diamminedichloroplatinum nephrotoxicity in rats by optimal circadian drug timing. *Cancer Res* **42**, 950-955 (1982).
- 350 Jodrell, D. I. *et al.* The renal effects of N10-propargyl-5,8-dideazafolic acid (CB3717) and a non-nephrotoxic analogue ICI D1694, in mice. *British Journal of Cancer* **64**, 833-838, doi:10.1038/bjc.1991.409 (1991).

Literature

- 351 Espandiari, P. *et al.* Age-related differences in susceptibility to cisplatin-induced renal toxicity. *J Appl Toxicol* **30**, 172-182, doi:10.1002/jat.1484 (2010).
- 352 Gautier, J. C. *et al.* Evaluation of novel biomarkers of nephrotoxicity in two strains of rat treated with Cisplatin. *Toxicol Pathol* **38**, 943-956, doi:10.1177/0192623310379139 (2010).
- 353 Parham, K. Can Intratympanic Dexamethasone Protect against Cisplatin Ototoxicity in Mice with Age-Related Hearing Loss? *Otolaryngology-Head and Neck Surgery* **145**, 635-640, doi:10.1177/0194599811409304 (2011).
- 354 Hill, G. W., Morest, D. K. & Parham, K. Cisplatin-induced ototoxicity: effect of intratympanic dexamethasone injections. *Otol Neurotol* **29**, 1005-1011, doi:10.1097/MAO.0b013e31818599d5 (2008).

7. Appendix

7.1. Plasmid sequences

7.1.1. GCDL-2A-DTR

CAATTGCATGAAGAATCTGCTTAGGGTTAGGCGTTTTGCGCTGCTTCGCGATGTACGGGCCA
GATATACGCGTTGACATTGATTATTGACTAGTTATTAATAGTAATCAATTACGGGGTCATTA
GTTTCATAGCCCATATATGGAGTTCGCGGTTACATAACTTACGGTAAATGGCCCCGCTGGCTG
ACCGCCCAACGACCCCGCCATTGACGTCAATAATGACGTATGTTCCCATAGTAACGCCAA
TAGGGACTTTCCATTGACGTCAATGGGTGGACTATTTACGGTAAACTGCCCACTTGGCAGTA
CATCAAGTGTATCATATGCCAAGTACGCCCCCTATTGACGTCAATGACGGTAAATGGCCCCG
CTGGCATTATGCCAGTACATGACCTTATGGGACTTTCCTACTTGGCAGTACATCTACGTAT
TAGTCATCGCTATTACCATGGTGATGCGGTTTTGGCAGTACATCAATGGGCGTGGATAGCGG
TTTGACTCACGGGGATTTCCAAGTCTCCACCCCATGACGTCAATGGGAGTTTTGTTTTGGCA
CCAAAATCAACGGGACTTTCCAAAATGTCGTAACAACCTCCGCCCCATTGACGCAAATGGGCG
GTAGGCGTGTACGGTGGGAGGTCTATATAAGCAGAGCTCTCTGGCTAACTAGAGAACCCACT
GCTTACTGGCTTATCGAAATTAATACGACTCACTATAGGGAGACCCAAGCTTCGAATTCTGC
AGTCGACGGTACCGCGGGGCCGGGATCCATCGCCACCATGGTGAGCAAGGGCGAGGAGCTGT
TCACCGGGGTGGTGCCCATCCTGGTTCGAGCTGGACGGCGACGTAAACGGCCACAAGTTCAGC
GTGTCCGGCGAGGGCGAGGGCGATGCCACCTACGGCAAGCTGACCCTGAAGTTCATCTGCAC
CACCGGCAAGCTGCCCGTGCCCTGGCCACCCTCGTGACCACCCTGACCTACGGCGTGCAGT
GCTTCAGCCGCTACCCCGACCACATGAAGCAGCACGACTTCTTCAAGTCCGCCATGCCCGAA
GGCTACGTCCAGGAGCGCACCATCTTCTTCAAGGACGACGGCAACTACAAGACCCGCGCCGA
GGTGAAGTTCGAGGGCGACACCCTGGTGAACCGCATCGAGCTGAAGGGCATCGACTTCAAGG
AGGACGGCAACATCCTGGGGCACAAGCTGGAGTACAACACTACAACAGCCACAACGTCTATATC
ATGGCCGACAAGCAGAAGAACGGCATCAAGGTGAACTTCAAGATCCGCCACAACATCGAGGA
CGGCAGCGTGCAGCTCGCCGACCACTACCAGCAGAACACCCCATCGGCGACGGCCCCGTGC
TGCTGCCCGACAACCACTACCTGAGCACCCAGTCCGCCCTGAGCAAAGACCCCAACGAGAAG
CGCGATCACATGGTCTTGCTGGAGTTCGTGACCGCCGCGGGATCACTCTCGGCATGGACGA
GCTGTACAAGGGTTCCGGTGCCACGAACCTTCTCTCTGTTAAAGCAAGCAGGAGACGTGGAAG
AAAACCCCGGTCCCATGGATATCTCCAACCTGCTGACTGTGCACCAAACCTGCCTGCCCTC
CCTGTGGATGCCACCTCTGATGAAGTCAGGAAGAACCTGATGGACATGTTCAAGGACAGGCA
GGCCTTCTCTGAACACACCTGGAAGATGCTCCTGTCTGTGTGCAGATCCTGGGCTGCCTGGT
GCAAGCTGAACAACAGGAAATGGTTCCCTGCTGAACCTGAGGATGTGAGGGACTACCTCCTG
TACCTGCAAGCCAGAGGCCTGGCTGTGAAGACCATCCAACAGCACCTGGGCCAGCTCAACAT
GCTGCACAGGAGATCTGGCCTGCCTCGCCCTTCTGACTCCAATGCTGTGTCCCTGGTGTGATGA
GGAGAATCAGAAAGGAGAATGTGGATGCTGGGGAGAGAGCCAAGCAGGCCCTGGCCTTTGAA
CGCACTGACTTTGACCAAGTCAGATCCCTGATGGAGAACTCTGACAGATGCCAGGACATCAG
GAACCTGGCCTTCCCTGGGCATTGCCTACAACACCCTGCTGCGCATTGCCGAAATGCCAGAA
TCAGAGTGAAGGACATCTCCCGCACCGATGGTGGGAGAATGCTGATCCACATTGGCAGGACC
AAGACCCCTGGTGTCCACAGCTGGTGTGGAGAAGGCCCTGTCCCTGGGGGTACCAAGCTGGT
GGAGAGATGGATCTCTGTGTCTGGTGTGGCTGATGACCCCAACAACCTACCTGTTCTGCCGGG
TCAGAAAGAATGGTGTGGCTGCCCTTCTGCCACCTCCCAACTGTCCACCCGGGCCCTGGAA
GGGATCTTTGAGGCCACCCACCGCTGATCTATGGTGCCAAGGATGACTCTGGGCAGAGATA
CCTGGCCTGGTCTGGCCACTCTGCCAGAGTGGGTGCTGCCAGGGACATGGCCAGGGCTGGTG
TGTCCATCCCTGAAATCATGCAGGCTGGTGGCTGGACCAATGTGAACATAGTGATGAACTAC

ATCAGAAACCTGGACTCTGAGACTGGGGCCATGGTGAGGCTGCTCGAAATCAAACGGTCGGC
CGCAGATCCAAAAAGAAGAGAAAGGTAGATCCAAAAAGAAGAGAAAGGTAGATCCAAAA
AGAAGAGAAAGGTAGATACGGCCGCATCCGGAGCCACGAACTTCTCTCTGTTAAAGCAAGCA
GGAGACGTGGAAGAAAACCCCGGTCCCATGAAGCTGCTGCCGTCCGTGGTGCTGAAGCTCTT
TCTGGCTGCAGTTCTCTCGGCACTGGTGACTGGCGAGAGCCTGGAGCGGCTTCGGAGAGGGC
TAGCTGCTGGAACCAGCAACCCGGACCCTCCCCTGTATCCACGGACCAGCTGCTACCCCTA
GGAGGCGGCCGGGACCGGAAAGTCCGTGACTTGCAAGAGGCAGATCTGGACCTTTTGAGAGT
CACTTTATCCTCCAAGCCACAAGCACTGGCCACACCAACAAGGAGGAGCACGGGAAAAGAA
AGAAGAAAGGCAAGGGGCTAGGGAAGAAGAGGGACCCATGTCTTCGGAAATACAAGGACTTC
TGCATCCATGGAGAATGCAAATATGTGAAGGAGCTCCGGGCTCCCTCCTGCATCTGCCACCC
GGGTTACCATGGAGAGAGGTGTCATGGGCTGAGCCTCCAGTGGAATAATCGCTTATATACCT
ATGACCACACAACCATCCTGGCCGTGGTGGCTGTGGTGCTGTCATCTGTCTGTCTGCTGGTC
ATCGTGGGGCTTCTCATGTTTAGGTACCATAGGAGAGGAGGTTATGATGTGGAATAATGAAGA
GAAAGTGAAGTTGGGCATGACTAATCCCACGGTTCGGGAGCCACGAACTTCTCTCTTTTAA
AGCAAGCAGGAGACGTGGAAGAAAACCCCGGTCCCATGGTGAAGCGTGAGAAAAATGTCATC
TATGGCCCTGAGCCTCTCCATCCTTTGGAGGATTTGACTGCCGGCGAAATGCTGTTTCGTGC
TCTCCGCAAGCACTCTCATTTCCTCAAGCCTTGGTCGATGTGGTCGGCGATGAATCTTTGA
GCTACAAGGAGTTTTTTGAGGCAACCGTCTTGCTGGCTCAGTCCCTCCACAATTGTGGCTAC
AAGATGAACGACGTCGTTAGTATCTGTGCTGAAAACAATACCCGTTTCTTCATTCCAGTCAT
CGCCGCATGGTATATCGGTATGATCGTGGCTCCAGTCAACGAGAGCTACATTCCCGACGAAC
TGTGTAAGTCAATGGGTATCTCTAAGCCACAGATTGTCTTCACCACTAAGAATATTCTGAAC
AAAGTCTGGAAGTCCAAAGCCGCACCAACTTTATTAAGCGTATCATCATCTTGACACTGT
GGAGAATATTCACGGTTGCGAATCTTTGCCTAATTTTCATCTCTCGCTATTCAGACGGCAACA
TCGAAACTTTAAACCACTCCACTTCGACCCTGTGGAACAAGTTGCAGCCATTCTGTGTAGC
AGCGGTACTACTGGACTCCCAAAGGGAGTCATGCAGACCCATCAAACATTTGCGTGCCTCT
GATCCATGCTCTCGATCCACGCGTGGGCACTCAGCTGATTCCCTGGTGTACCCGTCTTGGTCT
ACTTGCCTTTCTTCCATGCTTTCCGCTTTAGCATTACTTTGGGTACTTTATGGTCCGTCTC
CGCGTGATTATGTTCCGCCGTTTTGATCAGGAGGCTTTCTTGAAAGCCATCCAAGATTATGA
AGTCCGCAGTGTCAACGTGCCTAGCGTGATCCTGTTTTTGTCTAAGAGCCCACTCGTGG
ACAAGTACGACTTGTCTTCACTGCGTGAATTGTGTTGCGGTGCCGCTCCACTGGCTAAGGAG
GTCGCTGAAGTGGCCGCCAAACGCTTGAATCTTCCAGGGATTTCGTTGTGGCTTCGGCCTCAC
CGAATCTACCAGCGCTAACATTCACTCTCTCGGGGATGAGTTTAAAGAGCGGCTCTTTGGGCC
GTGTCACTCCACTCATGGCTGCTAAGATCGCTGATCGCGAAACTGGTAAGGCTTTGGGCCCG
AACCAAGTGGGCGAGCTGTGTATCAAAGGCCCTATGGTGAGCAAGGGTTATGTCAATAACGT
TGAAGCTACCAAGGAGGCCATCGACGACGACGGCTGGTTGCATTCTGGTGATTTTGGATATT
ACGACGAAGATGAGCATTTTTACGTCGTGGATCGTTACAAGGAGCTGATCAAATACAAGGGT
AGCCAGGTTGCTCCAGCTGAGTTGGAGGAGATTCTGTTGAAAAATCCATGCATTCCGCGATGT
CGCTGTGGTCCGCAATCCTGATCTGGAGGCCGGCGAACTGCCTTCTGCTTTCGTTGTCAAGC
AGCCTGGTAAAGAAATTACCGCCAAAGAAGTGTATGATTACCTGGCTGAACGTGTGAGCCAT
ACTAAGTACTTGCCTGGCGGCGTGCCTTTTGTGACTCCATCCCTCGTAACGTAACAGGCAA
AATTACCCGCAAGGAGCTGTTGAAACAATTGTTGGAGAAGGCCGGCGGTTAGGGATCAGCCT
CGACTGTGCCTTCTAGTTGCCAGCCATCTGTTGTTTGGCCCTCCCCGTGCCTTCTTGACC
CTGGAAGGTGCCACTCCACTGTCCTTTCTAATAAAATGAGGAAATTGCATCGCATTGTCT
GAGTAGGTGTCATTCTATTCTGGGGGGTGGGGTGGGGCAGGACAGCAAGGGGGAGGATTGGG
AAGACAATAGCAGGCATGCTGGGGATGCGGTGGGCTCTATGGCTTCTGAGGCGGAAAGAACC
AGCTGGGGCTCGAGGAAGTTCCTATTCTCTAGAAAGTATAGGAACTTCGCGGCCGCTCGCGC
ACTACTCAGCGACCTCAAACACACAAGCAGGGAGCAGATACTGGCTTAACTATGCGGCATCA
GAGCAGATTGTAAGTGCAGGATAGGGGATCGGGAGATCTCCCGATCCGTGACGTCATCA
GGTGGCACTTTTCGGGAAATGTGCGCGGAACCCCTATTTGTTTATTTTTCTAAATACATTC
AAATATGTATCCGCTCATGAGACAATAACCCGTGATAAATGCTTCAATAATATTGAAAAGGA
AGAGTATGAGTATTCAACATTTCCGTGTCGCCCTTATTCCCTTTTTTTCGGGCATTTTGCCTT

CCTGTTTTTGCTCACCCAGAAACGCTGGTCAAAGTAAAAGATGCTGAAGATCAGTTGGGTGC
 ACGAGTGGGTTACATCGAACTGGATCTCAACAGCGGTAAGATCCTTGAGAGTTTTCGCCCCG
 AAGAACGTTTTTCCAATGATGAGCACTTTTAAAGTTCTGCTATGTGGCGCGGTATTATCCCGT
 ATTGACGCCGGGCAAGAGCAACTCGGTCCCGCATACTACTATTCTCAGAATGACTTGGTTGA
 GTACTCACCGTACAGAAAAGCATCTTACGGATGGCATGACAGTAAGAGAATTATGCAGTG
 CTGCCATAACCATGAGTGATAACACTGCGGCCAACTTACTTCTGACAACGATCGGAGGACCG
 AAGGAGCTAACCGCTTTTTTGCACAACATGGGGGATCATGTAACCTCGCCTTGATCGTTGGGA
 ACCGGAGCTGAATGAAGCCATACCAAACGACGAGCGTGACACCACGATGCCTGTAGCAATGG
 CAACAACGTTGCGCAAATACTTAACTGGCGAACTACTTACTCTAGCTTCCCGGCAACAATTA
 ATAGACTGGATGGAGGCGGATAAAGTTGCAGGACCCTTCTGCGCTCGGCCCTTCCGGCTGG
 CTGGTTTTATTGCTGATAAATCTGGAGCCGGTGAGCGTGGGTCTCGCGGTATCATTGCAGCAC
 TGGGGCCAGATGGTAAGCCCTCCCGTATCGTAGTTATCTACACGACGGGGAGTCAGGCAACT
 ATGGATGAACGAAATAGACAGATCGCTGAGATAGGTGCCTCACTGATTAAGCATTTGGTAAGA
 AGTTCCCTATTCTCTAGAAAGTATAGGAACTTCTTAATTAACGGCTAGCTGCATTCTAGTTGT
 GGTTTGTCCAACTCATCAATGTATCTTATCATGTCTGTATAACCGTCGACCTCTAGCTAGAG
 CTTGGCGTAATCATGGTCATAGCTGTTTCTGTGTGAAATTGTTATCCGCTCACAAATCCAC
 ACAACATACGAGCCGGAAGCATAAAGTGTAAAGCCTGGGGTGCCTAATGAGTGAGCTAACTC
 ACATTAATTGCGTTGCGCTCACTGCCCGCTTCCAGTCGGGAAACCTGTCGTGCCAGCTGCA
 TTAATGAATCGGCCAACGCGCGGGGAGAGGCGGTTTGCCTATTGGGCGCTCTTCCGCTTCT
 CGCTCACTGACTCGCTGCGCTCGGTCTCGGCTGCGGCGAGCGGTATCAGCTCACTCAAAG
 GCGGTAATACGGTTATCCACAGAATCAGGGGATAACGCAGGAAAGAACATGTGAGCAAAGG
 CCAGCAAAGGCCAGGAACCGTAAAAAGGCCGCGTTGCTGGCGTTTTTCCATAGGCTCCGCC
 CCCCTGACGAGCATCACAAAATCGACGCTCAAGTCAGAGGTGGCGAAACCCGACAGGACTA
 TAAAGATACCAGGCGTTTCCCCTGGAAGCTCCCTCGTGCGCTCTCCTGTTCCGACCCTGCC
 GCTTACCGGATACCTGTCCGCTTTCTCCCTTCGGGAAGCGTGGCGCTTTCTCAATGCTCAC
 GCTGTAGGTATCTCAGTTCGGTGTAGGTCTTCCGCTCCAAGCTGGGCTGTGTGCACGAACCC
 CCCGTTTCCAGCCGACCGCTGCGCCTTATCCGTAACATATCGTCTTGAGTCCAACCCGGTAAG
 ACACGACTTATCGCCACTGGCAGCAGCCACTGGTAACAGGATTAGCAGAGCGAGGTATGTAG
 GCGGTGCTACAGAGTTCTTGAAGTGGTGGCCTAACTACGGCTACACTAGAAGGACAGTATTT
 GGTATCTGCGCTCTGCTGAAGCCAGTTACCTTCCGAAAAAGAGTTGGTAGCTCTTGATCCGG
 CAAACAAACCACCGCTGGTAGCGGTGGTTTTTTTTGTTTTGCAAGCAGCAGATTACGCGCAGAA
 AAAAAGGATCTCAAGAAGATCCTTTGATCTTTTCTACGGGGTCTGACGCTCAGTGGAACGAA
 AACTCACGTTAAGGGATTTTGGTCATGAGATTATCAAAAAGGATCTTACCTAGATCCTTTT
 AAATTAATAATGAAGTTTTAAATCAATCTAAAGTATATATGAGTAACTTGGTCTGACAG

7.1.2. 195 FrtneokanaFrt DTA

TAGATATCGATGGCCATAGCGGCCGCTCTAGAACTAGTGGATCCCCACCTGACTGATGAAG
 TTCCTATACTTTCTAGAGAATAGGAACTTCGAAGGGTTCCGCAAGCTCTAGTCGAGCCCCAG
 CTGGTTCTTTCCGCTCAGAAGCCATAGAGCCCACCGCATCCCCAGCATGCCTGCTATTGTC
 TTCCCAATCCTCCCCCTTGTGTCTGCTGCCCCACCCACCCCCAGAATAGAATGACACCTAC
 TCAGACAATGCGATGCAATTTCTCATTTTTATTAGGAAAGGACAGTGGGAGTGGCACCTTCC
 AGGGTCAAGGAAGGCACGGGGGAGGGGCAAACAACAGATGGCTGGCAACTAGAAGGCACAGT
 CGAGGCTGATCAGCGAGCTCTAGAGAATTGATCCCCCTCAGAAGAACTCGTCAAGAAGGCGAT
 AGAAGGCGATGCGCTGCGAATCGGGAGCGGCGATACCGTAAAGCACGAGGAAGCGGTGAGCC
 CATTCGCGCCAAGCTCTTACGCAATATCACGGGTAGCCAACGCTATGTCCTGATAGCGGTC
 CGCCACACCCAGCCGGCCACAGTCGATGAATCCAGAAAAGCGGCCATTTTCCACCATGATAT
 TCGGCAAGCAGGCATCGCCATGGGTACGACGAGATCATCGCCGTCGGGCATGCGCGCCTTG
 AGCCTGGCGAACAGTTCGGCTGGCGCGAGCCCCTGATGCTCTTCGTCCAGATCATCCTGATC
 GACAAGACCGGCTTCCATCCGAGTACGTGCTCGCTCGATGCGATGTTTTCGCTTGGTGGTCTGA

ATGGGCAGGTAGCCGGATCAAGCGTATGCAGCCGCCGCATTGCATCAGCCATGATGGATACT
 TTCTCGGCAGGAGCAAGGTGAGATGACAGGAGATCCTGCCCGGCACTTCGCCCAATAGCAG
 CCAGTCCCTTCCCGCTTCAGTGACAACGTCGAGCACAGCTGCGCAAGGAACGCCCGTTCGTGG
 CCAGCCACGATAGCCGCGCTGCCTCGTCCTGCAGTTCATTCAGGGCACCGGACAGGTTCGGTC
 TTGACAAAAAGAACCAGGGCGCCCTGCGCTGACAGCCGGAACACGGCGGCATCAGAGCAGCC
 GATTGTCTGTTGTGCCCAGTCATAGCCGAATAGCCTCTCCACCCAAGCGGGCCGGAGAACCCTG
 CGTGCAATCCATCTTGTTC AATGGCCGATCCCATGGTTTTAGTTCCCTCACCTTGTTCGTATTAT
 ACTATGCCGATATACTATGCCGATGATTAATTGTCAACAGGCTGCAGGTTCGAAAGGCCCGGA
 GATGAGGAAGAGGAGAACAGCGCGGCAGACGTGCGCTTTTGAAGCGTGCAGAATGCCGGGCC
 TCCGGAGGACCTTCGGGCGCCCGCCCGCCCTGAGCCCGCCCTGAGCCCGCCCCCGGACC
 CACCCCTTCCCAGCCTCTGAGCCAGAAAGCGAAGGAGCAAAGCTGCTATTGGCCGCTGCC
 CAAAGGCCTACCCGCTTCCATTGCTCAGCGGTGCTGTCCATCTGCACGAGACTAGTGAGACG
 TGCTACTTCCATTTGTACGTCCTGCACGACGCGAGCTGCGGGGCGGGGGGAACTTCCCTGA
 CTAGGGGAGGAGTAGAAGGTGGCGCGAAGGGGCCACCAAAGAACGGAGCCGGTTGGCGCCTA
 CCGGTGGATGTGGAATGTGTGCGAGGCCAGAGGCCACTTGTGTAGCGCCAAGTGCACGCGG
 GGCTGCTAAAGCGCATGCTCCAGACTGCCTTGGGAAAAGCGCCTCCCCTACCCGGTAGAATT
 TCGACGACCTGCAGCCAAGCTAGCTTGGCTGGACGTAAACTCCTCTTCAGACCTGAAGTTCC
 TATACTTTCTAGAGAATAGGAACTTCGGAATTCGATATCAAGCTTGCGGCCGGCCGCCACCT
 CGAGCCCCAGCTGGTTCTTTCCGCCTCAGAAGCCATAGAGCCCACCGCATCCCCAGCATGCC
 TGCTATTGTCTTCCCAATCCTCCCCCTTGTGTCTGCCCCACCCACCCCCAGAATAGAA
 TGACACCTACTCAGACAATGCGATGCAATTTCCCTCATTTTATTAGGAAAGGACAGTGGGAGT
 GGCACCTTCCAGGGTCAAGGAAGGCACGGGGGAGGGGGCAAACAACAGATGGCTGGCAACTAG
 AAGGCACAGTCGAGGCTGATCAGCGAGCTCTAGGATCTGCATTCCACCCTGCTCCCATTCA
 TCAGTTCCATAGGTTGGAATCTAAAATACACAACAATTAGAATCAGTAGTTTAAACACATTA
 TACACTTAAAAATTTTATATTTACCTTAGAGCTTTAAATCTCTGTAGGTAGTTTGTCCAATT
 ATGTCACACCACAGAAGTAAGGTTCCCTTACAAAGAGATCGCCTGACACGATTTCCCTGCACA
 GGCTTGAGCCATATACTCATACTCGCATCTTGGCCACGTTTTCCACGGGTTTCAAATTA
 TCTCAAGTTCTACGCTTAACGTTTTCGCCTGTTCCAGTTATTAATATATTC AACGCTAGAA
 CTCCCCTCAGCGAAGGGAAGGCTGAGCACTACACGCGAAGCACCATCACCGAACCTTTTGAT
 AAATCTTCCGTTCCGACTTGCTCCATCAACGGTTCAGTGAGACTTAAACCTAACTCTTTCT
 TAATAGTTTTCGGCATTATCCACTTTTAGTGCGAGAACCTTCGTCAGTCCTGGATACTGACT
 TTGACCACGCCTCCAGCTTTTCCAGAGAGCGGGTTTTTATTATCTACAGAGTATCCCGCAGC
 GTCGTATTTATTGTTCGGTACTATAAAACCTTTCCAATCATCGTCATAATTTCCCTTGTGTAC
 CAGATTTTGGCTTTTGTATACCTTTTTGAATGGAATCTACATAACCAGGTTTAGTCCCCTGG
 TACGAAGAAAAGTTTTCCATCACAAAAGATTTAGAAGAATCAACAACATCATCAGGATCCAT
 GCGGAGGACCTGCAGGTGCAAAGGCCCGGAGATGAGGAAGAGGAGAACAGCGCGGCAGACGT
 GCGCTTTTGAAGCGTGCAGAATGCCGGGCCCTCCGGAGGACCTTCGGGCGCCCGCCCGCCCC
 TGAGCCCGCCCTGAGCCCGCCCGGACCCACCCCTTCCCAGCCTCTGAGCCAGAAAGCG
 AAGGAGCAAAGCTGCTATTGGCCGCTGCCCCAAAGGCCTACCCGCTTCCATTGCTCAGCGGT
 GCTGTCCATCTGCACGAGACTAGTGAGACGTGCTACTTCCATTTGTCACGTCCTGCACGACG
 CGAGCTGCGGGGCGGGGGGAACTTCCCTGACTAGGGGAGGAGTAGAAGGTGGCGCGAAGGGG
 CCACCAAAGAACGGAGCCGGTTGGCGCCTACCGGTGGATGTGGAATGTGTGCGAGGCCAGAG
 GCCACTTGTGTAGCGCAAAGTGCCAGCGGGGCTGCTAAAGCGCATGCTCCAGACTGCCTTG
 GGAAAAGCGCCTCCCCTACCCGGTAGAATTCGATTGGAGCTCCAATTCGCCCTATAGTGAGT
 CGTATTACAATTCAGTGGCCGTGTTTTTACAACGTGCTGACTGGGAAAACCTTGGCGTTACC
 CAACTTAATCGCCTTGCAGCACATCCCCCTTTCGCCAGCTGGCGTAATAGCGAAGAGGCCCG
 CACCGATCGCCCTTCCCAACAGTTGCGCAGCCTGAATGGCGAATGGGACGCGCCCTGTAGCG
 GCGCATTAAGCGCGGGGGGTGTGGTGGTTACGCGCAGCGTGACCGCTACACTTGCCAGCGCC
 CTAGCGCCCGCTCCTTTTCGCTTTCTTCCCTTCCCTTCTCGCCACGTTTCGCCGGCTTTCCCG
 TCAAGCTCTAAATCGGGGGCTCCCTTTAGGGTTCCGATTTAGTGCTTTACGGCACCTCGACC
 CCAAAAAACTTGATTAGGGTGATGGTTCACGTAGTGGGCCATCGCCCTGATAGACGGTTTTT

CGCCCTTTGACGTTGGAGTCCACGTTCTTTAATAGTGGACTCTTGTTCCAAACCTGGAACAAC
ACTCAACCCTATCTCGGTCTATTCTTTTGATTTATAAGGGATTTTGCCGATTTTCGGCCTATT
GGTTAAAAAATGAGCTGATTTAACAAAAATTTAACGCGAATTTTAACAAAATATTAACGCTT
ACAATTTAGGTGGCACTTTTCGGGGAAATGTGCGCGGAACCCCTATTTGTTTATTTTTCTAA
ATACATTCAAATATGTATCCGCTCATGAGACAATAACCCTGATAAATGCTTCAATAATATTG
AAAAAGGAAGAGTATGAGTATTCAACATTTCCGTGTCGCCCTTATTCCTTTTTTTCGGGCAT
TTTGCCTTCTGTTTTTTGCTCACCCAGAAACGCTGGTGAAAGTAAAAGATGCTGAAGATCAG
TTGGGTGCACGAGTGGGTTACATCGAACTGGATCTCAACAGCGGTAAGATCCTTGAGAGTTT
TCGCCCCGAAGAACGTTTTCCAATGATGAGCACTTTTAAAGTTCTGCTATGTGGCGCGGTAT
TATCCCGTATTGACGCCGGGCAAGAGCAACTCGGTGCGCCGATACACTATTCTCAGAATGAC
TTGGTTGAGTACTCACAGTCCAGAAAAGCATCTTACGGATGGCATGACAGTAAGAGAATT
ATGCAGTGTGCCATAACCATGAGTGATAAACAACCTGCGGCCAACTTACTTCTGACAACGATCG
GAGGACCGAAGGAGCTAACCGCTTTTTTGCACAACATGGGGGATCATGTAACCTCGCCTTGAT
CGTTGGGAACCGGAGCTGAATGAAGCCATACCAAACGACGAGCGTGACACCACGATGCCTGT
AGCAATGGCAACAACGTTGCGCAAACCTATTAACCTGGCGAACTACTTACTCTAGCTTCCCGGC
AACAATTAATAGACTGGATGGAGGCGGATAAAGTTGCAGGACCACTTCTGCGCTCGGCCCTT
CCGGCTGGCTGGTTTTATTGCTGATAAATCTGGAGCCGGTGAGCGTGGGTCTCGCGGTATCAT
TGCAGCACTGGGGCCAGATGGTAAGCCCTCCCGTATCGTAGTTATCTACACGACGGGGAGTC
AGGCAACTATGGATGAACGAAATAGACAGATCGCTGAGATAGGTGCCTCACTGATTAAGCAT
TGTAACGTGCAGACCAAGTTTACTCATATATACTTTAGATTGATTTAAAACCTCATTTTTA
ATTTAAAAGGATCTAGGTGAAGATCCTTTTTTGATAATCTCATGACCAAAATCCCTTAACGTG
AGTTTTTCGTTCCACTGAGCGTCAGACCCCGTAGAAAAGATCAAAGGATCTTCTTGAGATCCT
TTTTTTCTGCGCTAATCTGCTGCTTGCAAACAAAAAACACCGCTACCAGCGGTGGTTTG
TTTGCCGGATCAAGAGCTACCAACTCTTTTTCCGAAGGTAACCTGGCTTCAGCAGAGCGCAGA
TACCAAACTGTCTTCTAGTGTAGCCGTAGTTAGGCCACCACTTCAAGAACTCTGTAGCA
CCGCTACATACTCGCTCTGCTAATCCTGTTACCAGTGGCTGCTGCCAGTGGCGATAAGTC
GTGTCTTACCGGTTGGACTCAAGACGATAGTTACCGGATAAGGCGCAGCGGTCCGGCTGAA
CGGGGGTTCGTGCACACAGCCAGCTTGGAGCGAACGACCTACACCGAACTGAGATACCTA
CAGCGTGAGCTATGAGAAAGCGCCACGCTTCCCGAAGGGAGAAAGGCGGACAGGTATCCGGT
AAGCGGCAGGGTCCGAACAGGAGAGCGCACGAGGGAGCTTCCAGGGGGAAACGCCTGGTATC
TTTATAGTCTGTGCGGTTTTCGCCACCTCTGACTTGAGCGTCGATTTTTTGATGCTCGTCA
GGGGGGCGGAGCCTATGGAAAAACGCCAGCAACGCGGCCTTTTTACGGTTCCTGGCCTTTTG
CTGGCCTTTTTGCTCACATGTTCTTTTCTGCGTTATCCCCTGATTCTGTGGATAACCGTATTA
CCGCTTTGAGTGAGCTGATACCGCTCGCCGACGCCGAACGACCGAGCGCAGCGAGTCAGTG
AGCGAGGAAGCGGAAGAGCGCCCAATACGCAAACCGCCTCTCCCGCGCGTTGGCCGATTCA
TTAATGCAGCTGGCACGACAGGTTTTCCCGACTGGAAAGCGGGCAGTGAGCGCAACGCAATTA
ATGTGAGTTAGCTCACTCATTAGGCACCCAGGCTTTACACTTTATGCTTCCGGCTCGTATG
TTGTGTGGAATTGTGAGCGGATAACAATTTACACAGGAAACAGCTATGACCATGATTACGC
CAAGCTCGAAATTAACCCTCACTAAAGGGAACAAAAGCTGTCGAGATCTAGA

7.1.3. pBlueScript[®] SK II (+)

CTAAATTGTAAGCGTTAATATTTTTGTTAAAAATTCGCGTTAAATTTTTGTTAAATCAGCTCAT
TTTTTAACCAATAGGCCGAAATCGGCAAATCCCTTATAAATCAAAGAATAGACCGAGATA
GGTTGAGTGTGTTCCAGTTTGAACAAGAGTCCACTATTAAGAACGTGGACTCCAACGT
CAAAGGGCGAAAACCGTCTATCAGGGCGATGGCCACTACGTGAACCATCACCTAATCAA
GTTTTTTGGGGTTCGAGGTGCCGTAAGCACTAAATCGGAACCCTAAAGGGAGCCCCGATTT
AGAGCTTGACGGGGAAAGCCGCGAACGTTGGCGAGAAAGGAAGGAAAGCGAAAGGAGC
GGGCGCTAGGGCGCTGGCAAGTGTAGCGGTACGCTGCGCGTAACCACCACACCCGCCGCGC
TTAATGCGCCGCTACAGGGCGCGTCCCATTGCCATTACGGCTGCGCAACTGTTGGGAAGGG

CGATCGGTGCGGGCCTCTTCGCTATTACGCCAGCTGGCGAAAGGGGGATGTGCTGCAAGGCG
ATTAAGTTGGGTAACGCCAGGGTTTTCCAGTCACGACGTTGTAAAACGACGGCCAGTGAGC
GCGCGTAATACGACTCACTATAGGGCGAATTGGGTACCGGGCCCCCCTCGAGGTGCGACGGT
ATCGATAAGCTTGATATCGAATTCCTGCAGCCCCGGGGATCCACTAGTTCTAGAGCGGCCGC
CACCGCGGTGGAGCTCCAGCTTTTGTTCCTTTAGTGAGGGTTAATTGCGCGCTTGCGGTAA
TCATGGTCATAGCTGTTTCCTGTGTGAAATTGTTATCCGCTCACAATTCCACACAACATACG
AGCCGGAAGCATAAAGTGTAAAGCCTGGGGTGCCTAATGAGTGAGCTAACTCACATTAATTG
CGTTGCGCTCACTGCCCCTTTCCAGTCGGGAAACCTGTGCGTCCAGCTGCATTAATGAATC
GGCCAACGCGCGGGGAGAGGCGGTTTGCCTATTGGGCGCTCTTCCGCTTCCCTCGCTCACTGA
CTCGCTGCGCTCGGTGTTCCGCTGCGGCGAGCGGTATCAGCTCACTCAAAGGCGGTAATAC
GGTTATCCACAGAATCAGGGGATAACGCAGGAAAGAACATGTGAGCAAAGGCCAGCAAAG
GCCAGGAACCGTAAAAAGGCCGCGTTGCTGGCGTTTTTCCATAGGCTCCGCCCCCTGACGA
GCATCACAAAAATCGACGCTCAAGTCAGAGGTGGCGAAACCCGACAGGACTATAAAGATAACC
AGGCGTTTTCCCCCTGGAAGCTCCCTCGTGCCTCTCCTGTTCCGACCCTGCCGCTTACCGGA
TACCTGTCCGCTTTTCTCCCTTCGGGAAGCGTGGCGTTTTCTCATAGCTCACGCTGTAGGTA
TCTCAGTTCGGTGTAGGTCGTTCCGCTCCAAGCTGGGCTGTGTGCACGAACCCCCGTTTACG
CCGACCGCTGCGCCTTATCCGGTAACTATCGTCTTGAGTCCAACCCGGTAAGACACGACTTA
TCGCCACTGGCAGCAGCCACTGGTAACAGGATTAGCAGAGCGAGGTATGTAGGCGGTGCTAC
AGAGTTCTTGAAGTGGTGGCCTAACTACGGCTACACTAGAAGGACAGTATTTGGTATCTGCG
CTCTGCTGAAGCCAGTTACCTTCGGAAAAAGAGTTGGTAGCTCTTGATCCGGCAAACAAACC
ACCGCTGGTAGCGGTGGTTTTTTTTGTTTGAAGCAGCAGATTACGCGCAGAAAAAAGGATC
TCAAGAAGATCCTTTGATCTTTTCTACGGGGTCTGACGCTCAGTGGAACGAAAACCTCACGTT
AAGGGATTTTGGTCATGAGATTATCAAAAAGGATCTTCACCTAGATCCTTTTAAATTAATAA
TGAAGTTTTAAATCAATCTAAAGTATATATGAGTAACTTGGTCTGACAGTTACCAATGCTT
AATCAGTGAGGCACCTATCTCAGCGATCTGTCTATTTTCGTTTCATCCATAGTTGCCCTGACTCC
CCGTGCTGTAGATAACTACGATACGGGAGGGCTTACCATCTGGCCCCAGTGCTGCAATGATA
CCGCGAGACCCACGCTCACCGGCTCCAGATTTATCAGCAATAAACCAGCCAGCCGGAAGGGC
CGAGCGCAGAAGTGGTCCGCAACTTTATCCGCCTCCATCCAGTCTATTAATTGTTGCCGGG
AAGCTAGAGTAAGTAGTTCCGCCAGTTAATAGTTTTCGCAACGTTGTTGCCATTGCTACAGGC
ATCGTGGTGTACGCTCGTCTGTTTGGTATGGCTTCATTCAGTCCGGTTCCCAACGATCAAG
GCGAGTTACATGATCCCCATGTTGTGCAAAAAGCGGTTAGCTCCTTCGGTCCCTCCGATCG
TTGTGAGAAGTAAGTTGGCCGAGTGTATCACTCATGGTTATGGCAGCACTGCATAATTCT
CTTACTGTGATGCCATCCGTAAGATGCTTTTCTGTGACTGGTGAGTACTCAACCAAGTCATT
CTGAGAATAGTGTATGCGGCGACCGAGTTGCTCTTGCCCGGCGTCAATACGGGATAATACCG
CGCCACATAGCAGAACTTTAAAAGTGCTCATCATTGGAAAACGTTCTTCGGGGCGAAAATC
TCAAGGATCTTACCGCTGTTGAGATCCAGTTCGATGTAACCCACTCGTGCACCCAACTGATC
TTCAGCATCTTTTACTTTTACCAGCGTTTTCTGGGTGAGCAAAAACAGGAAGGCAAAATGCCG
CAAAAAGGGAATAAGGGCGACACGGAAATGTTGAATACTCATACTCTTCTTTTTCAATAT
TATTGAAGCATTTATCAGGGTTATTGTCTCATGAGCGGATACATATTTGAATGTATTTAGAA
AAATAAACAAATAGGGGTTCCGCGCACATTTCCCCGAAAAGTGCCAC

7.2. Curriculum vitae

7.3.Affidavit



Affidavit

Pakalniškytė Dalia

Surname, first name

Street

Zip code, town

Germany

Country

I hereby declare, that the submitted thesis entitled

Novel CD64-DTR mouse model generation using CRISPR-Cas9 technology and functional characterization of renal dendritic cells

is my own work. I have only used the sources indicated and have not made unauthorised use of services of a third party. Where the work of others has been quoted or reproduced, the source is always given.

I further declare that the submitted thesis or parts thereof have not been presented as part of an examination degree to any other university.

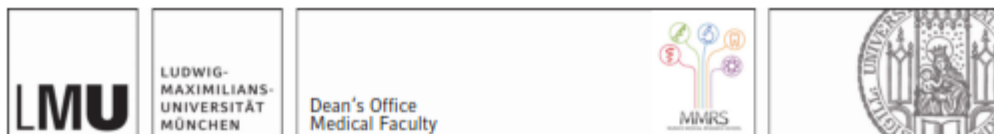
Munich, 09.07.2019

Place, date

Pakalniškytė Dalia

Signature doctoral candidate

7.4. Confirmation of congruency



Confirmation of congruency between printed and electronic version of the doctoral thesis

Pakalniškytė Dalia

Surname, first name

Street

Zip code, town

Germany

Country

I hereby declare that the electronic version of the submitted thesis, entitled
Novel CD64-DTR mouse model generation using CRISPR-Cas9 technology and functional
characterization of renal dendritic cells

is congruent with the printed version both in content and format.

Munich, 09.07.2019

Place, date

Pakalniškytė Dalia

Signature doctoral candidate

7.5. List of scientific publications

- Tissue-Specific Diversity and Functions of Conventional Dendritic Cells. **Pakalniškytė D**, Schraml BU. *Advances in Immunology*. 2017
- *Clec9a*-Mediated Ablation of Conventional Dendritic Cells Suggests a Lymphoid Path to Generating Dendritic Cells *In Vivo*. Salvermoser J, van Blijswijk J, Papaioannou NE, Rambichler S, Pasztoi M, **Pakalniškytė D**, Rogers NC, Keppler SJ, Straub T, Reis E Sousa C, Schraml BU. *Frontiers in Immunology*. 2018
- The kidney contains ontogenically distinct mononuclear phagocyte subtypes throughout development that differ in their inflammatory properties. Salei N, Rambichler S, Salvermoser J, Papaioannou NE, Schuchert R, **Pakalniškytė D**, Stremmel C, Cernilogar FM, Salvermoser M, Walzog B, Straub T, Schotta G, Schulz C, Schraml BU. *Journal of the American Society of Nephrology*. 2019 (Accepted)